TECHNICAL REPORT M-76-8

PROCEDURES FOR THE SYSTEMATIC EVALUATION OF REMOTE SENSOR PERFORMANCE AND QUANTITATIVE MISSION PLANNING

by

Lewis E. Link, Jr.

Mobility and Environmental Systems Laboratory
U. S. Army Engineer Waterways Experiment Station
P. O. Box 631, Vicksburg, Miss. 39180

August 1976

Final Report

Approved For Public Release; Distribution Unlimited

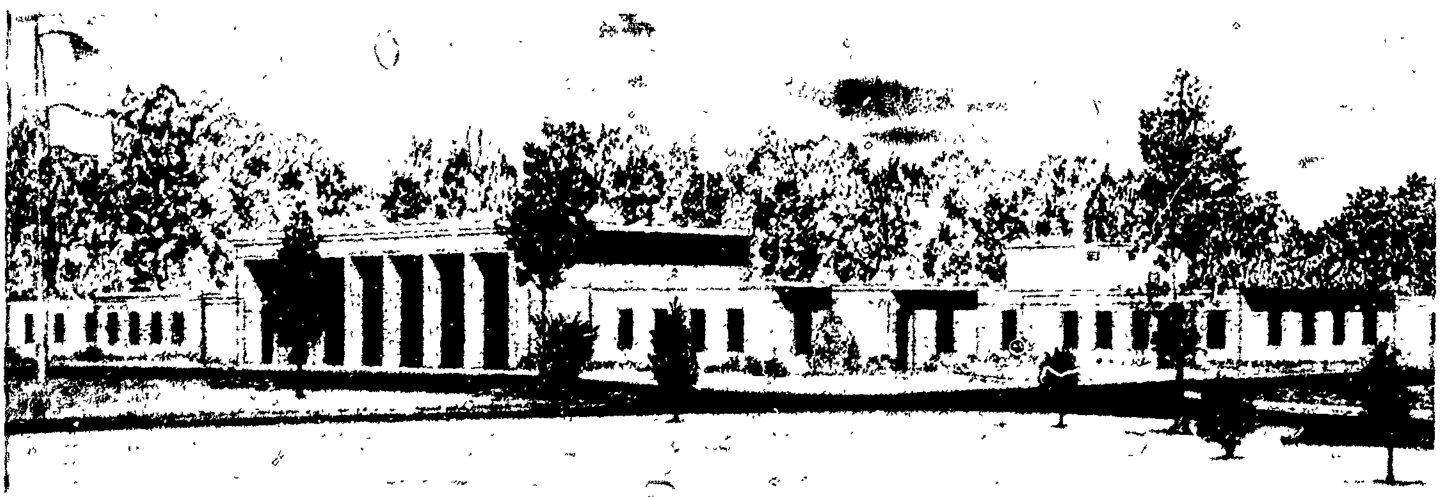

Prepared for Office, Chief of Engineers, U. S. Army
Washington, D. C. 20314

Under Project 4A162121A896, Ta[illegible]I

Destroy this report when no longer needed. Do not return it to the originator.

Unclassified

SECURITY CLASSIFICATION OF THIS PAGE (When Data Entered)

REPORT DOCUMENTATION PAGE		READ INSTRUCTIONS BEFORE COMPLETING FORM
1. REPORT NUMBER Technical Report M-76-8 (14) WES-TR-M-76-8	2. GOVT ACCESSION NO.	3. RECIPIENT'S CATALOG NUMBER
4. TITLE (and Subtitle) (6) PROCEDURES FOR THE SYSTEMATIC EVALUATION OF REMOTE SENSOR PERFORMANCE AND QUANTITATIVE MISSION PLANNING.		5. TYPE OF REPORT & PERIOD COVERED (9) Final report, 6. PERFORMING ORG. REPORT NUMBER
7. AUTHOR(s) (10) Lewis E. Link, Jr		8. CONTRACT OR GRANT NUMBER(s) (16) DA-4-A-162121-A-896
9. PERFORMING ORGANIZATION NAME AND ADDRESS U. S. Army Engineer Waterways Experiment Station Mobility and Environmental Systems Laboratory P. O. Box 631, Vicksburg, Miss. 39180		10. PROGRAM ELEMENT, PROJECT, TASK AREA & WORK UNIT NUMBERS Project 4A162121A896 Task 01, Work Unit 003
11. CONTROLLING OFFICE NAME AND ADDRESS Office, Chief of Engineers, U. S. Army Washington, D. C. 20314		12. REPORT DATE (11) Aug ~~ust 19~~76 13. NUMBER OF PAGES 287 (12) 291p.
14. MONITORING AGENCY NAME & ADDRESS(if different from Controlling Office) (17) 4-A-162121-A-896 01		15. SECURITY CLASS. (of this report) Unclassified 15a. DECLASSIFICATION/DOWNGRADING SCHEDULE
16. DISTRIBUTION STATEMENT (of this Report) Approved for public release; distribution unlimited.		
17. DISTRIBUTION STATEMENT (of the abstract entered in Block 20, if different from Report)		
18. SUPPLEMENTARY NOTES		
19. KEY WORDS (Continue on reverse side if necessary and identify by block number) Infrared scanners Mathematical models Remote sensing Sensors		
20. ABSTRACT (Continue on reverse side if necessary and identify by block number)		

Effective application of remote sensing techniques to civil engineering and environmental problems requires the selection of the sensor systems that will best provide the information desired. Because of the many phenomena involved and the lack of a simple means to consider them collectively, planning remote sensing missions has been done subjectively, quantitatively on a piecemeal basis, or solely on the experience of the investigator. None of these offers a systematic means to optimize the mission for acquisition of

(Continued)

DD FORM 1 JAN 73 1473 EDITION OF 1 NOV 65 IS OBSOLETE

SECURITY CLASSIFICATION OF THIS PAGE (When Data Entered)

038 100

20. ABSTRACT (Continued)

specific information types as a function of the many variables involved. The purpose of this study was to (a) quantitatively examine the natural phenomena that influence the information content of remote sensing imagery obtained in the visible and infrared (IR) portions of the electromagnetic spectrum, and (b) from the knowledge gained through these examinations, develop analytical tools for planning remote sensing missions and provide guidance for application of photographic and thermal IR sensor systems to civil engineering and environmental problems.

This study consisted of (a) the development of analytical models that allow systematic control of the major variables that influence the character of imagery produced by photographic and thermal IR scanning sensor systems, and (b) formulation from the models of simple, but comprehensive, tools for planning photographic and thermal IR remote sensing missions. The basic concept of the models and the mission planning tools is an organized and quantitative means for evaluating photographic and thermal IR sensor systems for particular data acquisition jobs by contrasting the magnitude and spectral content of energy received by the sensors with performance characteristics of the sensor systems. The ability to quantitatively predict performance provides the capability necessary to quantitatively plan missions for specified types of data. Variables considered include the source of electromagnetic radiation, interactions with terrain materials, interactions with the atmosphere, sensor altitude, time of day, time of year, source-sensor position, and sensor spectral and spatial characteristics.

The Photographic Systems Simulation Model and the Thermal IR Systems Simulation Models provide a new dimension for systematic evaluation of remote sensor performance and quantitative mission design previously unavailable to personnel applying remote sensors to civil engineering and environmental problems. The systems models and the graphical products derived from the models allow selection of the best (of those available) sensor system for a specific data acquisition problem by providing a means of quantitatively comparing the expected performances of a variety of sensors for the specific data needs. In addition, the models and derived products provide a means of quantitatively planning the remote sensing mission to optimize the information content of the resulting imagery for the specific data needs.

The systems models consider the major phenomena that influence the informational content of photographic and thermal IR sensors imagery. As is usually the case, a variety of analytical methods could have been used to model these phenomena. The methods used were chosen to provide a comprehensive description of the phenomena and yet minimize the number of hard-to-get inputs required to execute the models. As such, the models were oriented toward the people who apply remote sensors rather than those who design them.

THE CONTENTS OF THIS REPORT ARE NOT TO BE USED FOR ADVERTISING, PUBLICATION, OR PROMOTIONAL PURPOSES. CITATION OF TRADE NAMES DOES NOT CONSTITUTE AN OFFICIAL ENDORSEMENT OR APPROVAL OF THE USE OF SUCH COMMERCIAL PRODUCTS.

This Document Contains
Missing Page/s That Are
Unavailable In The
Original Document

OR are
Blank pgs
that have
Been Removed

BEST
AVAILABLE COPY

PREFACE

The work reported herein was conducted at the U. S. Army Engineer Waterways Experiment Station (WES), Vicksburg, Mississippi, as a portion of Work Unit 003, "Remote Sensing of the Environment," Task 01, "Environmental Quality Management for Military Facilities," Project 4A162121A896, "Environmental Quality for Construction and Operation of Military Facilities." This report is essentially a thesis submitted to the Graduate School of the Pennsylvania State University in partial fulfillment of the requirements for the degree of Doctor of Philosophy in the Department of Civil Engineering. The work is a comprehensive documentation of the procedures developed by the author for the systematic evaluation of remote sensor performance and quantitative mission planning.

This work was accomplished under the general supervision of Mr. W. G. Shockley, Chief of the Mobility and Environmental Systems Laboratory (MESL), and Mr. B. O. Benn, Chief of the Environmental Systems Division. This report was prepared by Mr. L. E. Link, Jr., Chief of the Environmental Research Branch (ERB). The author is indebted to the management personnel of the MESL for their support and invaluable guidance during the execution of this study. Particular appreciation is expressed to Messrs. Shockley, Benn, W. E. Grabau, and J. R. Lundien. The author also extends sincere appreciation to his faculty advisor, Dr. Gert Aron and the other members of his committee, Dr. F. Y. Borden, Dr. Harmer Weeden, and Dr. Arthur Miller. Appreciation is also to extended to Mr. J. R. Stabler, ERB, for his invaluable computer programming assistance.

COL G. H. Hilt, CE, and COL J. L. Cannon, CE, were Directors of the WES during this study and preparation of this report. Mr. F. R. Brown was Technical Director.

TABLE OF CONTENTS

	Page
PREFACE	v
LIST OF FIGURES	ix
LIST OF TABLES	xiii
LIST OF PLATES	xvii
CONVERSION FACTORS, U. S. CUSTOMARY TO METRIC (SI) UNITS OF MEASUREMENT	xix
PART I: INTRODUCTION	1
Background	1
Objective and Scope	7
PART II: PHOTOGRAPHIC SYSTEMS SIMULATION MODEL	10
Concept of the Model	10
Spectral Component of Model	13
Spatial Component of Model	35
Model Limitations	37
PART III: SIMULATION OF THERMAL IR SENSOR SYSTEMS	41
Introduction	41
Analytical Procedures for Simulation	42
Presentation of Model Forms and Their Outputs	55
PART IV: PLANNING TOOLS FOR PHOTOGRAPHIC MISSIONS	62
Introduction	62
Model Application in Photographic Mission Planning	66
A Nomogram for Computing Optical Density Contrast	80
PART V: PLANNING THERMAL IR MISSIONS	100
Introduction	100
Mission Planning Tools	107
Example Application of Mission Planning Tools	131
PART VI: SUMMARY	139

TABLE OF CONTENTS (Concluded)

		Page
LITERATURE CITED		142
SUPPLEMENTARY TABLES AND PLATES		145
APPENDIX A:	BIBLIOGRAPHY	206
APPENDIX B:	DOCUMENTATION OF PHOTOGRAPHIC SYSTEMS SIMULATION MODEL COMPUTER PROGRAM	210
	Program Identification	210
	Engineering Documentation	211
	System Documentation	213
APPENDIX C:	DOCUMENTATION OF SPECIFIC FORM OF THERMAL IR SYSTEMS SIMULATION MODEL COMPUTER PROGRAM	230
	Program Identification	230
	Engineering Documentation	231
	System Documentation	232
	Operating Instructions	235
APPENDIX D:	DOCUMENTATION OF GENERAL FORM OF THERMAL IR SYSTEMS SIMULATION MODEL COMPUTER PROGRAM	250
	Program Identification	250
	Engineering Documentation	251
	System Documentation	252
	Operating Instructions	256
APPENDIX E:	RELATION OF ABSOLUTE AND APPARENT TEMPERATURE	266

LIST OF FIGURES

Figure		Page
1	Concept of spectral component of Photographic Systems Simulation Model, energy reaching the sensor	11
2	Concept of spectral component of Photographic Systems Simulation Model, interaction with sensor system	12
3	Solar irradiance above the atmosphere as used in the model	14
4	Ratio of skylight to sunlight plus skylight	15
5	Atmospheric transmission curve for mid-latitude summer, 23-haze condition and 30-deg solar zenith angle	18
6	Example of solar irradiance that reaches the terrain by direct transmission through the atmosphere for mid-latitude summer, 23-km condition and 30-deg zenith angle	18
7	Geometric relation between solar zenith angle, solar azimuth, terrain surface slope, and terrain slope azimuth	20
8	Graphical means to compute effective sun angle . . .	21
9	Example of spectral reflectance curve for a mature cottonwood tree	23
10	Typical example of atmospheric transmission curve for transmission from the ground to the sensor at a specified altitude	24
11	Relative amplitudes of skylight at terrain surface and backscatter as a function of altitude for 23-km haze condition	27
12	Relative amplitudes of skylight at terrain surface and backscatter as a function of altitude for 5-km haze condition	27
13	Example of lens transmission curve	29
14	Transmission curve for Wratten No. 12 filter	30

LIST OF FIGURES

Figure		Page
15	Spectral sensitivity curve for Kodak Infrared Aerographic Film No. 2424	30
16	Representative output of Photographic Systems Simulation Model	33
17	Resolvable ground distance as a function of altitude for Kodak Plus-X Aerographic Film No. 2402	36
18	Schematic of Thermal IR Systems Simulation Models	42
19	Relative response curves for mercury-cadmium-telluride (a) and indium-antimonide (b) detectors operating in the 8- to 14- and 3- to 5.5-μm wavelength bands, respectively	49
20	Detector response curve for mercury-cadmium-telluride detector having a peak response of 1000 volts/watt	50
21	Illustration of situations where the feature area is less than the pixel area (a) and where the boundary between the feature and background occurs within individual pixels (b)	53
22	Spectral reflectance curves for silt and clay . . .	74
23	Simplified illustration of the basic structure of the nomogram for predicting optical density contrast	85
24	Diurnal temperature variations for bare soil and grass areas, Vicksburg, Mississippi	101
25	Schematic of typical thermal IR scanner system	103
26	Sensor spatial resolution for altitudes up to 1000 m	128
27	Sensor spatial resolution for altitudes from 0 to 10,000 m	129
28	Thermal IR imagery scale as a function of altitude, scan width, and film width	130

LIST OF FIGURES (Concluded)

Figure		Page
29	Temperature variations for alluvium and shale as adapted from Reference 33	133
B1	Condensed flow chart for remote sensing simulation model	214
C1	Condensed flow chart for specific form of Thermal IR Systems Simulation Model	233
D1	Example of graphical form of model output	253
D2	Condensed flowchart for specific form of Thermal IR Systems Simulation Model	254
E1	Apparent temperature versus actual temperature and emissivity for the 3.0- to 5.5-μm wavelength band	269
E2	Apparent temperature versus actual temperature and emissivity for the 8- to 14-μm wavelength band	270

LIST OF TABLES

Table		Page
1	Film Gamma (γ) Values Used in the Model	145
2	Output of Specific Form of Thermal IR Systems Simulation Model	145
3	Output of General Form of Thermal IR Systems Simulation Model	146
4	Film-Filter Combinations Considered for Example Problem in Text	147
5	Photographic Systems Simulation Model Output . . .	148
6	Photographic Systems Simulation Model Output . . .	149
7	Photographic Systems Simulation Model Output . . .	150
8	Photographic Systems Simulation Model Output . . .	151
9	Photographic Systems Simulation Model Output . . .	152
10	Photographic Systems Simulation Model Output . . .	153
11	Photographic Systems Simulation Model Output . . .	154
12	Photographic Systems Simulation Model Output . . .	155
13	Photographic Systems Simulation Model Output . . .	156
14	Photographic Systems Simulation Model Output . . .	157
15	Photographic Systems Simulation Model Output . . .	158
16	Photographic Systems Simulation Model Output . . .	159
17	Values of Transfer Function for Nomogram by Filter Type and Wavelength Band, Kodak Infrared Aerographic Film No. 2424, Summer Season	160
18	Approximate Gamma (γ) Values for Film as a Function of Processing Techniques	164
19	Values of Transfer Function for Nomogram by Emulsion Filter Type and Wavelength Band, Kodak Aerochrome Infrared Film No. 2443, Summer Season	165

LIST OF TABLES

Table		Page
20	Wavelength Sensitivities of Film-Filter Combinations	169
21	Solar Zenith Angle	170
22	Comparison of Computer- and Nomogram-Predicted Optical Density Contrast Values	174
23	Inputs to General Thermal IR Systems Simulation Model for Generating Mission Planning Graphics	174
24	Thermal Resolution for 8- to 14-μm Sensor Systems for Use in High-Performance Aircraft, Mid-latitude Summer Atmosphere	175
25	Thermal Resolution for 8- to 14-μm Sensor Systems for Use in High-Performance Aircraft, Mid-latitude Winter Atmosphere	176
26	Thermal Resolution for 8- to 14-μm Sensor Systems for Use in Low-Performance Aircraft, Mid-latitude Summer Atmosphere	177
27	Thermal Resolution for 8- to 14-μm Sensor Systems for Use in Low-Performance Aircraft, Mid-latitude Winter Atmosphere	178
28	Thermal Resolution for 3- to 5.5-μm Sensor Systems for Use in High-Performance Aircraft, Mid-latitude Summer Atmosphere	179
29	Thermal Resolution for 3- to 5.5-μm Sensor Systems for Use in High-Performance Aircraft, Mid-latitude Winter Atmosphere	180
30	Thermal Resolution for 3- to 5.5-μm Sensor Systems for Use in Low-Performance Aircraft, Mid-latitude Summer Atmosphere	181
31	Thermal Resolution for 3- to 5.5-μm Sensor Systems for Use in Low-Performance Aircraft, Mid-latitude Winter Atmosphere	182
32	Typical Emmissivity Values	183

LIST OF TABLES

Table		Page
33	Noise Equivalent Temperature Values as Derived from the Thermal IR Systems Simulation Model, °C	183
34	Approximate Scales for Thermal IR Imagery when Sensor Output is Recorded on Film	184
B1	List of Variables Input	217
B2	Example of Model Output	218
B3	Variable for Remote Sensing Simulation Model	219
B4	Structure of Input File for Sensors	221
B5	Structure of Input File for Spectral Sensitivity Curve	221
B6	Structure of Input File for Total and Ground-to-Sensor Atmospheres	222
B7	Structure of Input File for Spectral Reflectance, Skylight Irradiance, and Solar Irradiance Above Atmosphere	223
B8	Structure of Input File for Filter Data	223
B9	Example of Input File for Sensors	224
B10	Example of Input File for Film Spectral Sensitivity	225
B11	Example of Input File for Atmospheric Transmission	226
B12	Example of Input File for Spectral Reflectance	227
B13	Example of Input File for Filter	228
B14	List of Control Cards	229
C1	List of Variable Input	237
C2	Example of Model Output of IR Sensor Performance Prediction	238
C3	Variables for Thermal IR System Performance Prediction	239

LIST OF TABLES (Concluded)

Table		Page
C4	Structure of Input File for Total and Ground-to-Sensor Atmospheres	242
C5	Structure of Input File for Spectral Reflectance and Solar Irradiance Above Atmosphere	243
C6	Structure of Input File for Relative Response Curve	243
C7	Example of Variable Input	244
C8	Example of Solar Irradiance File	245
C9	Example of Input File for Detector Relative Response Curve	246
C10	Example of Input File for Atmospheric Transmission	247
C11	Example of Spectral Reflectance File	248
C12	List of Control Cards	249
D1	List of Variables Input	257
D2	Example of Graphical Output of Model	258
D3	Variable for Minimum Detectable Temperature Difference Model	259
D4	Structure of Input File for Ground-to-Sensor Atmospheres	261
D5	Structure of Input File for Relative Response Curve	261
D6	Example of Variable Inputs	262
D7	Example of Input File for Atmospheric Transmission	263
D8	Example of Detector Relative Response File	264
D9	List of Control Cards	265

LIST OF PLATES

Plate		Page
1	Total Atmospheric Scattering Coefficient Versus Altitude for $\lambda = 0.4880\ \mu m$	185
2	Total Atmospheric Scattering Coefficient Versus Altitude for $\lambda = 0.5145\ \mu m$	186
3	Total Atmospheric Scattering Coefficient Versus Altitude for $\lambda = 0.6328\ \mu m$	187
4	Total Atmospheric Scattering Coefficient Versus Altitude for $\lambda = 0.6943\ \mu m$	188
5	Total Atmospheric Scattering Versus Atltitude for $\lambda = 0.8600\ \mu m$	189
6	Part 1 of Nomogram for Predicting Photographic Optical Density Contrast	190
7	Part 2 of Nomogram for Predicting Photographic Optical Density Contrast	191
8	Example of Computation of Energy Index Values for Feature and Background in the 0.40- to 0.50-μm Band	192
9	Example of Computation of Energy Index Values for Feature and Background in the 0.50- to 0.58-μm Band	193
10	Example of Computation of Energy Index Values for Feature and Background in the 0.58- to 0.68-μm Band	194
11	Example of Computation of Energy Index Values for Feature and Background in the 0.68- to 0.80-μm Band	195
12	Example of Computation of Energy Index Values for Feature and Background in the 0.80- to 0.93-μm Band	196
13	Example of Computation of Optical Density Contrast Using Point on Reference Line and Appropriate γ Curve	197

LIST OF PLATES (Concluded)

Plate		Page
14	Thermal Resolution for 8- to 14-μm Sensor Systems for Use in High-Performance Aircraft, Mid-latitude Summer Atmosphere	198
15	Thermal Resolution for 8- to 14-μm Sensor Systems for Use in High-Performance Aircraft, Mid-latitude Winter Atmosphere	199
16	Thermal Resolution for 8- to 14-μm Sensor Systems for Use in Low-Performance Aircraft, Mid-latitude Summer Atmosphere	200
17	Thermal Resolution for 8- to 14-μm Sensor Systems for Use in Low-Performance Aircraft, Mid-latitude Winter Atmosphere	201
18	Thermal Resolution for 3- to 5.5-μm Sensor Systems for Use in High-Performance Aircraft, Mid-latitude Summer Atmosphere	202
19	Thermal Resolution for 3- to 5.5-μm Sensor Systems for Use in High-Performance Aircraft, Mid-latitude Winter Atmosphere	203
20	Thermal Resolution for 3- to 5.5-μm Sensor Systems for Use in Low-Performance Aircraft, Mid-latitude Summer Atmosphere	204
21	Thermal Resolution for 3- to 5.5-μm Sensor Systems for Use in Low-Performance Aircraft, Mid-latitude Winter Atmosphere	205

CONVERSION FACTORS, U. S. CUSTOMARY TO METRIC (SI) UNITS OF MEASUREMENT

Units of measurement used in this report can be converted as follows:

Multiply	By	To Obtain
	Metric (SI) to U. S. Customary	
micrometres	3.937007×10^{-5}	inches
millimetres	0.03937007	inches
centimetres	0.3937007	inches
metres	3.280839	feet
kilometres	0.6213711	miles (U. S. statute)
square centimetres	0.1550	square inches
watts per square centimetre	0.1550	watts per square inch
milliradians (angular)	0.05729578	degrees
Celsius degrees or Kelvins	1.8	Fahrenheit degrees*
	U. S. Customary to Metric (SI)	
inches	25.4	millimetres
feet per minute	0.3048	metres per minute
degrees (angular)	0.01745329	radians
Fahrenheit degrees	0.555	Celsius degrees or Kelvins**

* To obtain Fahrenheit (F) readings from Celsius readings, use the following formula: $F = 1.8(C) + 32$. To obtain Fahrenheit readings from Kelvins, use: $F = 1.8(K - 273.15) + 32$.

** To obtain Celsius (C) temperature readings from Fahrenheit (F) readings, use the following formula: $C = 0.555(F - 32)$. To obtain Kelvin (K) readings, use: $K = 0.555(F + 459.67)$.

PROCEDURES FOR THE SYSTEMATIC EVALUATION OF REMOTE SENSOR PERFORMANCE AND QUANTITATIVE MISSION PLANNING

PART I: INTRODUCTION

Background

General

1. Remote sensing began in 1840 when Gaspard Felix Tournachon took a photograph of an area near Paris from a balloon. Since then aerial photography and a variety of more exotic techniques have been used to acquire a staggering amount of data for application to engineering and environmental problems. In spite of this broad application, the methods employed by the user community to plan and execute remote sensing missions remain empirical and at times subjective. As the need increases for more detailed and specific data over larger and larger areas, remote sensing will be more and more in demand as a data acquisition tool. The added sophistication of the data needed will require added sophistication in the methods used to employ remote sensing to acquire that data. In the following paragraphs the field of hydrology is used to establish the need for generating new methods for evaluating remote sensor systems and planning missions. Although the discussion is limited to hydrology, the research needs established and the products resulting from the research are equally applicable to any field or discipline.

Data requirements for hydrology

2. The response of a watershed to a storm of given intensity, duration, and distribution is a function of the phenomena that control

the volume and time-phasing of the water reaching a given point within the watershed. These phenomena include interception storage, depression storage, evapotranspiration, surface runoff, interflow, infiltration, groundwater flow, subsurface storage, and routing and channel storage. Coupled with the above-mentioned phenomena are the antecedent conditions of the watershed. These "initial conditions" and the physical characteristics of the watershed (topography, geology, vegetation cover, etc.) essentially weigh the effects of the various phenomena to convert a storm into a response (i.e. a runoff hydrograph). Watershed response models are normally comprised of submodels or mathematical relations that simulate each phenomenon being considered. The number of phenomena included in a model may vary from the two or three considered to exert the most influence for a given situation to all of them (e.g. the Stanford Watershed Model). The accuracy of the watershed response predictions are a function of the following:

- a. The realism of the mathematical relations used to represent each phenomenon.
- b. The accurate translation of the physical conditions within the watershed into the inputs necessary for the various submodels.
- c. The accurate specification of the distribution within the watershed of those physical conditions that influence watershed response.

The following paragraphs address item c.

3. Examination of the mechanisms by which the phenomena mentioned in paragraph 2 operate, leads to a realization that the basic

physical characteristics that control the effect of each phenomenon on watershed response can be grouped into the following categories:

- a. Soils
- b. Vegetation
- c. Topography
- d. Bedrock

It is the knowledge of these characteristics and their distribution within the watershed, therefore, that comprises the basic terrain information required for predicting watershed response. The detail of the information required is a function of the sophistication of both the model used and the overall investigation.

4. For a comprehensive analysis of watershed response, it is necessary to know the changes in soil, vegetation, topography, and bedrock characteristics as a function of time as well as their spatial distribution at any given time. The time-dependent changes may only consist of variations in such things as soil moisture or plant vigor, which may influence the "antecedent conditions" of the watershed for a given storm. They may also involve gross changes in conditions such as clear cutting, land use, major excavations, etc., which may drastically alter the basic response character of the watershed. In any case, the requirement for basic terrain data is staggering if the investigator attempts to define the watershed in both a spatial and temporal framework. Nevertheless, if the possession of such data will help provide a reliable, quantitatively accurate response prediction, it behooves the researcher to investigate means for acquiring these data. Perhaps the only technique currently available that has potential for efficiently satisfying

these data needs in a cost-effective manner is remote sensing.

Remote sensing for data acquisition

5. Remote sensing techniques have been shown to be valuable tools for acquisition of environmental data pertinent to producing a baseline description of the environment of an area and for acquisition of data relevant to the detection of environmental changes as a function of time (Reference 1).* In this study the environmental factors of interest included vegetation type, vegetation density, vegetation height, wildlife habitat, soil type, depth to bedrock, surface water, depth to groundwater, pollution sources, and cultural features. Numerous reports have been written concerning the application of remote sensing to hydrology. (A comprehensive bibliography is presented in Appendix A.) They range from cursory overviews and evaluations of the applicability of remote sensing to hydrology (References 2 to 6) to evaluations and discussions of specific applications (References 7 to 13) and formulation of techniques for acquiring inputs for specific watershed response models (References 14 to 16). Within these reports, terrain factors are discussed, such as soil type and moisture content, drainage patterns, snow and ice conditions, land use, vegetation conditions, waterbody configuration, cloud cover, surface temperature, rainfall estimation, topography, soil depth, channel and floodplain topography, vegetation interception, overland flow roughness, and subsurface conditions. The general potential and applicability of remote sensing techniques for use in acquisition of environmental data relevant to hydrologic

---

* References in parentheses are listed at the end of the main text.

response has, to some extent, been documented and discussed. The primary and perhaps most demanding tasks remaining are to develop the techniques that allow remote sensing to be used effectively (i.e. to gather the most information possible concerning changes in watershed conditions on a spatial and temporal basis) by hydrologists not intimately familiar with the physics of the processes involved in remote sensing. As Robinove (Reference 6) so ably stated:

> Only by carefully studying the physics of electromagnetic radiation and its interactions with hydrologic features can the hydrologist utilize the proper sensing system or suggest the development of a specific sensing system for his purpose. The pitfall of thinking of aerial photography or infrared imagery as tools in themselves without consideration of the physics of these tools and the necessary ground control can often doom the hydrologist's efforts to failure.

Research needs

6. The informational content of a remote sensor image is entirely a function of the spatial variation of the optical density values (gray tones or colors) comprising the image and of the investigator's ability to place these variations within a meaningful context and translate them into desired information. It would be ideal if the variations in image optical density were always directly and exclusively related to changes in terrain material types (e.g. soil or vegetation types) or conditions (e.g. soil moisture content). Unfortunately, this is hardly ever the case. At best, variations in image optical density values are directly related to changes in the reflectance or radiation properties of terrain materials which may or may not be related directly to the material changes of interest to the hydrologist. Additional uncertainties are added in that the

optical density values on an image are the resultant of interactions of electromagnetic energy with the atmosphere and the sensor system itself as well as the aforementioned interaction with terrain materials (e.g. soils, vegetation, rock, etc.). The atmospheric and sensor system influences have been shown to be very significant with respect to the optical density variations resulting from changes in material type or condition (Reference 17). In addition to the above interactions, the reflectance geometry (i.e. the geometric relations among energy source, terrain feature, and sensor system) can have considerable influence on the optical density values that end up on an image. Because of the many interactions and complex geometry involved, it is entirely conceivable that variations in optical density values can occur without associated variations in the type or condition of terrain materials. Conversely, changes may occur in the terrain without producing a detectable change in optical density. The fact that these things can and do occur complicates the detection of change in both spatial and temporal frameworks.

7 An immediate need exists, therefore, for a quantitative definition of the influence of phenomena, other than changes in terrain material type and condition, on the informational content of remote sensor imagery. For the acquisition of hydrologic data at any given time, there is an immediate need for the hydrologist to have available a means for considering the complex phenomena that influence imagery informational content so as to minimize the effects of phenomena not related to changes in terrain material characteristics, in essence, a procedure for planning the remote sensing mission so as to optimize the resulting imagery with respect to the desired

information. Accomplishment of these research needs would be a significant step forward in the effort to provide the technology and technology products necessary for the effective use of remote sensing techniques by hydrologists concerned with watershed response and, in fact, for anyone concerned with the use of remote sensing techniques to acquire data relevant to civil engineering and environmental problems.

Objective and Scope

Objective

8. The overall objective of the research presented herein was to quantitatively examine the natural phenomena that influence the informational content of remote sensing imagery obtained in the visible and infrared (IR) regions of the electromagnetic spectrum, and from the understanding gained through these examinations, develop analytical tools for planning remote sensing missions and providing guidance for application of photographic and thermal IR sensor systems to fields such as hydrology.

Scope

9. The electromagnetic energy reaching a remote sensor is the resultant of a number of complex interactions, each varying as a function of wavelength. The sensor system also interacts with the energy to produce the signals recorded on film or magnetic tape. To determine the character of the final product, it is necessary to account quantitatively for each interaction. The number of variables involved and their dependence on wavelength make the determination of the character of the remote sensing product virtually impossible

without a systematic, analytical means of describing the interactions both individually and collectively.

10. The primary objective of the efforts reported in Parts II and III was to develop and computerize analytical models that allow systematic control of the major variables that influence the character of an image. In the models' development, the primary sensor systems available to the hydrologist (i.e. photographic systems and thermal IR scanner systems) were considered. Variables considered include the source of electromagnetic radiation, interactions with terrain materials, interactions with the atmosphere, sensor altitude, time of day, time of year, source-sensor position, and sensor spectral and spatial characteristics. The models provide a previously unavailable tool for examining quantitatively the effects of the major variables on the character of a remote sensing image.

11. Because of the many phenomena involved and the lack of a simple means to consider them collectively, planning of remote sensing missions has been done subjectively, quantitatively on a piecemeal basis, or solely on the experience of the investigator. None of these offer a systematic means to optimize the mission for acquisition of specific information types as a function of the many variables involved. A more comprehensive capability is needed, especially for those unfamiliar with the physics of the processes involved in remote sensing.

12. The primary objective of the efforts reported in Parts IV and V was to use the analytical models (Parts II and III) to formulate simple, but comprehensive, tools for planning photographic and thermal IR remote sensing missions. The final form of the planning

tools is graphical to provide easy dispersal to users and simplistic execution. An attempt was made to maintain the analytical rigor inherent in the models, although some simplification and loss of quantitative rigor was necessary. The simplification was based on inclusion of only those variables representing the phenomena that have a rather significant influence on image character.

13. The comprehensive planning tools provide the hydrologist with a new capability for optimizing the utility of remote sensing systems. Through the use of these tools, he will hopefully be able to select quantitatively the best sensor system (e.g. film type and filter) and mission characteristics (e.g. altitude, atmospheric conditions, time of day, etc.). Only by using adequate planning tools will the full potential of remote sensing techniques be realized in any discipline.

PART II: PHOTOGRAPHIC SYSTEMS SIMULATION MODEL

14. A computerized simulation model of the relations between photographic remote sensor systems and the environment was developed to provide an analytical capability for evaluating and comparing photographic remote sensor systems and optimization of mission profiles. The model allows for the systematic control of the major variables that affect the character of photographic imagery, including the electromagnetic (EM) radiation* source, atomsphere, terrain materials, time constraints, season, latitude, sensor characteristics, and altitude. The present form of the model is capable of handling any film-filter-lens-camera systems for both visible and near-IR (0.4 to 1.0 μm**) wavelengths. Since systems for these wavelengths are fairly well established and economical (as compared to the more exotic imagery types), they are the most readily available for acquisition of environmental data related to hydrologic phenomena.

Concept of the Model

15. The concept of the model is quite simple. The basic question to be answered is: What combination of sensor system and mission profile results in the greatest contrast between environmental features of interest? The approach to answering this question consists of separating the characteristics of the feature into spectral

---

* The physics of EM radiation and the use of EM radiation for remote sensing are discussed in detail in Appendix A of Reference 18.

** A table of factors for converting metric (SI) units of measurement to U. S. customary units and U. S. customary units to metric (SI) units is presented on page xix.

(energy level) and spatial (dimensional) components.

Spectral component

16. The basic concept of the spectral component of the model is illustrated pictorially in Figures 1 and 2. In this illustration the environmental problem consists of distinguishing between cottonwood and fir trees; however, the features may just as well have been two masses of water with different turbidity characteristics, or indeed any situation in which there is assumed to be a spectral distinction between two adjoining objects or factors. Using the sun

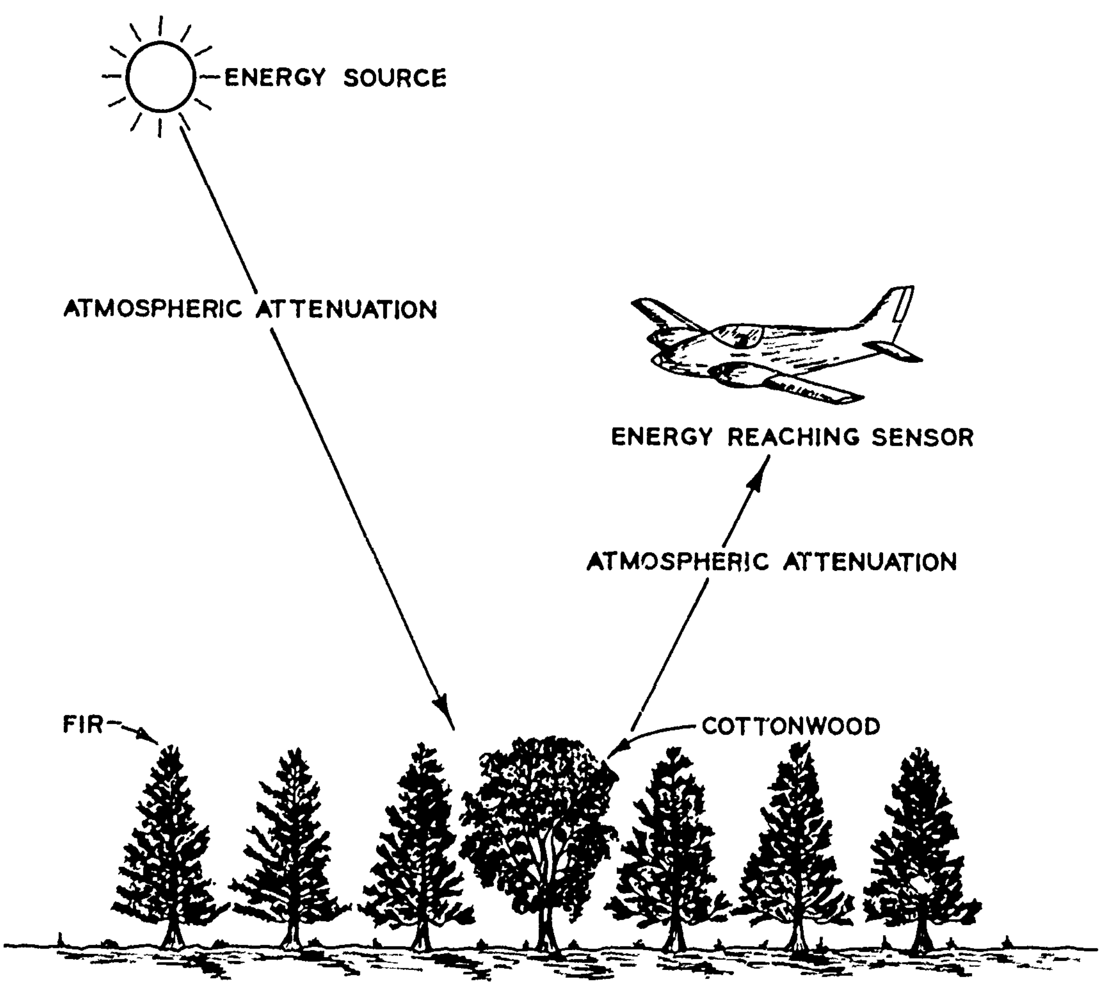

Figure 1. Concept of spectral component of Photographic Systems Simulation Model, energy reaching the sensor

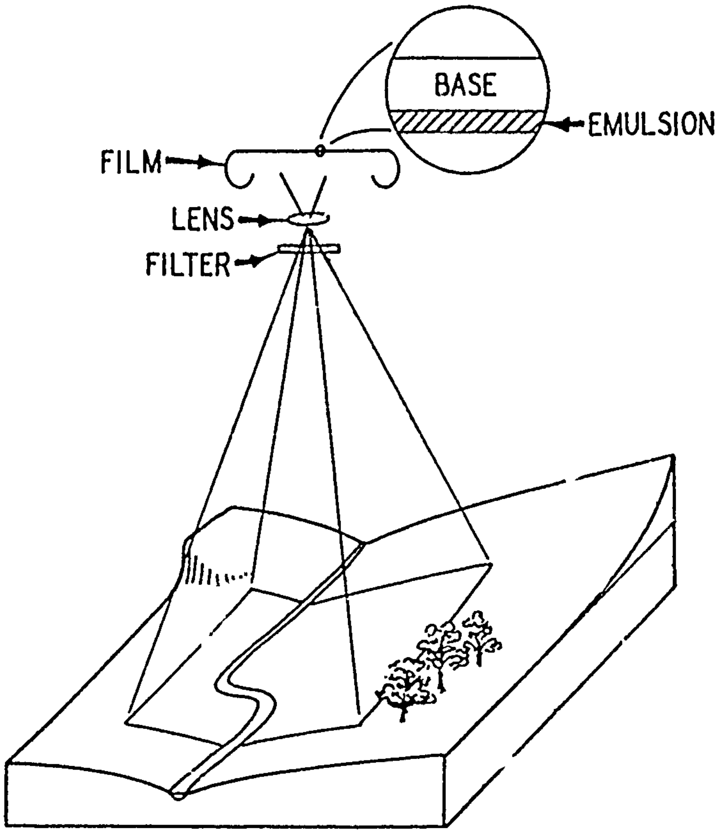

Figure 2. Concept of spectral component of Photographic Systems Simulation Model, interaction with sensor system

as the basic energy source, the model calculates the amount of solar energy reaching the remote sensor by considering the attenuating and scattering effects of the atmosphere and the reflectance properties of the environmental features under consideration. The energy per unit area reaching the remote sensor for each environmental feature (cottonwood and fir, or two bodies of water) is compared with the sensitivity (film, filter, and lens characteristics) of a given remote sensor to determine if the features would appear as different image tones, i.e. gray tones or colors, on the imagery produced by that sensor. The model output is image optical density contrast values for the specified features of interest (the model assumes a

feature is uniformly surrounded by a second terrain feature that is specified as the background).

Spatial component

17. The spatial component of the model uses the dimensions of an environmental feature, the sensor characteristics (lens focal length for photographic sensor systems), and the distance from the feature to the sensor to calculate the dimensions of the image of the feature as observed by the sensor. The image dimensions are compared with the spatial sensitivity of a given remote sensor to determine if the feature would appear as a discrete feature (on the basis of size only) on the imagery produced by that sensor at the specified altitude or distance from the features.

Overall concept

18. The overall concept of the model is, therefore, a means of evaluating a photographic remote sensing system for a particular problem by contrasting the energy content and dimensions of the images received by the sensor with the spectral and spatial sensitivities of the sensor. The following paragraphs discuss the technical content of the model in detail. The specific details concerning the computer program and the form of the various inputs to the model are presented in Appendix B.

Spectral Component of Model

Energy source

19. The sun is considered the primary energy source. The solar irradiance above the atmosphere as a function of wavelength is used in the model, as illustrated in Figure 3, to quantitatively

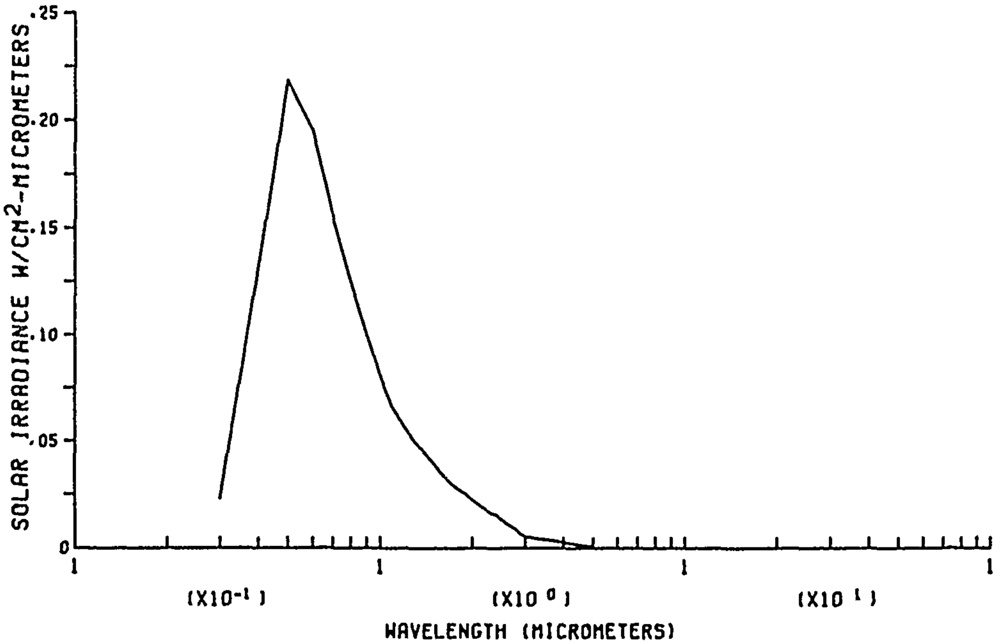

Figure 3. Solar irradiance above the atmosphere as used in the model

define the sun. Skylight, energy resulting from the scattering of sunlight by atmospheric constituents, is considered as a secondary source. The ratio of skylight to sunlight plus skylight as reported in Reference 19 and presented graphically in Figure 4 is used as the basis for computing the spectral distribution of skylight in the model. These data represent widely differing haze conditions that might be encountered on cloudless days. The precise method of employing the skylight-sunlight plus skylight ratio is discussed in the following paragraphs.

Factors affecting the transmission of radiation from the energy source to the terrain

20. Direct transmission through the atmosphere: To provide the model with the capability of predicting realistically the solar irradiance reaching the earth's surface, a capability had to be

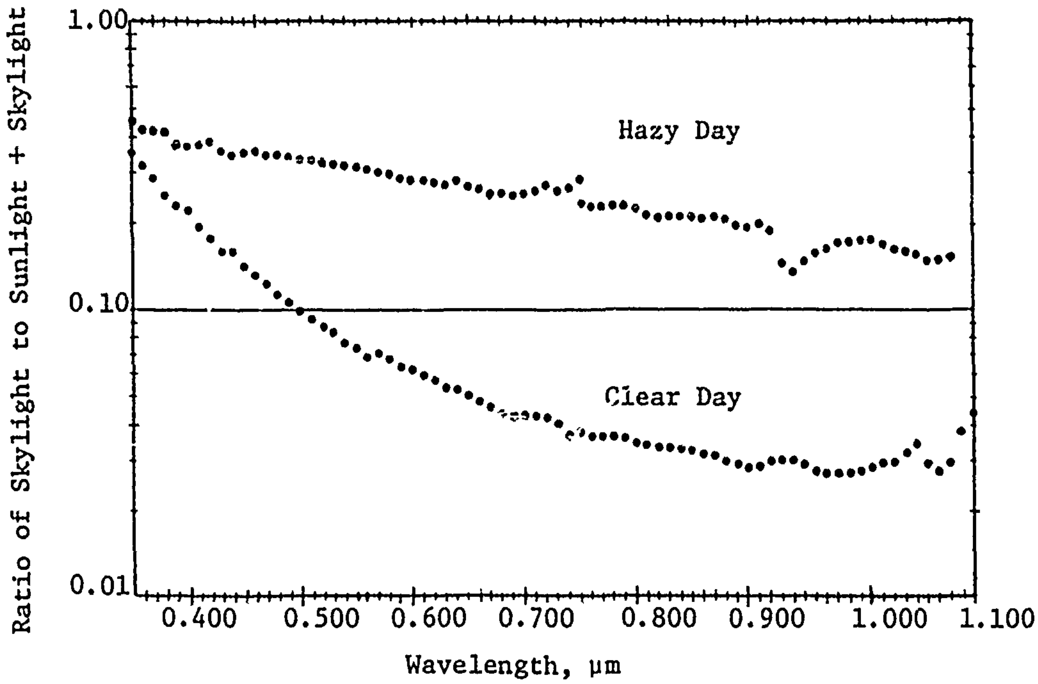

Figure 4. Ratio of skylight to sunlight plus skylight (Reference 19)

achieved for predicting total radiation transmitted through the atmosphere as a function of wavelength for a variety of atmospheric conditions and paths. This capability, of course, requires a set of mathematical relations that describe molecular and aerosol absorption and molecular and aerosol scattering, along with profiles of the basic gaseous and aerosol components for a variety of conditions.

21. A computerized model (LOWTRAN I) recently developed at the U. S. Air Force Cambridge Research Laboratories (Reference 20) was used to predict atmospheric transmission curves for the Photographic Systems Simulation Model. With LOWTRAN I, the total radiation transmitted directly through the atmosphere for the 0.25- to 28.5-μm wavelength region can be computed with a spectral resolution of 20 wave numbers (wave number is determined from the reciprocal of the wavelength expressed in centimetres). The wavelength region

encompassed by LOWTRAN I extends beyond the region required for modeling photographic sensor systems (0.3 to 1 μm). The resolution expressed in terms of wavelengths in this region is less than 0.002 μm, more than sufficient for accurate determination of the numerical quantities required for the simulation model. LOWTRAN I includes five geographic atmospheres: tropical, mid-latitude summer, mid-latitude winter, subarctic summer, and subarctic winter. Each atmosphere is defined by a profile of pressure, temperature, density, water vapor concentration, and ozone concentration as a function of altitude or height above sea level.

22. Two aerosol models are available to be run with the atmosphere models. The aerosol models describe "clear" and "hazy" atmospheric conditions corresponding to visibilities of 23 km and 5 km, respectively, at ground level. Together, the atmosphere and haze models provide the basic data for predicting radiation transmission through the atmosphere on geographic and seasonal bases for both good (clear) and poor (hazy) visibility conditions.

23. The atmosphere and haze models are constructed as series of parallel atmospheric layers, so LOWTRAN I can be used to calculate the radiation transmitted through the entire atmosphere or through only a portion thereof. In addition, transmission can be calculated for vertical, horizontal, or slant paths through the atmosphere. A detailed explanation of the mathematics used to account for the absorption and scattering phenomena is given in Reference 21.

24. For the purposes of this study, LOWTRAN I was used to predict radiation transmission through the atmosphere as a function of wavelength for the mid-latitude summer- and winter-modeled

atmospheres with both haze models and for solar zenith angles (slant paths) from 0 to 60 deg at increments of 10 deg. The result is 28 different transmission curves for use in predicting the solar energy reaching the terrain (the curves are presented in Reference 18). The consideration of solar zenith angle adds a degree of realism in that the effects of time of day, time of year, and latitude can be accounted for. Since the length of the path through the atmosphere increases with increasing zenith angle (angle from the vertical), the attenuation of EM energy is increased (transmission is decreased), and less solar energy reaches the terrain. The decrease in energy reaching the terrain can be very significant for large zenith angles (i.e. angles from the vertical greater than 30 deg).

25. An atmospheric transmission curve for mid-latitude summer, 23-km haze, and a zenith angle of 30 deg is presented in Figure 5. Within the remote sensing simulation model, curves such as this are multiplied (wavelength by wavelength) by the solar irradiance curve shown in Figure 3 to predict the solar energy reaching the terrain by direct transmission. A variety of curves defining the solar energy reaching the terrain by direct transmission are presented in Reference 18. Figure 6 presents a typical example of these curves.

26. <u>Geometric relations:</u> The curve in Figure 6 shows an example of the solar irradiance that reaches the terrain by direct transmission, but it does not present the actual irradiance that impinges on a given terrain surface. The actual flux per unit area (e.g. w/cm^2) is a function of the relative orientation of the sun and the terrain surface plus skylight. Thus, curves such as the one in Figure 6 must be modified by the factor $\cos\theta$ (where θ is the

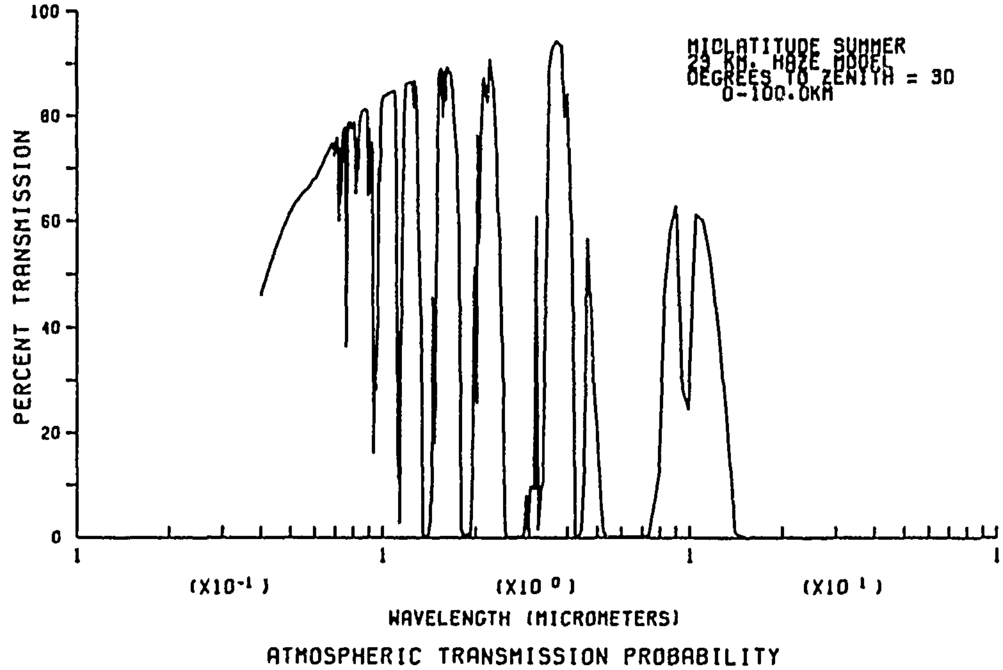

Figure 5. Atmospheric transmission curve for mid-latitude summer, 23-km haze condition and 30-deg solar zenith angle

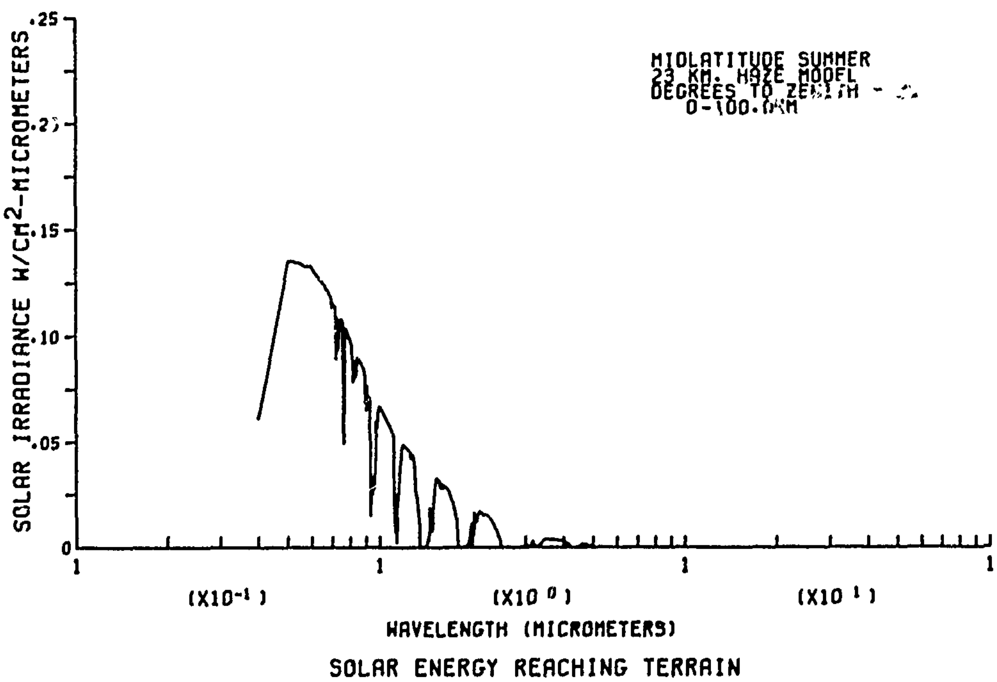

Figure 6. Example of solar irradiance that reaches the terrain by direct transmission through the atmosphere for mid-latitude summer, 23-km haze condition and 30-deg zenith angle

angle between the path of the impinging solar irradiance and the normal to the surface) to calculate the true irradiance incident (directly) on a given terrain surface. If the terrain is assumed to be perfectly horizontal (which is almost never the case), the angle θ becomes the value of the solar zenith angle. Unless otherwise specified, the model makes this assumption for the sake of simplicity.

27. Figure 7 shows the geometric relation among the solar zenith angle, solar azimuth, terrain surface slope, and the direction of maximum terrain surface slope (terrain slope azimuth). The solar and terrain slope azimuth are combined into a single parameter, the relative azimuth angle, for simplicity. The relative azimuth is the angular separation of the solar azimuth and terrain slope azimuth as illustrated in the figure. The interrelation of solar zenith, terrain slope, and the relative azimuth defines the effective sun angle which is the angle between the incoming solar energy and the normal to the terrain surface in the vertical plane defined by the solar azimuth. Figure 8 presents a graphical means of computing effective sun angle for combinations of solar zenith angle, terrain slope, and relative azimuth angle. The effective sun angle is obtained by adding the appropriate solar zenith angle to the value for the "effective slope angle" obtained for a given relative azimuth-terrain slope combination.

28. Skylight: In addition to the product of $\cos \theta$ and the solar energy reaching the terrain by direct transmission, skylight must also be considered to compute the total flux per unit area impinging on the terrain. The skylight energy (as a function of wavelength) reaching the terrain is computed using the ratio (R) of

Legend

ϕ= Solar zenith angle

ϕ_{eff}= Effective Sun angle

β= Maximum terrain slope

β_{eff}= Terrain slope in plane of solar azimuth

θ_1= Azimuth of maximum terrain slope from some reference (North)

θ_2= Azimuth of Sun from some reference (North)

To compute ϕ_{eff}

$\Delta\theta = |\theta_2 - \theta_1|$ = relative azimuth angle

$\beta_{eff} = \beta \cos(\Delta\theta)$

if

$\Delta\theta > 90°$

$\phi_{eff} = \phi + \beta_{eff}$

if

$\Delta\theta < 90°$

$\phi_{eff} = \phi - \beta_{eff}$

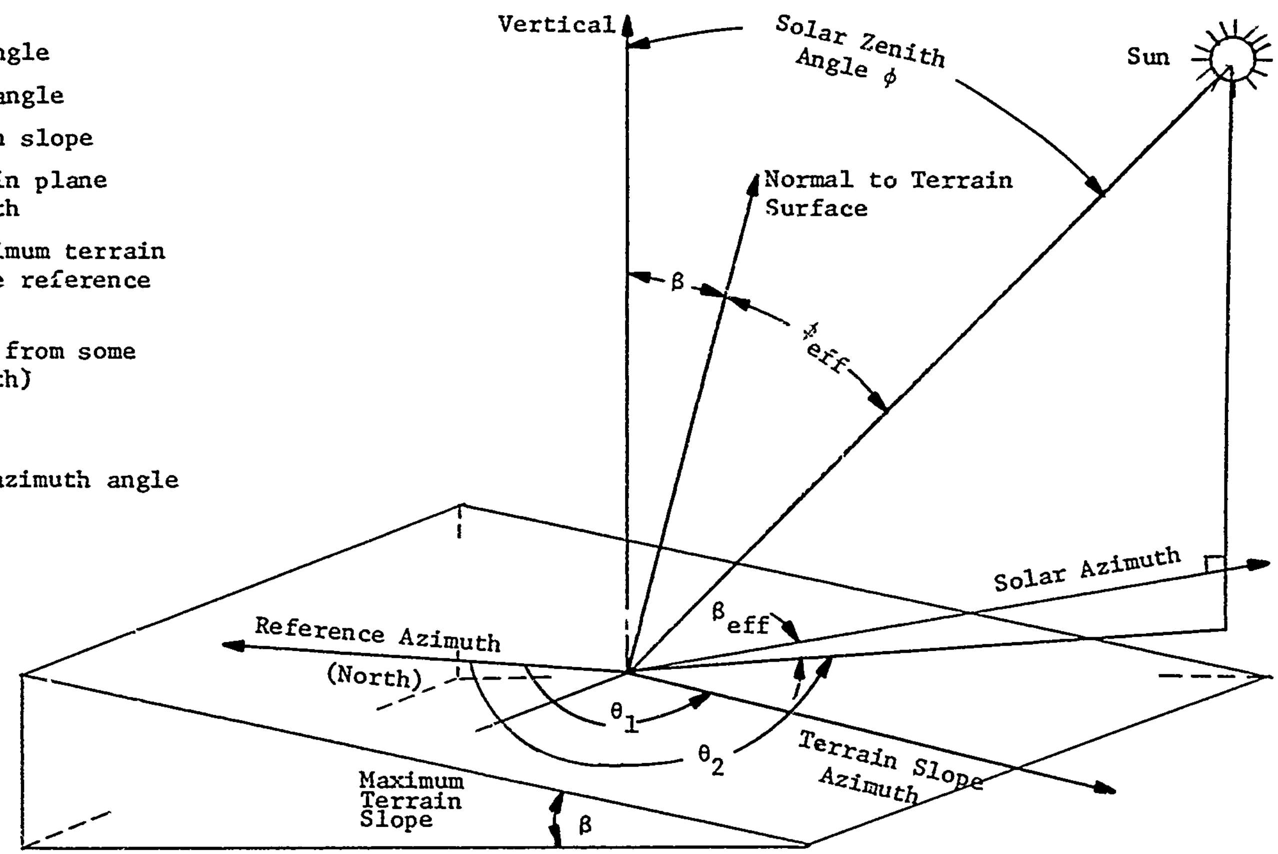

Figure 7. Geometric relation between solar zenith angle, solar azimuth, terrain surface slope, and terrain slope azimuth

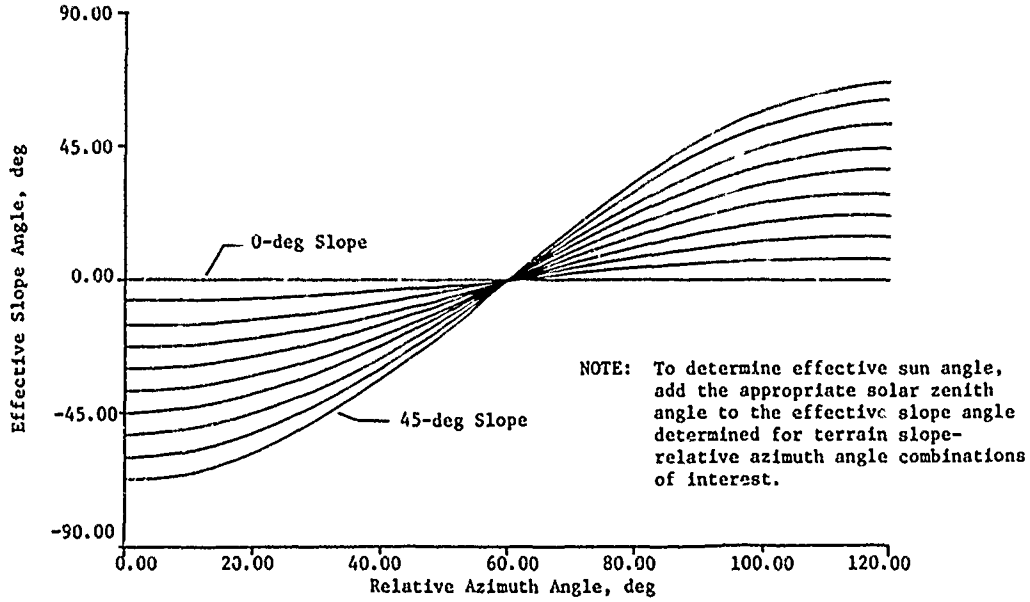

Figure 8. Graphical means to compute effective sun angle

skylight to sunlight plus skylight in the following manner.

29. At any given wavelength, λ, the solar energy reaching the terrain by direct transmission, SUN_λ, is known (i.e. calculated by the procedures previously described); however, the skylight, SKY_λ, is unknown. The ratio, R_λ, can be used to develop a simple expression for SKY_λ as follows:

$$R_\lambda = \frac{SKY_\lambda}{SUN_\lambda + SKY_\lambda} \tag{1}$$

then

$$R_\lambda(SUN_\lambda + SKY_\lambda) = SKY_\lambda$$

and

$$R_\lambda SUN_\lambda + R_\lambda SKY_\lambda = SKY_\lambda$$

which simplifies to

$$R_\lambda SUN_\lambda = (1 - R_\lambda)SKY_\lambda$$

and

$$\frac{R_\lambda SUN_\lambda}{(1 - R_\lambda)} = SKY_\lambda \qquad (2)$$

which can be used to compute skylight energy at any wavelength with the known values of R_λ and SUN_λ at that wavelength. This can be expanded to a single expression for computing the total EM energy reaching the terrain as follows:

$$Total_\lambda = SUN_\lambda + \frac{R_\lambda}{1 - R_\lambda} SUN_\lambda = \left(1 + \frac{R_\lambda}{1 - R_\lambda}\right) SUN_\lambda \qquad (3)$$

which is the relation used in the model. The curve for R_λ designated "HAZY" in Figure 4 is used in conjunction with the 5-km haze model (in LOWTRAN), and the R_λ curve designated as "CLEAR" is used with the LOWTRAN 23-km haze model.

Interaction of EM
radiation and the terrain

30. The Photographic Systems Simulation Model assumes that terrain features are essentially diffuse reflectors of EM radiation in the visible and near-IR spectral regions. This assumption is a limiting factor for the model in that many terrain features may reflect both specularly and diffusely, depending on their position with respect to the radiation source. The diffuse reflectance assumption was made, however, to limit the complexity of the necessary input data for the model and to provide for simplicity in the mathematics.

31. The model uses spectral reflectance (diffuse) curves for terrain features to define the interaction of the solar irradiance

impinging on the terrain. Figure 9 is an example of a reflectance curve for a mature cottonwood tree. These curves define the percentage of incident irradiance reflected as a function of wavelength for the visible and near-IR portions of the EM spectrum. By multiplying a curve for a terrain feature (wavelength by wavelength) by a curve for that portion of the solar irradiance reaching the terrain, the irradiance reflected from the feature is obtained.

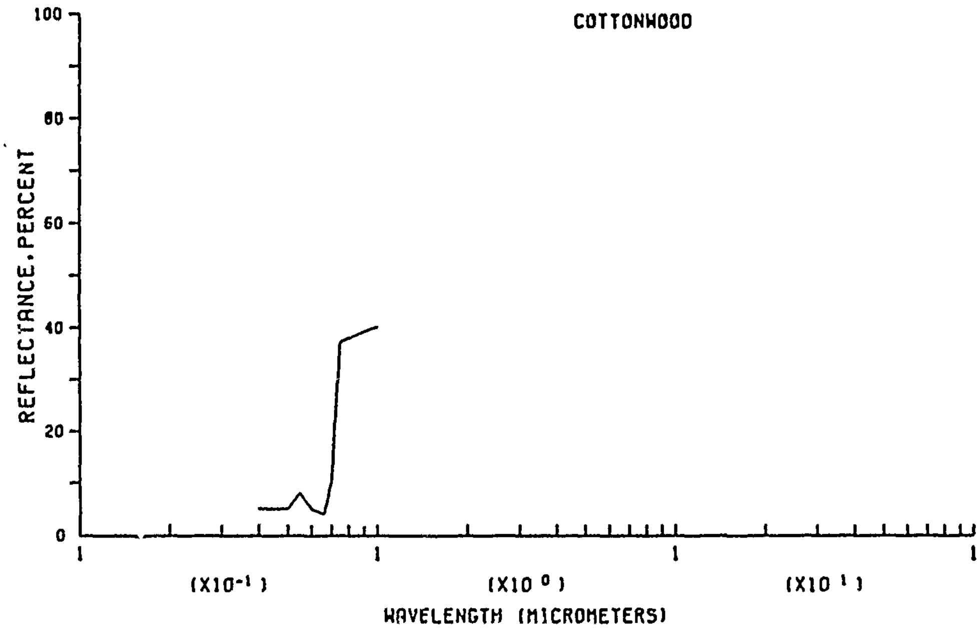

Figure 9. Example of spectral reflectance curve for a mature cottonwood tree

<u>Factors affecting the transmission of EM radiation from the terrain to an airborne remote sensor</u>

32. <u>Direct transmission through the atmosphere:</u> To provide the capability of predicting the amount of EM radiation that reaches a remote sensor at a given altitude, radiation transmission curves for various portions of the atmosphere had to be predicted. LOWTRAN I

was used to predict transmission for the following common altitudes for remote sensing missions:

a. Ground to 1.5 km

b. Ground to 3.0 km

c. Ground to 6.0 km

d. Ground to 15.0 km

These predictions were made with the mid-latitude summer and winter atmosphere models and both haze models. Only the 0-deg zenith angle (vertical path) was considered, since the model assumes that the sensor is located directly above the environmental features of interest. The predicted curves available for use in the model are presented in Reference 18; Figure 10 is a typical example.

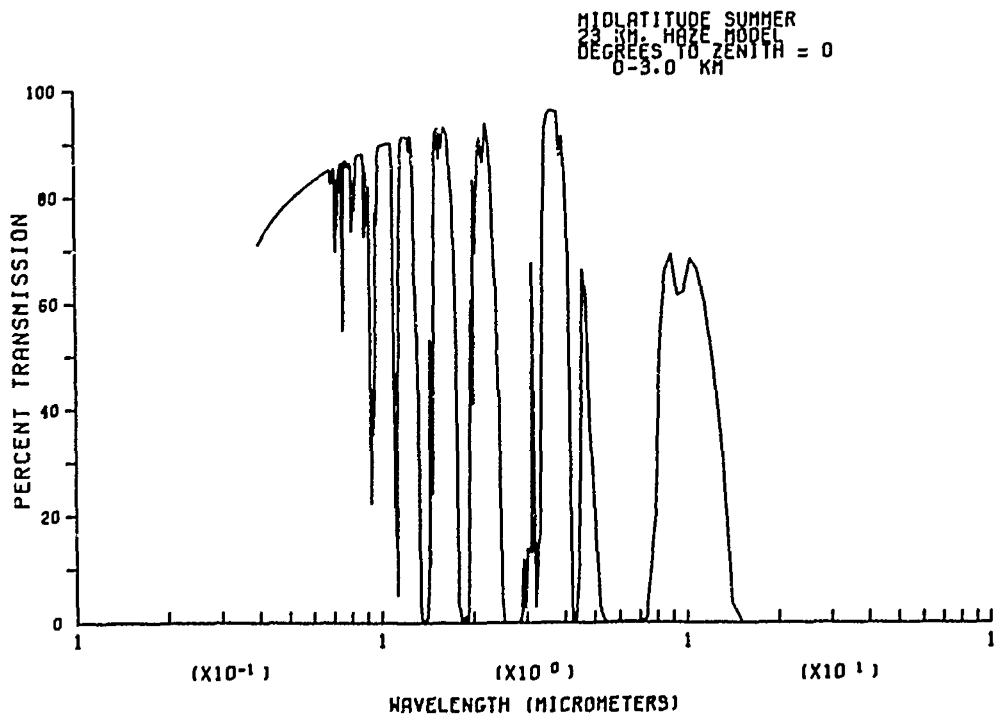

Figure 10. Typical example of atmospheric transmission curve for transmission from the ground to the sensor at a specified altitude

33. The total irradiance (as a function of wavelength) reaching a given altitude is calculated by multiplying, wavelength by wavelength, the irradiance reflected from a specific terrain feature by the appropriate transmission curve (e.g. Figure 10) and adding backscatter energy. Since backscatter is a diffuse energy source in the atmosphere like skylight, it is present in the field of view of the camera and must be added to the energy transmitted from the terrain to the camera to calculate the total energy received at the camera. When considering the energy received at the camera from two features (i.e. to calculate the contrast that will result on an image) the backscatter energy is added to the computed energy reaching the sensor for each feature individually. In this manner backscatter acts as a contrast attenuator within the model as it does in nature. The following is a brief description of backscatter and how it is handled in the model.

34. Backscatter: As solar energy is transmitted through the atmosphere, a portion is scattered by the molecular and aerosol constituents of the atmosphere. The scattered energy is redistributed in the atmosphere and becomes a somewhat diffuse energy source. An observer positioned on the terrain surface and looking up would perceive the scattered energy as skylight (see paragraph 19); whereas, an observer looking down from a position at some altitude above the earth's surface would perceive the scattered energy as backscatter. The quantity of backscatter or skylight perceived is a function of atmospheric conditions and the altitude (i.e. position within the atmosphere) of the observer. A means to compute skylight was discussed in paragraphs 19 to 29. The following paragraphs

present the simple, but rational, procedure used in the Photographic Systems Simulation Model to compute backscatter.

35. Skylight and backscatter result from the same phenomena, molecular and aerosol scattering of solar irradiance passing through the atmosphere. Because of their similar origin, the spectral character (i.e. the relative amplitude as a function of wavelength) of skylight and backscatter are considered to be the same. This simplifying assumption allows the shape of the curve of the skylight energy at the ground versus wavelength, as computed in the model (see paragraph 29), to be used to represent the spectral character of backscatter. The only remaining information needed is the relative amplitude of the backscatter with respect to the skylight.

36. Figures 11 and 12 show the relative amplitudes of skylight and backscatter as a function of altitude for clear (23-km visibility) and hazy (approximately 5-km visibility), respectively. These curves were adapted from Reference 22 and serve as the major tool for defining the relative amplitudes of skylight and backscatter. The original forms of the curves in Figures 11 and 12 were computed for a wavelength of 0.55 μm and for a homogeneous atmosphere. Use of these curves requires that some credibility be given to their applicability to the entire 0.40- to 0.93-μm wavelength band. Plates 1 to 5 present curves of the total atmospheric scattering coefficient (molecular plus aerosol scattering) as a function of altitude and atmospheric haze (from Reference 21) for wavelengths of 0.488, 0.515, 0.633, 0.694, and 0.860 μm, respectively. Close examination of these curves showed that they all had approximately the same shape. In addition, the relations of the change in the scattering coefficient

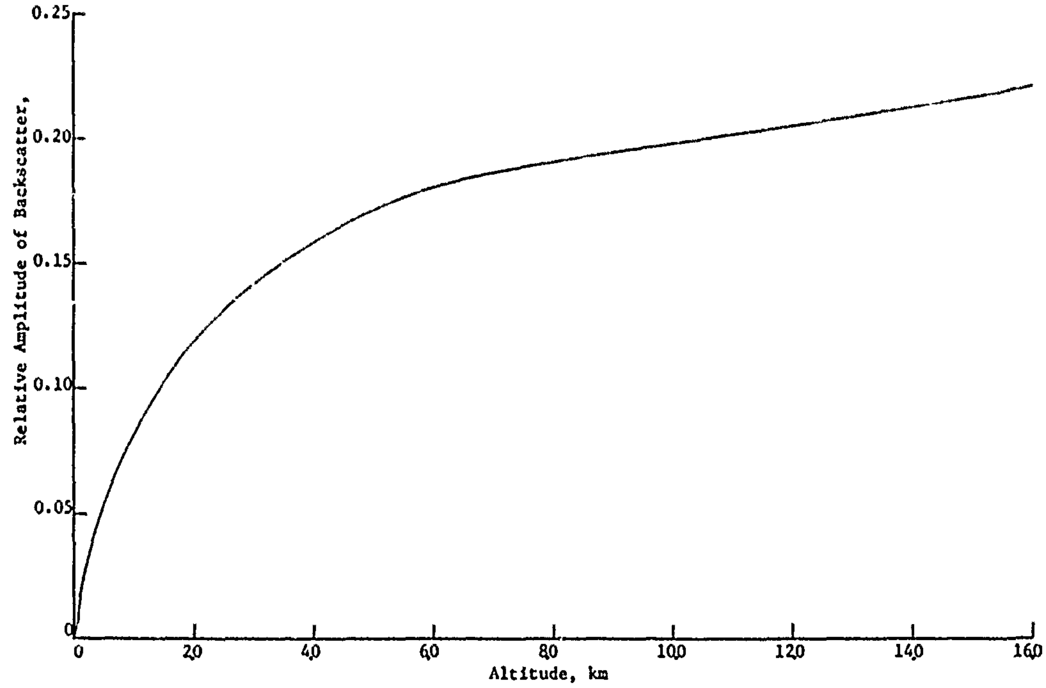

Figure 11. Relative amplitudes of skylight at terrain surface and backscatter as a function of altitude for 23-km haze condition (Reference 22)

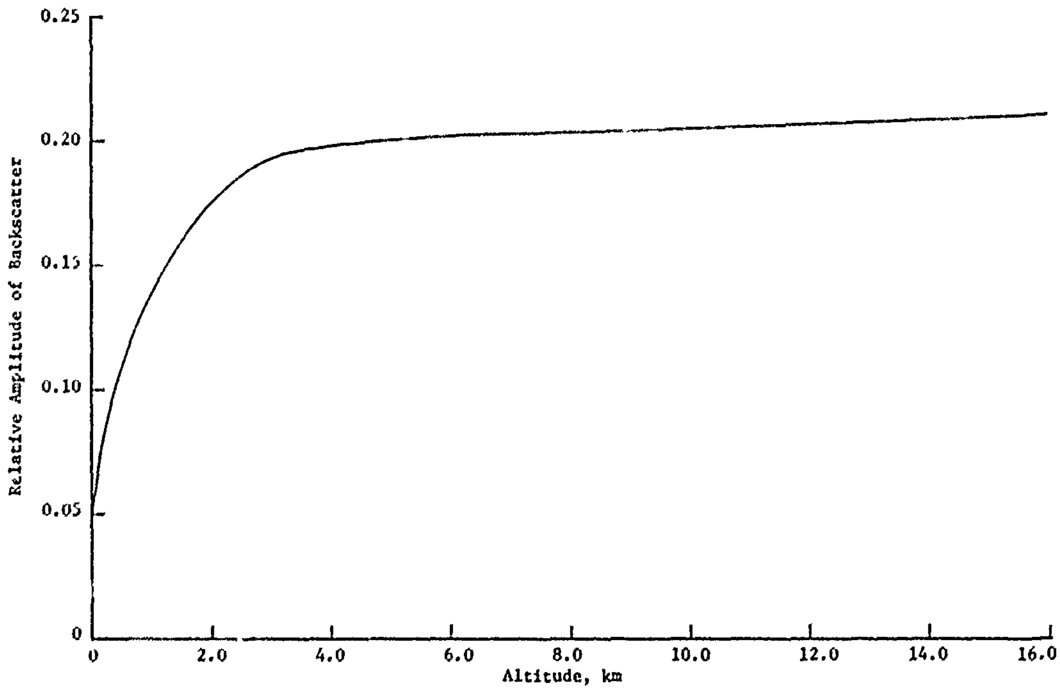

Figure 12. Relative amplitudes of skylight at terrain surface and backscatter as a function of altitude for 5-km haze condition (Reference 22)

with respect to a change in altitude was essentially the same for all of the curves. This indicated that if the curves were all normalized so that the scattering coefficient value was 1.0 at the terrain, the normalized relations between the scattering coefficient and altitude would be the same for all of the wavelengths.

37. Based on the similarities among the curves in Plates 1 to 5, it was assumed that the curves in Figures 11 and 12 were representative of all wavelengths in the 0.40- to 0.93-μm band for the purpose of defining the relative amplitude of backscatter with respect to skylight. Thus, the spectral character of skylight and backscatter are assumed to be the same, only their relative amplitudes differ.

38. The necessary tools are available for computing backscatter energy as a function of wavelength for specific altitude and haze combinations. The specific procedure used is as follows: The starting point is the previously computed skylight-wavelength curve for a given haze condition (23-km or 5-km visibility). The appropriate value for the relative amplitude of backscatter is then selected for the appropriate haze and altitude combination from Figure 11 or 12. The value selected from Figure 11 or 12 represents the percentage of the skylight energy reaching the terrain that is equivalent to the backscatter energy for the haze-altitude combination selected. The amplitude of the skylight curve (for each wavelength) is multiplied by the relative amplitude value to compute the backscatter energy as a function of wavelength. Thus, the computed backscatter is simply a proportion of the skylight energy reaching the terrain with the same spectral character.

39. Sensor components and their descriptors: In this portion of the model, the calculated irradiance (as a function of wavelength) reaching a specified photographic sensor system interacts with the components of the system to predict image optical density contrast for the feature and background (or other feature). The major system components considered are the lens, the filter, and the film.

40. The parameters used to describe the camera lens are the transmission for the lens as a function of wavelength (the 0.4- to 1.00-μm wavelength band) and the F-stop setting of the lens. Figure 13 presents an example of a lens transmission curve. The filter is described by a transmission curve that defines the percentage (as

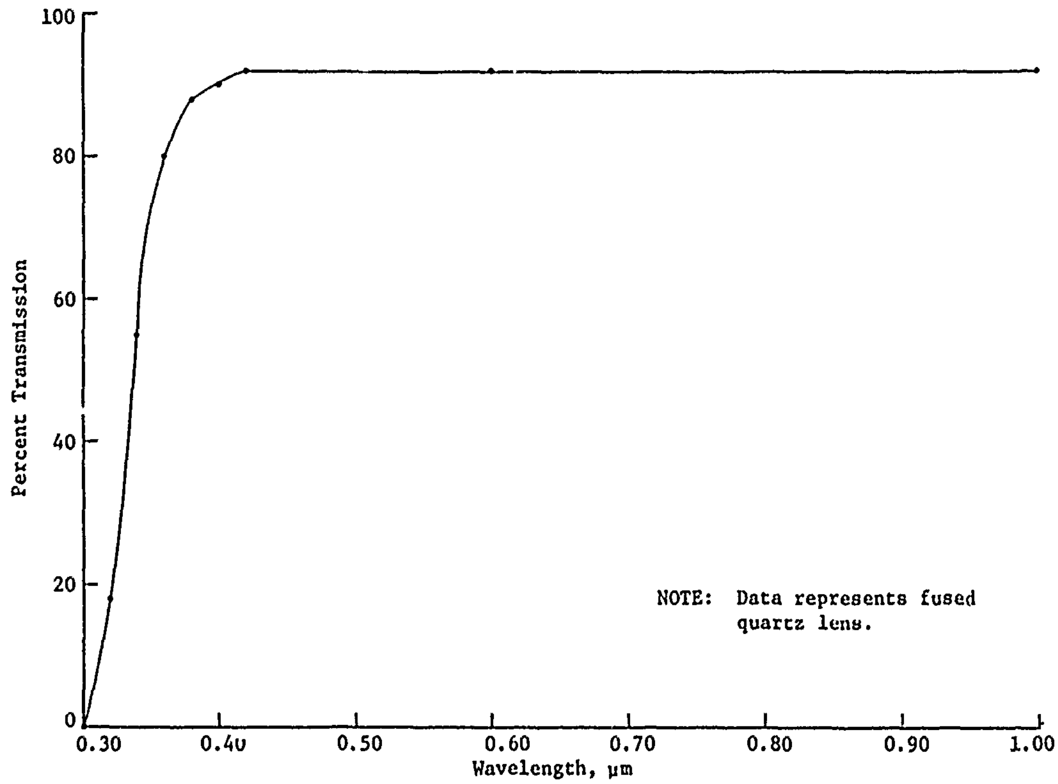

Figure 13. Example of lens transmission curve

a function of wavelength) of the impinging EM radiation that is transmitted by the filter. The most commonly used filters (and those included in the model) are the Wratten Nos. 12, 47B, 58, 25A, 87C, and 89B (Reference 23). Figure 14 presents a transmission curve for a Wratten No. 12 filter (Reference 23).

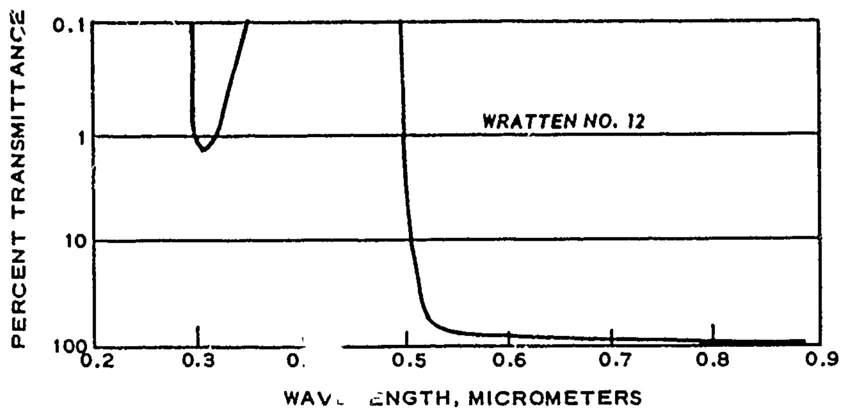

Figure 14. Transmission curve for Wratten No. 12 filter (Reference 23)

41. The films are described by their spectral sensitivity curves and gamma (λ) values. The spectral sensitivity curve defines the sensitivity of the film as a function of wavelength, as illustrated in Figure 15 for Kodak Infrared Aerographic Film No. 2424

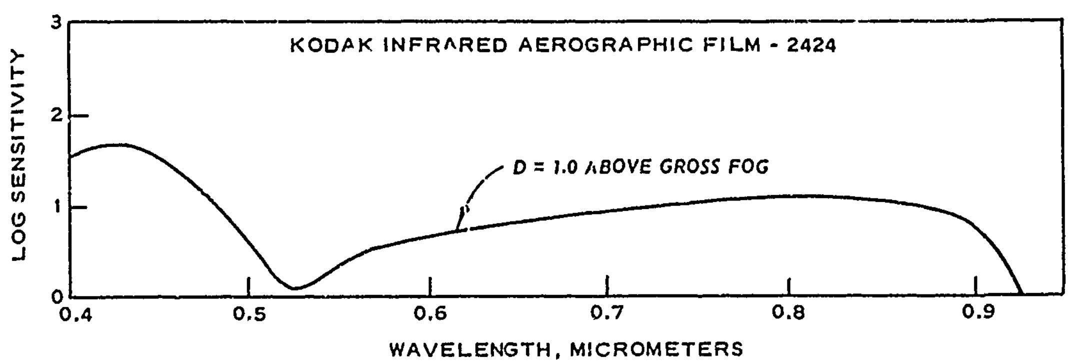

Figure 15. Spectral sensitivity curve for Kodak Infrared Aerographic Film No. 2424 (Reference 24)

(Reference 24). In the figure the ordinate is the logarithm of sensitivity (the reciprocal of the exposure in ergs cm^{-2} required to produce an optical density of 1.0 above base fog) and the abscissa is wavelength. Curves such as the one shown in Figure 15 are published by the film manufacturers.

42. The film gamma value is the slope of the linear portion of the curve relating optical density to the logarithm of exposure for the film (commonly referred to as the D log E curve). Exposure is a measure of the energy impinging on the film. D log E curves and their associated γ values are published for available films by the manufacturers. Since the γ value for a specific film varies with film processing techniques, choice of γ values for use in the model must be based on the film processing techniques available to the user.

43. Computation procedure: The procedure in the model used to compute the expected image optical density contrast for a specified feature and background and a specified film-filter combination is as follows:

a. The exposure time (t) in seconds required to reach an optical density of 1.0 above base fog is computed indivually for the feature and the background by

$$t = 4 \; (\text{F-stop})^2 \frac{1}{10^7 \int_{\lambda_1}^{\lambda_2} H_\lambda T_\lambda L_\lambda S_\lambda d\lambda} \qquad (4)$$

where

F-stop = the F-stop setting of the lens (assumed to be 5.6 unless otherwise specified)

$\lambda_1\lambda_2$ = wavelength limits of spectral sensitivity of the film-filter combination in μm

H_λ = irradiance, as a function of wavelength, reaching the sensor in watts cm^{-2} μm-1

T_λ = transmittance, as a function of wavelength, for the filter (1.0 for all wavelengths if no filter is used)

L_λ = transmittance, as a function of wavelength, for the lens

S_λ = sensitivity of the film as a function of wavelength, ergs cm^{-2}

b. The computed exposure time values for the feature (t_F) and background (t_B) are compared, and an optical density value of 1.0 is assigned to the one (feature or background) having the largest t value. For example, if $t_F > t_B$ the feature is assigned an optical density value of 1.0.

c. The optical density contrast ($D_F - D_B$) for the feature and background is computed by

$$D_F - D_B = \gamma \log \frac{t_B}{t_F} \qquad (5)$$

where

D_F = optical density of the feature

D_B = optical density of the background

γ = film gamma

44. Special consideration for color films: Since color films have three emulsions, each having a unique spectral sensitivity curve, optical density contrast values for a specified feature and

background are computed individually for each emulsion. The γ values for the films most commonly evaluated in the execution of the model (unless otherwise specified) are listed in Table 1. The γ values given in Table 1 represent average values obtained with a Versamat Processor and Number 855 chemicals (Reference 24).

45. Output of model: Figure 16 presents a representative output of the Photographic Systems Simulation Model. The legend in

FILMN	FILTER	FEATURE EXPT FOR D=1.0 (SEC)	BACKGROUND EXPT FOR D=1.0 (SEC)	FEATURE DENSITY (DF)	BACKGROUND DENSITY (DB)	DF-DB
2402	12	0.003390	0.001928	1.000000	1.404593	0.404593
2403	12	0.001170	0.000622	1.000000	1.356313	0.356313
2402	47B	0.033594	0.025463	1.000000	1.198597	0.198597
2403	47B	0.014355	0.011038	1.000000	1.148355	0.148355
2402	58	0.018516	0.012402	1.000000	1.287157	0.287157
2403	58	0.009077	0.006073	1.000000	1.226905	0.226905
2402	25A	0.006357	0.003210	1.000000	1.489718	0.489718
2403	25A	0.001855	0.000885	1.000000	1.417579	0.417579
2402	3	0.002653	0.001543	1.000000	1.388644	0.388644
2403	3	0.000973	0.000531	1.000000	1.342060	0.342060
2448C	3	0.006801	0.003546	1.000000	1.565799	0.565799
2448Y	3	0.020895	0.013152	1.000000	1.402102	0.402102
2448M	3	0.007187	0.004900	1.000000	1.332574	0.332574
2443C	3	0.006833	0.005622	1.000000	1.127092	0.127092
2443Y	3	0.003363	0.002233	1.000000	1.266872	0.266872
2443M	3	0.004301	0.002199	1.000000	1.437023	0.437023
2443C	12	0.007936	0.006800	1.000000	1.100670	0.100670
2443Y	12	0.005604	0.003808	1.000000	1.251794	0.251794
2443M	12	0.004639	0.002353	1.000000	1.442131	0.442131
2424	12	0.000776	0.000717	1.000000	1.069254	0.069254
2424	25A	0.000804	0.000753	1.000000	1.056171	0.056171
2424	87C	0.003701	0.003984	1.063936	1.000000	0.063936
2424	89B	0.000932	0.000990	1.053038	1.000000	0.053038

LEGEND

FEATURE PONDEROSA PINE HEALTHY
BACKGROUND PONDEROSA PINE DISEASED
ATMOSPHERE MIDLATITUDE SUMMER HAZE-5 KM
ZENITH ANGLE 30 DEG.
DISTANCE TO SENSOR 1.50 KM

Figure 16. Representative output of Photographic Systems Simulation Model

the lower left-hand corner documents the feature, background, atmospheric conditions, solar zenith angle, and sensor altitude. The first two columns specify the various film-filter combinations used in the execution of the model. The third and fourth columns present the calculated exposure times (t) necessary to reach an optical density of 1.0 above base fog for the feature and the background, respectively, for the various film-filter combinations. The fifth and sixth columns present the predicted optical density data for the feature and the background, respectively. The seventh column presents the optical density contrast values for the feature and the background.

46. Perhaps the most important information on the output printout is that presented in the seventh column, the optical density contrast for the feature and the background. By scanning this column the investigator can determine which, if any, of the film-filter combinations considered will provide an optical density contrast adequate to allow discrimination between the feature and the background, and those film-filter combinations best suited for discriminating between the feature and the background on a spectral or tonal basis. The adequacy of a film-filter combination is determined by comparing the predicted optical density contrast (D_F - D_B) to a threshold value that defines the minimum contrast necessary for discrimination. The threshold value varies with the means of examining the imagery. The human eye, for example, can reliably discriminate between 10 to 15 gray tone levels. Thus, an optical density contrast of 0.30 to 0.20 could be used as a threshold value for the human eye. These values are obtained by dividing the gray tone levels (10 and 15) by the

range of possible optical density values (0.0 to 3.0). The film-filter combinations having the greatest $D_F - D_B$ values (and therefore the greatest tonal contrast) are the best for the job (given the conditions represented by the various inputs to the model).

Spatial Component of Model

47. The spatial component of the Photographic Systems Simulation Model compares the minimum dimension of the image of the feature with the spatial sensitivity of the film in order to determine whether or not the feature can be resolved on the film. The relations presented in paragraph 5, Appendix B, Reference 18, are used in the model to calculate the minimum dimensions and area of the image of the feature for specified lens focal length and sensor-to-feature distances. The minimum dimensions and area of the calculated image are compared with the diameter and area of the smallest spot (pixel) that the film can resolve, as calculated from the line pairs per millimeter (lpm, see paragraphs 17-20, Appendix A, Reference 18) values published by the film manufacturer, as follows:

a. The published film lpm value for a target contrast ratio of 1.6:1 is obtained from the manufacturer. The lpm values are obtained by visual examination of test photographs.

b. The pixel radius (r_p) is calculated from the relation

$$r_p = \frac{0.5}{\text{lpm}} \qquad (6)$$

c. The pixel diameter (d_p) is calculated from the relation

$$d_p = 2r_p$$

d. The pixel area (A_p) is calculated from the relation

$$A_p = \pi(r_p)^2 \qquad (7)$$

The model then calculates the ratio of the minimum dimension of the image to the pixel diameter, and the area of the image to the area of the pixel. These ratios are used to assess the ability of the film to resolve the feature spatially for the specified distance and lens focal length. If both ratios are greater than 1.0, the feature has a high probability of appearing on the film as a distinct image (assuming that there is sufficient contrast between the feature and its surroundings). Figure 17 represents curves defining resolvable

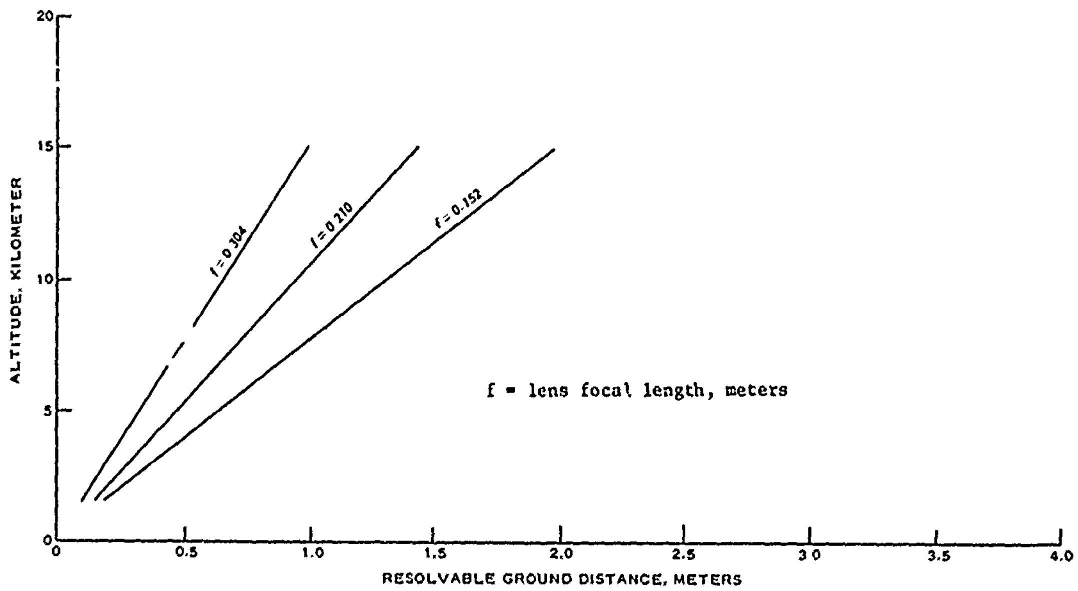

Figure 17. Resolvable ground distance as a function of altitude for Kodak Plus-X Aerographic Film No. 2402

ground distance as a function of altitude for Kodak Plus-X Aerographic film 2402 as computed using the spatial component of the model.

Model Limitations

48. The remote sensing simulation model discussed in the previous paragraphs is a first attempt at simulating the interactions of the terrain and remote sensors on a systems basis. To arrive at a usable product within the framework of this study, many simplifying assumptions were made. As is usually the case, the model can be improved considerably by additional sophistication. For example, there is a great need to improve the understanding of the basic phenomena of the reflection of EM radiation from terrain materials. To achieve the necessary or desired understanding would possibly require a major basic research effort. This was not feasible in the framework of this study. In the following paragraphs, an effort will be made to point out the most obvious weaknesses of the present form of the model, and to suggest possible avenues for improvement.

Atmospheric considerations

49. LOWTRAN I allows the calculation of curves for radiation directly transmitted through the atmosphere for standard summer and winter clear (23-km visibility) and hazy (5-km visibility) conditions. These curves represent good and poor conditions for a sunny day; thus, only the end members are included. LOWTRAN I does provide for inserting atmospheric data for any conditions as measured; however, acquisition of the complete set of data required (again only for sunny days) is an extremely difficult task. The ability to predict transmission curves for a larger variety of atmospheric conditions, including the effects of cloud cover (partial or full), would significantly increase the capability of the remote sensing simulation

model. Also, it would be desirable to simulate intermediate haze conditions indicative of urban and industrial areas.

Terrain considerations

50. In the present form of the model, terrain materials are assumed to be diffuse reflectors. This is obviously not always the case. The ability to include both the specular and diffuse components of reflected radiation would broaden the scope and realism of the model. However, the advantages of keeping this aspect of the model simple are assumed to outweigh the increased accuracy, as modeling the reflectance geometry of environmental features would complicate the model considerably.

51. Presently, all terrain features are assumed to have uniform diffuse surfaces. This assumption limits the accuracy with which the radiance of the terrain can be described. A technique for including the effects of the complex reflectance geometry of some terrain features (especially vegetation) would enchance the capability of the model. In addition to reflectance geometry, the effects of shadows on the resulting image should also be taken into account.

52. The spatial component of the model uses only the minimum dimensions and the area of a feature to determine its ability to be resolved spatially. The assumption is made that the feature is surrounded by an infinitely large background. Added realism could be obtained by expanding this component of the model to include the actual shape of the feature and the surrounding features in the analysis for spatial discrimination. In addition, the assumptions made for calculating the diameter and area of a pixel are based on limited data. Additional analysis in this area to solidify these

relations would contribute to the overall authenticity of the model.

Sensor considerations

53. The analysis of the interaction of EM radiation and the remote sensor relies quite heavily on published spectral sensitivity curves for the different films. It must be realized that these curves are only representative or average values for the respective films. Considerable variation may occur between the published data and the actual values measured for a particular batch of film. Since the model is basically used to compare the relative capabilities of the various films, this may not be of serious consequence. However, the published data cannot be reliably used for predicting discrete values of film optical density resulting from a given exposure. In addition to the variance in the published curves, additional variance may occur because of the inconsistences in film processing techniques (i.e. within a single film processing technique).

54. Another consideration is the resolution of the lens and the depth of focus. Most lenses are more precise when the aperture is reduced slightly. Thus, the lens should not be used at very low F-stop settings, unless necessary for proper film exposure. The depth of focus and the distance from the sensor to the terrain determine the depth of field or the range of distances within which objects are imaged within the depth of focus of the lens. Since aerial cameras are normally focused at infinity, the depth of field defines the altitude at which the sensor can be flown to ensure that the camera will remain in focus. The greater the F-stop setting used, the greater will be the depth of focus. Thus, higher F-stop settings are advantageous for increasing the depth of field. This is

not a serious problem, however, except for low-altitude photography missions.

55. The spatial sensitivity of a film can be effectively reduced in significant proportions by image motion. The usual means for combating image motion is using short exposure times; however, this is not always possible. A routine for assessing the degradation of spatial sensitivity caused by image motion would be a significant improvement to the model for evaluating photographic systems used under conditions where fast shutter speeds or image motion compensation devices cannot be applied. This routine would become a part of the spatial component of the model.

Summary

56. In the preceding paragraphs a substantial number of limitations of and desirable additions to the simulation model are discussed. Indeed, it would be desirable to add all of the suggested improvements; however, there is another aspect to be considered. With each new capability and with each expansion in the present capabilities comes an increase in the necessary inputs to the model. Thus, the model could become very cumbersome, if the additions are not made carefully. There are many trade-offs to be considered in this process, and the benefits to be derived from an addition must be carefully weighed against the price of obtaining those benefits.

PART III: SIMULATION OF THERMAL IR SENSOR SYSTEMS

Introduction

57. A capability to simulate the performance of thermal IR sensor systems, in the form of two computer models similar in makeup but differing in output format, was developed to provide an analytical means for quickly and easily evaluating and comparing such systems for specific data acquisition jobs and for optimization of mission profiles for those jobs. The computer models allow for the systematic control of the major variables that affect the character of thermal IR imagery, including EM radiation sources, atmospheric attenuation, time of day, season, latitude, sensor altitude, and sensor characteristics. The models in their present form are capable of handling thermal IR sensor systems that operate in the 3.0- to 14.0-μm wavelength band. These systems comprise those most commonly available to both the private and Government sectors.

58. The basic concept of the models is an organized and quantitative means for evaluating thermal IR systems for particular data acquisition jobs by contrasting the magnitude and spectral content of energy received by the sensor system with the performance characteristics of the sensor system. The ability to quantitatively predict performance provides the capabilities necessary to quantitatively plan missions for specified jobs.

59. In the following paragraphs the basic analytical procedures used in the models are presented and discussed, followed by presentation of the individual capabilities (i.e. the form of the model outputs) of the individual model forms.

Analytical Procedures for Simulation

60. The basic analytical framework of the computer models for simulating thermal IR system performance (essentially identical for both model forms) is outlined schematically in Figure 18. The models

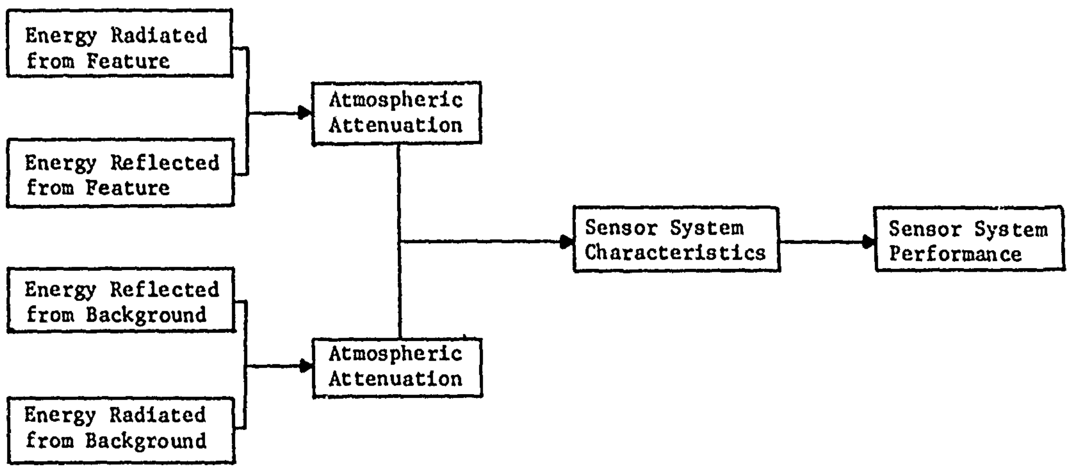

Figure 18. Schematic of Thermal IR Systems Simulation Models

have two basic components, the first concerning the calculation of the EM energy reaching the sensor system at some prescribed altitude, and the second concerning the interaction of the energy with the sensor system. The following paragraphs discuss the details of these model components. Specific details concerning the computer programs are presented in Appendixes C and D.

Energy reaching the sensor

61. Computation of the EM energy as a function of wavelength reaching a sensor at an altitude, R , is accomplished in three steps: computation of energy radiated from the terrain, computation of energy reflected from the terrain, and computation of the total energy reaching the sensor. The following paragraphs discuss these steps in detail.

62. Energy radiated from the terrain: The EM energy (radiant emittance) as a function of wavelength radiated from terrain materials is computed using the following version of Planck's Law:

$$W_\lambda = \frac{\varepsilon_\lambda C_1 \lambda^{-5}}{\left[e^{(C_2/\lambda T)} - 1\right]} \tag{8}$$

where

W_λ = radiant emittance at wavelength λ (W cm^{-2})

ε_λ = emissivity of terrain materials at wavelength λ

C_1 = constant (3.74×10^4 W μm^4 cm^{-2})

e = base to natural logarithm

C_2 = constant (14,388 μm K)

T = absolute temperature of terrain materials (K)

63. In the execution of the models, values for W_λ are computed at wavelength intervals equivalent to 50 cm^{-1} wave number (where wave number is defined by the relation 10^{-4} times wavelength in micrometers and expressed in units of cm^{-1}) for a feature and the background (the feature is assumed to be uniformly surrounded by the background) over the wavelength band of interest. The feature and the background are defined by their respective temperatures and emissivities. Emissivity may be considered a constant over a given wavelength band or a variable with wavelength. By specifying λ bounds, any portion of the 3.0- to 14.0-μm wavelength band can be isolated for individual consideration.

64. Energy reflected from the terrain: The sun is considered the basic source of EM radiation reflected from the terrain surface. The curve in Figure 3, which shows the solar irradiance as a function of wavelength above the earth's atmosphere, is used in the model to

define the sun. The amount of solar energy that reaches the terrain surface is computed (as in the Photographic Systems Simulation Model) by using an atmospheric transmission curve that, for a specified combination of season, haze, and solar zenith angle, defines the percentage of incident EM energy that is transmitted directly through the atmosphere to the terrain surface (i.e. as a function of wavelength). The atmospheric transmission curves are computed with the model LOWTRAN I as previously described in the discussion of the Photographic Systems Simulation Model (see Part II). The atmospheric transmission curves currently on file in the computer for use in execution of the Thermal TR Systems Simulation Models are the same as those used for the Photographic Systems Simulation Model and are presented in Reference 18.

65. Combining the solar irradiance curve (Figure 3) and a selected atmospheric transmission curve (such as that presented in Figure 5 on a wavelength-by-wavelength basis results in computation of the solar energy reaching the terrain surface. The value of the energy reaching the terrain surface is modified by the cosine of the solar zenith angle (or the effective sun angle) if slope, zenith, and solar azimuth are considered as was discussed previously to account for the effect of the angular relation between the impinging solar energy and the terrain surface. This correction is considered to be a constant for all wavelengths.

66. The energy as a function of wavelength reflected from the terrain is computed by combining, wavelength by wavelength, the values representing the solar energy impinging on the terrain and the values for the spectral reflectance of the terrain materials of

interest (feature and background). The spectral reflectance values define the percentage of the incident EM radiation that is reflected (for any given wavelength) by the feature and the background. The end result is curves defining the solar energy (in units of W cm^{-2} μm^{-1}) reflected from the feature and the background terrain materials for the specified atmospheric conditions (season, haze, zenith angle) and terrain surface geometry with respect to the incident radiation.

67. Since in most instances the sun is only of concern as a source during daylight hours and the solar energy available is confined to the 3.0- to 5.0-μm band (i.e. within the 3.0- to 14.0-μm band), the inclusion of the computation of reflected energy is an option within the Thermal IR Systems Simulation Model. It need only be executed if the investigator is interested in the daytime performance of sensor systems operating partially or wholly in the 3.0- to 5.5-μm band, or in special cases for the 8- to 14-μm band.

68. <u>Total energy reaching the sensor:</u> Addition (on a wavelength-by-wavelength basis) of the EM energy radiated by the terrain materials of interest (feature and background) and the energy reflected from the terrain materials (if applicable) results in the total EM energy coming from the terrain surface (as a function of wavelength). Computation of the total EM energy as a function of wavelength reaching the thermal IR sensor system is accomplished by applying an atmospheric transmission curve (from LOWTRAN I) that defines the percentage of the energy coming from the terrain as a function of wavelength that is transmitted through the atmosphere from the terrain to the altitude at which the sensor is located. The atmospheric transmission curves used assume a vertical path through

the atmosphere for specified season, atmospheric haze, and sensor altitude combinations. The curves available for execution in the model are the same as those used in the Photographic Systems Simulation Model and are presented in Reference 18.

69. The products of this component of the Thermal IR Systems Simulation Model are curves defining the energy (W cm^{-2} μm^{-1}) as a function of wavelength reaching the thermal IR sensor system at an altitude, R , from the feature and the background of interest and for a specified combination of season, atmospheric haze, solar zenith angle, and relative orientation between the terrain and incident solar energy (if pertinent). The basic information needed to execute this component of the model (i.e. unless an atmospheric transmission curve is desired other than those provided on file for ready access) consists of temperature and emissivity values for the feature and the background terrain materials, and if the performance of sensors operating in the 3.0- to 5.5-μm wavelength band during daylight hours is to be considered, the spectral reflectance character of the feature and the background.

Interaction of EM energy and the sensor system

70. Calculation of the interaction of the EM energy reaching the sensor system and the sensor system is handled in three steps that result in the prediction of the capability of the sensor system to discriminate between the feature and the background (i.e. given the previously assumed atmospheric conditions). The three steps (calculation of the energy impinging on the detector, calculation of the detector output voltage, and calculation of sensor system noise) and the procedures for predicting sensor performance capabilities are

discussed in the following paragraphs. The techniques used were selected to present a simple, yet fairly comprehensive, representation of the actual interactions. It should be emphasized that the resulting product is essentially a signal-to-noise ratio that simply designates whether the difference in the signals resulting from the feature and the background is greater or less than the noise (voltage) signal of the sensor system. The occurrence of a signal-to-noise ratio greater than 1.0 indicates the potential for detecting a difference between the sensor output for the feature and that for the background. It does not address the question of detection (i.e. recognition of an anomaly in the sensor output caused by the feature) versus recognition (i.e. identification of the exact character of the feature). The detection-recognition problem* is complicated by the response and recognition capabilities of the instrument (such as the eye) used to view or analyze the sensor output and is beyond the scope of this modeling effort.

71. Energy impinging on the detector: The energy impinging on the detector of the sensor system is computed by considering the energy as a function of wavelength reaching the sensor system (as calculated in the first component of the model), the spatial resolution of the sensor system, and the character of the sensor optics. Specifically, the calculation is made as follows:

$$W_{\lambda D} = W_{\lambda S} \times \pi \tan^2 \left(\frac{0.180 MR}{2\pi} \right) \times AA \qquad (9)$$

* Empirical studies concerning this problem are being conducted at the U. S. Army Night Vision Laboratories, Fort Belvoir, Virginia.

where

$W_{\lambda D}$ = EM radiation as a function of wavelength impinging on the sensor detector, W μm^{-1}

$W_{\lambda S}$ = EM energy as a function of wavelength reaching the remote sensor, W cm^{-2} μm^{-1}

MR = sensor system spatial resolution, mrad

AA = area of sensor optical aperture, cm^2

The term $\pi \tan^2 \left(\frac{0.180MR}{2\pi}\right)$ takes into account the cone of energy viewed by the sensor at any given time (i.e. the instantaneous field of view of the sensor system). The "AA" value defines the effective area of sensor optics for collecting incoming radiation and channeling it to the detector. The value of AA is usually fixed with the sensor system design and is a basic descriptor of the optics of the scanner system. The overall result is the watts (power) as a function of wavelength impinging on the detector.

72. Detector output voltage: The power incident on the detector is converted to an electrical voltage by photovoltaic, photoconductive, or photoelectromagnetic processes (depending on the type of detector used). In the model the spectral response characteristics of the detector are defined by a relative response curve, such as those shown in Figure 19, and a peak response value, $R_{\lambda max}$, which defines the voltage output of the detector per unit power input (watts) at the wavelength of peak detector response. The relative response curve and the $R_{\lambda max}$ value (both available from manufacturers literature) are combined to generate a response curve for the detector that defines (as a function of wavelength) the voltage output of the detector per watt of incident power. For example, if the relative

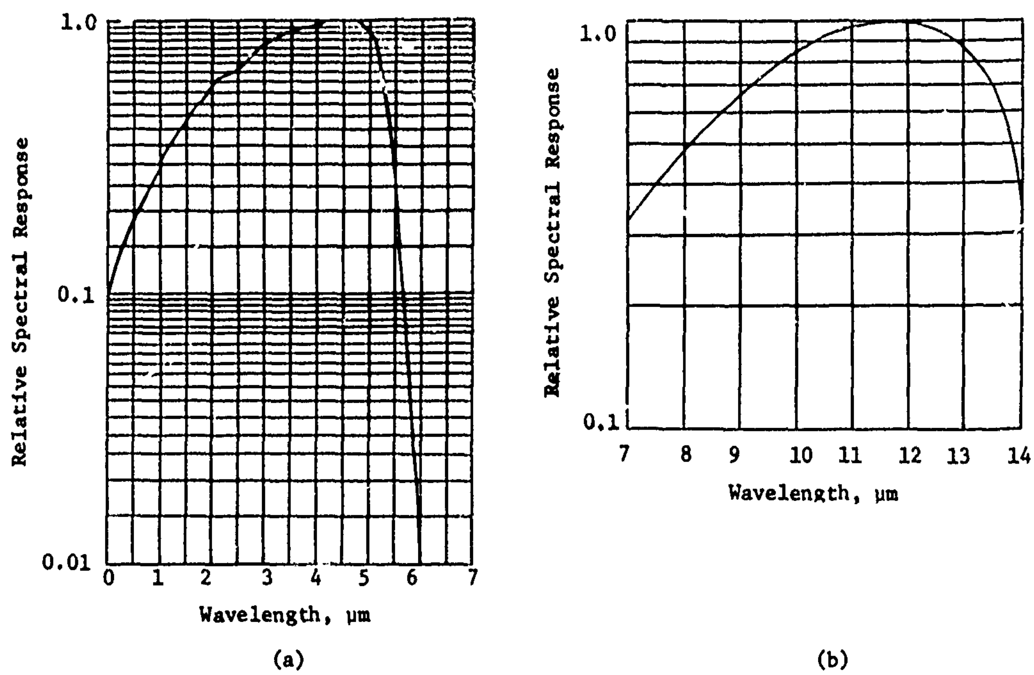

Figure 19. Relative response curves for mercury-cadmium-telluride (a) and indium-antimonide (b) detectors operating in the 8- to 14- and 3- to 5.5-μm wavelength bands, respectively

response curve shown in Figure 19 for the HgCdTe detector is coupled with an $R_{\lambda max}$ value of 1000 v/w, the result is the detector response curve shown in Figure 20. Combining the relative response curve and the curve defining the power as a function of wavelength, incident on the detector $S_{\lambda D}$ and integrating results in computation of the output voltage of the detector. The specific form of the equation is as follows:

$$V_D = \int_{\lambda_1}^{\lambda_2} R_\lambda S_{\lambda D} d\lambda \tag{10}$$

where

V_D = output voltage of the detector, v

R_λ = response of detector as a function of wavelength, v/w^{-1} (this variable is a function of detector area)

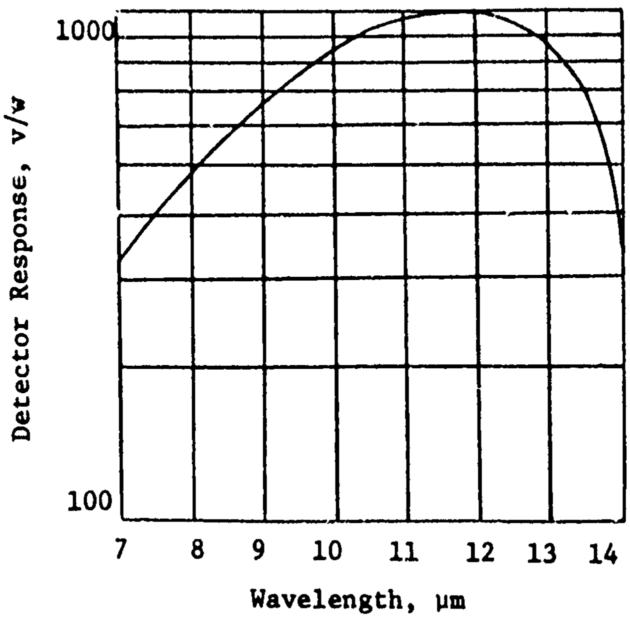

Figure 20. Detector response curve for mercury-cadmium-telluride detector having a peak response of 1000 volts/watt

73. In the execution of the model, the detector voltage output is computed for the feature (V_{DF}) and the background (V_{DB}) individually. These voltage values are used to determine the sensor system's capability for discriminating between the feature and the background. The discrimination capability evaluation is also based on the sensor noise voltage, which is discussed in the following paragraph.

74. <u>Sensor system noise:</u> Sensor system noise voltage is computed based on the detector noise voltage. The first step involves computing the detector noise voltage, which is a function of the detector "noise voltage index" and the electrical bandwidth of the sensor system as follows:

$$DNV = NVI(\Delta F)^{1/2} \tag{11}$$

where

DNV = detector noise voltage, v

NVI = detector noise voltage index, v-$Hz^{-1/2}$

ΔF = electrical bandwidth of sensor system, Hz

The noise voltage index is a published value for the detector. For example, Barnes Engineering, Incorporated, publishes a noise voltage value of 900×10^{-9} v-$Hz^{-1/2}$ for their lead-tin telluride (Pb-Sn-Te) infrared detector (Series A-500 photoconductive crystal) for an operating temperature of 77 K and a background temperature of 300 K. The noise voltage index value is a function of the detector characteristics and the environment within which it is placed (i.e. the sources of IR radiation, internal detector noise, etc.) and other factors; thus, it represents a gross or simplified parameter for detector noise. The electrical bandwidth is a function of the sensor system design. It is assumed to be a value of approximately 1.25×10^6 Hz for sensor systems designed for operation of high-performance aircraft and 0.30×10^6 Hz for sensor systems designed for operation in slower aircraft.* The total sensor system noise (V_N) is assumed to be 1.5 times the detector noise voltage* as follows:

$$V_N = 1.5 \text{ DNV} \tag{12}$$

75. System performance evaluation: System performance evaluation concerns the ability of a sensor system to detect a meaningful change in terrain conditions through a recognizable or detectable

---

* Conversations with HRB Singer personnel, State College, Pennsylvania, and with detector manufacturers and IR system designers.

change in the output signal of the sensor system. Within the framework of this work, the evaluation is based on the comparison of the sensor output voltage for adjacent pixels (i.e. the areas on the ground represented by adjacent pixels) and the sensor system noise voltage. For an individual pixel (i.e. the area on the ground viewed instantaneously by the sensor - a function of sensor system spatial resolution and sensor altitude), three conditions are possible: the area on the ground covered by the pixel can be comprised totally of the background, totally of the feature, or of a portion of each. The voltage output of the sensor system for a given pixel will, of course, be dependent upon which of the three conditions exist.

76. The simplest case for evaluation of sensor performance occurs when one pixel is considered to be comprised completely of the background and the second completely of the feature. The evaluation is accomplished by comparing the difference between the detector output voltages computed for the feature and the background with the computed sensor system noise voltage as follows:

$$V_R = \frac{V_F - V_B}{V_N} \tag{13}$$

where

V_R = voltage ratio

V_F = computed detector output voltage for the feature, v

V_B = computed detector output voltage for the background, v

V_N = computed sensor system noise voltage, v

77. If the value of the voltage ratio (V_R) is greater than 1.0 the difference in sensor system responses for the feature and the background is sufficiently large to theoretically allow discrimination

between the pixel comprised of the background and the pixel comprised of the feature. Of course, the larger the value of V_R , the greater is the potential for actually being able to distinguish between the pixels on the final output product of the sensor system (e.g. magnetic tape, imagery).

78. The evaluation procedure becomes more complicated if one of the pixels to be considered is comprised of portions of both the feature and the background.

79. Figure 21 illustrates situations wherein the feature area

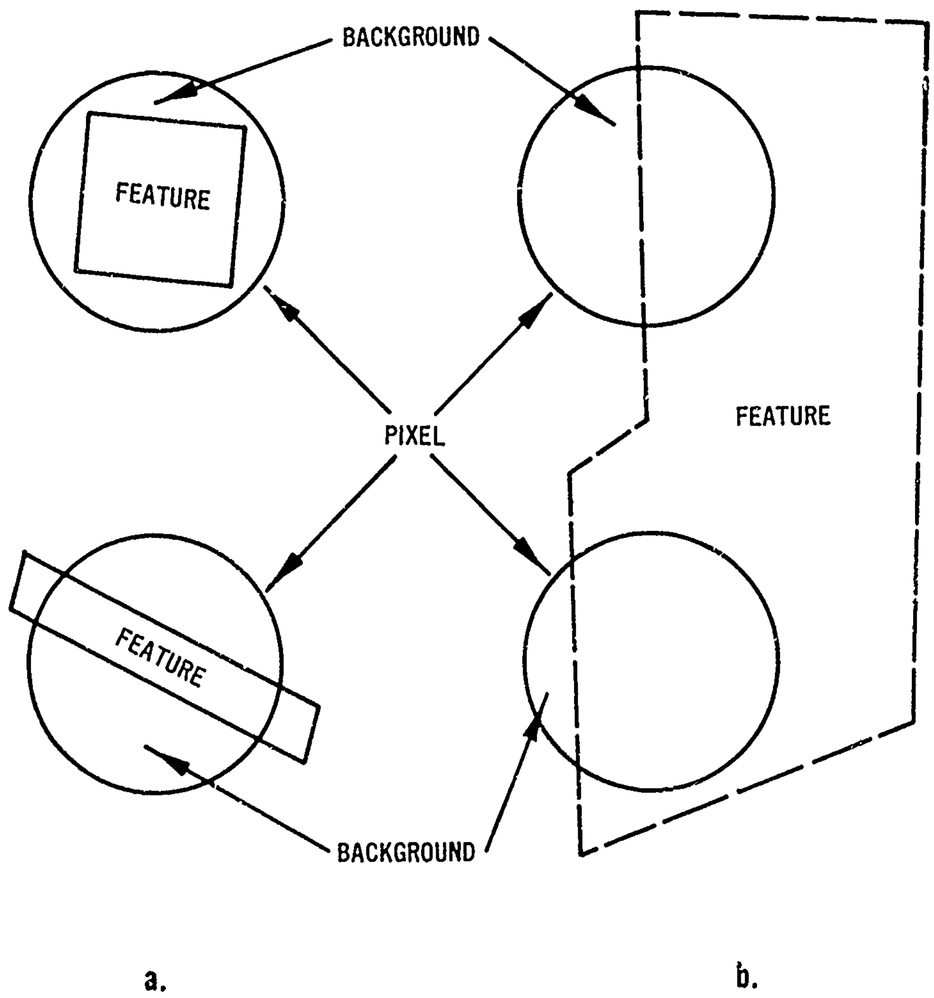

Figure 21. Illustration of situations where the feature area is less than the pixel area (a) and where the boundary between the feature and background occurs within individual pixels (b)

is less than the ground area covered by the pixel (a) and the boundary between feature and background occurs within the ground area covered by the pixel (b). Obviously, a multitude of other situations (i.e. in addition to those illustrated in Figure 21) are possible. For the purposes of this model, the evaluation of system performance is limited to comparing the sensor response (output voltage) for a pixel comprised entirely of the background to that of a pixel comprised of portions of both the feature and the background, and on the basis of the simple ratio of the ground area of the pixel to the area of the feature within the bounds of the pixel. If the feature is entirely within the ground area of the pixel, the parameter PARFAR is calculated as follows:

$$\text{PARFAR} = \frac{A_F}{\text{APG}} \tag{14}$$

where

PARFAR = proportion of the ground area of the pixel comprised of the feature

A_F = area of the feature, m^2

APG = ground area of pixel, m^2

The value of APG is computed by the following relation:

$$\text{APG} = \pi R^2 \tan^2 \left(\frac{0.180\text{MR}}{2\pi}\right) \tag{15}$$

where the R represents sensor height above the ground and the other parameters are defined as previously discussed in paragraph 71. If the ratio of A_F to APG (PARFAR) is greater than 1.0, it is assumed to be 1.0. That is, the pixel is considered to be comprised entirely of the feature (the simple case previously described in

paragraph 71). If this procedure is not acceptable for the situation of interest, an appropriate value for PARFAR can be entered to override that computed by the ratio.

80. Calculation of PARFAR is followed by calculation of the parameter PARBAR (the proportion of the pixel area comprised of the background) by the following relation:

$$PARBAR = 1.0 - PARFAR$$

The values of PARFAR and PARBAR are used to calculate the detector output voltage (i.e. for the pixel comprised of a portion of both the feature and the background) in the following manner:

$$V_{FB} = PARFAR\ (V_F) + PARBAR\ (V_B)$$

where V_{FB} is the detector output voltage for the pixel. The value of V_{FB} is used to compute V_R as follows:

$$V_R = \frac{|V_{FB} - V_B|}{V_N} \qquad (16)$$

Thus, the value of V_R is the evaluation parameter in all cases. If V_R is greater than 1.0, it is theoretically possible to detect the feature from the background for the sensor, atmosphere, and terrain conditions specified by the values of the inputs to the models.

Presentation of Model Forms and Their Outputs

81. As mentioned in paragraph 57 two computer models for simulation of the performance of thermal IR sensors were developed. The models have identical analytical frameworks with the same computational routines. They differ slightly in the input data

required, the general execution of the computations, and the type of information output. For the purposes of this discussion, the model forms will be designated as the "Specific" and "General" Thermal IR Systems Simulation Models, respectively. The following paragraphs briefly discuss these models and present their outputs. The computer programs for the specific and general models are presented in detail in Appendices C and D, respectively.

Specific performance model

82. The Specific Thermal IR Systems Simulation Model was designed to provide a means of evaluating the capabilities of a specific sensor system for discriminating between a feature (defined by values of T , ε , and ground area) and a background (defined by values of T and ε) for specified atmospheric conditions and sensor altitude. The major sensor, atmosphere, and terrain descriptor inputs are as follows (see Appendix C for details):

Sensor

Response curve
Peak response
Area of aperture
Detector noise voltage index
Electrical bandwidth
Wavelength band
Spatial resolution
Altitude

Atmosphere

Season
Latitude
Haze
Solar zenith angle*

---

* Necessary only when considering daytime flights.

Terrain

Feature temperature
Feature emissivity
Feature area
Background temperature
Background emissivity
Feature reflectance*
Background reflectance*

Using the analytical computations described in the previous sections of this part of the report (paragraphs 61 to 80), the voltage output of the detector for the feature (i.e. V_F if the feature area is larger than the ground area of the pixel and V_{FB} if not, as discussed in paragraph 80), the voltage output of the detector for the background (V_B), the sensor noise voltage (V_N), and the voltage ratio (V_R) are computed and output as shown in Table 2, the output format for this model form. The value of V_R is used to specify the ability of the sensor system to discriminate between the feature and the background for the specified conditions. If V_R is greater than 1.0, the sensor system as described can potentially discriminate between the feature and the background (for the terrain and atmospheric conditions specified). If V_R is less than 1.0 (or equal), the sensor noise voltage exceeds the difference in the output voltages for the feature and the background and discrimination is not possible. It should be emphasized at this point that the model predictions represent the best possible (i.e. theoretical limit) sensor performance under specified conditions. The means of recording the sensor output (i.e. digital or analog magnetic tape, film, etc.) can strongly influence the performance of the system and must

* Necessary only when considering daytime flights.

be considered on an individual basis. Guidance concerning this problem is provided in Part V of this report.

General performance model

83. The General Thermal IR Systems Simulation Model was designed to provide sensor performance information over a broad range of terrain material temperature and emissivity values. The information provided in the model output is, by necessity, less specific than that provided by the "Specific" Model form; however, it is for a wider variety of applications. The necessary model inputs describing sensor, atmosphere, and terrain conditions are as follows (see Appendix D for details):

Sensor

Response curve
Peak response
Area of aperture
Detector noise voltage index
Electrical bandwidth
Wavelength band
Spatial resolution
Altitude

Atmosphere

Season
Latitude
Haze

Terrain

Emissivity

84. A review of paragraph 82 will show that only the terrain descriptor inputs differ from the inputs for the Specific Model form. In the General Model form a single emissivity value is used for all computations. This does not restrict use of the model output to the condition where $\varepsilon_F = \varepsilon_B$, as will be discussed later; it simply makes the computational routines in the computer program much simpler.

85. In the execution of the model (given a specified ε value, sensor characteristics, and atmospheric conditions), the value for the minimum temperature difference detectable by the sensor system is computed as a function of background temperature. This is accomplished essentially by assigning a value to the feature temperature and then varying the background temperature (i.e. from the assigned feature temperature) until the value of V_R is greater than 1.0 (using the analytical relations described in paragraphs 61 to 76). By systematically varying the feature temperature over a broad range (e.g. 200 to 400 K), the model computes the minimum resolvable temperature differences for the spectrum of background temperatures. It should be noted that the feature area is not considered in the computations; thus, the assumption is made that the feature area is greater than the ground area of the pixel (i.e. given the sensor spatial resolution).

86. The basic output of the model is a tabular listing of the minimum resolvable temperature differences for a spectrum of background temperature values (for the specified conditions). Table 3 presents a sample output for sensor characteristics, atmospheric conditions, and emissivity as specified in the legend included in the table. To generate these data the feature temperature was initially assigned a value of 200 K and increased by 20 K increments to a maximum value of 400 K. The sensor characteristics used are, approximately, those of the HRB Singer Reconofax XIII A scanner system. The published (Reference 25) temperature resolution value for this sensor is 0.2 K for a blackbody radiator ($\varepsilon = 1.0$) at a temperature of approximately 300 K and a sensor spatial resolution of

1.0 milliradian. The corresponding value predicted* with the General Model form was 0.20°C, which is identical to the published value.

87. In any given wavelength band (e.g. 3- to 3.5-μm or 8- to 14-μm), thermal IR sensor performance can be defined by a single parameter, apparent temperature, which combines ε and T. The apparent temperature, T_{app}, of a material is the temperature of a blackbody that would radiate, within a given wavelength band, the same amount of EM energy as the material (i.e. the material having a specified temperature, T, and emissivity, ε). The relation between absolute and apparent temperature for a specified wavelength band can be described as follows:

$$T_{app} = \frac{1}{\frac{1}{T} - \frac{\Delta\lambda \ln \varepsilon}{C_2 \ln (\lambda_2/\lambda_1)}} \qquad (17)$$

where

T_{app} = apparent temperature, K

T = absolute temperature, K

$\Delta\lambda = \lambda_2 - \lambda_1$

ε = emissivity

C_2 = 14,388 μm K

λ_2 = upper (longer) wavelength limit of band, μm

λ_1 = lower (shorter) wavelength limit of band, μm

This relation is derived and presented in Appendix E, along with graphics relating T and T_{app} for the 3- to 5.5-μm and 8- to 14-μm bands (Figures E1 and E2, respectively).

---

* Atmospheric effects were ignored in this computation to make the model prediction compatible with the co utations used to arrive at the published value.

88. Using the graphics (i.e. or others like them) presented in Figures E1 and E2 and the output of the General Model form (ΔT_{min} versus T) it is feasible to examine the performance of a given sensor system for any feature background combination of temperatures and emissivities. Since apparent temperature is defined as a blackbody temperature (with ε given as 1.0), the output of the General Model form can be interpreted to be the minimum resolvable apparent temperature difference as a function of the apparent temperature of the background. Thus, if the temperature and emissivity values for the feature and the background are transformed to apparent temperature, using graphics such as those in Figures E1 and E2 or using equation E3, it is possible to evaluate a particular sensor system for its ability to delineate a "Specific" feature-background situation as accomplished with the Specific Model form. The difference in the apparent temperatures of the feature and the background can be compared to the ΔT_{min} value (computed from the General Model form) at the apparent temperature of the feature. If the difference in the apparent temperatures of the feature and the background exceeds the value of ΔT_{min}, the sensor system can theoretically detect the feature from the background.

PART IV: PLANNING TOOLS FOR PHOTOGRAPHIC MISSIONS

Introduction

89. Remote sensors, particularly airborne sensors, have been shown to be a most effective means for acquiring environmental data over large areas (Reference 1). Although remote sensing techniques can by no means supply all of the data necessary for the hydrologic evaluation of an area, they can provide a very efficient and cost-effective means for acquiring a wide variety of pertinent information. The phrase "can provide" must be emphasized in that planning a successful multipurpose remote sensor data acquisition program is not a simple task.

90. Successful application of remote sensing to data acquisition requires that the following six steps be implemented:

a. Problem specification

b. Acquisition of ground control data

c. Remote sensor data acquisition

d. Data manipulation

e. Information extraction

f. Information presentation

Problem specification

91. Problem specification consists of defining the problem to be solved, specifying the types of data that are necessary to solve it, and determining the applicability of remote sensing techniques for supplying any or all of the necessary data. In general, this usually means that some kind of sc[illegible] for solving the problem must be visualized. The scheme, or model, of the phenomena should contain

a careful statement of the objective and an equally careful identification of each step in the information flow from present state of the art to final solution. Such schemes allow rational specification of data requirements for the solution of the problem. Determining the applicability of remote sensing techniques for acquisition of the specified data requires a similar understanding of the phenomena that affect remote sensor data acquisition.

Acquisition of ground control data

92. Acquisition of ground control data consists of obtaining information necessary for accurate interpretation of remotely sensed data and possible specification of the remote sensing techniques best suited for the problem. This may mean determination of how the factors of interest are related on the ground in selected locations to serve as a basis for interpreting those relations over the entire time and region of interest. In addition, it may also consist of acquiring basic information concerning the reflectance properties of terrain materials or other such information that could be used in an analytical scheme (model) to specify a favorable data acquisition mission profile to enhance the data obtained.

Remote sensor data acquisition

93. Remote sensor data acquisition consists of the actual process of sensing and recording data on the region of interest at the time of interest. Integrated in this process is the design of the data acquisition mission, which consists of the specification of such things as flight time, altitude, sensor type, and sensor adjustments (e.g. exposure times and F-stop settings for aerial cameras). These parameters must be carefully matched to the problem at hand;

and considering the almost infinite number of possible combinations of data requirements, mission profiles, and remote sensing systems, it is essential that the mission be designed in as rational and quantitative a way as possible. This is especially important in the case of a multipurpose (i.e. for a variety of data types) data acquisition mission.

Data manipulation

94. Data manipulation consists of putting the information obtained by the remote sensor system into a form suitable for analysis or interpretation. Remotely sensed data as recorded by the sensor are seldom in the best form for data extraction, particularly data recorded on magnetic tape. Some information may be directly obtainable from the data by measurement or interpretative techniques, but other types of information may require application of geometric rectification algorithms or image enhancement techniques before a meaningful analysis can be made.

Information extraction

95. Information extraction is the actual analysis or interpretation of the remotely sensed data to obtain the needed information. This step may be, and many times is, closely associated and integrated with the data manipulation. The information extraction can be in the form of a rigid mathematical process, such as density slicing and spectrum matching, or it can be achieved by essentially subjective procedures, such as classical photo interpretation. If the desired data consist of things inherent in the three-dimensional geometry of the landscape, information extraction can be achieved by

photogrammetric processes. Usually all three processes are required in a multipurpose program.

Information presentation

96. Information presentation consists of putting the extracted data into a form in which it can be used to assist in solving the problem(s) at hand. The most useful form for a particular set of data depends, of course, on how those data are to be applied to the solution of a problem. Topographic data, for example, can assume the form of contour maps, cross sections, pseudo-three-dimensional images, etc., the most appropriate form varying as the intended use of the data varies.

Summary

97. The implementation of the previously discussed steps is considerably more complicated for a multipurpose data acquisition program than for acquiring data of a specific type because a greater number of parameters must be considered. In either case, effective implementation of these procedures demands a rational, analytical procedure for mission planning (evaluating the use of remote sensing techniques for acquisition of specific data types and for detailed planning of the data acquisition mission to ensure its success). The following paragraphs present and discuss basic analytical mission planning tools. Use of the computerized Photographic Systems Simulation Model for mission planning is first presented followed by the formulation of a graphical (nomogram) version of the computer model prediction capability and illustration of its use. These tools and a number of associated capabilities provide a quantitative mission planning capability previously unavailable. The procedures presented

herein are by no means comprehensive; however, they provide a significant advancement in the ability to answer critical questions for mission planning.

Model Application in Photographic Mission Planning

General

98. Within the remote sensing data acquisition and interpretation scheme presented in the previous paragraphs, the Photographic Systems Simulation Model can be applied effectively in two of the six steps: problem specification and remote sensor data acquisition (in a way that can be collectively termed mission planning). A major consideration in the problem specification step is the identification of those factors that will cause a visible change in the imagery (or some measurable change in any remotely sensed data) and those factors for which changes must be inferred from other changes visible on the imagery. Since the Photographic Systems Simulation Model calculates the contrast that will occur on a photographic image (between two features or conditions of interest) as a function of material reflectance properties (as related to physical properties) for a given mission profile, the model can be directly applied to this problem.

99. For a specific problem (requiring a single type of data), appropriate reflectance data for the two features or conditions of a single feature can be input to the model and the contrast predicted for a number of film-filter combinations. These predicted values can be used directly to determine if the change in feature or conditions will be detectable directly on the imagery.

100. For a multipurpose data acquisition program, the model

can be applied to each individual data type required and the results combined to determine, overall, those data types whose variations would be directly observable on remote imagery. For those items not directly visible on the imagery, additional analysis must be made. First, the investigator must relate the changes in these data types to physical changes in other features. This can be accomplished only by one knowledgeable in the interrelations of the surface and near-surface terrain materials. Once these relations have been defined, the model can be applied to determine if variations in the "indicator" feature(s) can be directly observed on remote imagery.

101. The application of the Photographic Systems Simulation Model to the remote sensing data acquisition step involves the planning or design of the mission profile. This entails selection of the best sensor (film-filter combination) for the job and specification of acceptable mission profile parameters, such as sensor altitude, acceptable atmospheric conditions, acceptable solar zenith (time of day for a particular season at a particular location), and optimum sensor adjustments or calibration for the problem at hand.

102. The use of the model for specifying the best or most acceptable film-filter combinations for a specific purpose from a number of selected combinations is simply a matter of executing the model with the appropriate reflectance data. Application of the model for a multipurpose data acquisition program would entail repeated use of the model and an analysis of the results to determine a single or minimum number of film-filter combinations that would be adequate for acquiring the necessary data. However, the specified "best" sensor system may and probably will vary for each required

data type. In this case, the film-filter combinations deemed adequate for each data type can be compared, and a selection of the sensor system(s) can be made for the data acquisition mission based on those film-filter combinations shown to be adequate for the largest number of the individual data types. Another alternative consists of flying several missions using different sensors, or if possible, one mission with multispectral capability.

103. Specification of acceptable mission profile parameters requires examination of the effects of variations of these parameters on the informational content of the remote imagery. This means that the effects of variations in sensor altitude, atmospheric haze conditions, solar zenith angle, and sensor adjustments must be examined in an orderly fashion to determine those conditions most conducive to a successful data acquisition mission. Since the Photographic Systems Simulation Model allows for the systematic control of these variables, it can be used to examine the effects of their vari' 'on on the contrast between the images of specific features as o' ne with a specified sensor or sensor package.

104. Specifically, the model can be used to predic' trast between the images of specific features or feature cond... at various altitudes, for different atmospheric haze conditions, f different solar zenith angles, and for various sensor adjustments (e.g. F-stop). The predicted contrast values are then used to examine the effect of each mission parameter on the contrast. If, for example, an increase in altitude decreases the contrast significantly, or below an acceptable level, the altitude at which the mission is flown must be tailored to prevent a significant loss in

contrast. Predictions at a number of altitudes would allow specification of the maximum acceptable altitude on a spectral basis. On the other hand, if an increase in altitude does not affect the image contrast, the mission flight altitude can be selected on the basis of scale factors alone, using the spatial component of the model.

105. In the analysis of the predicted contrast values, it is necessary to examine combined effects of parameters in addition to individual parameter effects. For example, the effect of variations in atomspheric haze should be investigated for various sensor altitudes, because a change in haze conditions may not cause a significant change in contrast on images obtained at low altitudes, but may, indeed, create an undesirably large contrast change (decrease) for images obtained at relatively high altitudes. Similar analogies can be drawn for the other mission parameters. The increase in solar zenith angle, for example, will effectively magnify atmospheric attenuation. Similarly, variations in altitude, atmospheric haze, and solar zenith angle affect the optimum values for camera adjustments such as F-stop and exposure time.

Illustration problem

106. General: Perhaps the most effective means for illustrating the use of the model is by applying it to a hypothetical, yet realistic, problem. In the following example, a hydrologic-related data acquisition problem concerning the mapping of soil conditions in a watershed (perhaps as input for computing infiltration losses) is hypothesized, and the model is applied to obtain information regarding the following questions:

a. Are photographic remote sensing techniques capable of

providing the necessary data?

b. What are the optimum film-filter combinations for data acquisition?

c. What are the mission profile constraints regarding atmospheric conditions, altitude, etc.?

107. The first question concerns the amount of contrast that will occur on an image obtained under specified conditions. The contrast must be of sufficient magnitude that the feature and the background (second feature) can be distinguished on the imagery either by eye or by an automated optical device, such as a scanning microdensitometer. In this case we are concerned with the contrast between soil types.

108. The second question concerns the relative magnitudes of the contrasts in optical density that will occur on images obtained using various film-filter combinations. The film-filter combination that provides the maximum optical density contrast would be the optimum system for acquisition of data concerning the particular feature and background. This, of course, is a function of other factors such as altitude and atmospheric haze conditions.

109. The third question concerns the effects of altitude, atmospheric haze conditions, solar zenith angle, sensor characteristics, etc., on the magnitude of the contrast between optical density of the feature and that of the background, or between two features. If atmospheric haze conditions have a very great effect on the resulting optical density contrast on the imagery, it may be necessary to obtain imagery only in very clear atmospheric conditions to ensure acquisition of the desired data. At times the size of a feature may

create a constraint on altitude of the sensor in that it is necessary to have imagery at a scale that will allow recognition of a particular feature from among neighboring features. In addition, because of incre ~d atmospheric attenuation with higher altitudes (i.e. a longer path for the EM radiation to traverse), the altitude at which a successful mission can be flown may vary to some degree with atmospheric conditions.

110. The soil mapping problem presented herein is idealized in that the obscuring effects of vegetation are not considered. In addition, the ability to interpret soil type by topographic or landform conditions, is not considered. For simplicity, two soil types (silt and clay) at three moisture contents (10, 20, and 30 percent) were selected for this illustration. The soils data presented herein should be considered representative only for the specific soil formations from which the reflectance data were derived and should not be considered as representative of other soil formations having similar physical properties. The applicability of photographic systems to this problem concerns primarily the contrast in optical density of the resulting images of adjacent soil areas. There is not a direct image scale requirement, except that the imagery scale must be sufficient to obtain the desired accuracy for the soil boundaries and for identification of isolated patches that differ from the surrounding soil. Since the contrast in the optical densities for the soils may vary with soil moisture conditions, a mission constraint concerning antecedent soil moisture conditions may be pertinent. For example, if two soils can be best distinguished from each other when they are relatively dry, the acquisition of imagery in wet conditions

(e.g. just after a rain) may seriously affect the usefulness of the imagery.

111. Model application: For the purposes of this study the film-filter combinations shown in Table 4 were considered. These films and filters represent those most commonly used for conventional aerial photographic surveys. The spectral sensitivity curves and gamma values for the films were obtained from Reference 24, and the filter transmission curves were obtained from Reference 23. The lens transmission curve used is shown in Figure 13.

112. The Photographic Systems Simulation Model is capable of predicting feature and background image optical density values for a variety of atmospheric conditions, solar zenith angles, sensor altitudes, etc. To keep the illustration at a reasonably simple level, however, only a limited number of such combinations were used. Both the 23- and 5-km-visibility haze models were used with the mid-latitude summer atmosphere model. The 23-km-visibility model represents nearly optimum conditions for transmittance of EM radiation; the 5-km-visibility model represents somewhat marginal conditions.

113. A solar zenith angle of 30 deg was used for all predictions made in this application of the model. This value was chosen to represent an average value for solar zenith angles occurring for the time period of 2 hr before and after local apparent noon for the summer months in the contiguous United States.

114. For this study, the remote sensor was considered to be at altitudes of 1.5 and 6.0 km. These altitudes represent the lower and upper bounds, respectively, for most conventional aerial photography surveys conducted with a lens with a 15.2-cm focal length and a

22.5- by 22.5-cm film format. With the lens-film format above, the scale of the photography obtained at 1.5 and 6.0 km is about 1:10,000 and 1:40,000, respectively. The spectral reflectance curves for the soils are presented in Figures 22a and 22b for silt and clay, respectively (from Reference 26). The reflectance curves represent only those samples from which they were obtained. The curves for silt, for example, cannot be used to represent all silts, but merely the particular series from which the sample was obtained. The spectral reflectance curves were placed on file in the computer for subsequent use in the execution of the model.

115. Results. The F-stop value (assumed to be 5.6) and the curves for spectral reflectance, transmission, spectral sensitivity for the selected films, and lens and filter transmission curves were used in the model to predict optical density values for specified feature and background pairs for sensor altitudes of 1.5 and 6.0 km and atmospheric haze conditions of 23- and 5-km visibility. The feature and background pairs for the soils problem were as follows:

a. Feature: silt, 10 percent moisture content
   Background: clay, 10 percent moisture content
b. Feature: silt, 20 percent moisture content
   Background: clay, 20 percent moisture content
c. Feature: silt, 30 percent moisture content
   Background: clay, 30 percent moisture content

116. The optical density contrast predictions for the above feature-background combinations are presented in Tables 3 to 31. The data in the tables are the output of the model as previously presented and described in Figure 16 and paragraph 50.

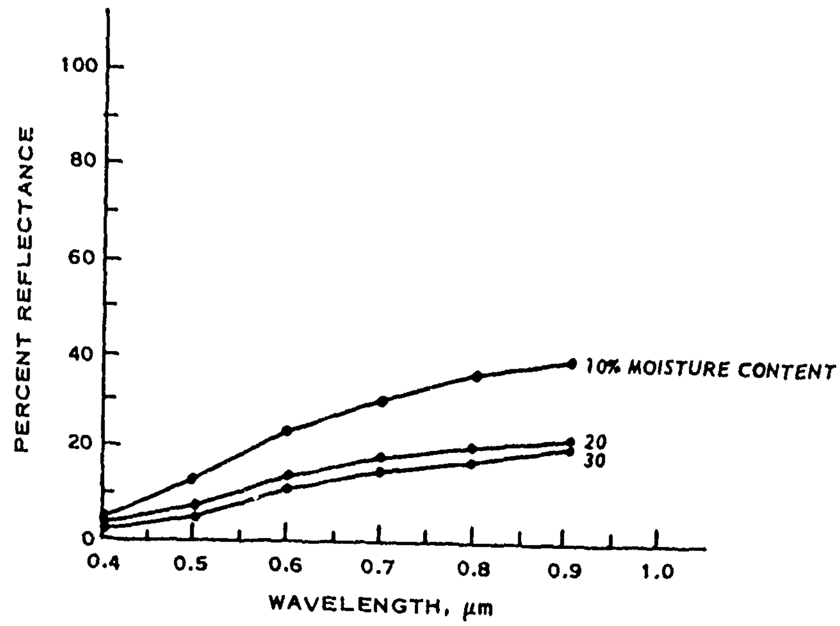

(a) Silt

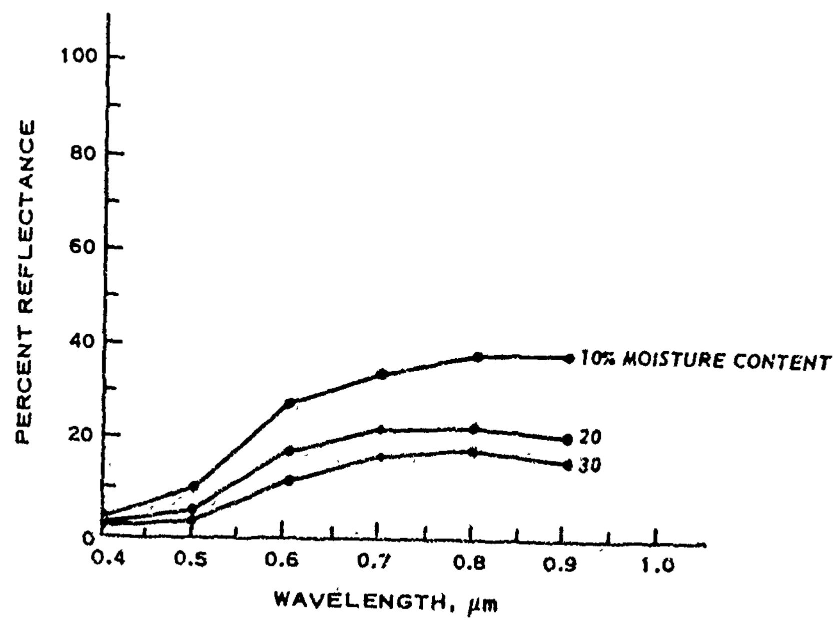

(b) Clay

Figure 22. Spectral reflectance curves for silt and clay (Reference 26)

117. In the following paragraphs the predicted optical density values are evaluated with respect to a threshold optical density contrast value of 0.20. This threshold value is based on the assumption that the human eye can discriminate approximately 15 image tones (optical density levels) in the range of 0.0 to 3.0. The numerical value of 0.20 is the resultant of dividing the total optical density range (3.0) by the number of levels (15).

118. The predicted contrast values ($D_F - D_B$) for the silt and clay soils at moisture contents of 10, 20, and 30 percent (Tables 5-16) were examined to determine if any of the film-filter combinations considered in the analysis were adequate for distinguishing between the soil types. Several film-filter combinations were found to have absolute contrast values greater than the previously selected minimum of 0.20. Thus, for the problem at hand, the feasibility exists for distinguishing between the soil types by means of photographic remote sensing techniques.

119. The next step was the examination of the predicted $D_F - D_B$ (contrast) values to determine the optimum film-filter combination(s) for acquiring the desired data. This examination must be conducted with the atmospheric haze condition and sensor altitude in mind, since the optimum film-filter combination may vary somewhat with changes in these features, e.g., the best film-filter combination for a clear day may not be the best for a hazy day. The maximum contrast within one emulsion of the color films (i.e. cyan, yellow, or magenta) is the criterion for determining the capability of the color film to discriminate between feature and background. First, the predicted contrast values for soils at 10 percent moisture content (Tables 5-8) were

examined to determine the optimum film-filter combination(s) for distinguishing between the silt and clay soils when they are relatively dry. The examination showed that for the 23-km-visibility condition (Tables 5 and 6), the following film-filter combinations had the four largest contrast values (ranked by the contrast values for 1.5-km altitude).

		$D_F - D_B$	
Film	Filter	1.5 km	6.0 km
2402	47B	0.27	0.21
2403	47B	0.23	0.18
2448	3	0.22	0.20
2402	25A	0.11	0.10

For the 5-km-visibility haze condition (Tables 7 and 8), the following film-filter combinations had the four largest contrast values.

		$D_F - D_B$	
Film	Filter	1.5 km	6.0 km
2402	47B	0.12	0.08
2448	3	0.12	0.09
2403	47B	0.10	0.07
2402	25A	0.08	0.08

For the 23-km (clear) haze condition, the 2402-47B and 2448-3 film-filter combinations had contrasts greater than the threshold (0.20) for both 1.5- and 6.0-km altitudes. For the 5-km (hazy) haze condition, none of the film-filter combinations had an optical density contrast close to the 0.20 threshold.

120. Further examination of the contrast values showed that in general a small decrease in contrast occurred (for a given haze condition) from an altitude of 1.5 to 6.0 km. A much more significant decrease in contrast occurred for a change in atmospheric haze conditions from clear (23-km visibility) to hazy (5-km visibility).

For example, the predicted optical density contrast value for the 2402-473 film-filter combination was 0.27 for the 23-km haze, 1.5-km altitude condition and 0.12 for the 5-km haze, 1.5-km altitude condition.

121. The predicted contrast values for soils at 20 percent moisture content (Tables 9 to 12) were examined next to determine the best film-filter combinations for distinguishing between the silt and clay soils when they are fairly moist. The examination showed that for the 23-km-visibility haze condition (Tables 9 and 10), the following film-filter combinations had the four greatest contrast values (ranked by the contrast values for 1.5-km altitude).

Film	Filter	$D_F - D_B$ 1.5 km	$D_F - D_B$ 6.0 km
2448	3	0.31	0.30
2402	25A	0.26	0.25
2443	12	0.23	0.22
2402	12	0.23	0.22

For the 5-km-visibility haze condition (Tables 11 and 12), the following film-filter combinations had the four greatest contrast values.

Film	Filter	$D_F - D_B$ 1.5 km	$D_F - D_B$ 6.0 km
2448	3	0.21	0.18
2402	25A	0.18	0.15
2424	25A	0.17	0.15
2424	12	0.17	0.15

122. Examination of the predicted contrast values showed that for the 23-km haze condition all four film-filter combinations had adequate contrast values (i.e. greater than 0.20) for detection of the feature from the background. The 2448-3 film-filter combination had

the largest predicted contrast value for both haze conditions and, in fact, was the only film-filter combination with a predicted contrast value greater than 0.20 for the 5-km haze condition. Once again the contrast values for 6.0-km altitude were slightly less than the corresponding values for 1.5-km altitude. A slightly more significant decrease in contrast occurred for a change in haze conditions from 23- to 5-km visibility.

123. The predicted contrast values for soils at 30 percent moisture content (Tables 13 to 16) were examined to determine the best film-filter combination(s) for distinguishing between the silt and clay when they are relatively wet. The examination showed that for the 23-km-visibility haze condition (Tables 13 and 14), the following film-filter combinations had the four greatest predicted contrast values (ranked by the contrast values for 1.5-km altitude).

		$D_F - D_B$	
Film	Filter	1.5 km	6.0 km
2448	3	0.15	0.14
2402	25A	0.13	0.12
2402	12	0.12	0.11
2443	12	0.11	0.11

For the 5-km-visibility haze condition (Tables 15 and 16), the following film-filter combinations had the four greatest contrast values.

		$D_F - D_B$	
Film	Filter	1.5 km	6.0 km
2448	3	[illegible]	0.08
2402	24A	[illegible]	0.07
2443	12	0.07	0.06
2402	12	0.07	0.06

124. Examination of the above optical density contrast values revealed that none of the film-filter combinations had predicted contrast values greater than the 0.20 threshold. In fact, the maximum value computed (0.15 for the 2448-3 film-filter combination; 23-km haze 1.5-km altitude condition) was significantly less than the threshold value (0.20). Thus, the film-filter combinations considered herein do not appear adequate for discriminating between the silt and clay soils at 30 percent moisture content.

125. Considering the predicted contrast values for the 10, 20, and 30 percent soil moisture conditions, it is evident that the imagery should not be obtained when the soils are relatively wet (i.e. 30 percent or greater moisture content) or when they are very dry (i.e. 10 percent or less moisture content). The best situation is when the soils are fairly moist (i.e. approximately 20 percent moisture content); thus, the imagery should not be obtained immediately after a rain, during periods of high antecedent moisture conditions, or during a long period without rain. The best film-filter combination for the mission is the 2448-3 combination, since it had the greatest predicted contrast for the 20 percent soil moisture condition and had predicted contrast values in excess of the 0.20 threshold value for the 10 percent soil moisture condition. In addition, for the 20 percent soil moisture condition, the predicted contrast values for the 2448-3 film-filter combination were greater than 0.20 at both altitudes for the 23-km haze condition and at the 1.5-km altitude for the 5-km haze condition (the contrast value for the 1.5-km altitude, 5-km haze condition was just less than the threshold).

126. Haze conditions have a significant effect on the predicted

contrast values and, if at all possible, the mission should be flown during clear conditions. Altitude has little bearing on the contrast values and does not appear to be a factor in mission design, except for determining the expected accuracy of the locations of the soil boundaries. The imagery should be obtained at the highest altitude possible (to reduce mission time and film costs) without sacrificing desired levels of precision.

127. Vegetation cover will present a constraint for soil data acquisition. A fairly thick cover of almost any vegetation type may mask the soils to a degree that may prohibit their identification or discrimination. Thus, the optimum time for imagery acquisition may be in the spring when most agricultural areas are recently plowed.

128. The Photographic Systems Simulation Model should be regarded as an aid in mission planning that enables the planner to project a suitable mission profile to ensure good contrast and resolution. The predictions can be no better than the accuracy of the reflectance data provided to the model. Other interpretation aids, such as landforms and drainage patterns, can provide invaluable clues as to the soil types, depth to bedrock, etc. The illustrations were presented here solely to demonstrate the use of the model. The results of the analyses in the illustrations should not be taken as being generally applicable for similar situations.

A Nomogram for Computing Optical Density Contrast

Introduction

129. Part II of this report documented a computerized simulation model for predicting image optical density contrasts in

photographic remote sensing systems. The model, called the Photographic Systems Simulation Model, provides for the first time a rigorous, quantitative means of examining the effects of the major variables that influence the informational content of aerial photographs. Specifically, the model can be used to predict the contrast between the images of specific features or feature conditions, taken at various altitudes, in different atmospheric haze conditions, at different solar zenith angles, during different seasons, and with different sensor characteristics (i.e films, filters, etc.). This makes possible the objective selection of a sensor system and mission profile to enhance the success of a data acquisition program.

130. Execution of the simulation model requires personnel knowledgeable in the operation of computer facilities and the basic character of the model and its inputs. Clearly, such personnel and, for that matter, appropriate computer facilities are not always available. For this reason it was deemed necessary to generate a graphical form of the model (i.e. a nomogram), thereby providing all potential users of photographic systems with a means for predicting image optical density contrasts for quantitatively planning remote sensing missions.

131. This portion of the report describes that nomogram. A brief description of its formulation is first presented followed by its presentation, including a step-by-step example problem to illustrate the correct procedures for using it and an evaluation of its accuracy with respect to the computer model from which it was generated.

Concept of the nomogram

132. The basic criteria for design of the nomogram were as follows:

a. Maintain the accuracy of the computer model as much as possible.

b. Consolidate or combine as many variables as possible to simplify the structure of the nomogram.

c. Create a flexible or generally applicable basic structure that will allow the consideration of new film-filter combinations, atmospheric conditions, etc., in the future.

d. Include a spectrum of conditions for the major variables influencing image optical density values and yet maintain a level of simplicity sufficient to ensure ease of use.

133. To satisfy the above criteria, it was deemed necessary to:

a. Maintain the spectral character of the variables considered.

b. Make computations in a manner that minimizes error due to rounding and other such phenomena.

c. Provide a stable nomogram format with the basic inputs in tabular form, thus allowing future additions by adding to the tables rather than changing the format of the nomogram.

d. Initially, consider one latitude atmospheric condition, two seasonal atmospheric conditions, two atmospheric haze conditions, three solar zenith angles, and four altitudes for the spectrum of conditions of the nonsensor-related variables of interest.

e. Initially, consider five films that are representative of the films commonly used for aerial photographic work and six commonly used filters that effectively divide the visible and near-IR spectral regions into somewhat equal wavelength bands.

Nomogram structure

134. In the computer model the spectral character of the wavelength-dependent variables is maintained by representing each variable as a continuous variate with wavelength (i.e. a continuous curve). This is not feasible for a nomogram, and to maintain the spectral character of the variables for the nomogram, it was necessary to divide the visible and near-IR spectral regions (0.40 to 0.93 μm) into a number of discrete wavelength bands. All of the computations made in the execution of the nomogram are made with respect to these wavelength bands, which are:

a. 0.40 to 0.50 μm

b. 0.50 to 0.58 μm

c. 0.58 to 0.68 μm

d. 0.68 to 0.80 μm

e. 0.80 to 0.93 μm

The bands were selected to provide coverage over the 0.40- to 0.93-μm spectral region in wavelength bands that coincide with the transmission windows of the following filters:

a. Wratten No. 12

b. Wratten No. 25A

c. Wratten No. 47B

d. Wratten No. 58

e. Wratten No. 89B

f. Wratten No. 87C

The transmission curves for the above filters are available in Reference 23. These filters are among those most commonly used in remote sensing and, when combined with the commonly used aerial films (see Table 4), can be used to obtain images in the wavelength bands specified above. The sensitivity curves for the films considered in this work are available in Reference 24.

135. The reflectance characteristics of the feature and the background of interest are the only material-related input data necessary for predicting optical density contrasts with the computer model. All other variables (e.g. atmospheric transmission, haze, altitude, film sensitivity, etc.) are handled in the model as discrete points within a spectrum of conditions. For example, atmospheric transmission curves for the various combinations of summer or winter seasons, 0-, 30-, or 60-deg solar zenith angles, and 1.5-, 3.0-, 6.0-, 15.2-, and 100-km altitudes are on file in the computer. Thus, to predict the optical density contrast for a given combination of season, zenith angle, and altitude, the proper files are called and used in the execution of the program. Although this does not allow prediction of contrast values for the infinite combinations of values that exist among those on file, the combinations available provide a variety of conditions that span the spectrum of those observed in the real world.

136. Figure 23 shows, in simplified form, the basic structure chosen for the nomogram. The reflectance data for the feature and the background of interest (average values of reflectance for each

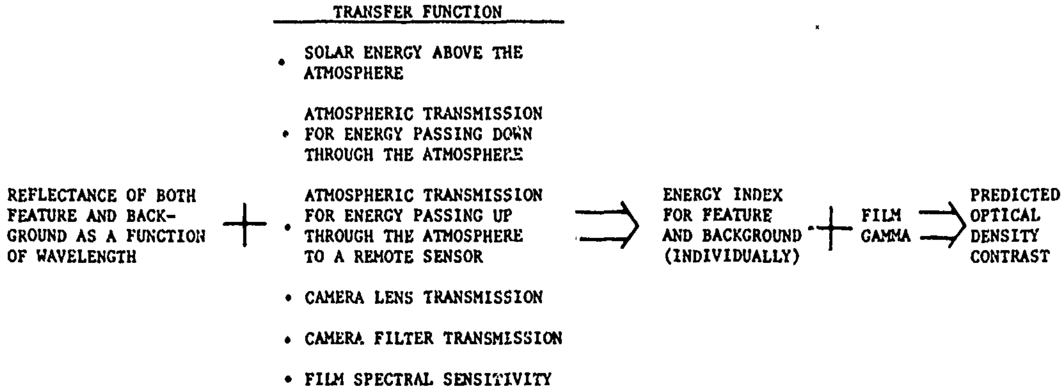

Figure 23. Simplified illustration of the basic structure of the nomogram for predicting optical density contrast

specific wavelength interval) are the only information that must be acquired from an outside source (i.e. the literature or by laboratory or field measurement). As such, reflectance is the only unknown and must be isolated as a single entity in the nomogram.

137. For the sake of simplicity, the other wavelength-dependent variables are combined to form a composite variable (see Figure 23), hereafter termed the transfer function. Specifically, the transfer function is a continuous variate with wavelength resulting from the mathematical combination of the solar energy above the atmosphere, atmospheric transmission for energy passing down through the atmosphere (as a function of season, zenith angle, and haze), atmospheric transmission for energy reflected from the terrain up to a sensor at a given altitude, lens transmission, filter transmission, and film spectral sensitivity. For the purposes of this study the computer files for the individual variables as used in the Photographic Systems Simulation Model were combined mathematically to compute values of the transfer function. The mathematical combination consisted of a simple multiplication or division of file values as necessary and as a

function of wavelength. The resulting data for the transfer function were averaged over the wavelength bands presented in paragraph 134 and tabulated for use with the nomogram. The computed transfer function values are presented in tabular form (see Table 17 for an example). The full set of tables are available in Reference 27.

138. The reflectance data for the feature and the background of interest are combined with the trans er function for a specific set of conditions (i.e. atmospheric conditions, sensor altitude and lens-filter-film characteristics) to compute an energy index. Since the reflectance data and transfer function are both wavelength-dependent, the energy index values for the feature and the background must be obtained by summing partial energy index values for each of the wavelength bands listed in paragraph 134. The energy index values for the feature and the background (totals of partial index values for feature and background individually) are then combined with the gamma of the film being considered for the final step in the computation of the optical density contrast between the feature and the background.

139. In summary, the basic structure of the nomogram is based on three paremeters:

a. Reflectance

b. Transfer function

c. Film gamma

The values for film gamma can be extracted from the literature (see Table 18) or measured if the proper sensitometric equipment is available. The values of the transfer function are computer using the mathematics and files within the computer model and, once obtained, are tabulated for future use with the nomogram. Any future data acquired

concerning atmospheric conditions, films, etc., can be considered by simply computing the appropriate transfer function values and adding them to those previously computed (see Tables 17 and 19).

Presentation of nomogram

140. The nomogram for predicting photographic optical density contrast is presented in two parts in Plates 6 and 7. Part 1 (Plate 6) concerns computation of energy index values for each wavelength band, and Part 2 (Plate 7) concerns computation of optical density contrast using the total energy indices for the feature and the background (computed with Part 1) and the gamma value for the film of interest. Literature-derived values for film gamma are tabulated in Table 18. Example values for the transfer function by season and film type are presented in Tables 17 and 19. The following is a brief description of the procedures for using the nomogram.

Steps for use of nomogram

141. The systematic use of the nomogram consists of the execution of the following steps:

- a. Obtain reflectance data for the feature and the background of interest and compute average reflectance values for the wavelength bands listed in paragraph 134.
- b. Choose film type, filter, season, atmospheric haze, solar zenith angle, and sensor altitude combination of interest.
- c. Obtain from the appropriate table (e. g. Table 17 or 18) the transfer function value for the combination selected in b for each wavelength band.

Special considerations must be made for multiple emulsion films such as color IR (film No. 2443). These considerations are discussed in paragraph 155.

d. For the 0.4- to 0.5-μm wavelength band (see paragraph 134) locate the appropriate reflectance value for the feature and the transfer function value on the appropriate axes of Part 1 of the nomograph (Plate 6).

e. Connect the points with a straight line and read the energy index value where the line connecting the points intersects the energy index axis.

f. Record this value as the partial energy index for the feature in the 0.4- to 0.5-μm wavelength band.

g. Repeat steps d through f for the 0.4- to 0.5-μm wavelength band for the background.

h. Repeat steps d through g for the other wavelength bands (0.5-0.58, 0.58-0.68, 0.68-0.80, and 0.80-0.93 μm).

i. Sum the five partial energy index values for the feature and for the background (separately) to obtain a total energy index value for the feature and a total energy index value for the background.

j. On Part 2 of the nomogram (Plate 2), locate the total energy index values (from step i) for the feature and the background on the appropriate axes.

k. Select the appropriate film gamma (γ) value from Table 18.

l. Project a straight line between the feature and

background energy index values on Part 2 of the nomogram and locate the point where this line intersects the reference line.

m. Project a line perpendicular to the reference line and locate the point of intersection with the appropriate sloping (γ) line. If the γ value obtained from Table 18 does not match numerically one of the γ lines in Part 2 of the nomogram, a linear interpolation can be made between the intersections of the projected line mentioned above and the γ lines on the nomogram that bound the γ value of interest. For example, if a γ value of 1.5 is of interest, the appropriate point for execution of step n below would be the midpoint between the intersections of the projected line and the $\gamma = 1.0$ curve and $\gamma = 2.0$ curve. If the projected line misses all of the γ lines on the nomogram, the optical density contrast value can be assumed to be 3.00.

n. From the point of intersection with the γ line, project a line, parallel to the total energy index and reference lines, to the optical density contrast axis and obtain the photographic optical density difference for the feature and the background with the conditions specified in step b.

Example problem

142. Execution of the steps presented in the previous paragraph can be best illustrated with an example mission design problem. The

following paragraphs present an example of the use of the nomogram and related information to plan a hypothetical photographic remote sensing mission. The problem of interest is to discriminate between juniper trees (feature) and lodgepole pines (background).

143. Step a: As previously stated in paragraph 136, the reflectance values needed for use of the nomogram consist of average values for each wavelength band. If the raw reflectance data available are in the form of a continuous curve, it is necessary to average the data within each wavelength band to obtain the appropriate values for use in the nomograph. The average reflectance values (by wavelength band) for the feature (juniper) and background (lodgepole pines) are as follows:

Wavelength Band, μm	Reflectance, %	
	Juniper	Lodgepole Pine
0.40-0.50	6	6
0.40-0.58	12	10
0.58-0.68	11	10
0.68-0.80	12	32
0.80-0.93	28	51

These data represent mature trees during the late-summer conditions in the northwestern contiguous United States. In some instances, reflectance data for the en[illegible] 40- to 0.93-μm band are not available. The optical density contrast value computed with only a portion of the wavelength bands may differ considerably from the actual value, especially if the reflectances of the feature and the background differ significantly in the wavelength band(s) not considered.

144. Step b: The film-filter combinations that can be considered

to have the most potential for discrimination between a given feature and its background are those with wavelength sensitivities that correspond to wavelength bands in which the reflectances of the feature and the background differ the most. Table 20 presents a summary of the approximate wavelength sensitivities of the film-filter combinations considered in the nomogram. Thus, by visually examining the reflectance data for the feature and the background, determining the wavelength bands of maximum difference, and referring to Table 20, a number of potentially "best" film-filter combinations can be identified for prediction of optical density contrast. The reflectance data presented in paragraph 143 show that the juniper and lodgepole pines have very similar reflectance characteristics in the 0.40- to 0.50-, 0.50- to 0.58-, and 0.58- to 0.68-μm wavelength bands. The reflectance of the lodgepole pines, however, is significantly greater than that of the juniper in the 0.68- to 0.80- and 0.80- to 0.93-μm wavelength bands. Thus, film-filter combinations with sensitivity in these bands would be the best, potentially, for discriminating between the feature and the background. Examination of Table 20 reveals that the film-filter combinations having wavelength sensitivities in the 0.68- to 0.93-μm wavelength range are as follows:

Film	Filter
2424	12
	25
	89B
	87C
2443	None
	12

145. In practice it would be desirable to compute with the

nomogram the image optical density contrast values for each of the film-filter combinations listed in paragraph 134 to determine which would provide the most contrast between the juniper and lodgepole pines. Since the procedures followed for each film-filter combination would be identical, the purpose of this example problem would not be served by the repetitive calculations. To keep the example as simple as possible, the assumption was made that only the 2424-12 film-filter combination was available for use. The following discussion is, therefore, limited to consideration of the adequacy of the 2424-12 film-filter combination for discriminating between the juniper and the lodgepole pines.

146. The remainder of step b concerns selection of season, atmospheric haze, zenith angle, and sensor altitude values. Season is probably the easiest of all the parameters to choose in that only winter and summer conditions are offered. Selection of the appropriate option is obviously a function of the time of year in which the reflectance data were obtained, in this case summer is specified (see paragraph 133).

147. Atmospheric haze can be selected on the basis of the predominant conditions existing in the area to be photographed. The "clear" option represents a 23-km horizontal visibility, and the "hazy" option represents a 5-km horizontal visibility (at sea level). For the purposes of this example problem, the clear condition was assumed.

148. Solar zenith angle is a function of the following:

a. Latitude of the area to be imaged.

b. Time of year.

_c_. Time of day.

Since it is normally (but not always) beneficial to acquire aerial photographs during maximum solar illumination of the terrain, and this condition exists at local apparent noon, it is usually most meaningful to use in the nomogram the solar zenith angle representative of this time of day. During the winter months the zenith angle at local apparent noon will be considerably larger than that for the summer months. An approximate value for solar zenith angle as a function of latitude, time of year, and time of day can be obtained from Table 21, which has been modified from Reference 28. By assuming a latitude of approximately 40 deg (north) and the specified time of year as late summer (paragraph 133), the approximate solar zenith angle for local apparent noon can be obtained from Table 21 as follows:

_a_. Locate the portion of the table for latitude 40 deg.

_b_. Determine the appropriate date symbol from the date table on the right side of the sheets in Table 21. In this case let the appropriate symbol be "I" (assuming 20 August to represent late summer conditions).

_c_. Read the approximate solar zenith angle in the "I" row under the time of 1200 hr (local apparent noon), which in this case turns out to be 32 deg.

Since the nomogram currently considers zenith angles of only 0, 30, or 60 deg, it was assumed that the 30-deg condition was representative for this problem.

149. The optimum sensor altitude for acquiring aerial photographs is a function of the desired image scale and spatial or ground resolution (assuming a film format of 9 × 9 in). Image scale is

purely dependent on the focal length of the camera lens (f) and the altitude of the sensor (H). Scale (S) can be computed by the following relation:

$$S = \frac{H}{f}$$

where scale is expressed as a dimensionless ratio of 1:S. The ground resolution of an image (i.e. the size of an object on the ground that can be detected as a discrete object on the imagery) is a function of altitude, lens focal length, and film spatial sensitivity. For the purpose of this example, it is arbitrarily assumed that a ground resolution of approximately 0.6 m is necessary to enable the interpreter to identify individual tree crowns on the imagery. Examination of Figure 17 reveals that a sensor altitude of no more than approximately 3.0 km would be necessary (i.e. using an 0.152-m focal length lens) to achieve a ground resolution of 0.6 m with 2424 film. A sensor altitude of 3.0 km was assumed for this example.

150. Step c: The values for the transfer function as obtained from Table 17 for film-filter combination 2424-12, mid-latitude, summer, clear, 30-deg zenith angle, and sensor altitude of 3.0 km are as follows:

Wavelength Band, μm	Transfer Function Value
0.40-0.50	0.0025
0.50-0.58	0.0136
0.58-0.68	0.0594
0.68-0.80	0.1020
0.80-0.93	0.0849

It should be noted that in nomogram computation for films with more

than one emulsion, a transfer function value must be obtained and the nomogram applied for each emulsion individually. For example, if the nomogram were used to compute the optical density contrast expected for juniper and lodgepole pines on Kodak Aerochrome Infrared Film (film No. 2443) with a No. 12 filter, it would be necessary to:

<u>a</u>. Obtain transfer function values from Table 19 for each emulsion (cyan, yellow, and magenta) in each wavelength band.

<u>b</u>. Using the nomogram, compute for each emulsion the optical density contrast for the juniper and lodgepole pines.

<u>c</u>. Compare the computed contrast values (one for each emulsion) and adopt the largest value as the contrast representative of that film-filter combination.

If a transfer function in the tables (Tables 17 and 19) has a value of 0.0 it indicates that the film-filter combination to which the transfer function applies is not sensitive to energy in that wavelength band, and the partial energy index for both the feature and the background (i.e. in that wavelength band) can be assumed to be 0.0.

151. <u>Steps d to i:</u> With the above reflectance data and transfer function values, use of the nomogram becomes a simple process. Plates 8-12 illustrate the use of Part 1 of the nomogram to compute the partial energy index values in each wavelength band for the feature and the background, using the appropriate reflectance and transfer function values for each wavelength band. The partial energy index values obtained from Plates 8-12 are summarized below.

Wavelength Band, μm	Energy Index Values	
	Juniper	Lodgepole Pine
0.40-0.50	0.0002	0.0001
0.50-0.58	0.0018	0.0012
0.58-0.68	0.0070	0.0060
0.68-0.80	0.0120	0.0320
0.80-0.93	0.0230	0.0480
Total	0.0440	0.0873

152. Steps j to n: The sums of the partial energy indices (see totals in paragraph 151) provide the total energy index for the feature (juniper) and the background (lodgepole pines). The total energy index values are input to Part 2 of the nomogram (see Plate 13) to determine the intersection on the reference line. A line perpendicular to the reference line is projected from the point on the reference line to the line representing the gamma (γ) of the film of interest. A γ value of 2.0 was used for this example. The intersection of the projected line to the gamma line provides another reference point from which a line is projected down to the density contrast axis to determine the expected optical density contrast. For this example, the expected optical density contrast was computed with the nomogram to be 0.59.

153. The adequacy of a film-filter for a particular application is determined by comparing the predicted optical density contrast to a threshold value that defines the minimum contrast necessary for discrimination. The threshold value varies with the means of examining the imagery. The human eye, for example, can easily discriminate 10 to 15 gray tone levels. A threshold value for the human eye can be obtained by dividing the range of possible optical density values

(0.0 to 3.0) equal to 3.0 by the number of discernable gray tone levels (10 to 15). Thus, an optical density contrast value of 0.30 (3.0 divided by 10.0) or 0.20 (3.0 divided by 15.0) could be specified as a threshold for the human eye. Assuming a threshold value of 0.20 for this example, the computed optical density contrast value of 0.59 indicates that the 2424-12 film-filter combination flown at an altitude of 3.0 km at noon on a clear summer day and in a camera with an 0.152-m focal length lens would be adequate for discriminating between juniper and lodgepole pine trees on a tonal basis.

Evaluation of nomogram

154. The nomogram is intended as a substitute for the computer program of the Photographic Systems Simulation Model. It is thus essential that the predicted values of optical density contrast from the nomogram agree closely with those from the computer program. Table 22 presents a comparison of optical density contrast values for a number of feature-background combinations and two commonly used film-filter combinations (Nos. 2403-12 and 2424-12) as computed with the computer model and with the nomogram. The features and backgrounds were selected to represent a cross section of terrain materials (i.e. soils, rock, and vegetation). Examination of Table 22 shows that the computer- and nomogram-predicted optical density contrast values are in very close agreement for all feature-background and film-filter combinations.

155. Further examination of the data in Table 22 is pertinent for interpreting the optical density contrast values computed with the nomogram. For example, by comparing the nomogram-computed optical density contrast values in Table 22 with the previously adopted

threshold value of 0.20, it is possible to assess the utility of the film-filter combinations considered (2403-12 and 2424-12) for discriminating between the various features and backgrounds in the table. The computed optical density contrast value of 0.59 (well above the 0.20 threshold) indicates that the 2424-12 film-filter combination would provide sufficient contrast for the human eye to discriminate between juniper and lodgepole pines. Conversely, the computed contrast value of 0.04 indicates that the 2403-12 film-filter combination would not provide adequate contrast for the eye to discriminate between juniper and lodgepole pines. In the juniper-lodgepole pine examples, the decision concerning adequacy or inadequacy for discrimination is fairly obvious because of the significant differences between the computed optical density contrast values and the threshold. In other cases the computed contrast value may be very close to the threshold (for example, the computed contrast value of 0.30 for juniper and sagebrush when using the 2403-12 film-filter combination) and judgments concerning the adequacy of the film-filter combination for that specific purpose should be made cautiously.

Summary of results

156. The nomogram in Plates 6 and 7 is essentially a graphical version of the computer program for the Photographic Systems Simulation Model. It provides a previously nonexistent quantitative graphical tool for planning photographic remote sensing missions to enhance the success of a remote sensing data acquisition program. Comparisons of predicted values (Table 22) demonstrates that the nomogram-predicted optical density contrast values are, indeed, representative of those computed with the computer model; therefore, the nomogram is an adequate

substitute for the computer model when computer facilities are not available.

157. Use of the nomogram is simple and straightforward as illustrated in the example problem. The only inputs required are reflectance data for the features and backgrounds of interest. Although only five commonly used films are currently included in the tables of transfer function values, these films cover the spectrum of film types. Additional film types can be added in the future.

PART V: PLANNING THERMAL IR MISSIONS

Introduction

158. The six steps presented in paragraph 86 are equally important for the successful application of thermal IR sensor systems as for photographic remote sensing systems. The problem specification and data acquisition steps (mission planning and execution) are the keystones of the process, since a failure to record the necessary basic information during the imagery acquisition precludes the ability to successfully execute the remaining steps (see paragraph 89) and obtain a useful product. The primary items of concern in planning a thermal IR mission can be summarized in the following questions:

- a. When should the mission be flown?
- b. What sensor system should be used?
- c. How high should the aircraft be?

When to fly

159. The first question (when...) concerns the best time (time of year and time of day) to acquire thermal IR imagery so as to record the information desired. Time of year is often a constraint because of seasonal changes in the terrain surface and corresponding changes in the thermal characteristics of terrain materials. In addition, the average terrain temperature may vary considerably from season to season, i.e., the average terrain temperatures are usually considerably lower in winter months than in the summer because of smaller amounts of solar energy available for warming and generally lower atmospheric temperatures, which can significantly influence thermal IR sensor performance.

160. The diurnal temperature variations for a bare soil area and an adjacent grass area are presented in Figure 24. These data were

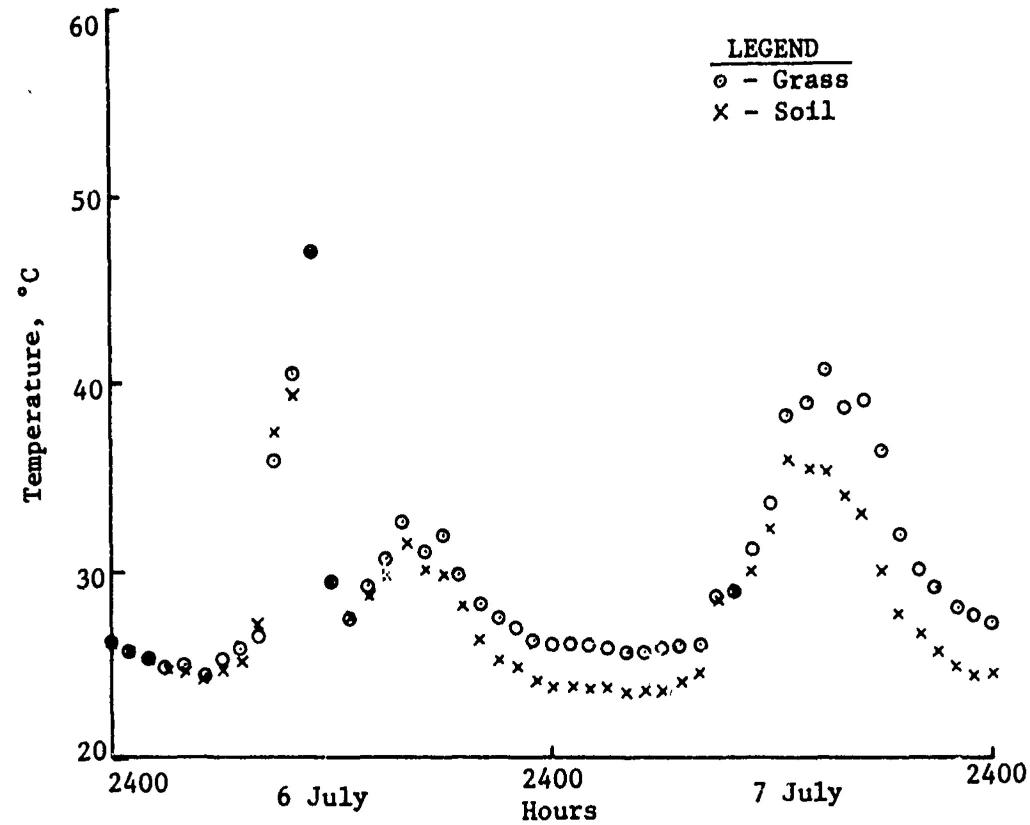

Figure 24. Diurnal temperature variations for bare soil and grass areas, Vicksburg, Mississippi

obtained with an automatic recording device using thermistors accurate to approximately 1°C during July 1973 at the U. S. Army Engineer Waterways Experiment Station. The soil is the Vicksburg loess and the grass is primarily the Bermuda grass native to the area. If an investigator desired to obtain thermal IR imagery on which the bare-soil and grass areas could be distinguished from one another, temperature data such as those in Figure 24 would be essential to plan the mission. With regard to the question of "when," comparison of the bare-soil and grass temperature curves provides a simple means of determining the time of day when the maximum temperature contrast

(temperature differences) occurs and the temperature contrast is a function of time. The optimum time to acquire thermal IR imagery would be the time corresponding to the maximum temperature contrast. Examination of Figure 24 reveals that the maximum contrast occurred generally between 1400 to 1700 hr during daylight hours and between 0300 and 0500 hr during the night. The contrast appeared to be slightly greater during the 1400- to 1700-hr period; however, the contrast was more consistent at night (i.e., very little contrast occurred on 6 July between 1400 to 1700 hr, but a large contrast, up to 4°C, occurred during the same period on 7 July). The lack of contrast on the afternoon of 6 July is attributed to a brief rain that morning and cloud cover that prevented effective warming of the terrain. It appears that the best time for a mission to acquire thermal IR imagery on which the bare soil and grass areas could be distinguished would be between 0300 and 0500 hr, or during 1400 to 1700 hr on clear, sunny days (if rain has not occurred for the previous 24-hr period).

161. The discussion in the previous paragraph illustrates the basic thought processes for selecting the optimum time for a thermal IR mission. Somewhat buried in the discussion is the fact that such items as cloud cover can have a significant bearing on the temperature contrast existing between two terrain features. Contrast will occur only if the differences in material thermal properties are allowed to manifest themselves in the heating and cooling that occur during the diurnal cycle. Any suppression of the heating or the cooling phenomena or "outside" interference from wind (which can have a cooling effect by evaporating surface moisture) can significantly reduce the temperature contrasts that could potentially occur.

What sensor system to fly

162. The second question (what...) in paragraph 158 concerns the sensor system that should be used to acquire the thermal IR imagery. Perhaps an additional question should be inserted at this point: Should the mission be flown at all? Before the mission is flown, it should first be determined if the available thermal IR sensor systems are capable of acquiring the information desired. This can only be determined by having temperature data such as that previously shown in Figure 24, knowledge of the emissivity of the materials, and knowledge of the thermal resolution capabilities of available sensor systems.

163. Figure 25 shows a schematic of a typical thermal IR

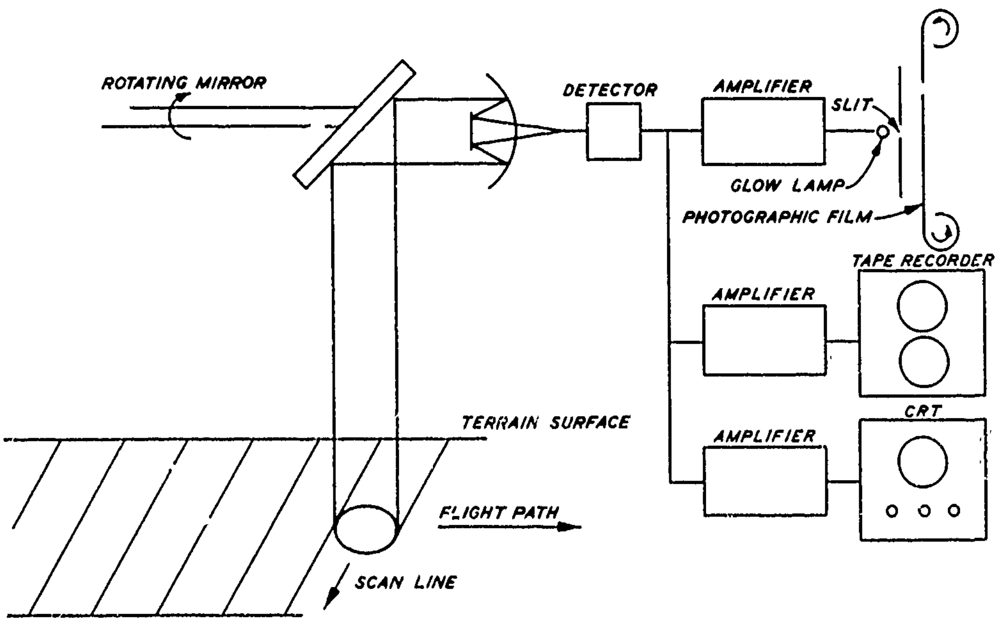

Figure 25. Schematic of typical thermal IR scanner system

sensor system. The rotating mirror reflects the impinging energy from the terrain to the detector. As the mirror rotates, the detector receives energy from a path on the terrain perpendicular to the flight of the aircraft. Successive scan lines are produced by repetition of

this cycle. The detector, normally a semiconductor device, transforms the impinging energy into an electrical analog signal. The detector output is normally amplified and then recorded directly on film on an analog or digital recorder (i.e. magnetic tape) or displayed on a cathode-ray-tube (CRT) screen, or both. To record the detector output directly on film, the amplified signal is used to vary the intensity of a glow lamp. The photographic film advances at a rate dependent on the speed and altitude of the aircraft. The light from the glow lamp is deflected along a line perpendicular to the direction of film advance synchronously with rotation of the rotating mirror, so that the light from the glow lamp that exposes the film will define a photographic image of the EM radiation from the terrain. Thermal IR sensor systems that record information directly on film are normally used for reconnaissance purposes, since the information is rapidly available for visual inspection. It should be noted, however, that directly recording the sensor output on film results in a significant loss in information. This information loss will be discussed in more detail in subsequent paragraphs.

164. In most state-of-the-art thermal IR sensor systems not used for reconnaissance purposes, the detector output is both displayed in real-time on a CRT screen and recorded on magnetic tape using an analog recorder. The production of a film image is accomplished from the analog magnetic tape with the aid of computer processing. The computer processing techniques allow very specialized analyses of the thermal IR system output signal. The real-time display on the CRT screen is used to adjust sensor gain settings. The use of digital magnetic tape recorders is not widespread because

of cost and operational constraints; however, they can be used to very good advantage because of their large dynamic range.

165. In the 3- to 5.5-μm wavelength band, the most popular detector is an indium antimonide (InSb) semiconductor crystal. The InSb detectors are capable of operating as photovoltaic, photoconductive, or photoelectromagnetic devices. The spectral sensitivity ranges from approximately 2.0 to 7.0 μm depending on the operating mode. Efficient use of InSb detectors requires cryogenic cooling to approximately 77 K, primarily to achieve acceptable sensitivity levels.

166. In the 8- to 14-μm wavelength band, mercury-doped-germanium (Ge:Hg) or mercury-cadmium-telluride (HgCdTe) are the most commonly used detectors. The Ge:Hg detectors are photoconductive devices and require cooling to approximately 28 K to achieve acceptable sensitivity levels. The HgCdTe detectors are photoconductive devices that require cooling to approximately 77 K; thus, they have an advantage over the Ge:Hg detectors in that cooling can be achieved with low-cost liquid nitrogen rather than the more expensive coolants needed to reach the 28 K temperature required by Ge:Hg detectors.

167. For wavelengths longer than 3 μm (i.e. for intermediate- and far-IR remote sensing), lenses must be constructed of materials such as semiconductor crystals and plastics (polyethylene and polymethylmethacrylate). These materials are capable of transmitting wavelengths out to 15 μm although their efficiencies are sometimes quite low. The other alternative is reflecting optics. Reflectors coated with an evaporated aluminum film have virtually no transmission losses for IR wavelengths and they have the advantage of being free

of aberrations. Most intermediate- and far-IR scanners utilize reflecting optics for these reasons.

168. Operation of a scanner must meet two requirements: (a) The scanner must dwell a sufficient amount of time on each picture element (pixel), and (b) there must be no underlap of scan lines (overlap is acceptable). The time requirement for each pixel (as determined by the spatial sensitivity of the sensor system) is a function of the time constant of the detector. The dwell time for modern scanners with semiconductor detectors can be in the neighborhood of 10^{-6} sec per pixel (Reference 29). The width of the terrain path scanned per second is equal to the product of the diameter of the pixel, the number of pixels per scan line, altitude, and the revolutions per second of the scanner mirror. To prevent underlap the terrain path scanned per second must be greater than the velocity of the aircraft. Thus, the limits on the revolutions per second for the scanner are set basically by the detector time constant (upper limit) and by the ratio of the velocity to altitude of the aircraft (lower limit), which controls the overlap of scan lines. In addition, the maximum-revolutions-per-second value is limited by the mechanical and strength characteristics of the scanning system.

169. Spatial sensitivities on the order of 1.0 mrad can be achieved with modern scanner systems (Reference 30), although commerical systems commonly have resolutions on the order of 2.0 to 3.0 mrad.

170. Successful application of thermal IR sensors requires a quantitative knowledge of how the major sensor system components affect the informational content of the resulting imagery. The Thermal IR

Systems Simulation Models were developed to provide information concerning sensor system constraints for mission planning. Application of the models and products derived from the models will be presented in subsequent sections.

How high to fly

171. The altitude of the aircraft or, more specifically, the distance between the sensor system and the terrain surface determines the scale of the resulting imagery and the spatial resolution (i.e. the minimum resolvable ground distance). Selection of the proper mission altitude requires consideration of sensor spatial resolution, sensor field of view (scan width), and the required scale for extracting the desired information from the imagery.

Mission Planning Tools

172. In the following paragraphs quantitative tools are presented to aid in the design of thermal IR imagery missions. The tools were designed to provide guidance for answering the previously discussed questions of when, what, and how high to fly. Emphasis is first placed on using the computer models as they are and then using generalized graphical tools developed from the computer models.

When to fly

173. A contrast in energy radiated from terrain materials is the key to contrast on thermal IR imagery and the corresponding ability to properly interpret information about those terrain features on the imagery. The thermal IR sensor systems detect energy differences; thus, it is obvious that the imagery acquisition mission will be most successful if flown when the terrain materials of interest have

the most difference in radiated energy. Since the energy radiated is a function of the temperature and emissivity of the materials, and emissivity of a given material can be considered to be a constant within a specified wavelength band, the time at which the maximum change in radiated energy occurs (i.e. between some feature and background) can be assumed to be the time of maximum temperature difference.

174. As previously discussed in paragraphs 159 to 161, temperature data such as that shown in Figure 24 can be effectively used to determine the time of maximum temperature difference and, thus, the best time of day to fly a thermal IR mission. Examination of the temperature data in Figure 24 shows that there are two times during a diurnal cycle when significant temperature differences can occur, one during daylight hours and one at night. For terrain materials such as soils, previous experiments (Reference 31) have shown that the largest contrast during daylight hours usually occurs between 1400 and 1600 hr. At night the largest contrast usually occurs between 0200 and 0500 hr. The mid-afternoon time occurs because the terrain materials have warmed up to their maximum temperatures during daylight hours and any differences in material thermal properties such as heat capacity have manifested themselves in the form of temperature differences. In the case of wet and dry soils, the dry soils will have a higher temperature than the wet soils (the wet soils have a higher heat capacity and require more energy to reach the same temperature).

175. After sundown the materials start to cool because of conduction losses to the atmosphere and radiation of EM energy. The dry materials, such as soils with low moisture contents, decrease in temperature much more rapidly than wet materials (e.g. soils with high

moisture contents); thus, by 0200 to 0300 hr, the dry soil areas are significantly cooler than the wet soil areas. The time of the maximum temperature difference is a function of wind, soil moisture contents, and atmospheric conditions. It should be noted that moisture content is the largest factor in the thermal properties of soils because it has a heat capacity much higher than soil materials or the air that fills the voids between soil particles in the absence of water.

176. It is important to note that the time of maximum temperature contrast does not occur between 0200 and 0500 hr for all materials. Recent temperature measurements by the author on roofs of large buildings showed that the maximum contrast between roof areas with entrapped moisture in the insulation and adjacent areas with no entrapped moisture occurred between 2000 and 2200 hr. Since roof systems are by no means capable of storing energy in the amounts stored by "Mother Nature" in the terrain, this result is not too surprising; however, it should serve as a reminder that the 0200- to 0500-hr period is not always the time of maximum temperature contrast. The roof temperature example points out the need for temperature data such as that presented in Figure 24.

177. An additional note is necessary concerning the afternoon and nighttime periods of maximum temperature contrast. During the daylight hours the temperature regime is considerably more complex than at night. Solar radiation impinging on the terrain causes warming and corresponding rises in temperature. Energy is lost because of evaporation (aided by the wind) and radiation of EM energy. The warming process may be sporadic due to partial cloud cover or significantly retarded due to long periods of total cloud cover. In the 3- to

5.5-μm band, some solar energy is reflected from the terrain creating an additional energy source. At night, the situation is much simpler with the primary phenomenon being radiation of EM energy from the terrain. Significant cloud cover may reflect some of the emitted energy back to the terrain and radiate a significant amount of EM energy, and the presence of wind may accelerate the cooling process. In most cases, it is beneficial to acquire thermal IR imagery at night to eliminate the "noise" created by the additional complexities of the daylight thermal regime, especially if the sensor system to be used operates in the 3- to 5.5-μm band. The effects of the reflectance of EM energy in the 3- to 5.5-μm wavelength band can be investigated using the "Specific" form of the Thermal IR Systems Simulation Model.

178. In summary, the optimum time for conducting a thermal IR imagery acquisition mission is at the time of maximum temperature difference between the feature of interest and the background or materials surrounding the feature. In most instances, unless warranted by the phenomena being studied or flight constraints, the time of the maximum nighttime temperature contrast is usually better than the daylight maximum contrast period. Temperature data as a function of time are needed to ascertain not only the time of maximum contrast, but also the magnitude of the temperature contrast. The magnitude of the temperature contrast is needed to determine the sensor system thermal resolution necessary to allow detection of a given feature from a background on thermal IR imagery. The required system resolution is, in turn, the primary parameter for evaluation of the adequacy of available or potentially available thermal IR sensor systems to acquire the needed information. The following paragraphs discuss the

evaluation of sensor systems and answer the question: What sensor system to fly?

What sensor system to fly

179. Sensor resolution: The question of what to fly (i.e. the specific sensor system that will be adequate for acquiring the data desired), and for that matter, the more basic question of whether or not the mission can be executed successfully, boils down to a comparison of the thermal resolution capabilities of available sensor systems and the magnitude of the apparent temperature difference between the feature and the background of interest. Since thermal IR sensor systems respond to differences or changes in the EM energy received at the detector, not to temperature changes alone, the thermal resolution of the sensor systems must be defined in terms of apparent temperature. Similarly, the difference in the EM energy radiated from the feature and the background must be described in terms of apparent temperature to account for variations in actual temperature and emissivity and to provide an easy means of evaluating the adequacy of available sensor systems for detecting the feature from the background. The relation between actual and apparent temperature is discussed in detail in Appendix E.

180. If the actual temperature and emissivity of a material are known, the apparent temperature can be computed (i.e. for a specified wavelength band) with Equation E3 in Appendix E or determined with graphs such as those in Figures E1 and E2 for the 3- to 5.5-μm and 8- to 14-μm wavelength bands, respectively. Calculation of apparent temperature for the feature and the background (i.e. using the feature and background temperatures representing the time of

maximum temperature difference) allows determination of the maximum apparent temperature contrast for the feature and the background. For example, if the feature has a temperature of 300 K and an emissivity of 0.90, and the background has a temperature of 303 K and an emissivity of 0.85, the apparent temperatures for the feature and the background (from Equation E3 in Appendix E and for the 3- to 5.5-μm wavelength band) are 297.3 K and 298.7 K, respectively. The apparent temperatures for the feature and the background in the 8- to 14-μm wavelength band (assuming the same ε values are valid) are 293.1 K and 292.3 K, respectively. The resulting apparent temperature differences (contrast) for the 3- to 5.5-μm and 8- to 14-μm wavelength bands are 1.4 K and 0.8 K, respectively. Note that in this example, the apparent temperature differences are smaller than the actual temperature differences, which is not always the case.

181. Planning a mission to acquire imagery on which the feature of interest can be detected within its background requires that the investigator first determine if the thermal IR sensor system or systems available can produce imagery of that quality. Essentially, the thermal resolution, minimum detectable change in apparent temperature, of the sensor system must be less than the apparent temperature contrast for the feature and the background. Secondly, the investigator must determine which sensor system (if more than one is available) would be best for the specific job at hand.

182. Determination of the thermal resolution of a specific system requires consideration of the thermal IR sensor and the means of recording the output signal from the sensor (together the sensor and recorder form the complete sensor system). The resolution

capabilities of the sensor can be determined using the current forms of the Thermal IR Systems Simulation Model. The Specific Model form allows the investigator to examine the adequacy of a specific thermal IR sensor for a specific feature and background (i.e. for given temperature and emissivity values for the feature and the background). Special problems such as daytime missions can be evaluated along with examination of situations wherein the feature area may be less than the pixel area. The General Model form provides definition of the minimum resolvable temperature difference as a function of average terrain temperature for a specific sensor system. Reflectance phenomena or feature area-pixel area relations cannot be examined with the General Model form, but it does provide broad information concerning the resolution capabilities of thermal IR sensor systems.

183. Using the feature-background temperature and emissivity data presented in paragraph 180 and specifying the following sensor parameters:

Detector type: HgCdTe

Detector noise voltage index: 1×10^{-8} v-Hz$^{-1/2}$

Electrical bandwidth: 1.25×10^{6} Hz

Spatial resolution: 2.0 mrad

Wavelength band: 8-14 μm

Effective aperture area: 40 cm^2

Peak response: 2000 v/w

and the following atmospheric conditions:

Mid-latitude summer

23-km haze

1.5-km altitude

the Specific Thermal IR Systems Simulation Model was run to examine the feasibility of obtaining imagery with this particular scanner system on which the feature could be detected from the background. The output of the model was as follows:

Feature Voltage	Background Voltage	Noise Voltage	Voltage Ratio
0.00173	0.00171	0.00001677	1.088

Since the value of the voltage ratio (1.088) is greater than 1.0, the sensor is adequate (theoretically) to detect the feature from the background. This does not include the influence of the recording system, which will be discussed in subsequent paragraphs.

184. Using similar parameters (i.e. for the sensor and atmospheric conditions), the General Thermal IR Systems Simulation Model was run to obtain the following output:

Temperature K	Emissivity	Minimum Detectable Temperature Difference C
200	1.0	2.50
220	1.0	1.56
240	1.0	1.09
260	1.0	0.86
280	1.0	0.70
300	1.0	0.55
320	1.0	0.47
340	1.0	0.39
360	1.0	0.35
380	1.0	0.31
400	1.0	0.27

Examination of the above information shows that the sensor system being evaluated (as described by the parameters input to the model) has a much better thermal resolution for higher temperatures (i.e. for higher average terrain temperatures) than for the lower temperatures. This is primarily because a 1-degree change in temperature in the lower

temperature ranges does not result in as much of a change in the energy radiated as a 1-degree change in temperature in a higher temperature range.

185. It is significant to note that the output from the General Model is in the form of minimum detectable temperature difference as a function of background or average terrain temperature. If emissivity is input as 1.0 (i.e. the value for a blackbody), the same data can be directly interpreted as <u>minimum detectable apparent temperature difference</u> as a function of the <u>apparent temperature</u> of the <u>background</u> or average apparent terrain temperature. The direct interpretability of these data in either actual or apparent temperature stems from the basic definition of apparent temperature as presented in Appendix E; apparent temperature is the temperature of a blackbody ($\varepsilon = 1.0$) that would radiate the same amount of energy (i.e. within a given wavelength band) as an imperfect radiator at a higher actual temperature. Thus, if the value of the apparent temperature of the background (or average terrain temperature) is known, it is possible to determine the thermal resolution of a specific sensor system (minimum detectable apparent temperature difference) directly from the output of the General Thermal IR Systems Simulation Model as presented in paragraph 184.

186. Going back to the apparent temperature contrast value specified for the feature and the background (8- to 14-μm wavelength band) in paragraph 180, it is now possible to rapidly evaluate the capability of the sensor specified in paragraph 183 for detecting the feature from the background. Examination of the model output data in paragraph 184 reveals that the minimum detectable apparent temperature

difference for a background apparent temperature of 292 K is somewhere between 0.55°C and 0.70°C (the values for 300 K and 280 K, respectively). A rapid linear interpolation results in a ΔT_{min} value of approximately 0.61°C for a background apparent temperature of 292 K. Comparison of this value (0.61) to the apparent temperature difference calculated for the feature and the background in paragraph 180 (0.80°C) reveals that the sensor thermal resolution is adequate (i.e. less than the contrast between the feature and the background) to detect the feature from the background. It is important to note that only the sensor has been considered. In the following paragraphs the influence of the recording component of the sensor systems is presented and discussed.

187. Recorder effects on sensor resolution: As mentioned previously in the introduction to this part of the report, the output signal from a thermal IR sensor can be recorded and displayed in a variety of ways. The principal methods used and those discussed herein are direct recording on photographic film, recording on analog magnetic tape, and recording on digital magnetic tape. In all of these recording methods, the signal can be first displayed on a CRT screen for real-time viewing and confirmation of informational content. Direct recording of the sensor output on photographic film is the fastest, but least precise, means of displaying the information gathered with the sensor. Recording on magnetic tape has significant advantages in that more of the basic information (resolution) of the sensor can be retained and analyzed; however, it creates an additional step to acquire a hard copy of the sensor output. Digital tape recorders, because of their larger dynamic range, provide a more

accurate record of the actual sensor output than analog recorders. Analog recorders provide a significant improvement in dynamic range over film, however, and they are easier to use in the aircraft environment.

188. The primary point of interest is, specifically, how does the means of recording the sensor output influence or degrade the thermal resolution of the sensor? That is, what is the effective minimum resolvable temperature difference (at a specified background temperature and for a given wavelength band) when the entire sensor system (sensor and recording components) is considered as a single unit? The following paragraphs present simple, yet rational and quantitative, criteria for evaluating the influence of recording systems on overall thermal IR sensor system performance.

189. The main objective of the following analysis is to determine how the various recording methods available influence the effective thermal resolution of thermal IR sensors. An analysis of the many phenomena involved could go to great depths and analytical extremes; however, such sophistication would not benefit the majority of potential users. Rather, a simple concept has been formulated to arrive at "resolution degradation indices" by considering the recording system noise, sensor system noise, and sensor amplifier gain values. The exact procedure for computing a resolution degradation index is as follows:

a. Calculate recorder system noise.

b. Calculate or determine sensor gain.

c. Calculate or determine sensor noise.

d. Compute total effective sensor system noise.

e. Divide total effective sensor system noise by sensor noise to obtain the resolution degradation index.

190. The recording system noise is computed as if all methods of recording the sensor output were magnetic tape recorders. A full-scale amplitude deflection of 3.0 v is assumed, and the recording system noise voltage is computed by the simple relation:

$$\text{recording system noise voltage} = \frac{3.0 \text{ v}}{\text{amplitude levels}}$$

where the number of amplitude levels (i.e. the number of amplitude levels recordable) is determined from the relation

$$\text{amplitude levels} = 10^{\left(\frac{\text{dynamic range}}{10}\right)^{(1/2)}}$$

with the recording system dynamic range given in decibels (db).

191. The sensor gain is determined by dividing 1.5 v (the mid-range of the recorder amplitude scale) by the sensor output voltage for a 300 K blackbody radiator target and clear summer atmospheric conditions. The output voltages for a 300 K blackbody of a state-of-the-art sensor system operating in the 3- to 5.5-μm and 8- to 14-μm wavelength bands were determined to be approximately 0.00033 v and 0.004 v, respectively, using the Specific Thermal IR Systems Simulation Model. The resulting sensor gain values were approximately 4545 and 375 for the 3- to 5.5-μm and 8- to 14-μm wavelength bands, respectively. The sensor noise voltage for state-of-the-art thermal IR sensors operating in the 3- to 5.5-μm and 8- to 14-μm wavelength bands are approximately 5.61×10^{-6} v and 4.5×10^{-5} v, respectively

(from the Specific Thermal IR Systems Simulation Model).

192. The total effective sensor system noise is computed by the following relation:

$$\left[\left(\frac{\text{recording system noise voltage}}{\text{sensor gain}}\right)^2 + \left(\text{sensor noise voltage}\right)^2\right]^{1/2} = \left(\text{total effective sensor noise voltage}\right)$$

and the resolution degradation index is computed by simply dividing the total effective sensor noise voltage by the original sensor noise voltage.

193. The procedure outlined in the previous paragraphs was applied to determine resolution degradation indices for digital magnetic tape recorders, analog magnetic tape recorders, direct recording on film for analysis with densitometer procedures, and direct recording on film for visual (eyeball) analysis. The resulting approximate resolution degradation indices, the assumed dynamic range values, and corresponding amplitude levels are:

Recording System	Assumed Dynamic Range db	Amplitude Levels	Resolution Degradation Index by Wavelength Band 3-5.5 μm	8-14 μm
Digital tape recorder	60	1000	1.0	1.0
Analog tape recorder	44	158	1.25	1.50
Film analysis by densitometer	36	63	2.0	3.0
Film analysis by visual interpretation	24	15	8.0	12.0

The resolution degradation indices presented above are intended as guidance for assessing the effects of recording systems on sensor

system resolution; they are approximate and should be considered as such. The actual effect is variable depending on a number of factors, such as gain values, sensor noise, and recording system noise, that change from flight to flight and sensor system to sensor system.

194. Use of the resolution degradation indices to compute overall system resolution (for the general form of the Thermal IR Systems Simulation Model) or overall system performance (for the Specific Model form) is as follows: The overall or effective sensor system thermal resolution is simply the product of the minimum detectable apparent temperature difference (from the output of the General Model form) and the appropriate resolution degradation index. Thus, for the model output presented in paragraph 184, the effective thermal resolution for an average background apparent temperature of 300 K and using an analog recording system (8- to 14-μm band) is the product of 0.55 and 1.5, or approximately 0.83 C. Going back to the example feature and background discussed in paragraph 180, the thermal resolution (in the 8- to 14-μm band) for an average background apparent temperature of 292 K is approximately (0.61 × 1.5) 0.92 C. Comparison of the effective thermal resolution (0.92 C) to the feature-background maximum apparent temperature contrast (0.80 C) reveals that the overall system does not have adequate resolution to detect the feature from the background when the analog recording system is considered.

195. System performance as specified by the "voltage ratio" in the output of the Specific Model is modified by dividing the voltage ratio by the square root of the resolution degradation index to obtain an effective voltage ratio, which includes the influence of

the recording system on overall sensor system performance. From the example in paragraph 184, division of the voltage ratio (1.088) by the square root of the resolution degradation index ($1.5^{1/2} = 1.225$) representing the effect of an analog recorder (for the 8- to 14-μm wavelength band) results in an effective voltage ratio of 0.89. Since the effective voltage ratio is less than 1.0, it indicates that the specified sensor with an analog recorder would not be adequate to detect the feature from the background. It is interesting to note that for this example, similar results were obtained by both forms of the Thermal IR Systems Simulation Model. The same resolution degradation indices are applied to the basic output of both model forms to determine effective sensor system thermal resolution. The output from the Specific Model form does not contain much additional information; however, the output of the General Model form provides information on sensor effective thermal resolution over a wide spectrum of background temperature conditions.

Generation of graphics for mission planning

196. The previous paragraphs have emphasized the use of computerized models for evaluating the potential performance of thermal IR sensor systems for specific data acquisition jobs. Computer facilities and personnel trained in their use are at times not at hand, and often inconvenient to use. For this reason the General Model form of the Thermal IR Systems Simulation Model was used to generate graphics defining the thermal resolution capabilities for "state-of-the-art" sensors operating in the 3.0- to 5.5-μm and 8- to 14-μm wavelength bands. Values for the sensor descriptor model

inputs were selected that represent approximate "state-of-the-art" operational capabilities for sensor systems (unclassified) currently available in commercial and military aircraft. The sensor descriptor inputs were obtained from the literature and conversations with commercial sensor designers. The following paragraphs present and discuss the sensor input descriptors used, the predicted sensor thermal resolution capabilities, and graphics summarizing the predictions. The graphics are intended as general, yet quantitative, guidance for planning thermal IR imagery missions.

197. The sensor descriptors input to the model are presented in Table 23. The model predictions for the mission planning graphics were separated into groups representing sensors used in high-performance (jet) aircraft and low-performance (propeller) aircraft. The primary difference between these groups was the electrical bandwidth value, which is commonly four times larger for high-performance aircraft than for low-performance aircraft. In addition, three different values for spatial resolution were considered, the values spanning the spectrum of spatial resolution values normally encountered with currently available thermal IR sensor systems. It should be emphasized at this point that although the subsequent model predictions were limited to the simple combination of descriptor values presented in Table 23, individual sensor systems can be designed to optimize their performance for a given aircraft. In this case, their performance may indeed exceed the predicted values generated with the given inputs and the computer model. Nevertheless, the thermal resolution values generated with the inputs shown in Table 23 are representative of most systems available to both the

private and military (nonstrategic) user for environmental applications. The data generated by the model are not representative of sensors developed or under development that use detector arrays. In addition to the sensor inputs, a clear (23-km visibility) haze condition and a sensor altitude of 1.5 km were assumed for the model execution. Predictions of sensor thermal resolution were made for both the mid-latitude summer and mid-latitude winter atmospheric models.

198. The model (General Model form of the Thermal IR Systems Simulation Model) outputs for the previously defined input parameter values were plotted to provide graphical tools for mission planning. The graphs, which present the minimum detectable apparent temperature difference as a function of background (or average terrain) apparent temperature are presented in Plates 14 to 21. The sensor thermal resolution curves and the resolution degradation indices included in the plates can be used to compute the effective thermal resolution of sensor systems (i.e. to include the effect of the means used to record or display the sensor output). The model outputs from which the graphics were derived are presented in Tables 24 to 31.

199. A quick review of the curves in Plates 14 to 21 reveals that a consistent functional relation exists between sensor thermal resolution (minimum detectable apparent temperature difference) and background apparent temperature. Thermal resolution becomes significantly better (the values become smaller) as the background apparent temperature increases (this relation was previously mentioned in paragraph 184). Another obvious relation is that thermal resolution (at a given background temperature) is slightly better in winter than

in summer. This is primarily because of differences in the atmospheric constituent profile. It should be noted, however, that this effect is somewhat nullified because the average terrain temperature is significantly less in the winter than in summer (i.e. at mid-latitude positions on the earth).

200. Perhaps the most obvious relation is that between sensor thermal resolution and sensor spatial resolution. The thermal resolution, at a given background apparent temperature, increases significantly with an increase in the size of the pixel area on the ground viewed instantaneously by the sensor system. An increase in the pixel area provides a corresponding increase in the energy impinging on the detector (for a given pixel and time of observation), since the energy from a larger ground area is collected by the optics and integrated by the detector. Thus, a sensor system with a spatial resolution of 1 mrad (all other things being equal) has a poorer thermal resolution than a similar sensor with a 2-mrad spatial resolution. Most sensor systems currently in use have spatial resolution values from approximately 1 to 3 mrad. The 5-mrad predicted values of thermal resolution were included to demonstrate the potential significance of sensor spatial resolution on sensor thermal resolution. Clearly, the mission planner must make a trade-off between these two important parameters. Additional aspects of spatial resolution will be discussed in a later portion of the report.

201. Comparison of the thermal resolution curves for high-performance aircraft (Plates 14, 15, 18, and 19) and corresponding curves for low-performance aircraft (Plates 16, 17, 20, and 21) reveals that sensor systems designed for use in low-performance aircraft

have slightly better thermal resolution values. The better thermal resolution occurs as a result of low system noise. The lower system noise results from the smaller electrical bandwidth of sensors used in low-performance aircraft (0.30×10^6 Hz as compared to approximately 1.25×10^6 Hz for high-performance aircraft).

202. An additional comparison is warranted between the sensor systems operating in the 3- to 5.5-μm and 8- to 14-μm wavelength bands. Comparison of the summertime thermal resolution curves for high-performance aircraft sensors in the 3- to 5.5-μm wavelength band (Plate 16) to corresponding curves for the 8- to 14-μm wavelength band (Plate 14) reveals that the thermal resolution of 3- to 5.5-μm sensors is better for warm or higher temperature conditions (e.g. above 320 K), and the thermal resolution of 8- to 14-μm sensor systems is better for cool or low temperatures (e.g. below 320 K). Thus, the latter sensor systems work better for "cool" features and for feature and background temperatures up to approximately 320 K. Sensor systems operating in the former wavelength band are best for "hot" features or feature and background temperatures above 320 K. It should be emphasized again that it is the apparent temperatures of the feature and the background that are important with respect to thermal IR sensor performance. This fact, coupled with the fact that most terrain materials have ε values less than 1.0 (normally in the 0.70 to 0.95 range; see Table 32 for typical ε values (Reference 32)) makes the 8- to 14-μm wavelength band sensors the most versatile for environmental data acquisition. However, in many cases, such as definition of temperature variations within an effluent plume from an industry or power plant, use of the 3- to 5.5-μm wavelength band sensor

systems can provide a significant advantage. Similar relations as discussed above occur for sensors used in low-performance aircraft.

203. Many times a sensor resolution parameter called the "noise equivalent temperature" and expressed as $NE\Delta T$ is used to compare thermal IR sensor system performance. The $NE\Delta T$ is defined as the change in absolute temperature (of a blackbody) required to produce a signal-to-noise ratio of 1.0 in the sensor system (i.e. for a given target temperature usually assumed to be 300 K). The minimum detectable temperature difference parameter predicted by the General Model form of the Thermal IR Systems Simulation Model (for a temperature of 300 K) is essentially equivalent to the $NE\Delta T$ parameter. Thus, the ΔT_{min} parameter can be used as a convenient method to compare the performance of sensor systems. Use of $NE\Delta T$ or ΔT_{min} to compare sensors should be done with the realization that the comparison is being made for a blackbody radiator at 300 K temperature, a very limited comparison at best. Nevertheless, the ΔT_{min} values for the curves presented in Plates 14 to 21 were tabulated for convenience of comparing these values to those published for available sensor systems (see Table 33). It is interesting to note that the $NE\Delta T$ value can vary significantly with respect to season. Published $NE\Delta T$ values seldom consider atmospheric conditions or sensor altitude.

How high to fly

204. The best altitude for execution of a thermal IR imagery mission is a trade-off between the size of the feature about which information is desired and the total area to be imaged. For best results, the size of the pixel or the ground area viewed instantaneously

by the sensor optics should be less than the size of the feature. The pixel diameter (assuming a circular pixel) is a function of sensor altitude (height above the ground) and sensor spatial resolution. The diameter of the pixel is given by the relation (from the computer model)

$$d_{pixel} = 2H \tan\left(\frac{0.180\ mr}{2\pi}\right) \tag{18}$$

where

d_{pixel} = pixel diameter, m

H = sensor height above ground, m

mr = sensor spatial resolution, mrad

The pixel diameter, d_{pixel}, is essentially the resolvable ground distance for the sensor. It is pertinent to point out, however, that the resolvable ground distance is not always discernable on the imagery with the unaided eye. This point will be discussed more in subsequent paragraphs. The above relation for d_{pixel} was used to generate curves defining resolvable ground distance as a function of sensor altitude and spatial resolution. The curves are presented in Figures 26 and 27. The data in the figures are intended as a guidance for planning how high to fly a thermal IR imagery mission.

205. The total terrain area to be imaged can be a factor in selecting the flight altitude and imagery scale. If a very large area is to be imaged, it may be advantageous to obtain imagery at a large scale so the number of flight lines and length of film required can be reduced to a manageable level. It should be emphasized, however, that the spatial resolution (ground resolvable distance) required

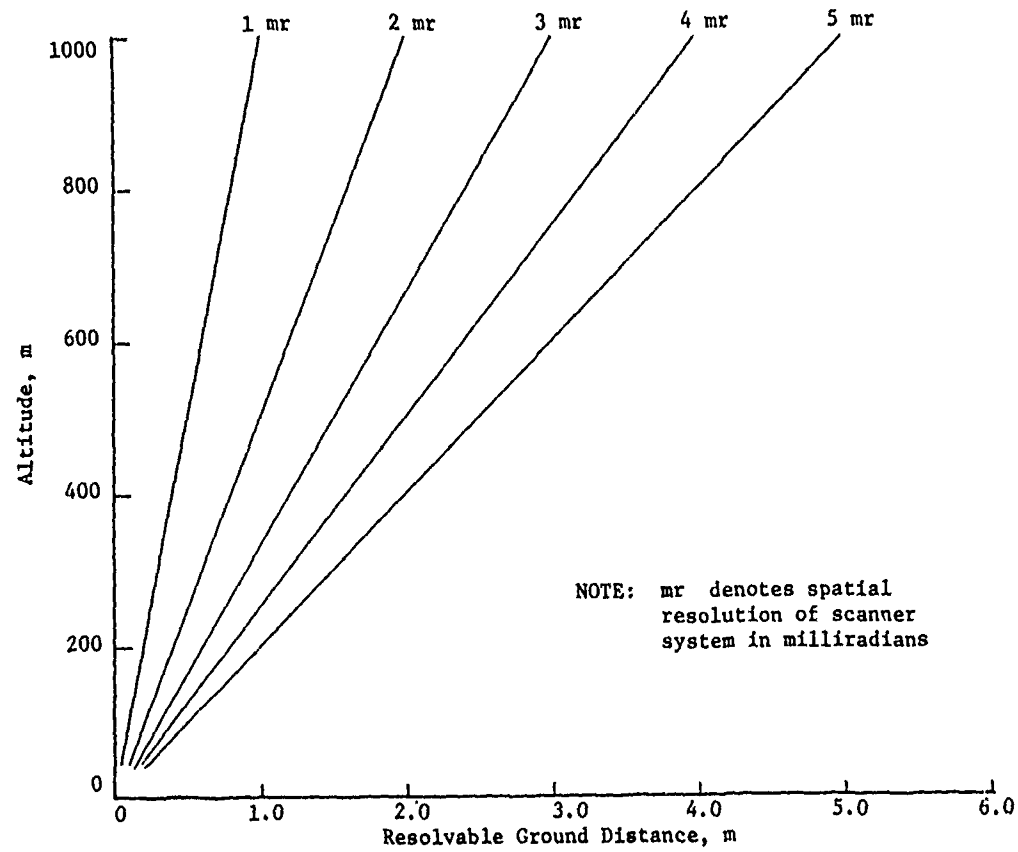

Figure 26. Sensor spatial resolution for altitudes up to 1000 m

for extracting the needed information from the imagery should be the primary factor in selection of the mission altitude. The savings in flight-time or film costs will be to no avail if the imagery obtained is inadequate for the original purpose of the mission. Obviously, a trade-off must be made between ground resolvable distance and imagery scale.

206. The imagery scale for thermal IR systems that record the sensor output directly on film is a function of sensor height above the ground, the total sensor scan width or scan angle, and the width of the film on which the information is recorded. The relation can be expressed as follows:

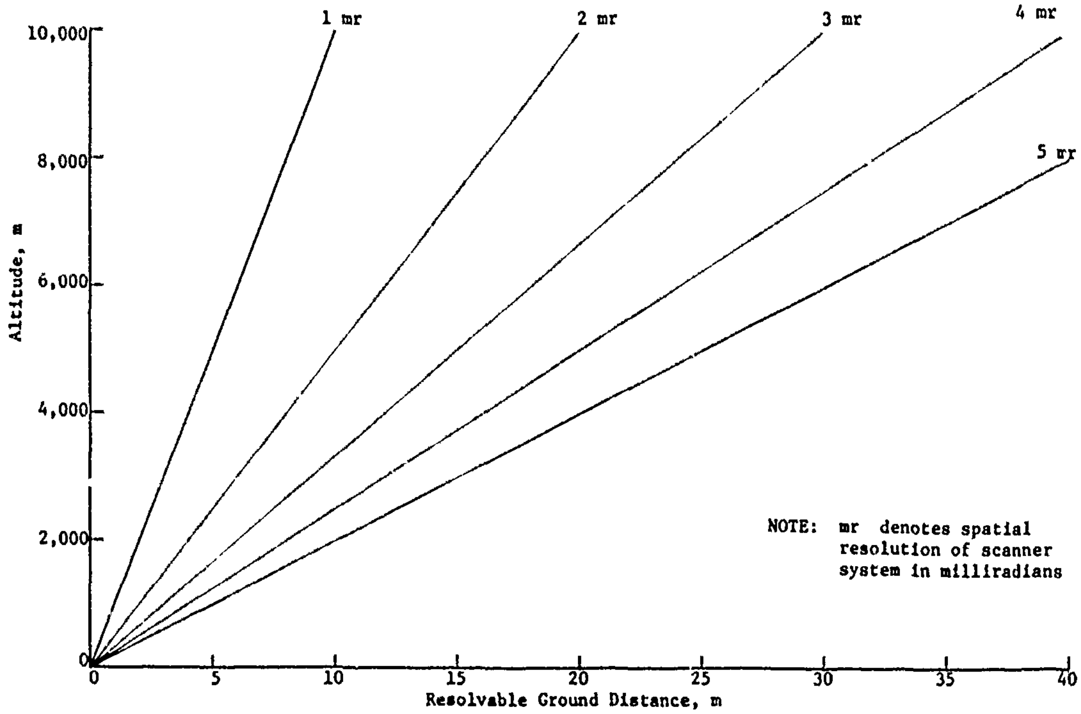

Figure 27. Sensor spatial resolution for altitudes from 0 to 10,000 m

$$\text{image scale} = \frac{200H \tan \phi}{f_w} \tag{19}$$

where

H = sensor height above ground, m

ϕ = one-half the scan angle or total scan width, deg

f_w = width of film, cm

The above equation was used to generate the data presented in Table 34 and Figure 28, which relate imagery scale to sensor height above the ground, scan width, and film width for selected values of each. Scan widths are typically 60 to 120 deg and film widths are typically 7 cm (70-mm film) or 12.7 cm (5-in.-wide film), although others can be used. The curves in Figure 28 are intended as general guidance for planning thermal IR imagery missions. If sensor systems are used that

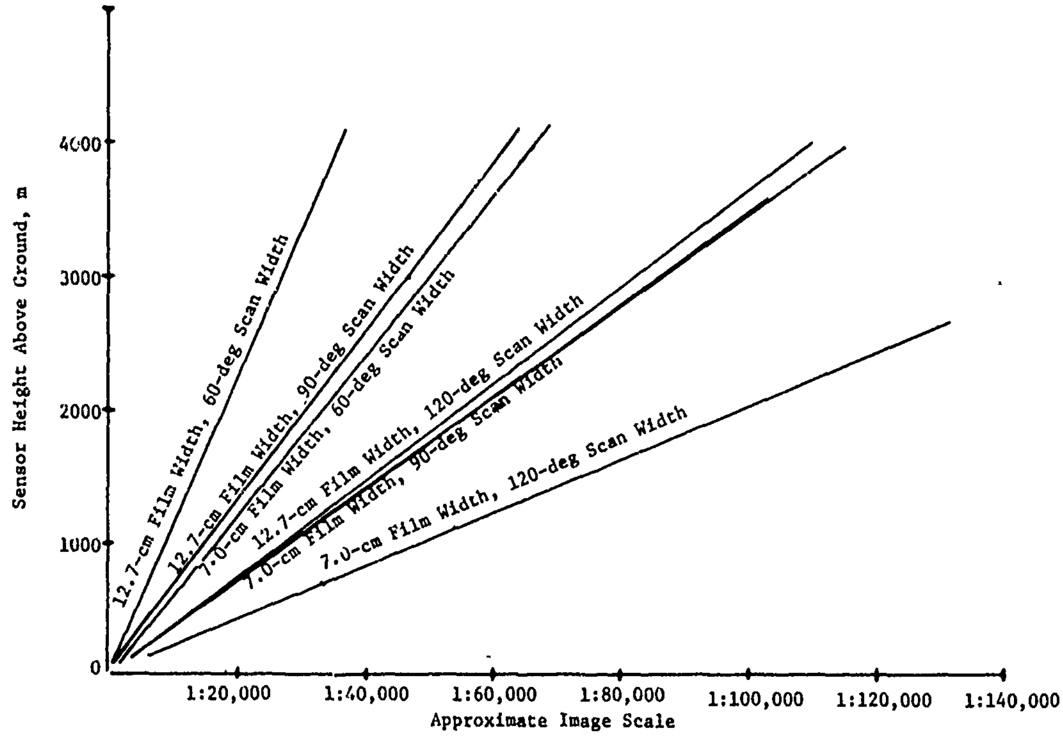

Figure 28. Thermal IR imagery scale as a function of altitude, scan width, and film width

record the sensor output on magnetic tape and the tape is then used to produce a photographic image, a variety of scale options are available since machine processing techniques can be used to produce a multitude of products.

207. At this point it is pertinent to examine for a given set of sensor descriptors the resolvable ground distance and imagery scale. For example, a sensor system flown at 300 m above the ground and having a 1.0-mrad spatial resolution has a resolvable ground distance of approximately 0.30 m. If the output of the sensor is recorded on film 12.7 cm wide (for a 120-deg scan angle), the resulting imagery has a scale of approximately 1:8200. The significance of the 1:8200 scale is that 1 cm on the film represents approximately 8200 cm on the ground. Thus, the resolvable ground distance (theoretical)

of 0.30 m is represented by a mere 0.0037 cm or 37 μm, which is roughly the order of magnitude of the EM energy wavelengths being detected by the sensor! The 37-μm distance is not easily depicted with the unaided eye; however, since films commonly have silver halide grains (crystals) with dimensions on the order of 0.1 to 5.0 μm, the films have latent resolution capabilities adequate to record the information. It requires sophisticated devices such as scanning microdensitometers to use the spatial information inherent in the film image. One such device, the Photomation Mark II system manufactured by Optronics International, Inc., used at the U. S. Army Engineer Waterways Experiment Station is capable of examining the spatial information of film transparencies with a 12.5-μm scanning spot size. It is important to realize, however, that the sensor resolvable ground distance cannot always be observed physically on the image by the unaided eye.

Example Application of Mission Planning Tools

Problem hypothesis

208. The following paragraphs illustrate the use of the thermal IR mission planning tools reported herein by designing a mission for a hypothetical problem. The problem concerns mapping the distribution of major geologic conditions within a watershed to estimate watershed response and loss rates. To keep the problem simple (so as not to mask the illustrations with unnecessary detail), the hypothetical watershed is comprised of only two major geologic units, alluvium and shale. The alluvium is considered to be fairly porous and permeable, and the shale is nearly impervious. The desired product is a map

showing the distribution of these geologic units. The following paragraphs address when, what, and how high to fly using the tools presented herein.

When to fly

209. Time of year: The first question addressed is when to fly. The time of year has considerable influence on the mission since the hypothetical watershed, hereafter termed watershed "H," is snow covered from late fall to early spring. Thus, the imagery cannot be obtained successfully during the winter months. The summer months present a different problem. By midsummer the alluvial and, to some extent, the shale areas are covered with vegetation. The presence of different types of density of vegetation on the different geologic units may in itself supply a sufficient temperature contrast between the respective areas to allow discrimination by thermal IR systems. The reliance on vegetation differences to map geologic variations places a great dependence on the consistency of the vegetation-geologic unit relations. It would be more advantageous to use a more direct measure of the geologic units.

210. During the late spring months, some vegetation is present; however, the majority of the area is still quite barren from the winter cold. The solar energy incident on the terrain surface is considerably greater than during the winter months and, thus, provides the advantage of a higher average terrain temperature (resulting in better sensor performance). For these reasons late spring is considered the best time of year for this particular mission.

211. Time of day: Selection of the best time of day requires knowledge of the diurnal variations in the temperature of the alluvium

and shale. Figure 29 presents a late May temperature history for

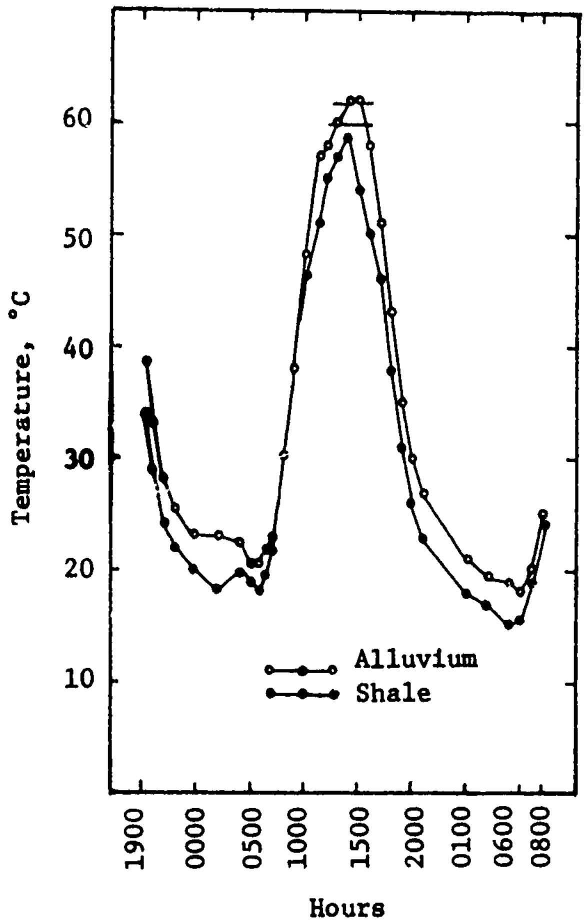

Figure 29. Temperature variations for alluvium and shale as adapted from Reference 33

alluvium and shale as adapted from Reference 33. Examination of the curves in the figure reveals that the shale is consistently cooler than the alluvium. The relatively cool temperature of the shale with respect to the alluvium can be explained by the difference in thermal inertia of the two materials. The thermal inertia, a measure of the resistance of a material surface to temperature change, is defined by the relation (Reference 33)

$$\text{thermal inertia} = K\rho C$$

where

K = thermal conductivity

ρ = specific gravity

C = specific heat

The shale had a measured specific gravity of approximately 1.0 and the alluvium, a corresponding value of approximately 1.3. The higher thermal inertia of the alluvium caused those areas to react more slowly to external temperature changes than the shale areas, thus resulting in the alluvium having a higher temperature during predawn hours.

212. Further examination of the curves in Figure 29 reveals that the maximum temperature difference between the alluvium and shale occurred between 0400 and 0600 hr during the night and between 1530 and 1630 hr during the daytime. Because of the additional complications of the thermal regime during the daytime (see paragraph 160), only the nighttime temperature contrast will be considered further. Thus, the best time of day for the flight was selected to be 0500 hr.

213. One additional note should be included concerning the time of day for a mission. Most missions for acquiring imagery require a considerable amount of time in the air, especially if a fairly large ground area is to be imaged. It is often necessary to compute the total air time required to complete the mission (by considering number of flight lines, total length of each flight line, and aircraft speed) and compare this time period to temperature, data such as that shown in Figure 29, to ensure that the entire area of interest can be imaged within the time period of maximum temperature difference. For example,

a flight that would require 1.5 hr for execution would fit well within the 0400- to 0600-hr time of maximum temperature difference for the alluvium and shale. The same mission may not be as successful if conducted during the daytime (1530 to 1630 hr) because the temperatures of the alluvium and shale are changing very rapidly during this period and the temperature difference changes also. The imagery obtained during afternoon hours may not be uniform from the beginning to the end of the flight (i.e., the same gray tones will not necessarily represent the same ground conditions at the beginning and at the end of the mission).

What sensor system to fly

214. For the purpose of this example problem, the emissivity of shale was assumed to be 0.75 and 0.92 for the 3- to 5.5-μm and 8- to 14-μm wavelength bands, respectively. The emissivity of the alluvium was assumed to be 0.75 and 0.93 for the two bands, respectively. From the curves in Figure 29, the temperature of the shale and alluvium at 0500 hr were approximately 288.0 K (15.0 C) and 291.5 K (18.5 C), respectively. Using equation E3 in Appendix E or the graphs in Figures E1 and E2, the apparent temperatures for the shale and alluvium can be found to be as follows:

	Apparent Temperature, K	
	3-5.5 μm	8-14 μm
Shale	281	282.9
Alluvium	285	286.9

From these data it is obvious that the apparent temperature difference between the shale and alluvium is 4.0 C for both the 3- to 5.5-μm and 8- to 14-μm wavelength bands. The computed apparent temperature

difference and average terrain apparent temperature (approximately 283 K for the 3- to 5.5-μm band and 285 K for the 8- to 14-μm band) are the data needed to examine potential sensor systems for acquiring the shale-alluvium distribution data for watershed "H."

215. For the purpose of this example problem the assumption was made that three thermal IR scanner systems are available for use. The available sensor systems (hereafter called sensor 1, sensor 2, and sensor 3) have the following characteristics:

Sensor*	Aircraft Type	Wavelength Sensitivity μm	Spatial Resolution mrad	Recording System
1	High performance	3-5.5	2.0	Film
2	High performance	8-14	2.0	Film
3	Low performance	8-14	2.0	Analog recorder

* All have a scan angle width of 120 deg.

216. Examination of the appropriate thermal resolution-background temperature curves in Plates 14 to 21 reveals that the thermal resolution (minimum detectable apparent temperature difference) of the sensors for the appropriate average terrain (background) apparent temperatures for the shale and clay are as follows for summer atmospheric conditions:

Sensor	Thermal Resolution, °C
1	1.56
2	0.70
3	0.31

If the recording systems are considered, the effective thermal

resolution of the sensors (realizing that the film product from sensors 1 and 2 can be interpreted visually or by a densitometer) can be easily computed with the resolution degradation indices presented in paragraph 198. The effective thermal resolution values for the sensors were computed to be:

Sensor	Effective Thermal Resolution, °C
1 (visual)	12.5
1 (densitometer)	3.1
2 (visual)	8.4
2 (densitometer)	2.1
3	0.47

217. The apparent temperature difference for the shale and alluvium was computed to be 4.0°C for both the 3- to 5.5-μm and 8- to 14-μm wavelength bands. Comparison of this value with the effective thermal resolution values presented in the previous paragraph clearly eliminates the use of sensors 1 and 2 if the imagery is interpreted visually. Both sensors 1 and 2 would be adequate if the film was interpreted with the aid of a densitometer. Sensor 2 would be better than sensor 1 because of its significantly better effective thermal resolution. Sensor 3 is clearly the best for the job with respect to effective thermal resolution. The product from sensor 3 is an analog magnetic tape, which will require an additional step to produce interpretable imagery. The resources available to produce these images in-house or to interpret the film output of sensor 2 with a densitometer must be weighed to make this decision.

218. Another consideration is the time required to obtain the imagery both from the previously discussed point of the time period of

an acceptable temperature contrast and the cost per hour for conducting the mission. The high-performance aircraft (sensor 2) would be able to obtain the imagery in a significantly shorter time than the low-performance aircraft. For this reason, assuming that the watershed is quite large, the high-performance aircraft (sensor 2) combination may be the best compromise for the mission.

<u>How high to fly</u>

219. The best altitude for the mission can be selected only if the precise size of the area to be imaged is known and the desired ground resolution can be specified. The curves in Figures 27 and 28 provide a quick reference to determine the resolvable ground distance and imagery scale as a function of aircraft altitude. A mission flown with sensor 2 at an altitude of 3000 m would result in a resolvable ground distance of approximately 6 m and an imagery scale (assuming a 12.5-cm-wide film is used) of approximately 1:40,000. A single flight line would cover a terrain swath approximately 5-km (approximately 3 miles) wide at this scale.

PART VI: SUMMARY

220. The Photographic Systems Simulation Model and the Thermal IR Systems Simulation Models provide a new dimension for systematic evaluation of remote sensor performance and quantitative mission design previously unavailable to personnel applying remote sensors to civil engineering and environmental problems. The systems models and the graphical products derived from the models allow selection of the best (of those available) sensor system for a specific data acquisition problem by providing a means of quantitatively comparing the expected performance of a variety of sensors for the specific data needs. In addition, the models and derived products provide a means of quantitatively planning the remote sensing mission to optimize the informational content of the resulting imagery for the specific data needs.

221. The systems models consider the major phenomena that influence the informational content of photographic and thermal IR sensors imagery. As is usually the case, a variety of analytical methods could have been used to model these phenomena. The methods used were chosen to provide a comprehensive description of the phenomena and yet minimize the number of hard-to-get inputs required to execute the models. As such, the models were oriented toward the people who apply remote sensors rather than those who design them.

222. The existing, on-the-machine forms of the systems models have a variety of atmospheric condition-sensor altitude-sensor characteristic combinations on file that can be used for general evaluation and mission planning. The variable combinations on file are

intended to represent the spectrum of conditions that the user might encounter or be interested in. It should be emphasized, however, that the framework of the systems models has been designed to allow incorporation of the descriptors of additional sensor systems, atmospheric conditions, etc., for more specific or detailed investigations. In addition, simple modifications can be made to the analytical procedures used to account for additional variables currently not considered or to change the method used to describe individual variables presently incorporated in the models. The systems models as they are reported are, thus, intended to be a first step toward the total capability desired by individual users.

223. Minimizing the inputs necessary for model execution required a number of simplifying assumptions concerning such items as the interrelation of the complex atmospheric phenomena and the interaction of EM energy with sensor systems. These assumptions, in the opinion of the author, do not significantly influence the relative performance predictions output by the models. The simplifying assumptions do limit the use of the models for such things as sensor system design in that not all of the specific parameters used by sensor designers are considered individually. The models and the graphics derived from the models provide new and powerful tools that will significantly enhance the cost-effectiveness of applying remote sensing techniques to civil engineering and environmental problems, such as those involved in predicting the hydrologic response of watersheds. A detailed sensitivity analysis is currently being conducted for both the Photographic and Thermal IR Systems Simulation

Models to identify the input parameters that most influence the models' outputs. The results of these studies will be documented in the near future.

LITERATURE CITED

1. Link, L. E., Jr., and Shamberger, J. H., "Application of Remote Sensors to Army Facility Management," Technical Report M-74-2, Feb 1974, U. S. Army Engineer Waterways Experiment Station, E, Vicksburg, Miss.

2. Badgley, P. C., "Planetary Exploration from Orbital Altitudes," Photogrammetric Engineering, Mar 1966.

3. Salomonson, V. V., "Advances in Water Resources Monitoring from Space," NASA Goddard Space Flight Center Reprint X-913-74-44, 1974.

4. Burgy, R. H., and Algazi, V. R., "An Assessment of Remote Sensing Applications in Hydrologic Engineering," Research Note No. 4, Sep 1974, U. S. Army Engineer Hydrologic Engineering Center, Davis, Calif.

5. Robinove, C. J., "Remote-Sensor Applications in Hydrology," Proceedings of the Fourth Symposium on Romote Sensing of the Environment, University of Michigan, Ann Arbor, Mich., Apr 1966.

6. Robinove, C. J., "The Status of Remote Sensing in Hydrology," Proceedings of the Fifth Symposium on Remote Sensing of the Environment, University of Michigan, Ann Arbor, Mich., Apr 1968.

7. Cannon, P. J., "The Application of Radar and Infrared Imagery to Quantitative Geomorphic Investigations," Remote Sensing of Earth Resources, Vol II, University of Tennessee, Tullahoma, Tenn., Mar 1973.

8. Stevens, A. R., "Land Cover Delineation Methods and Presentation Alternatives Applicable to the Tennessee River Watershed," Remote Sensing of Earth Resources, Vol II, University of Tennessee, Tullahoma, Tenn., Mar 1973.

9. Schmugge, T. J., et al., "Hydrologic Applications of NIMBUS 5 ESMR Data," NASA Goddard Space Flight Center Reprint X-910-74-51, Feb 1974.

10. Meier, M. F., Campbell, W. V., and ALEXANDER, R. H., "Multispectral Sensing Test at South Cascade Glacier, Washington," Proceedings of the Fourth Symposium on Remote Sensing of Environment, University of Michigan, Ann Arbor, Mich., Apr 1966.

11. Moxhman, R. M., "Aerial Infrared Surveys in Water Resources Studies," U. S. Geological Survey Technical Letter NASA-74, 1967.

12. Stingelin, R. W., and Fischer, W., "Advancements in Airborne Infrared Imaging Techniques in Hydrological Studies," American Water Resources Conference, San Francisco, Calif., 1967.

13. Wood, C. R., "Evidences of Ground-Water Flow into the Lehigh River, Pennsylvania," Proceedings of the 37th Annual Convention of the American Society of Photogrammetry, Washington, D. C., Mar 1971.

14. Castruccio, P. A., "Use of Remote Sensing in Hydrology," XXII International Astronautics Congress, Brussels, 1971.

15. Blanchard, J. K., "Measuring Watershed Runoff Capability with ERTS-1," Presented at the 3rd ERTS-1 Symposium, Washington D. C., Dec 1973.

16. Ambaruch, R., and Simmons, J. W., "Developments in Applications of Remote Sensing to Hydrology Through Continuous Simulation," Remote Sensing of Earth Resources, Vol II, University of Tennessee, Tullahoma, Tenn., Mar 1973.

17. Link, L. E., Jr., "Sensitivity of Normalized Classification Procedures for Floodplain Soils," Pennsylvania State University, State College, Pa. (to be published).

18. Link, L. E., Jr., "The Use of Remote Sensing Systems for Acquiring Data for Environmental Management Purposes; A Procedure for Predicting Image Contrasts in Photographic Remote Sensor Systems," Technical Report M-74-8, Report 1, Nov 1974, U. S. Army Engineer Waterways Experiment Station, CE, Vicksburg, Miss.

19. McDowell, D. Q., "Spectral Distribution of Skylight Energy for Two Haze Conditions," Photogrammetric Engineering, Vol XL, No. 5, May 1974.

20. Selby, J. E. A., and McClatchey, R. M., "Atmospheric Transmittance from 0-25 to 28.5 μm: Computer Code LOWTRAN 2," AFCRL Report 72-0745, Dec 1972, U. S. Air Force Cambridge Research Laboratories, Bedford, Mass.

21. McClatchey, R. A., et al., "Optical Properties of the Atmosphere," AFCRL Report 71-0279, May 1971, U. S. Air Force Cambridge Research Laboratories, Bedford, Mass.

22. Legault, R. R., "Summary of Michigan Multispectral Investigations Program," Third Annual Earth Resources Program Review, Vol II, Agricultural, Forestry, and Sensor Studies, NASA Manned Spacecraft Center, Houston, Tex., Dec 1970.

23. "Kodak Filters for Scientific and Technical Uses," Kodak Publication B-3, Eastman Kodak Company, Rochester, N. Y., 1970.

24. "Kodak Data for Aerial Photography," Kodak Publication M-29, Eastman Kodak Company, Rochester, N. Y., 1971.

25. American Society of Photogrammetry, "Manual of Remote Sensing," Theory, Instruments, and Techniques, Vol 1, Falls Church, Va., 1975.

26. Tanguay, M. G., Hoffner, R. M., and Miles, R. D., "Multispectral Imagery and Automatic Classification of Spectral Response for Detailed Engineering Soils Mapping," Proceedings, Sixth International Symposium of Remote Sensing of Environment, Vol 1, University of Michigan, Ann Arbor, Mich., Oct 1969.

27. Link, L. E., Jr., and Stabler, J. R., "The Use of Remote Sensing Systems for Acquiring Data for Environmental Management Purposes; Technical Report M-74-8, Report 3 (in preparation), U. S. Army Engineer Waterways Experiment Station, CE, Vicksburg, Miss.

28. "Kodak Aerial Exposure Computer," Kodak Publication R-10, Eastman Kodak Company, Rochester, N. Y., 1970.

29. "Remote Sensing with Special Reference to Agriculture and Forestry," National Academy of Sciences, Washington, D. C., 1970.

30. Colwell, R. N., "A Summary of the Uses and Limitations of Multispectral Remote Sensing," Proceedings, First Annual International Remote Sensing Institute Symposium, Vol 2, Sacramento, Calif., 1969.

31. Link, L.E., Jr., "Aerial Infrared Survey of the Walter F. George Lock and Dam, Chattahoochee River, Alabama-Georgia," Miscellaneous Paper M-70-3, May 1970, U. S. Army Engineer Waterways Experiment Station, CE, Vicksburg, Miss.

32. Office of Naval Research, Handbook of Military Infrared Technology, Department of the Navy, Washington, D. C., 1965.

33. Wolfe, E. W., "Thermal IR for Geology," Photogrammetric Engineering, Vol 37, No. 1, Jan 1971.

SUPPLEMENTARY TABLES AND PLATES

Table 1

Film Gamma (γ) Values Used in the Model

Film No.	Gamma, γ	Film Description
2402	1.65	Kodak Plus-X Aerographic
2403	1.30	Kodak Tri-X Panchromatic
2448	2.00	Kodak Ektachrome MS Aerographic
2443	2.00	Kodak Aerochrome Infrared
2424	1.50	Kodak Infrared Aerographic

Table 2

Output of Specific Form of Thermal IR Systems Simulation Model

Temperature K	Feature Emissivity	Voltage v	Temperature K	Background Emissivity	Voltage v	Noise Voltage, v	Voltage Ratio
300.0	0.90	0.00270	303.0	0.85	0.00267	0.00001677	1.70036

LEGEND

Sensor Characteristic

Detector Type: HGCDTE
Detector Noise Voltage Index (volt/sqrt (Hertz)): 0.1000E-07
Electrical Bandwidth (Hertz): 0.1250E 07
Spatial Resolution (milliradians): 2.5
Wavelength Band (micrometers): 14.0
Effective Aperture Area (cm^2): 40.0
Peak Response (volt/watt): 0.2000E 04

Atmosphere Condition

Latitude-Season: Mid-latitude Summer
Haze (km): 23
Altitude (km): 1.5

If voltage ratio >1.0, detection is possible.

Table 3

Output of General Form of Thermal IR Systems Simulation Model

Background Temperature K	Emissivity	Minimum Detectable Temperature Difference °C
200.0	1.0	2.50
220.0	1.0	1.56
240.0	1.0	1.09
260.0	1.0	0.86
280.0	1.0	0.70
300.0	1.0	0.55
320.0	1.0	0.47
340.0	1.0	0.39
360.0	1.0	0.35
380.0	1.0	0.31
400.0	1.0	0.27

LEGEND:

Sensor Characteristics

Detector Type: HGCDTE

Detector Noise Voltage Index (volt/sqrt (Hertz)): 0.1000E-07

Electrical Bandwidth (Hertz): 0.1250E 07

Spatial Resolution (milligradians): 2.0

Wavelength Band (micrometer): 14.0 - 8.0

Effective Aperature Area (cm^2): 40.0

Peak Response (volt/watt): 2000.0

Atmosphere Condition

Latitude-Season: Mid-latitude Summer

Haze (km): 23

Altitude (km): 1.5

Table 4

Film-Filter Combinations Considered for Example Problem in Text

Film Number	Filter Number
2402	3 (Haze)
	12 (Yellow)
	47B (Blue)
	58 (Green)
	25A (Red)
2403	3
	12
	47B
	58
	25A
2448	3
2443	3
	12
2424	12
	25A
	87C (Infrared)
	89B (Infrared)

Table 5

Photographic Systems Simulation Model Output

FILMN	FILTER	FEATURE EXPT FOR D=1.0 (SEC)	BACKGROUND EXPT FOR D=1.0 (SEC)	FEATURE DENSITY (DF)	BACKGROUND DENSITY (DB)	DF-DB
2402	12	0.001513	0.001326	1.000000	1.094529	0.094529
2403	12	0.000463	0.000402	1.000000	1.079448	0.079448
2402	47B	0.018861	0.027418	1.268085	1.000000	0.268085
2403	47B	0.007943	0.011902	1.228347	1.000000	0.228347
2402	58	0.011974	0.011754	1.000000	1.013305	0.013305
2403	58	0.005833	0.005697	1.000000	1.013401	0.013401
2402	25A	0.002336	0.002013	1.000000	1.106829	0.106829
2403	25A	0.000617	0.000530	1.000000	1.085560	0.085560
2402	3	0.001246	0.001135	1.000000	1.067347	0.067347
2403	3	0.000404	0.000359	1.000000	1.066131	0.066131
2448C	3	0.002421	0.002078	1.000000	1.132404	0.132404
2448Y	3	0.012483	0.016142	1.223302	1.000000	0.223302
2448M	3	0.004812	0.004824	1.002141	1.000000	0.002141
2443C	3	0.005243	0.005006	1.000000	1.030200	0.030200
2443Y	3	0.002103	0.002143	1.012217	1.000000	0.012217
2443M	3	0.001517	0.001306	1.000000	1.097632	0.097632
2443C	12	0.006393	0.005801	1.000000	1.063316	0.063316
2443Y	12	0.003539	0.003312	1.000000	1.043074	0.043074
2443M	12	0.001612	0.001382	1.000000	1.100234	0.100234
2424	12	0.000701	0.000646	1.000000	1.071941	0.071941
2424	25A	0.000742	0.000684	1.000000	1.070306	0.070306
2424	87C	0.004490	0.004473	1.000000	1.003184	0.003184
2424	89B	0.001080	0.001027	1.000000	1.043777	0.043777

LEGEND

FEATURE SILT 10% MOISTURE CONTENT
BACKGROUND CLAY 10% MOISTURE CONTENT
ATMOSPHERE MIDLATITUDE SUMMER HAZE=23 KM
ZENITH ANGLE 30 DEG.
DISTANCE TO SENSOR 1.50 KM

Table 6

Photographic Systems Simulation Model Output

FILMN	FILTER	FEATURE EXPT FOR D=1.0 (SEC)	BACKGROUND EXPT FOR D=1.0 (SEC)	FEATURE DENSITY (DF)	BACKGROUND DENSITY (DB)	DF-DB
2402	12	0.001587	0.001396	1.000000	1.092072	0.092072
2403	12	0.000485	0.000423	1.000000	1.077492	0.077492
2402	47B	0.018408	0.024852	1.215096	1.000000	0.215096
2403	47B	0.007710	0.010628	1.181225	1.000000	0.181225
2402	58	0.012473	0.012245	1.000000	1.013245	0.013245
2403	58	0.006077	0.005937	1.000000	1.013146	0.013146
2402	25A	0.002453	0.002120	1.000000	1.104532	0.104532
2403	25A	0.003647	0.000558	1.000000	1.083715	0.083715
2402	3	0.001302	0.001187	1.000000	1.066051	0.066051
2403	3	0.000423	0.000377	1.000000	1.064689	0.064689
2448C	3	0.002540	0.002188	1.000000	1.129356	0.129356
2448Y	3	0.012612	0.015800	1.195755	1.000000	0.195755
2448M	3	0.005004	0.005011	1.001341	1.000000	0.001341
2443C	3	0.005479	0.005226	1.000000	1.030755	0.030755
2443Y	3	0.002177	0.002210	1.010056	1.000000	0.010056
2443M	3	0.001591	0.001374	1.000000	1.095419	0.095419
2443C	12	0.006731	0.006119	1.000000	1.062135	0.062135
2443Y	12	0.003698	0.003471	1.000000	1.041344	0.041344
2443M	12	0.001691	0.001455	1.000000	1.097943	0.097943
2424	12	0.000738	0.000680	1.000000	1.070545	0.070545
2424	25A	0.000701	0.000721	1.000000	1.069038	0.069038
2424	87C	0.004705	0.004688	1.000000	1.003148	0.003148
2424	89B	0.001138	0.001083	1.000000	1.043051	0.043051

LEGEND

FEATURE SILT 10% MOISTURE CONTENT
BACKGROUND CLAY 10% MOISTURE CONTENT
ATMOSPHERE MIDLATITUDE SUMMER HAZE=23 KM
ZENITH ANGLE 30 DEG.
DISTANCE TO SENSOR 6.00 KM

Table 7

Photgraphic Systems Simulation Model Output

FILMN	FILTER	FEATURE EXPT FOR D=1.0 (SEC)	BACKGROUND EXPT FOR D=1.0 (SEC)	FEATURE DENSITY (DF)	BACKGROUND DENSITY (DB)	DF-DB
2402	12	0.002365	0.002137	1.000000	1.072487	0.072487
2403	12	0.000728	0.000653	1.000000	1.061537	0.061537
2402	47B	0.028868	0.034237	1.122230	1.000000	0.122230
2403	47B	0.012230	0.014699	1.103816	1.000000	0.103816
2402	58	0.017808	0.017539	1.000000	1.010922	0.010922
2403	58	0.008698	0.008542	1.000000	1.010191	0.010191
2402	25A	0.003692	0.003282	1.000000	1.084403	0.084403
2403	25A	0.000978	0.000868	1.000000	1.067673	0.067673
2402	3	0.001927	0.001789	1.000000	1.053368	0.053368
2403	3	0.000631	0.000576	1.000000	1.051942	0.051942
2448C	3	0.003824	0.003394	1.000000	1.103635	0.103635
2448Y	3	0.017920	0.020462	1.115194	1.000000	0.115194
2448M	3	0.007118	0.007113	1.000000	1.000659	0.000659
2443C	3	0.007956	0.007609	1.000000	1.029001	0.029001
2443Y	3	0.003124	0.003142	1.003707	1.000000	0.003707
2443M	3	0.002397	0.002131	1.000000	1.076609	0.076609
2443C	12	0.009784	0.009053	1.000000	1.050559	0.050559
2443Y	12	0.005349	0.005107	1.000000	1.030080	0.030080
2443M	12	0.002551	0.002261	1.000000	1.078578	0.078578
2424	12	0.001072	0.001003	1.000000	1.057231	0.057231
2424	25A	0.001133	0.001062	1.000000	1.056413	0.056413
2424	87C	0.006685	0.006666	1.000000	1.002486	0.002486
2424	89B	0.001630	0.001563	1.000000	1.036464	0.036464

LEGEND

FEATURE SILT 10% MOISTURE CONTENT
BACKGROUND CLAY 10% MOISTURE CONTENT
ATMOSPHERE MIDLATITUDE SUMMER HAZE=5 KM
ZENITH ANGLE 30 DEG.
DISTANCE TO SENSOR 1.50 KM

Table 8

Photographic Systems Simulation Model Output

FILMN	FILTER	FEATURE EXPT FOR D=1.0 (SEC)	BACKGROUND EXPT FOR D=1.0 (SEC)	FEATURE DENSITY (DF)	BACKGROUND DENSITY (DB)	DF-DB
2402	12	0.002475	0.002263	1.000000	1.064090	0.064090
2403	12	0.000764	0.000693	1.000000	1.054691	0.054691
2402	47B	0.027654	0.031129	1.084810	1.000000	0.084810
2403	47B	0.011658	0.013232	1.071502	1.000000	0.071502
2402	58	0.018044	0.017805	1.000000	1.009577	0.009577
2403	58	0.008811	0.008675	1.000000	1.008788	0.008788
2402	25A	0.003906	0.003514	1.000000	1.075882	0.075882
2403	25A	0.001034	0.000929	1.000000	1.060837	0.060837
2402	3	0.001997	0.001869	1.000000	1.047264	0.047264
2403	3	0.000658	0.000607	1.000000	1.046126	0.046126
2448C	3	0.004028	0.003621	1.000000	1.092584	0.092584
2448Y	3	0.017438	0.019248	1.085798	1.000000	0.085798
2448M	3	0.007176	0.007167	1.000000	1.001041	0.001041
2443C	3	0.008328	0.007990	1.000000	1.026953	0.026953
2443Y	3	0.003141	0.003151	1.002000	1.000000	0.002000
2443M	3	0.002525	0.002273	1.000000	1.068488	0.068488
2443C	12	0.010409	0.009701	1.000000	1.045882	0.045882
2443Y	12	0.005458	0.005249	1.000000	1.025392	0.025392
2443M	12	0.002690	0.002415	1.000000	1.070296	0.070296
2424	12	0.001144	0.001077	1.000000	1.052092	0.052092
2424	25A	0.001212	0.001143	1.000000	1.051563	0.051563
2424	87C	0.007170	0.007151	1.000000	1.002306	0.002306
2424	89B	0.001750	0.001684	1.000000	1.033667	0.033667

LEGEND

FEATURE SILT 10% MOISTURE CONTENT
BACKGROUND CLAY 10% MOISTURE CONTENT
ATMOSPHERE MIDLATITUDE SUMMER HAZE-5 KM
ZENITH ANGLE 30 DEG.
DISTANCE TO SENSOR 6.00 KM

Table 9

Photographic Systems Simulation Model Output

FILMN	FILTER	FEATURE EXPT FOR D=1.0 (SEC)	BACKGROUND EXPT FOR D=1.0 (SEC)	FEATURE DENSITY (DF)	BACKGROUND DENSITY (DB)	DF-DB
2402	12	0,002860	0,002069	1,000000	1,232050	0.232050
2403	12	0,000877	0,000626	1,000000	1,190816	0.190816
2402	47B	0,034231	0,042717	1,158703	1,000000	0.158703
2403	47B	0,014383	0,018517	1,142644	1,000000	0.142644
2402	58	0,022057	0,018666	1,000000	1,119622	0.119622
2403	58	0,010734	0,009054	1,000000	1,096101	0,096101
2402	25A	0,004475	0,003117	1,000000	1,259056	0.259056
2403	25A	0,001181	0,000821	1,000000	1,205028	0,205028
2402	3	0,002342	0,001775	1.000000	1,198640	0,198640
2403	3	0,000763	0,000561	1,000000	1,174139	0,174139
2448C	3	0,004603	0,003231	1,000000	1,307297	0,307297
2448Y	3	0,022621	0,025927	1,118450	1,000000	0.118450
2448M	3	0,008837	0,007683	1,000000	1,121556	0.121556
2443C	3	0,009834	0,007798	1,000000	1,151114	0.151114
2443Y	3	0,003856	0,003409	1,000000	1,080354	0,080354
2443M	3	0,002886	0,002030	1,000000	1,229352	0,229352
2443C	12	0,012074	0,009004	1,000000	1,191108	0.191108
2443Y	12	0,006523	0,005252	1,000000	1,141099	0.141099
2443M	12	0,003070	0,002147	1,000000	1,232891	0,232891
2424	12	0,001316	0,001010	1,000000	1,230170	0.230170
2424	25A	0,001394	0,001070	1,000000	1,230068	0.230068
2424	87C	0,008250	0,007351	1,000000	1,100138	0.100138
2424	89B	0,002008	0,001617	1,000000	1,187888	0.187888

LEGEND

FEATURE SILT 20% MOISTURE CONTENT
BACKGROUND CLAY 20% MOISTURE CONTENT
ATMOSPHERE MIDLATITUDE SUMMER HAZE=23 KM
ZENTTH ANGLE 30 DEG,
DISTANCE TO SENSOR 1.50 KM

Table 10

Photographic Systems Simulation Model Output

FILMN	FILTER	FEATURE EXPT FOR D=1.0 (SEC)	BACKGROUND EXPT FOR D=1.0 (SEC)	FEATURE DENSITY (DF)	BACKGROUND DENSITY (DB)	DF-DB
2402	12	0.002921	0.002145	1.000000	1.221322	0.221322
2403	12	0.000898	0.000650	1.000000	1.182637	0.182637
2402	47B	0.029512	0.034505	1.112015	1.000000	0.112015
2403	47B	0.012263	0.014623	1.099381	1.000000	0.099381
2402	58	0.021946	0.018836	1.000000	1.109504	0.109504
2403	58	0.010681	0.009141	1.000000	1.087904	0.087984
2402	25A	0.004604	0.003249	1.000000	1.249860	0.249860
2403	25A	0.001214	0.000855	1.000000	1.197713	0.197713
2402	3	0.002364	0.001819	1.000000	1.187594	0.187594
2403	3	0.000775	0.000578	1.000000	1.165607	0.165607
2448C	3	0.004721	0.003361	1.000000	1.295115	0.295115
2448Y	3	0.021024	0.023467	1.095473	1.000000	0.095473
2448M	3	0.008748	0.007705	1.000000	1.110218	0.110218
2443C	3	0.009973	0.007991	1.000000	1.144307	0.144307
2443Y	3	0.003782	0.003382	1.000000	1.072976	0.072976
2443M	3	0.002959	0.002110	1.000000	1.220247	0.220247
2443C	12	0.012506	0.009410	1.000000	1.185259	0.185259
2443Y	12	0.006542	0.005356	1.000000	1.130212	0.130212
2443M	12	0.003151	0.002235	1.000000	1.223925	0.223925
2424	12	0.001366	0.001056	1.000000	1.223722	0.223722
2424	25A	0.001449	0.001120	1.000000	1.224182	0.224182
2424	87C	0.008578	0.007658	1.000000	1.098607	0.098607
2424	89B	0.002094	0.001695	1.000000	1.183882	0.183882

LEGEND

FEATURE SILT 20% MOISTURE CONTENT
BACKGROUND CLAY 20% MOISTURE CONTENT
ATMOSPHERE MIDLATITUDE SUMMER HAZE-23 KM
ZENITH ANGLE 30 DEG.
DISTANCE TO SENSOR 6.00 KM

Table 11

Photograpic Systems Simulation Model Output

FILMN	FILTER	FEATURE EXPT FOR D=1,0 (SEC)	BACKGROUND EXPT FOR D=1,0 (SEC)	FEATURE DENSITY (DF)	BACKGROUND DENSITY (DB)	DF-DB
2402	12	0,003650	0,002954	1,000000	1.151659	0.151659
2403	12	0,001134	0,000906	1,000000	1.126852	0.126852
2402	47B	0,037858	0,040644	1,050890	1.000000	0.050890
2403	47B	0,015906	0,017285	1,046929	1.000000	0.046929
2402	58	0,025369	0,023166	1,000000	1.065099	0.065099
2403	58	0,012370	0,011287	1,000000	1.051724	0.051724
2402	25A	0,005896	0,004593	1,000000	1.179029	0.179029
2403	25A	0,001561	0,001214	1,000000	1.141549	0.141549
2402	3	0,002911	0,002440	1,000000	1.126544	0.126544
2403	3	0,000969	0,000792	1,000000	1.113745	0.113745
2448C	3	0,006012	0,004733	1,000000	1.207690	0.207690
2448Y	3	0,023867	0,025140	1,045137	1.000000	0.045137
2448M	3	0,010027	0,009322	1,000000	1.063328	0.063328
2443C	3	0,012361	0,010513	1,000000	1.105499	0.105499
2443Y	3	0,004389	0,004104	1,000000	1.043769	0.043769
2443M	3	0,003771	0,002972	1,000000	1.155235	0.155235
2443C	12	0,015754	0,012783	1,000000	1.136146	0.136146
2443Y	12	0,007701	0,006829	1,000000	1.078332	0.078332
2443M	12	0,004025	0,003157	1,000000	1.158254	0.158254
2424	12	0,001739	0,001436	1,000000	1.166660	0.166660
2424	25A	0,001852	0,001525	1,000000	1.168656	0.168656
2424	87C	0,011043	0,010090	1,000000	1.078353	0.078353
2424	89B	0,002680	0,002273	1,000000	1.143156	0.143156

LEGEND

FEATURE SILT 20% MOISTURE CONTENT
BACKGROUND CLAY 20% MOISTURE CONTENT
ATMOSPHERE MIDLATITUDE SUMMER HAZE-5 KM
ZENITH ANGLE 30 DEG,
DISTANCE TO SENSOR 1.50 KM

Table 12

Photographic Systems Simulation Model Output

FILMN	FILTER	FEATURE EXPT FOR D=1,0 (SEC)	BACKGROUND EXPT FOR D=1,0 (SEC)	FEATURE DENSITY (DF)	BACKGROUND DENSITY (DB)	DF-DB
2402	12	0,003579	0,002997	1,000000	1.127058	0.127058
2403	12	0,001117	0,000924	1,000000	1.107036	0.107036
2402	47B	0,033402	0,034942	1,032303	1.000000	0.032303
2403	47B	0,013962	0,014724	1,029970	1.000000	0.029970
2402	58	0,023898	0,022262	1,000000	1.050833	0.050833
2403	58	0,011650	0,010848	1,000000	1.040270	0.040270
2402	25A	0,005869	0,004737	1,000000	1.153549	0.153549
2403	25A	0,001553	0,001252	1,000000	1.121357	0.121357
2402	3	0,002817	0,002434	1,000000	1.104634	0.104634
2403	3	0,000946	0,000799	1,000000	1.095113	0.095113
2448C	3	0,005948	0,004855	1,000000	1.176419	0.176419
2448Y	3	0,021515	0,022304	1,031289	1.000000	0.031289
2448M	3	0,009391	0,008879	1,000000	1.048690	0.048690
2443C	3	0,012156	0,010588	1,000000	1.089971	0.089971
2443Y	3	0,004097	0,003889	1,000000	1.034026	0.034026
2443M	3	0,003730	0,003047	1,000000	1.131921	0.131921
2443C	12	0,015868	0,013230	1,000000	1.118456	0.118456
2443Y	12	0,007313	0,006653	1,000000	1.061638	0.061638
2443M	12	0,003989	0,003244	1,000000	1.134755	0.134755
2424	12	0,001765	0,001492	1,000000	1.146294	0.146294
2424	25A	0,001886	0,001589	1,000000	1.148851	0.148851
2424	87C	0,011403	0,010505	1,000000	1.071237	0.071237
2424	89B	0,002755	0,002378	1,000000	1.128082	0.128082

LEGEND

FEATURE SILT 20% MOISTURE CONTENT
BACKGROUND CLAY 20% MOISTURE CONTENT
ATMOSPHERE MIDLATITUDE SUMMER HAZE-5 KM
ZENITH ANGLE 30 DEG.
DISTANCE TO SENSOR 6.00 KM

Table 13

Photographic Systems Simulation Model Output

FILMN	FILTER	FEATURE EXPT FOR D=1.0 (SEC)	BACKGROUND EXPT FOR D=1.0 (SEC)	FEATURE DENSITY (DF)	BACKGROUND DENSITY (DB)	DF-DB
2402	12	0.003253	0.002769	1.000000	1.115452	0.115452
2403	12	0.000994	0.000841	1.000000	1.094557	0.094557
2402	47B	0.040015	0.043502	1.059879	1.000000	0.059879
2403	47B	0.016875	0.018632	1.055916	1.000000	0.055916
2402	58	0.025749	0.023344	1.000000	1.070259	0.070259
2403	58	0.012571	0.011386	1.000000	1.055901	0.055901
2402	25A	0.004991	0.004178	1.000000	1.127469	0.127469
2403	25A	0.001320	0.001103	1.000000	1.101004	0.101004
2402	3	0.002674	0.002321	1.000000	1.101385	0.101385
2403	3	0.000868	0.000743	1.000000	1.087418	0.087418
2448C	3	0.005203	0.004373	1.000000	1.150981	0.150981
2448Y	3	0.026283	0.026624	1.011198	1.000000	0.011198
2448M	3	0.010352	0.009483	1.000000	1.076097	0.076097
2443C	3	0.010876	0.009859	1.000000	1.063944	0.063944
2443Y	3	0.004516	0.004173	1.000000	1.051534	0.051534
2443M	3	0.003258	0.002740	1.000000	1.112857	0.112857
2443C	12	0.013214	0.011731	1.000000	1.077542	0.077542
2443Y	12	0.007667	0.006830	1.000000	1.075300	0.075300
2443M	12	0.003462	0.002904	1.000000	1.114401	0.114401
2424	12	0.001432	0.001314	1.000000	1.074816	0.074816
2424	25A	0.001509	0.001388	1.000000	1.072525	0.072525
2424	87C	0.008759	0.009369	1.058459	1.000000	0.058459
2424	89B	0.002154	0.002075	1.000000	1.032466	0.032466

LEGEND

FEATURE SILT 30% MOISTURE CONTENT
BACKGROUND CLAY 30% MOISTURE CONTENT
ATMOSPHERE MIDLATITUDE SUMMER HAZE=23 KM
ZENITH ANGLE 30 DEG.
DISTANCE TO SENSOR 1.50 KM

Table 14

Photographic Systems Simulation Model Output

FILMN	FILTER	FEATURE EXPT FOR D=1.0 (SEC)	BACKGROUND EXPT FOR D=1.0 (SEC)	FEATURE DENSITY (DF)	BACKGROUND DENSITY (DB)	DF-DB
2402	12	0.003296	0.002831	1.000000	1.108878	0.108878
2403	12	0.001010	0.000862	1.000000	1.089580	0.089580
2402	47B	0.033035	0.034978	1.040959	1.000000	0.040959
2403	47B	0.013739	0.014690	1.037819	1.000000	0.037819
2402	58	0.025203	0.023084	1.000000	1.062949	0.062949
2403	58	0.012302	0.011259	1.000000	1.050045	0.050045
2402	25A	0.005109	0.004309	1.000000	1.122010	0.122010
2403	25A	0.001350	0.001137	1.000000	1.096646	0.096646
2402	3	0.002670	0.002341	1.000000	1.094287	0.094287
2403	3	0.000873	0.000755	1.000000	1.082073	0.082073
2448C	3	0.005302	0.004494	1.000000	1.143644	0.143644
2448Y	3	0.023739	0.023976	1.008643	1.000000	0.008643
2448M	3	0.010065	0.009313	1.000000	1.067465	0.067465
2443C	3	0.010948	0.009982	1.000000	1.060170	0.060170
2443Y	3	0.004344	0.004051	1.000000	1.045464	0.045464
2443M	3	0.003319	0.002814	1.000000	1.107364	0.107364
2443C	12	0.013638	0.012163	1.000000	1.074577	0.074577
2443Y	12	0.007572	0.006820	1.000000	1.068146	0.068146
2443M	12	0.003532	0.002958	1.000000	1.109023	0.109023
2424	12	0.001462	0.001364	1.000000	1.071996	0.071996
2424	25A	0.001565	0.001444	1.000000	1.070026	0.070026
2424	87C	0.009098	0.009719	1.057311	1.000000	0.057311
2424	89B	0.002243	0.002164	1.000000	1.031262	0.031262

LEGEND

FEATURE SILT 30% MOISTURE CONTENT
BACKGROUND CLAY 30% MOISTURE CONTENT
ATMOSPHERE MIDLATITUDE SUMMER HAZE=23 KM
ZENITH ANGLE 30 DEG.
DISTANCE TO SENSOR 6.00 KM

Table 15

Photographic Systems Simulation Model Output

FILMN	FILTER	FEATURE EXPT FOR D=1,0 (SEC)	BACKGROUND EXPT FOR D=1,0 (SEC)	FEATURE DENSITY (DF)	BACKGROUND DENSITY (DB)	DF-DB
2402	12	0,003936	0,003571	1,000000	1.069692	0.069692
2403	12	0,001222	0,001102	1,000000	1.058258	0.058258
2402	47B	0,040024	0,041018	1,017567	1.000000	0.017567
2403	47B	0,016820	0,017336	1,017063	1.000000	0.017063
2402	58	0,027334	0,026055	1,000000	1.034322	0.034322
2403	58	0,013350	0,012726	1,000000	1.027029	0.027029
2402	25A	0,006317	0,005630	1,000000	1.082531	0.082531
2403	25A	0,001674	0,001491	1,000000	1.065266	0.065266
2402	3	0,003133	0,002885	1,000000	1.059115	0.059115
2403	3	0,001043	0,000951	1,000000	1.052613	0.052613
2448C	3	0,006483	0,005813	1,000000	1.094784	0.094784
2448Y	3	0,025306	0,025409	1,003518	1.000000	0.003518
2448M	3	0,010799	0,010366	1,000000	1.035608	0.035608
2443C	3	0,013120	0,012324	1,000000	1.040764	0.040764
2443Y	3	0,004724	0,004548	1,000000	1.024710	0.024710
2443M	3	0,004063	0,003644	1,000000	1.070994	0.070994
2443C	12	0,016723	0,015453	1,000000	1.051430	0.051430
2443Y	12	0,008352	0,007883	1,000000	1.037621	0.037621
2443M	12	0,004337	0,003881	1,000000	1.072342	0.072342
2424	12	0,001843	0,001741	1,000000	1.049446	0.049446
2424	25A	0,001958	0,001851	1,000000	1.048745	0.048745
2424	87C	0,011565	0,012182	1,045119	1.000000	0.045119
2424	89B	0,002824	0,002751	1,000000	1.022469	0.022469

LEGEND

FEATURE SILT 30% MOISTURE CONTENT
BACKGROUND CLAY 30% MOISTURE CONTENT
ATMOSPHERE MIDLATITUDE SUMMER HAZE-5 KM
ZENITH ANGLE 30 DEG,
DISTANCE TO SENSOR 1,50 KM

Table 16

Photographic Systems Simultion Model Output

FILMN	FILTER	FEATURE EXPT FOR D=1.0 (SEC)	BACKGROUND EXPT FOR D=1.0 (SEC)	FEATURE DENSITY (DF)	BACKGROUND DENSITY (DB)	DF-DB
2402	12	0.003804	0.003512	1.000000	1.057056	0.057056
2403	12	0.001187	0.001090	1.000000	1.048063	0.048063
2402	47B	0.034645	0.035175	1.010893	1.000000	0.010893
2403	47B	0.014478	0.014755	1.010710	1.000000	0.010710
2402	58	0.025285	0.024381	1.000000	1.026089	0.026089
2403	58	0.012341	0.011901	1.000000	1.020488	0.020488
2402	25A	0.006217	0.005643	1.000000	1.069378	0.069378
2403	25A	0.001646	0.001494	1.000000	1.054826	0.054826
2402	3	0.00298[illegible]	0.002794	1.000000	1.047681	0.047681
2403	3	0.001004	0.000930	1.000000	1.042966	0.042966
2448C	3	0.006330	0.005782	1.000000	1.078736	0.078736
2448Y	3	0.022412	0.022472	1.002310	1.000000	0.002310
2448M	3	0.009927	0.009627	1.000000	1.026678	0.026678
2443C	3	0.012762	0.012116	1.000000	1.033878	0.033878
2443Y	3	0.004329	0.004207	1.000000	1.018606	0.018606
2443M	3	0.003968	0.003624	1.000000	1.059011	0.059011
2443C	12	0.016695	0.015610	1.000000	1.043787	0.043787
2443Y	12	0.007782	0.007445	1.000000	1.028817	0.028817
2443M	12	0.004244	0.003869	1.000000	1.060267	0.060267
2424	12	0.001855	0.001767	1.000000	1.042228	0.042228
2424	25A	0.001980	0.001887	1.000000	1.041901	0.041901
2424	87C	0.011889	0.012458	1.040582	1.000000	0.040582
2424	89B	0.002886	0.002822	1.000000	1.019370	0.019370

LEGEND

FEATURE SILT 30% MOISTURE CONTENT
BACKGROUND CLAY 30% MOISTURE CONTENT
ATMOSPHERE MIDLATITUDE SUMMER HAZE-5 KM
ZENITH ANGLE 30 DEG.
DISTANCE TO SENSOR 6.00 KM

Table 17

Values of Transfer Function for Nomogram by Filter Type and Wavelength Band, Kodak Infrared Aerographic Film No. 2424, Summer Season

Haze	Solar Zenith deg	Altitude km	Filter Type 12	25A	87C	89B
			Wavelength Band, 0.4-0.5 μm			
Clear	0	1.5	0.0029	0	0	0
		3.0	0.0027	0	0	0
		6.0	0.0025	0	0	0
		15.2	0.0023	0	0	0
	30	1.5	0.0027	0	0	0
		3.0	0.0025	0	0	0
		6.0	0.0024	0	0	0
		15.2	0.0022	0	0	0
	60	1.5	0.0019	0	0	0
		3.0	0.0017	0	0	0
		6.0	0.0016	0	0	0
		15.2	0.0015	0	0	0
Hazy	0	1.5	0.0008	0	0	0
		3.0	0.0007	0	0	0
		6.0	0.0006	0	0	0
		15.2	0.0006	0	0	0
	30	1.5	0.0007	0	0	0
		3.0	0.0006	0	0	0
		6.0	0.0006	0	0	0
		15.2	0.0005	0	0	0
	60	1.5	0.0003	0	0	0
		3.0	0.0002	0	0	0
		6.0	0.0002	0	0	0
		15.2	0.0002	0	0	0
			Wavelength Band, 0.5-0.58 μm			
Clear	0	1.5	0.0152	0.0005	0	0
		3.0	0.0144	0.0005	0	0
		6.0	0.0139	0.0005	0	0
		15.2	0.0130	0.0005	0	0
	30	1.5	0.0144	0.0005	0	0
		3.0	0.0136	0.0005	0	0
		6.0	0.0131	0.0005	0	0
		15.2	0.0122	0.0004	0	0

(Continued)

(Sheet 1 of 4)

Table 17 (Continued)

Haze	Solar Zenith deg	Altitude km	Filter Type 12	25A	87C	89B
			Wavelength Band, 0.5-0.58 μm (Continued)			
Clear	60	1.5	0.0105	0.0004	0	0
		3.0	0.0100	0.0004	0	0
		6.0	0.0096	0.0003	0	0
		15.2	0.0090	0.0003	0	0
Hazy	0	1.5	0.0050	0.0002	0	0
		3.0	0.0043	0.0002	0	0
		6.0	0.0041	0.0002	0	0
		15.2	0.0038	0.0001	0	0
	30	1.5	0.0043	0.0002	0	0
		3.0	0.0037	0.0001	0	0
		6.0	0.0035	0.0001	0	0
		15.2	0.0033	0.0001	0	0
	60	1.5	0.0019	0.0001	0	0
		3.0	0.0017	0.0001	0	0
		6.0	0.0016	0.0001	0	0
		15.2	0.0015	0.0001	0	0
			Wavelength Band, 0.58-0.68 μm			
Clear	0	1.5	0.0650	0.0558	0	0
		3.0	0.0622	0.0535	0	0
		6.0	0.0603	0.0519	0	0
		15.2	0.0574	0.0495	0	0
	30	1.5	0.0620	0.0533	0	0
		3.0	0.0594	0.0511	0	0
		6.0	0.0576	0.0496	0	0
		15.2	0.0548	0.0473	0	0
	60	1.5	0.0480	0.0416	0	0
		3.0	0.0460	0.0398	0	0
		6.0	0.0446	0.0386	0	0
		15.2	0.0425	0.0368	0	0
Hazy	0	1.5	0.0236	0.0205	0	0
		3.0	0.0208	0.0180	0	0
		6.0	0.0199	0.0173	0	0
		15.2	0.0189	0.0164	0	0
	30	1.5	0.0208	0.0180	0	0
		3.0	0.0183	0.0159	0	0
		6.0	0.0175	0.0152	0	0
		15.2	0.0167	0.0145	0	0

(Continued)

(Sheet 2 of 4)

Table 17 (Continued)

Haze	Solar Zenith deg	Altitude km	Filter Type 12	25A	87C	89B
			Wavelength Band, 0.58-0.68 μm (Continued)			
Hazy	60	1.5	0.0104	0.0091	0	0
		3.0	0.0091	0.0080	0	0
		6.0	0.0087	0.0077	0	0
		15.2	0.0083	0.0073	0	0
			Wavelength Band, 0.68-0.80 μm			
Clear	0	1.5	0.1105	0.1111	0.0004	0.0717
		3.0	0.1060	0.1065	0.0004	0.0688
		6.0	0.1031	0.1037	0.0003	0.0669
		15.2	0.0994	0.1000	0.0003	0.0646
	30	1.5	0.1063	0.1069	0.0004	0.0691
		3.0	0.1020	0.1025	0.0003	0.0662
		6.0	0.0993	0.0998	0.0003	0.0645
		15.2	0.0957	0.0962	0.0003	0.0622
	60	1.5	0.0865	0.0869	0.0003	0.0564
		3.0	0.0830	0.0834	0.0003	0.0542
		6.0	0.0808	0.0812	0.0003	0.0528
		15.2	0.0780	0.0784	0.0003	0.0509
Hazy	0	1.5	0.0462	0.0465	0.0002	0.0302
		3.0	0.0412	0.0414	0.0002	0.0270
		6.0	0.0396	0.0398	0.0001	0.0259
		15.2	0.0382	0.0384	0.0001	0.0250
	30	1.5	0.0414	0.0417	0.0002	0.0272
		3.0	0.0369	0.0371	0.0001	0.0243
		6.0	0.0355	0.0357	0.0001	0.0233
		15.2	0.0342	0.0344	0.0001	0.0225
	60	1.5	0.0229	0.0230	0.0001	0.0152
		3.0	0.0204	0.0206	0.0001	0.0136
		6.0	0.0197	0.0198	0.0001	0.0131
		15.2	0.0190	0.0191	0.0001	0.0126
			Wavelength Band, 0.80-0.93 μm			
Clear	0	1.5	0.0912	0.0911	0.0369	0.0936
		3.0	0.0878	0.0877	0.0356	0.0901
		6.0	0.0859	0.0859	0.0349	0.0882
		15.2	0.0837	0.0836	0.0340	0.0859

(Continued)

(Sheet 3 of 4)

Table 17 (Concluded)

Haze	Solar Zenith deg	Altitude km	Filter Type 12	25A	87C	89B
			Wavelength Band, 0.80-0.93 μm (Continued)			
Clear	30	1.5	0.0882	0.0882	0.0357	0.0905
		3.0	0.0849	0.0849	0.0345	0.0872
		6.0	0.0831	0.0831	0.0334	0.0853
		15.2	0.0810	0.0809	0.0329	0.0831
	60	1.5	0.0738	0.0738	0.0301	0.0757
		3.0	0.0711	0.0711	0.0290	0.0730
		6.0	0.0696	0.0696	0.0285	0.0715
		15.2	0.0678	0.0678	0.0278	0.0696
Hazy	0	1.5	0.0415	0.0414	0.0169	0.0426
		3.0	0.0374	0.0374	0.0153	0.0384
		6.0	0.0362	0.0362	0.0148	0.0372
		15.2	0.0353	0.0352	0.0145	0.0362
	30	1.5	0.0377	0.0376	0.0154	0.0387
		3.0	0.0340	0.0340	0.0140	0.0349
		6.0	0.0329	0.0329	0.0135	0.0338
		15.2	0.0320	0.0320	0.0132	0.0329
	60	1.5	0.0224	0.0224	0.0093	0.0230
		3.0	0.0202	0.0202	0.0084	0.0207
		6.0	0.0196	0.0195	0.0081	0.0201
		15.2	0.0190	0.0190	0.0079	0.0196

(Sheet 4 of 4)

Table 19

Values of Transfer Function for Nomogram by Emulsion Filter Type and Wavelength Band, Kodak Aerochrome Infrared Film No. 2443, Summer Season

Haze	Solar Zenith deg	Altitude km	Cyan None	Cyan 12	Yellow None	Yellow 12	Magenta None	Magenta 12
			Wavelength Band, 0.4-0.5 μm					
Clear	0	1.5	0.0576	0	0.1097	0.0004	0.0178	0
		3.0	0.0530	0	0.1014	0.0004	0.0163	0
		6.0	0.0490	0	0.0943	0.0003	0.0150	0
		15.2	0.0433	0	0.0843	0.0003	0.0132	0
	30	1.5	0.0529	0	0.1012	0.0004	0.0163	0
		3.0	0.0487	0	0.0936	0.0003	0.0150	0
		6.0	0.0450	0	0.0871	0.0003	0.0137	0
		15.2	0.0398	0	0.0779	0.0003	0.0121	0
	60	1.5	0.0332	0	0.0655	0.0002	0.0100	0
		3.0	0.0306	0	0.0606	0.0002	0.0092	0
		6.0	0.0283	0	0.0564	0.0002	0.0085	0
		15.2	0.0251	0	0.0505	0.0002	0.0075	0
Hazy	0	1.5	0.0149	0	0.0294	0.0001	0.0045	0
		3.0	0.0123	0	0.0243	0.0001	0.0037	0
		6.0	0.0111	0	0.0221	0.0001	0.0033	0
		15.2	0.0098	0	0.0199	0.0001	0.0029	0
	30	1.5	0.0123	0	0.0244	0.0001	0.0037	0
		3.0	0.0101	0	0.0202	0.0001	0.0030	0
		6.0	0.0091	0	0.0184	0.0001	0.0027	0
		15.2	0.0081	0	0.0165	0.0001	0.0024	0
	60	1.5	0.0042	0	0.0088	0	0.0012	0
		3.0	0.0035	0	0.0073	0	0.0010	0
		6.0	0.0032	0	0.0067	0	0.0009	0
		15.2	0.0028	0	0.0060	0	0.0008	0
			Wavelength Band, 0.5-0.58 μm					
Clear	0	1.5	0.0061	0.0034	0.1280	0.0777	0.0112	0.0078
		3.0	0.0058	0.0032	0.1211	0.0736	0.0106	0.0074
		6.0	0.0055	0.0031	0.1158	0.0705	0.0102	0.0071
		15.2	0.0052	0.0029	0.1079	0.0658	0.0095	0.0066
	30	1.5	0.0058	0.0032	0.1206	0.0733	0.0106	0.0074
		3.0	0.0055	0.0031	0.1141	0.0695	0.0100	0.0070
		6.0	0.0052	0.0029	0.1092	0.0665	0.0096	0.0067
		15.2	0.0049	0.0027	0.1017	0.0621	0.0090	0.0063

(Continued)

(Sheet 1 of 4)

Table 19

Values of Transfer Function for Nomogram by Emulsion Filter Type and Wavelength Band, Kodak Aerochrome Infrared Film No. 2443, Summer Season

Haze	Solar Zenith deg	Altitude km	Cyan None	Cyan 12	Yellow None	Yellow 12	Magenta None	Magenta 12
			Wavelength Band, 0.4-0.5 μm					
Clear	0	1.5	0.0576	0	0.1097	0.0004	0.0178	0
		3.0	0.0530	0	0.1014	0.0004	0.0163	0
		6.0	0.0490	0	0.0943	0.0003	0.0150	0
		15.2	0.0433	0	0.0843	0.0003	0.0132	0
	30	1.5	0.0529	0	0.1012	0.0004	0.0163	0
		3.0	0.0487	0	0.0936	0.0003	0.0150	0
		6.0	0.0450	0	0.0871	0.0003	0.0137	0
		15.2	0.0398	0	0.0779	0.0003	0.0121	0
	60	1.5	0.0332	0	0.0655	0.0002	0.0100	0
		3.0	0.0306	0	0.0606	0.0002	0.0092	0
		6.0	0.0283	0	0.0564	0.0002	0.0085	0
		15.2	0.0251	0	0.0505	0.0002	0.0075	0
Hazy	0	1.5	0.0149	0	0.0294	0.0001	0.0045	0
		3.0	0.0123	0	0.0243	0.0001	0.0037	0
		6.0	0.0111	0	0.0221	0.0001	0.0033	0
		15.2	0.0098	0	0.0199	0.0001	0.0029	0
	30	1.5	0.0123	0	0.0244	0.0001	0.0037	0
		3.0	0.0101	0	0.0202	0.0001	0.0030	0
		6.0	0.0091	0	0.0184	0.0001	0.0027	0
		15.2	0.0081	0	0.0165	0.0001	0.0024	0
	60	1.5	0.0042	0	0.0088	0	0.0012	0
		3.0	0.0035	0	0.0073	0	0.0010	0
		6.0	0.0032	0	0.0067	0	0.0009	0
		15.2	0.0028	0	0.0060	0	0.0008	0
			Wavelength Band, 0.5-0.58 μm					
Clear	0	1.5	0.0061	0.0034	0.1280	0.0777	0.0112	0.0078
		3.0	0.0058	0.0032	0.1211	0.0736	0.0106	0.0074
		6.0	0.0055	0.0031	0.1158	0.0705	0.0102	0.0071
		15.2	0.0052	0.0029	0.1079	0.0658	0.0095	0.0066
	30	1.5	0.0058	0.0032	0.1206	0.0733	0.0106	0.0074
		3.0	0.0055	0.0031	0.1141	0.0695	0.0100	0.0070
		6.0	0.0052	0.0029	0.1092	0.0665	0.0096	0.0067
		15.2	0.0049	0.0027	0.1017	0.0621	0.0090	0.0063

(Continued)

(Sheet 1 of 4)

Table 19 (Continued)

Haze	Solar Zenith deg	Altitude km	Cyan None	Cyan 12	Yellow None	Yellow 12	Magenta None	Magenta 12
			Wavelength Band, 0.5-0.58 μm (Continued)					
Clear	60	1.5	0.0042	0.0024	0.0874	0.0534	0.0077	0.0054
		3.0	0.0039	0.0022	0.0827	0.0506	0.0073	0.0051
		6.0	0.0038	0.0021	0.0791	0.0484	0.0070	0.0049
		15.2	0.0035	0.0020	0.0737	0.0452	0.0066	0.0046
Hazy	0	1.5	0.0019	0.0011	0.0409	0.0252	0.0037	0.0026
		3.0	0.0017	0.0009	0.0351	0.0217	0.0032	0.0022
		6.0	0.0016	0.0009	0.0330	0.0204	0.0030	0.0021
		15.2	0.0015	0.0008	0.0308	0.0191	0.0028	0.0020
	30	1.5	0.0017	0.0010	0.0351	0.0217	0.0032	0.0022
		3.0	0.0014	0.0008	0.0302	0.0187	0.0027	0.0019
		6.0	0.0013	0.0008	0.0284	0.0176	0.0026	0.0018
		15.2	0.0013	0.0007	0.0265	0.0164	0.0024	0.0017
	60	1.5	0.0007	0.0004	0.0154	0.0096	0.0014	0.0010
		3.0	0.0006	0.0004	0.0132	0.0083	0.0012	0.0009
		6.0	0.0006	0.0003	0.0124	0.0078	0.0012	0.0008
		15.2	0.0005	0.0003	0.0116	0.0073	0.0011	0.0008
			Wavelength Band, 0.58-0.68 μm					
Clear	0	1.5	0.0099	0.0085	0.0108	0.0090	0.1496	0.1293
		3.0	0.0095	0.0082	0.0103	0.0085	0.1432	0.1239
		6.0	0.0092	0.0079	0.0100	0.0082	0.1390	0.1202
		15.2	0.0088	0.0076	0.0094	0.0078	0.1324	0.1145
	30	1.5	0.0095	0.0082	0.0103	0.0085	0.1428	0.1235
		3.0	0.0091	0.0078	0.0098	0.0081	0.1368	0.1184
		6.0	0.0088	0.0076	0.0094	0.0078	0.1328	0.1148
		15.2	0.0084	0.0072	0.0089	0.0074	0.1265	0.1094
	60	1.5	0.0073	0.0063	0.0077	0.0064	0.1111	0.0961
		3.0	0.0070	0.0061	0.0073	0.0061	0.1064	0.0921
		6.0	0.0068	0.0059	0.0071	0.0058	0.1033	0.0894
		15.2	0.0065	0.0056	0.0067	0.0055	0.0984	0.0851
Hazy	0	1.5	0.0036	0.0031	0.0038	0.0031	0.0553	0.0479
		3.0	0.0032	0.0027	0.0033	0.0027	0.0488	0.0422
		6.0	0.0030	0.0026	0.0031	0.0026	0.0466	0.0403
		15.2	0.0029	0.0025	0.0029	0.0024	0.0444	0.0384
	30	1.5	0.0032	0.0027	0.0033	0.0027	0.0487	0.0422
		3.0	0.0028	0.0024	0.0029	0.0024	0.0430	0.0372
		6.0	0.0027	0.0023	0.0027	0.0023	0.0411	0.0356
		15.2	0.0026	0.0022	0.0026	0.0021	0.0391	0.0339

(Continued)

(Sheet 2 of 4)

Table 19 (Continued)

Haze	Solar Zenith deg	Altitude km	Emulsion Filter Type: Cyan None	Cyan 12	Yellow None	Yellow 12	Magenta None	Magenta 12
			Wavelength Band, 0.58-0.68 μm (Continued)					
Hazy	60	1.5	0.0016	0.0014	0.0015	0.0013	0.0245	0.0212
		3.0	0.0014	0.0012	0.0013	0.0011	0.0216	0.0187
		6.0	0.0013	0.0012	0.0013	0.0011	0.0206	0.0179
		15.2	0.0013	0.0011	0.0012	0.0010	0.0197	0.0170
			Wavelength Band, 0.68-0.80 μm					
Clear	0	1.5	0.0165	0.0148	0	0	0.0045	0.0040
		3.0	0.0158	0.0142	0	0	0.0043	0.0038
		6.0	0.0153	0.0138	0	0	0.0042	0.0038
		15.2	0.0148	0.0133	0	0	0.0040	0.0036
	30	1.5	0.0158	0.0142	0	0	0.0043	0.0038
		3.0	0.0152	0.0136	0	0	0.0041	0.0037
		6.0	0.0148	0.0133	0	0	0.0040	0.0036
		15.2	0.0142	0.0128	0	0	0.0039	0.0035
	60	1.5	0.0128	0.0115	0	0	0.0035	0.0031
		3.0	0.0123	0.0111	0	0	0.0033	0.0030
		6.0	0.0120	0.0108	0	0	0.0032	0.0029
		15.2	0.0116	0.0104	0	0	0.0031	0.0028
Hazy	0	1.5	0.0069	0.0062	0	0	0.0018	0.0017
		3.0	0.0061	0.0055	0	0	0.0016	0.0015
		6.0	0.0059	0.0053	0	0	0.0016	0.0014
		15.2	0.0056	0.0051	0	0	0.0015	0.0014
	30	1.5	0.0061	0.0055	0	0	0.0016	0.0015
		3.0	0.0055	0.0049	0	0	0.0015	0.0013
		6.0	0.0053	0.0047	0	0	0.0014	0.0013
		15.2	0.0051	0.0046	0	0	0.0013	0.0012
	60	1.5	0.0034	0.0030	0	0	0.0009	0.0008
		3.0	0.0030	0.0027	0	0	0.0008	0.0007
		6.0	0.0029	0.0026	0	0	0.0008	0.0007
		15.2	0.0028	0.0025	0	0	0.0007	0.0006
			Wavelength Band, 0.80-0.93 μm					
Clear	0	1.5	0.0063	0.0057	0	0	0	0
		3.0	0.0061	0.0055	0	0	0	0
		6.0	0.0060	0.0054	0	0	0	0
		15.2	0.0058	0.0052	0	0	0	0

(Continued)

(Sheet 3 of 4)

Table 19 (Concluded)

Haze	Solar Zenith deg	Alti- tude km	Emulsion Filter Type: Cyan None	Cyan 12	Yellow None	Yellow 12	Magenta None	Magenta 12
			Wavelength Band, 0.80-0.93 μm (Continued)					
Clear	30	1.5	0.0061	0.0055	0	0	0	0
		3.0	0.0059	0.0053	0	0	0	0
		6.0	0.0058	0.0052	0	0	0	0
		15.2	0.0056	0.0051	0	0	0	0
	60	1.5	0.0051	0.0046	0	0	0	0
		3.0	0.0049	0.0044	0	0	0	0
		6.0	0.0048	0.0043	0	0	0	0
		15.2	0.0047	0.0042	0	0	0	0
Hazy	0	1.5	0.0029	0.0026	0	0	0	0
		3.0	0.0026	0.0023	0	0	0	0
		6.0	0.0025	0.0023	0	0	0	0
		15.2	0.0024	0.0022	0	0	0	0
	30	1.5	0.0026	0.0024	0	0	0	0
		3.0	0.0024	0.0021	0	0	0	0
		6.0	0.0023	0.0021	0	0	0	0
		15.2	0.0022	0.0020	0	0	0	0
	60	1.5	0.0015	0.0014	0	0	0	0
		3.0	0.0014	0.0013	0	0	0	0
		6.0	0.0014	0.0012	0	0	0	0
		15.2	0.0013	0.0012	0	0	0	0

(Sheet 4 of 4)

Table 20

Wavelength Sensitivities of Film-Filter Combinations

Film No.	Filter No.	Approximate Range of Sensitivity, m
2402	3	0.40-0.68
2402	12	0.50-0.68
2402	47B	0.40-0.50
2402	58	0.50-0.60
2402	25	0.58-0.60
2403	3	0.40-0.71
2403	12	0.50-0.71
2403	47B	0.40-0.50
2403	58	0.50-0.60
2403	25	0.58-0.71
2424	12	0.50-0.93
2424	25	0.58-0.93
2424	89B	0.68-0.93
2424	87C	0.80-0.93
2448	3	0.40-0.68
2443	3	0.40-0.89
2443	12	0.50-0.89

Table 21

Solar Zenith Angle

Date Code	Time of Day: 1600 or 0800	1530 or 0830	1500 or 0900	1430 or 0930	1400 or 1000	1330 or 1030	1300 or 1100	1230 or 1130	1200
					Latitude - 20 degrees				
A	73	67	62	57	52	49	46	46	46
B	72	67	62	56	51	48	45	45	45
C	71	66	60	55	49	46	42	42	42
D	69	63	57	51	46	42	39	39	39
E	67	60	54	48	42	38	34	34	34
F	64	57	51	45	39	34	29	29	29
G	62	55	48	42	35	30	24	24	24
H	60	53	46	39	32	26	20	20	20
I	58	51	44	37	30	23	17	17	17
J	57	50	43	36	29	22	15	15	15
K	56	49	42	35	28	21	14	14	14
L	55	49	42	35	28	21	14	14	14
M	55	49	42	35	28	21	14	14	14

(Continued)

Date Table

Date Code	Date		Date Code
A	Dec 21	Dec 21	A
B	Dec 5	Jan 5	B
C	Nov 20	Jan 20	C
D	Nov 4	Feb 5	D
E	Oct 20	Feb 20	E
F	Oct 5	Mar 7	F
G	[illegible] 20	Mar 22	G
H	Sep 5	Apr 6	H
I	Aug 20	Apr 22	I
J	Aug 5	May 7	J
K	Jul 21	May 22	K
L	Jul 6	Jun 6	L
M	Jun 21	Jun 21	M

(Sheet 1 of 4)

Table 21 (Continued)

Date Code	Time of Day: 1600 or 0800	1530 or 0830	1500 or 0900	1430 or 0930	1400 or 1000	1330 or 1030	1300 or 1100	1230 or 1130	1200
						Latitude - 30 degrees			
A	78	73	69	65	61	58	55	54	53
B	78	73	68	64	60	57	54	53	53
C	77	71	66	62	57	55	52	51	50
D	74	69	63	58	54	51	48	47	46
E	71	65	60	55	50	46	43	42	41
F	68	67	55	50	45	42	38	37	35
G	65	58	52	46	41	37	33	31	29
H	61	55	48	43	37	32	27	26	24
I	58	52	45	39	33	28	23	20	18
J	56	50	43	37	31	25	19	16	15
K	55	48	42	35	29	23	17	13	10
L	54	47	41	34	28	22	16	11	8
M	53	47	40	34	27	21	15	17	7

Date Table

Date Code	Date		Date Code
A	Dec 21	Dec 21	A
B	Dec 5	Jan 5	B
C	Nov 20	Jan 20	C
D	Nov 4	Feb 5	D
E	Oct 20	Feb 20	E
F	Oct 5	Mar 7	F
G	Sep 20	Mar 22	G
H	Sep 5	Apr 6	H
I	Aug 20	Apr 22	I
J	Aug 5	May 7	J
K	Jul 21	May 22	K
L	Jul 6	Jun 6	L
M	Jun 21	Jun 21	M

(Continued)

(Sheet 2 of 4)

Table 21 (Continued)

Date Code	1600 or 0800	1530 or 0830	1500 or 0900	1430 or 0930	1400 or 1000	1330 or 1030	1300 or 1100	1230 or 1130	1200		Date Table: Date Code	Date		Date Code
	Latitude 40 degrees													
A	84	80	76	73	69	67	65	64	63		A	Dec 21	Dec 21	A
B	84	80	76	72	68	66	63	63	62		B	Dec 5	Jan 5	B
C	82	78	74	70	66	64	61	61	60		C	Nov 20	Jan 20	C
D	79	74	70	67	63	60	58	57	56		D	Nov 4	Feb 5	D
E	76	71	66	62	58	55	53	52	51		E	Oct 20	Feb 20	E
F	72	67	62	57	53	50	47	46	45		F	Oct 5	Mar 7	F
G	67	62	57	52	48	45	42	41	40		G	Sep 20	Mar 22	G
H	63	58	53	48	43	40	36	35	34		H	Sep 5	Apr 6	H
I	60	54	48	43	39	35	31	29	28		I	Aug 20	Apr 22	I
J	57	51	45	40	35	31	27	25	23		J	Aug 5	May 7	J
K	54	49	43	38	32	28	23	22	20		K	Jul 21	May 22	K
L	53	47	42	36	31	26	22	20	18		L	Jul 6	Jun 6	L
M	52	46	41	35	30	25	21	19	17		M	Jun 21	Jun 21	M

(Continued)

(Sheet 3 of 4)

Table 21 (Concluded)

Date Code	Time of Day: 1600 or 0800	1530 or 0830	1500 or 0900	1430 or 0930	1400 or 1000	1330 or 1030	1300 or 1100	1230 or 1130	1200	Date Table: Date Code	Date	Date	Date Code
					Latitude - 50 degrees								
A	90	90	84	81	78	76	74	74	73	A	Dec 21	Dec 21	A
B	90	87	83	80	78	76	74	74	73	B	Dec 5	Jan 5	B
C	90	87	81	78	75	73	72	41	70	C	Nov 20	Jan 20	C
D	86	82	77	74	72	70	68	68	67	D	Nov 4	Feb 5	D
E	81	77	73	70	67	65	63	63	62	E	Oct 20	Feb 20	E
F	76	72	68	65	62	59	57	56	56	F	Oct 5	Mar 7	F
G	71	67	63	59	56	53	51	50	50	G	Sep 20	Mar 22	G
H	68	62	58	54	51	48	46	45	44	H	Sep 5	Apr 6	H
I	62	57	53	49	45	43	40	39	38	I	Aug 20	Apr 22	I
J	58	54	49	45	41	39	36	34	33	J	Aug 5	May 7	J
K	55	51	46	42	38	35	32	31	30	K	Jul 21	May 22	K
L	54	49	45	41	36	33	30	28	27	L	Jul 6	Jun 6	L
M	53	48	44	40	35	32	29	27	26	M	Jun 21	Jun 21	M

(Sheet 4 of 4)

Table 22

Comparison of Computer- and Nomogram-Predicted Optical Density Contrast Values

Feature	Background	Film No.	Filter No.	Optical Density Contrast: Computer Model	Optical Density Contrast: Nomogram
Wet Clay	Dry Clay	2403	12	0.17	0.15
Wet Clay	Dry Clay	2424	12	0.16	0.15
Weathered Tuff	Fresh Tuff	2403	12	0.39	0.42
Weathered Tuff	Fresh Tuff	2424	12	0.35	0.39
Sagebrush	Lodgepole Pine	2403	12	0.26	0.29
Sagebrush	Lodgepole Pine	2424	12	0.47	0.44
Juniper	Sagebrush	2403	12	0.28	0.30
Juniper	Sagebrush	2424	12	0.13	0.15
Juniper	Lodgepole Pine	2403	12	0.02	0.04
Juniper	Lodgepole Pine	2424	12	0.60	0.59

Table 23

Inputs to General Thermal IR Systems Simulation Model for Generating Mission Planning Graphics

Sensor Descriptor	High-Performance Aircraft Wavelength Band, m: 3.0-5.5	High-Performance Aircraft Wavelength Band, m: 8-14	Low-Performance Aircraft Wavelength Band, m: 3.0-5.5	Low-Performance Aircraft Wavelength Band, m: 8-14
Detector	InSb	HgCdTe	InSb	HgCdTe
Noise Voltage Index, $v/Hz^{1/2}$	3.74×10^{-9}	1.0×10^{-8}	3.74×10^{-10}	1.0×10^{-8}
Electrical Band Width, Hz	1.25×10^{6}	1.25×10^{6}	0.30×10^{6}	0.30×10^{6}
Peak Response, v/w	6.0×10^{3}	2.0×10^{3}	6.0×10^{3}	2.0×10^{3}
Area Aperture, cm^2	40	40	40	40
Spatial Resolution, mrad	1,2,5	1,2,5	1,2,5	1,2,5

Table 24

Thermal Resolution for 8- to 14-μm Sensor Systems for Use in High-Performance Aircraft, Mid-latitude Summer Atmosphere

Temperature K	Thermal Resolution, °C		
	1 mrad	2 mrad	5 mrad
200.0	8.75	2.50	0.39
220.0	6.25	1.56	0.27
240.0	4.38	1.09	0.20
260.0	3.44	0.86	0.14
280.0	2.81	0.70	0.11
300.0	2.19	0.55	0.09
320.0	1.88	0.47	0.08
340.0	1.56	0.39	0.07
360.0	1.41	0.35	0.06
380.0	1.25	0.31	0.05
400.0	1.09	0.27	0.05

LEGEND:
Sensor Characteristics
Detector Type: HGCDTE
Detector Noise Voltage Index (volt/sqrt (Hertz)): 0.100E-07
Electrical Bandwidth (Hertz): 0.1250E 07
Wavelength Band (micrometer): 14.0-8.0
Effective Aperature Area (cm^2): 40.0
Peak Response (volt/watt): 2000.0
Atmosphere Condition
Latitude-Season: Mid-latitude Summer
Haze (km): 23
Altitude (km): 1.5

Table 25

Thermal Resolution for 8- to 14-μm Sensor Systems for Use in High-Performance Aircraft, Mid-latitude Winter Atmosphere

Temperature K	Thermal Resolution, °C		
	1 mrad	2 mrad	5 mrad
200.0	6.25	1.72	0.27
220.0	4.38	1.09	0.18
240.0	3.13	0.78	0.13
260.0	2.50	0.63	0.10
280.0	1.88	0.47	0.08
300.0	1.56	0.39	0.06
320.0	1.25	0.31	0.05
340.0	1.09	0.27	0.05
360.0	1.02	0.25	0.04
380.0	0.94	0.23	0.04
400.0	0.86	0.21	0.03

LEGEND:

Sensor Characteristics

Detector Type: HGCDTE

Detector Noise Voltage Index (volt/Sqrt (Hertz)): 0.1000E-07

Electrical Bandwidth (Hertz): 0.1250E 07

Wavelength Band (micrometers): 14.0-8.0

Effective Aperature Area (cm^2): 40.0

Peak Response (volt/watt): 2000.0

Atmosphere Condition

Latitude-Season: Mid-latitude Winter

Haze (km): 23

Altitude (km): 1.5

Table 26

Thermal Resolution for 8- to 14-μm Sensor Systems for Use in Low-Performance Aircraft, Mid-latitude Summer Atmosphere

Temperature K	Thermal Resolution, °C 1 mrad	2 mrad	5 mrad
200.0	5.00	1.25	0.20
220.0	3.13	0.78	0.12
240.0	2.50	0.63	0.10
260.0	1.88	0.47	0.07
280.0	1.25	0.31	0.06
300.0	1.09	0.27	0.04
320.0	0.94	0.23	0.04
340.0	0.78	0.20	0.03
360.0	0.63	0.16	0.03
380.0	0.63	0.16	0.02
400.0	0.63	0.16	0.02

LEGEND:

Sensor Characteristics

Detector Type: HGCDTE

Detector Noise Voltage Index (volt/sqrt (Hertz)): 0.1000E-07

Electrical Bandwidth (Hertz): 0.1250E 07

Wavelength Band (micrometer): 14.0-8.0

Effective Aperature Area (cm^2): 40.0

Peak Response (volt/watt): 2000.0

Atmosphere Condition

Latitude-Season: Mid-latitude Summer

Haze (km): 23

Altitude (km): 1.5

Table 27

Thermal Resolution for 8- to 14-μm Sensor Systems for Use in Low-Performance Aircraft, Mid-latitude Winter Atmosphere

Temperature K	Thermal Resolution, °C 1 mrad	2 mrad	5 mrad
200.0	3.13	0.78	0.12
220.0	2.19	0.55	0.08
240.0	1.56	0.39	0.06
260.0	1.25	0.31	0.05
280.0	0.94	0.23	0.04
300.0	0.78	0.20	0.03
320.0	0.63	0.16	0.02
340.0	0.63	0.16	0.02
360.0	0.47	0.12	0.02
380.0	0.47	0.12	0.02
400.0	0.39	0.10	0.01

LEGEND:

Sensor Characteristics

Detector Type: HGCDTE

Detector Noise Voltage Index (volt/sqrt (Hertz)): 0.1000E-07

Wavelength Band (micrometer): 14.0-8.0

Effective Aperature Area (cm^2): 40.0

Peak Response (volt/watt): 2000.0

Atmosphere Condition

Latitude-season: Mid-latitude Winter

Haze (km): 23

Altitude (km): 1.5

Table 28

Thermal Resolution for 3- to 5.5-μm Sensor Systems for Use in High-Performance Aircraft, Mid-latitude Summer Atmosphere

Temperature K	Thermal Resolution, °C 1 mrad	2 mrad	5 mrad
200.0	50.00	30.00	10.00
220.0	35.00	15.00	3.75
240.0	20.00	7.50	1.25
260.0	10.00	3.13	0.47
280.0	5.00	1.56	0.23
300.0	3.13	0.78	0.12
320.0	1.88	0.47	0.08
340.0	0.94	0.31	0.04
360.0	0.63	0.16	0.03
380.0	0.47	0.12	0.02
400.0	0.31	0.08	0.01

LEGEND:

Sensor Characteristics

Detector Type: HGCDTE

Detector Noise Voltage Index (volt/sqrt (Hertz)): 0.1000E-07

Electrical Bandwidth (Hertz): 0.1250E 07

Wavelength Band (micrometer): 14.0-0.8

Effective Aperature Area (cm^2): 10.0

Peak Response (volt/watt): 2000.0

Atmosphere Condition

Latitude-Season: Mid-latitude Summer

Haze (km): 23

Altitude (km): 1.5

Table 29

Thermal Resolution for 3- to 5.5-μm Sensor Systems for Use in High-Performance Aircraft, Mid-latitude Winter Atmosphere

Temperature K	Thermal Resolution, °C 1 mrad	2 mrad	5 mrad
200.0	40.00	20.00	6.25
220.0	25.00	10.00	1.88
240.0	15.00	5.00	0.78
260.0	7.50	1.88	0.31
280.0	3.75	0.94	0.16
300.0	2.50	0.63	0.08
320.0	1.25	0.31	0.06
340.0	0.78	0.20	0.03
360.0	0.47	0.12	0.02
380.0	0.31	0.08	0.01
400.0	0.23	0.06	0.01

LEGEND:

Sensor Characteristics

Detector Type: HGCDTE

Detector Noise Voltage Index (volt/sqrt (Hertz)): 0.1000E-07

Electrical Bandwidth (Hertz): 0.1250E 07

Wavelength Band (micrometer): 14.0-8.0

Effective Aperature Area (cm^2): 40.0

Peak Response (volt/watt): 2000.0

Atmosphere Condition

Latitude-Season: Mid-latitude Winter

Haze (km): 23

Altitude (km): 1.5

Table 30

Thermal Resolution for 3- to 5.5-μm Sensor Systems for Use in Low-Performance Aircraft, Mid-latitude Summer Atmosphere

Temperature K	Thermal Resolution, °C 1 mrad	2 mrad	5 mrad
200.0	40.00	20.00	5.00
220.0	20.00	10.00	1.25
240.0	10.00	2.50	0.63
260.0	5.00	1.25	0.31
280.0	2.50	0.63	0.08
300.0	1.25	0.31	0.08
320.0	0.63	0.16	0.04
340.0	0.63	0.16	0.02
360.0	0.31	0.08	0.01
380.0	0.16	0.04	0.01
400.0	0.16	0.04	0.00

LEGEND:

Sensor Characteristics

Detector Type: HGCDTE

Detector Noise Voltage Index (volt/sqrt (Hertz)): 0.1000E-07

Electrical Bandwidth (Hertz): 0.1250E 07

Wavelength Band (micrometer): 14.0-8.0

Effective Aperature Area (cm^2): 40.0

Peak Response (volt/watt): 2000.0

Atmosphere Condition

Latitude-Season: Mid-latitude Summer

Haze (km): 23

Altitude (km): 1.5

Table 31

Thermal Resolution for 3- to 5.5-μm Sensor Systems for Use in Low-Performance Aircraft, Mid-latitude Winter Atmosphere

Temperature K	Thermal Resolution, °C 1 mrad	2 mrad	5 mrad
200.0	30.00	15.00	2.50
220.0	20.00	5.00	1.25
240.0	10.00	2.50	0.31
260.0	5.00	1.25	0.16
280.0	2.50	0.63	0.08
300.0	1.25	0.31	0.04
320.0	0.63	0.16	0.02
340.0	0.31	0.08	0.01
360.0	0.31	0.08	0.01
380.0	0.16	0.04	0.00
400.0	0.16	0.04	0.00

LEGEND:

Sensor Characteristics

Detector Type: HGCDTE

Detector Noise Voltage Index (volt/sqrt (Hertz)): 0.1000E-07

Electrical Bandwidth (Hertz): 0.1250E 07

Wavelength Band (micrometer): 14.0-8.0

Effective Aperature Area (cm^2): 2000.0

Peak Response (volt/watt): 2000.0

Atmosphere Condition

Latitude-Season: Mid-latitude Winter

Haze (km): 23

Altitude (km): 1.5

Table 32

Typical Emissivity Values*

Terrain Feature	Wavelength Band, m 3.0-5.5	8.0-14.0
Green Mountain Laurel	≈ 0.90	≈ 0.92
Young Willow Leaf (dry, top)	0.94	0.96
Holly Leaf (dry, top)	0.90	0.90
Holly Leaf (dry, bottom)	0.86	0.94
Pressed Dormant Maple Leaf (dry, top)	0.87	0.92
Green Leaf Winter Color - Oak Leaf (dry, top)	0.90	0.92
Green Coniferous Twigs (Jack Pine)	0.96	0.97
Grass - Meadow Fescue (dry)	0.82	0.88
Sand - Hainamanu Silt Loam - Hawaii	0.84	0.94
Sand - Barnes Fine Silt Loam - South Dakota	0.78	0.93
Sand - Gooah Fine Silt Loam - Oregon	0.80	0.98
Sand - Vereiniging - Africa	0.82	0.94
Sand - Maury Silt Loam - Tennessee	0.74	0.95
Sand - Dublin Clay Loam - California	0.88	0.97
Sand - Pullman Loam - New Mexico	0.78	0.93
Sand - Grady Silt Loam - Georgia	0.85	0.94
Sand - Colts Neck Loam - New Jersey	0.90	0.94
Sand - Mesita Negra - lower test site	0.75	0.92
Bark - Northern Red Oak	0.90	0.96
Bark - Northern American Jack Pine	0.88	0.97
Bark - Colorado Spruce	0.87	0.94

* From Reference 31.

Table 33

Noise Equivalent Temperature* Values as Derived from the Thermal IR Systems Simulation Model, °C

Sensor Spatial Resolution, mrad	Wavelength Band, μm 3.0-5.5 Season Winter	Summer	8.0-14.0 Season Winter	Summer
Sensors for High-Performance Aircraft				
1	2.50	3.13	1.56	2.19
2	0.63	0.78	0.39	0.55
5	0.08	0.12	0.06	0.09
Sensors for Low-Performance Aircraft				
1	1.25	1.25	0.78	1.09
2	0.31	0.31	0.20	0.27
5	0.04	0.08	0.03	0.04

* Values include the influence of atmospheric conditions.

Table 34

Approximate Scales for Thermal IR Imagery
When Sensor Output is Recorded on Film

Film Width cm	Scan Width deg	Sensor Height m	Approximate Image Scale
7.0	60	300	1:5,000
		600	1:10,000
		900	1:15,000
		1500	1:25,000
		3000	1:50,000
	90	300	1:8,600
		600	1:17,100
		900	1:25,700
		1500	1:42,900
		3000	1:85,700
12.7	60	300	1:2,700
		600	1:5,500
		900	1:8,200
		1500	1:13,600
		3000	1:27,000
	90	300	1:4,700
		600	1:9,400
		900	1:14,200
		1500	1:23,600
		3000	1:47,200
	120	300	1:8,200
		600	1:16,400
		900	1:25,700
		1500	1:41,000
		3000	1:82,000

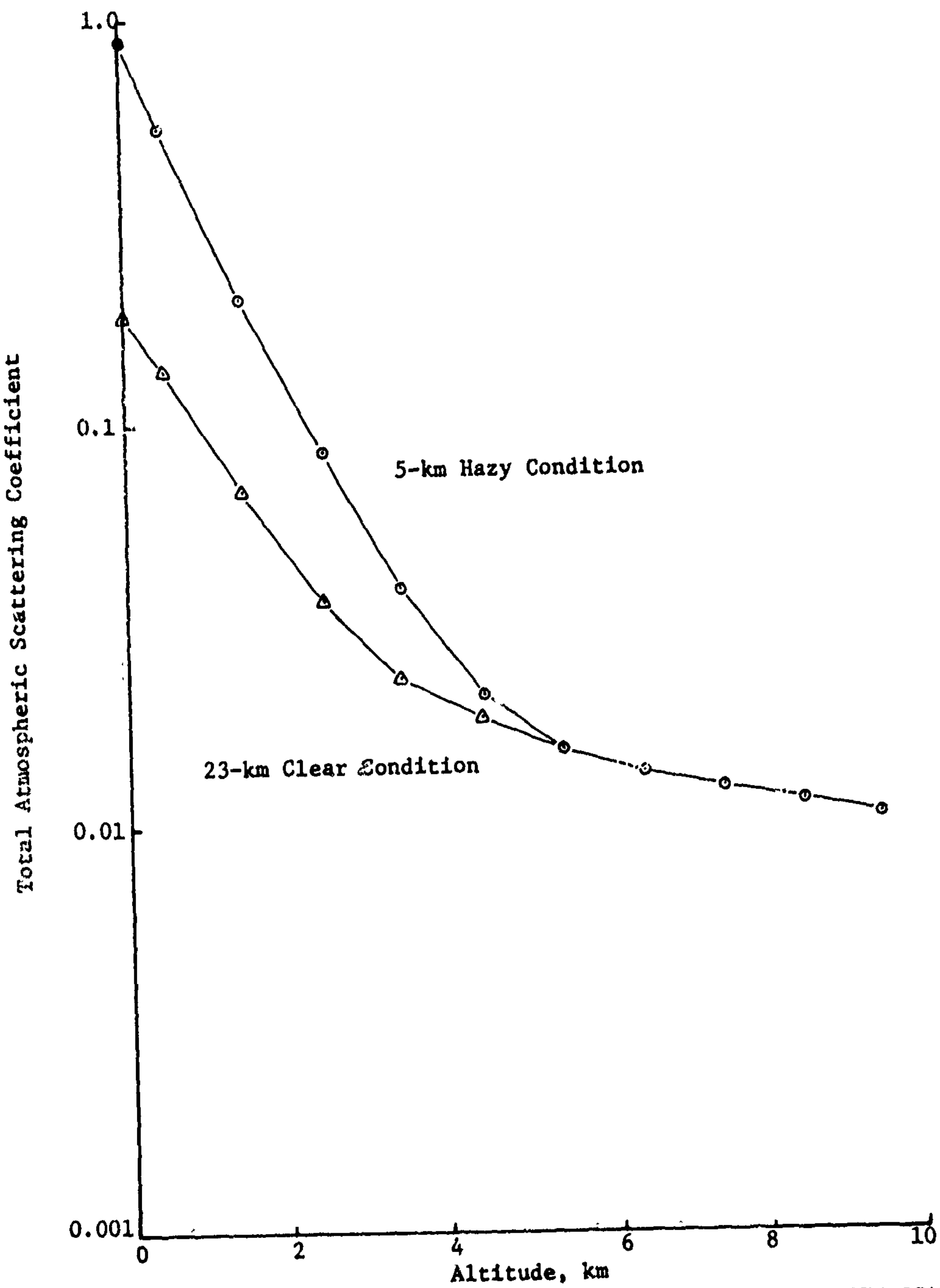

TOTAL ATMOSPHERIC SCATTERING
COEFFICIENT VERSUS
ALTITUDE FOR $\lambda = 0.4880\ \mu m$

PLATE 1

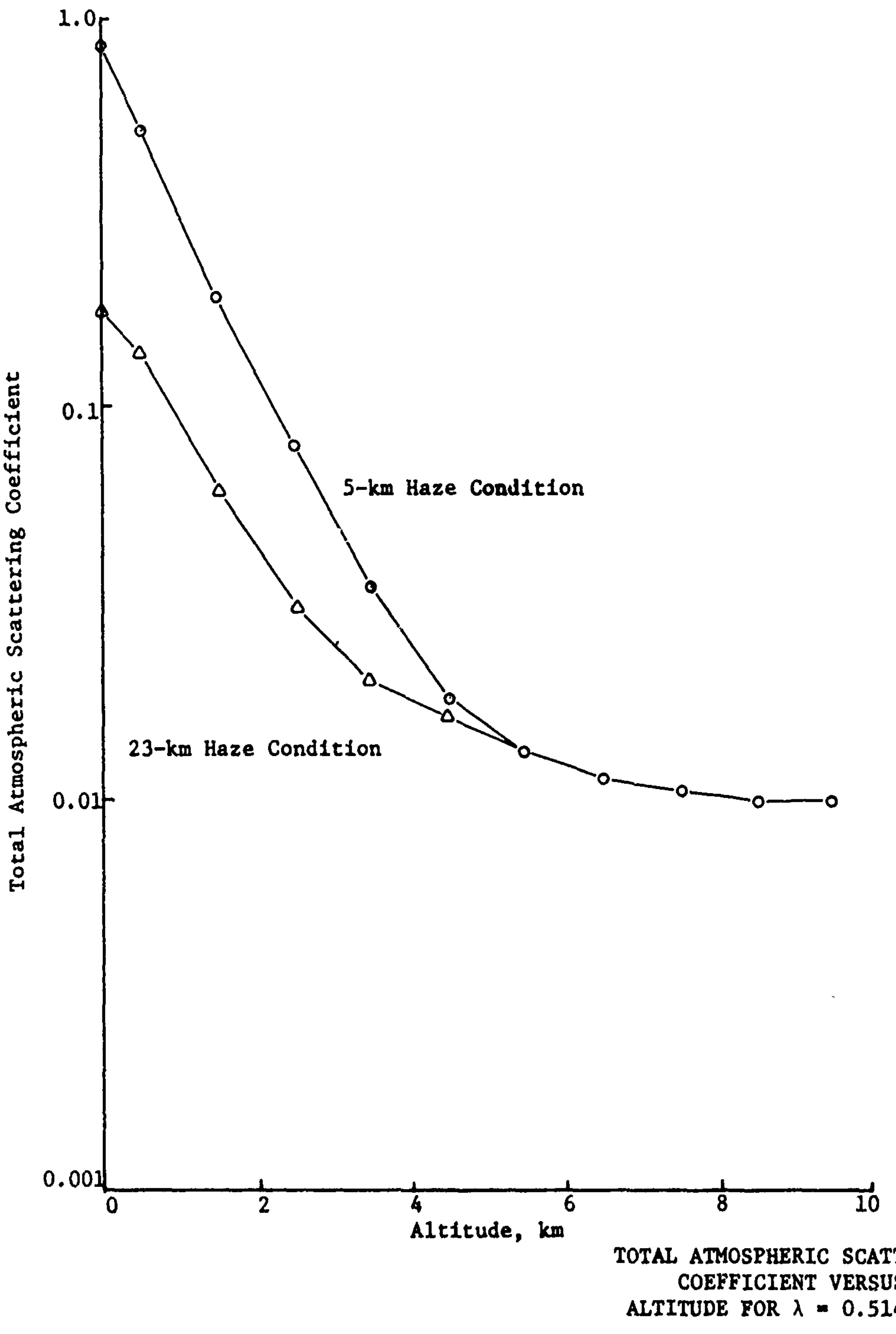

TOTAL ATMOSPHERIC SCATTERING
COEFFICIENT VERSUS
ALTITUDE FOR $\lambda = 0.5145\ \mu m$

PLATE 2

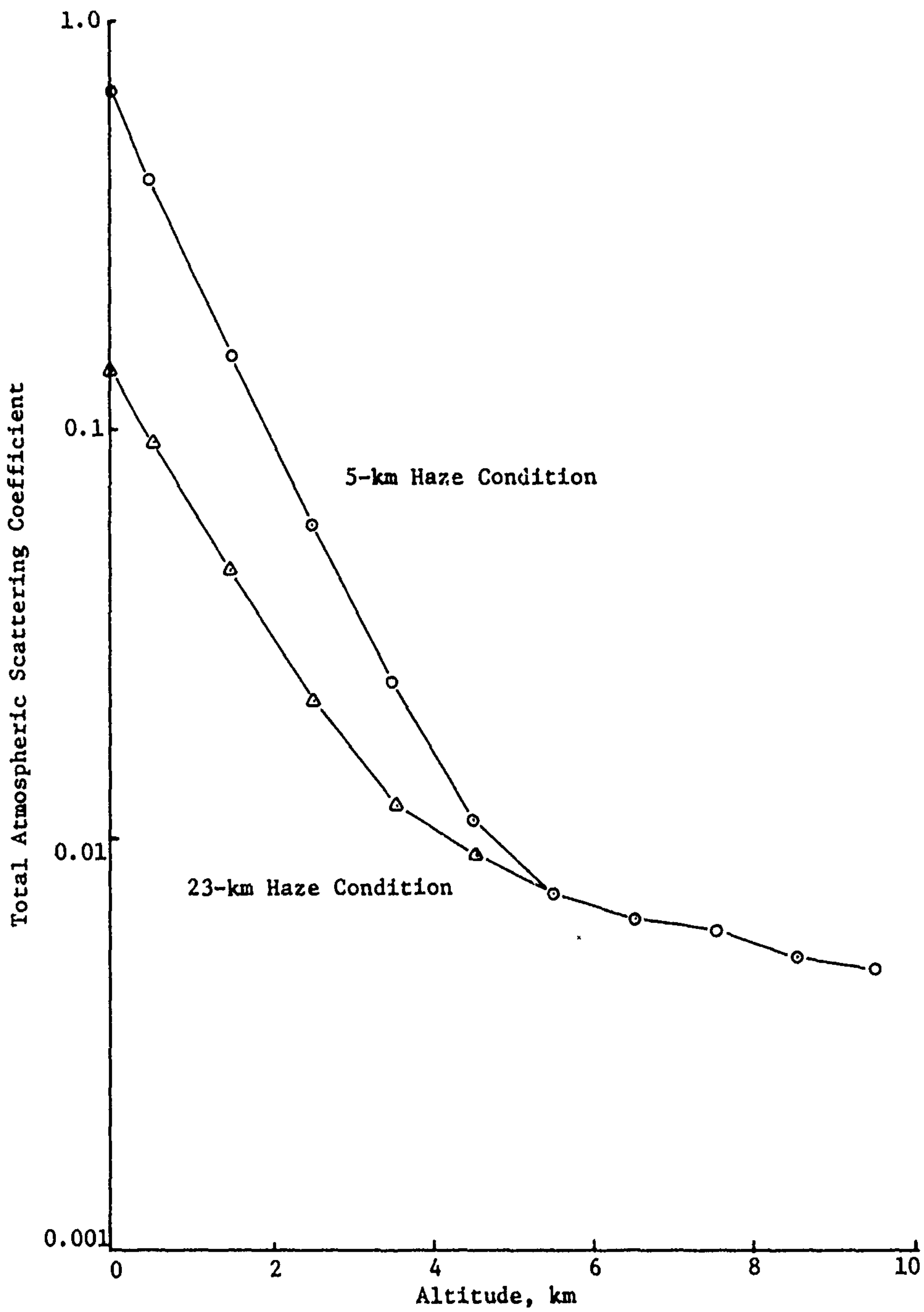

TOTAL ATMOSPHERIC SCATTERING
COEFFICIENT VERSUS
ALTITUDE FOR $\lambda = 0.6328\ \mu m$

PLATE 3

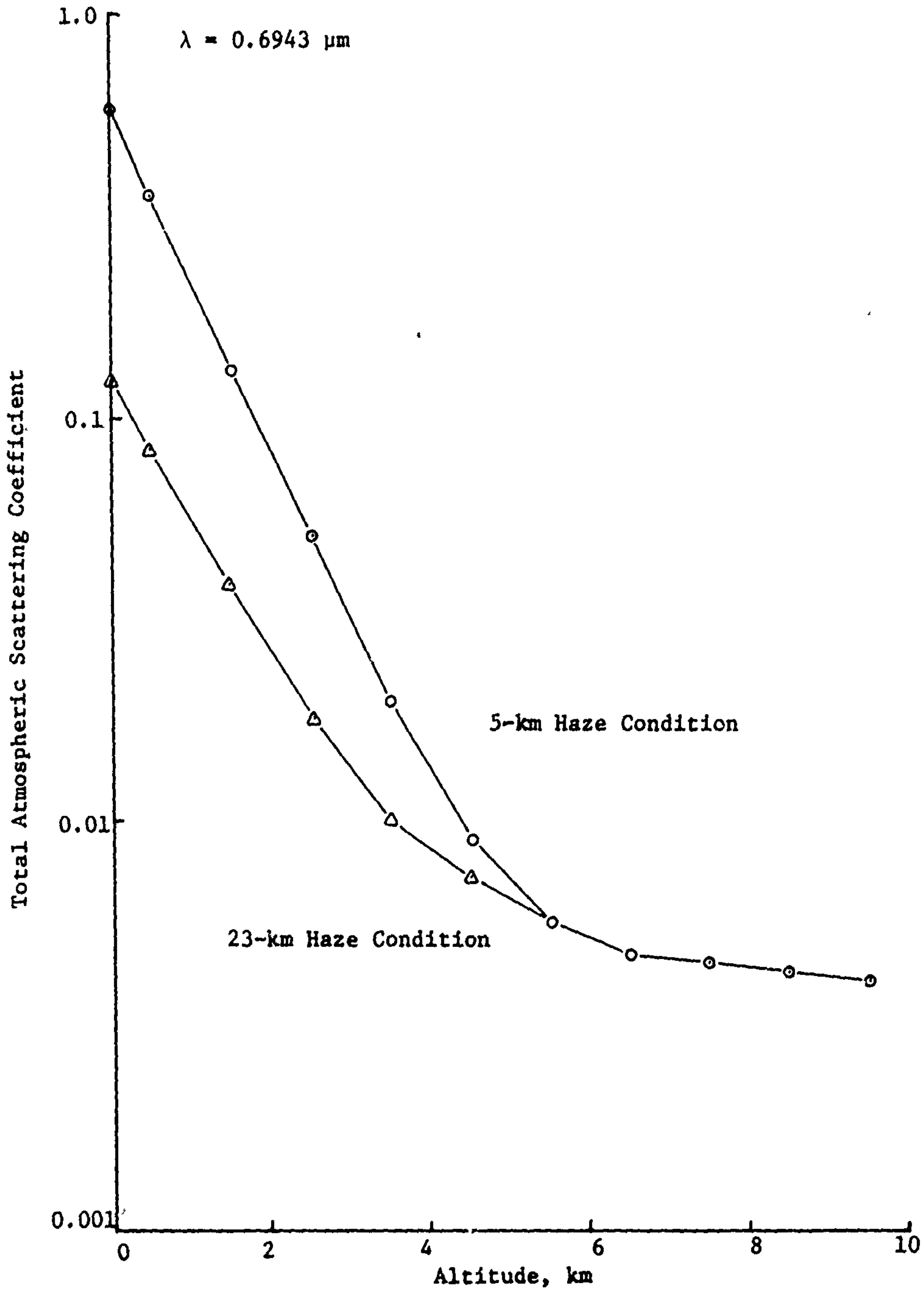

TOTAL ATMOSPHERIC SCATTERING
COEFFICIENT VERSUS
ALTITUDE FOR λ = 0.6943 μm

PLATE 4

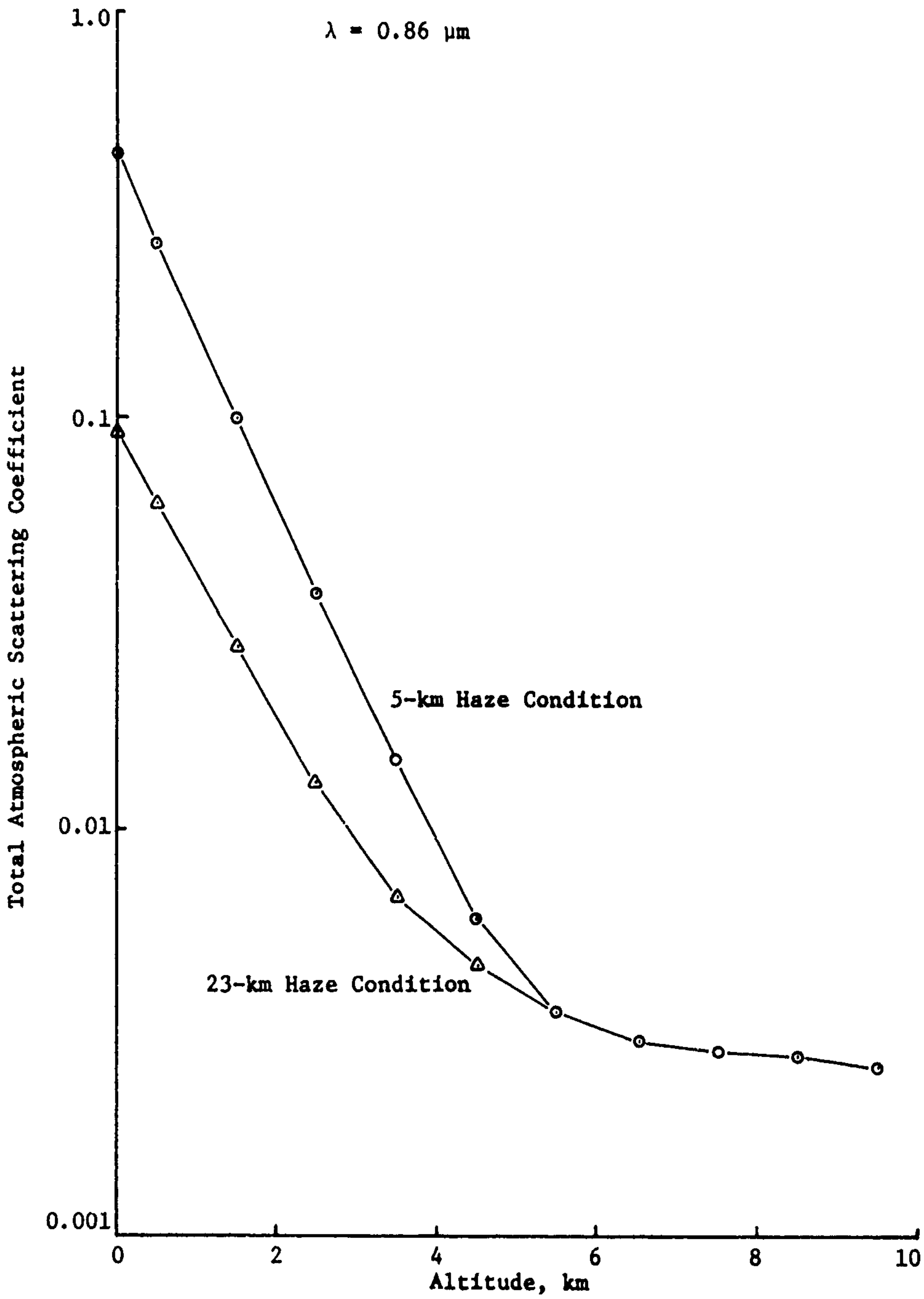

TOTAL ATMOSPHERIC SCATTERING
VERSUS
ALTITUDE FOR λ = 0.8600 μm

PLATE 5

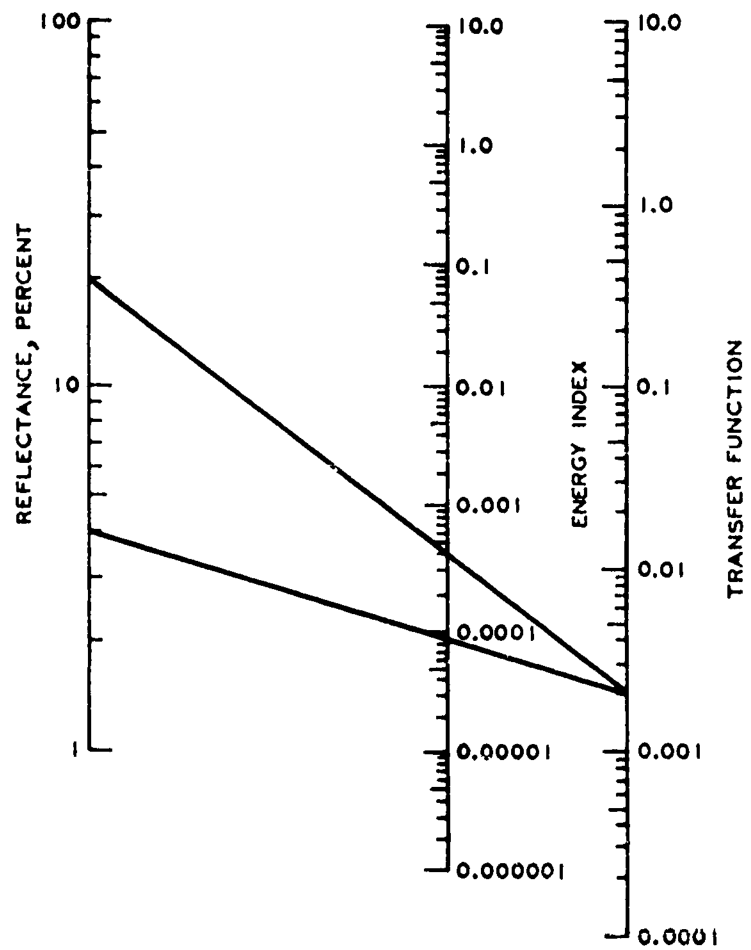

PART 1 OF NOMOGRAM
FOR PREDICTING PHOTOGRAPHIC
OPTICAL DENSITY CONTRAST

PLATE 6

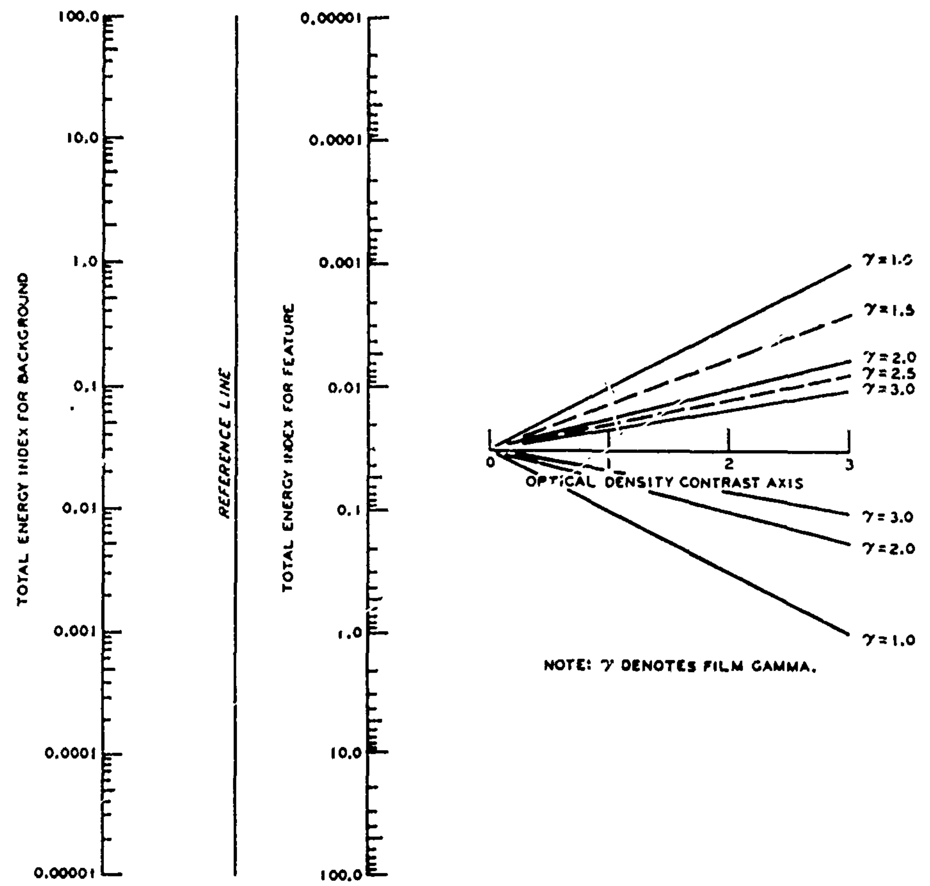

PART 2 OF NOMOGRAM
FOR PREDICTING PHOTOGRAPHIC
OPTICAL DENSITY CONTRAST

PLATE 7

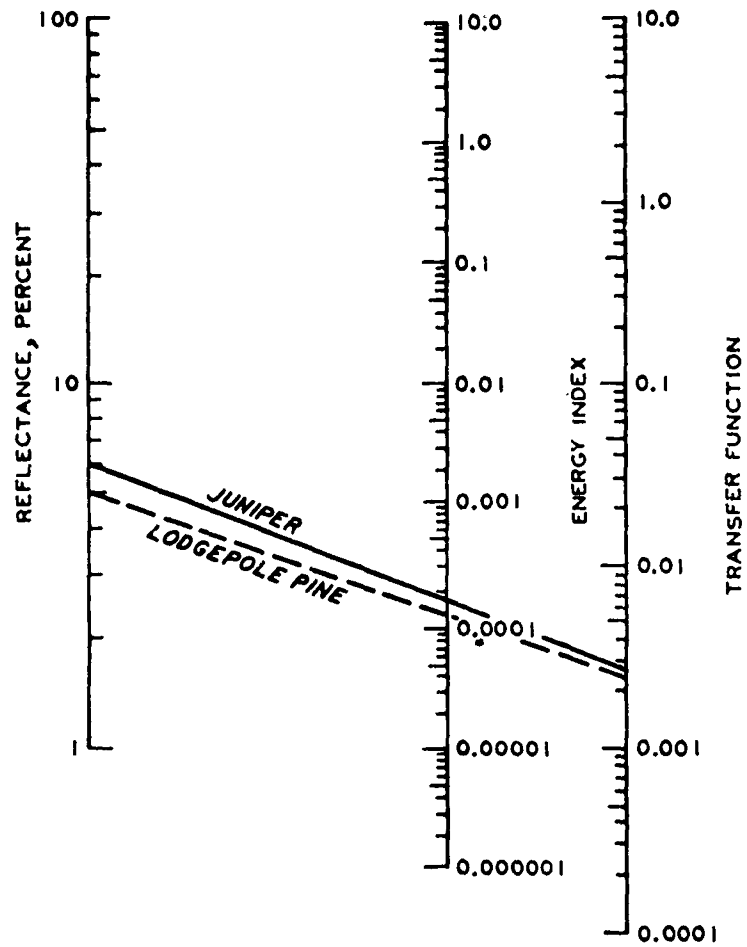

EXAMPLE OF COMPUTATION OF ENERGY INDEX VALUES FOR FEATURE AND BACKGROUND IN THE 0.40- TO 0.50-μM BAND

PLATE 8

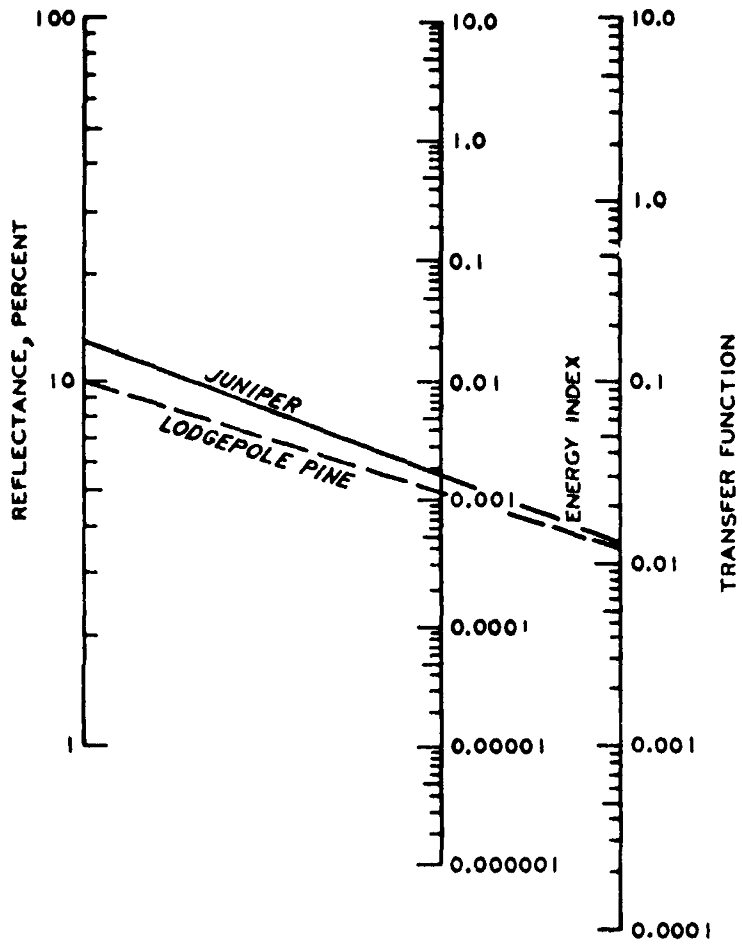

EXAMPLE OF COMPUTATION
OF ENERGY INDEX VALUES
FOR FEATURE AND BACKGROUND
IN THE 0.50- TO 0.58-μM BAND

PLATE 9

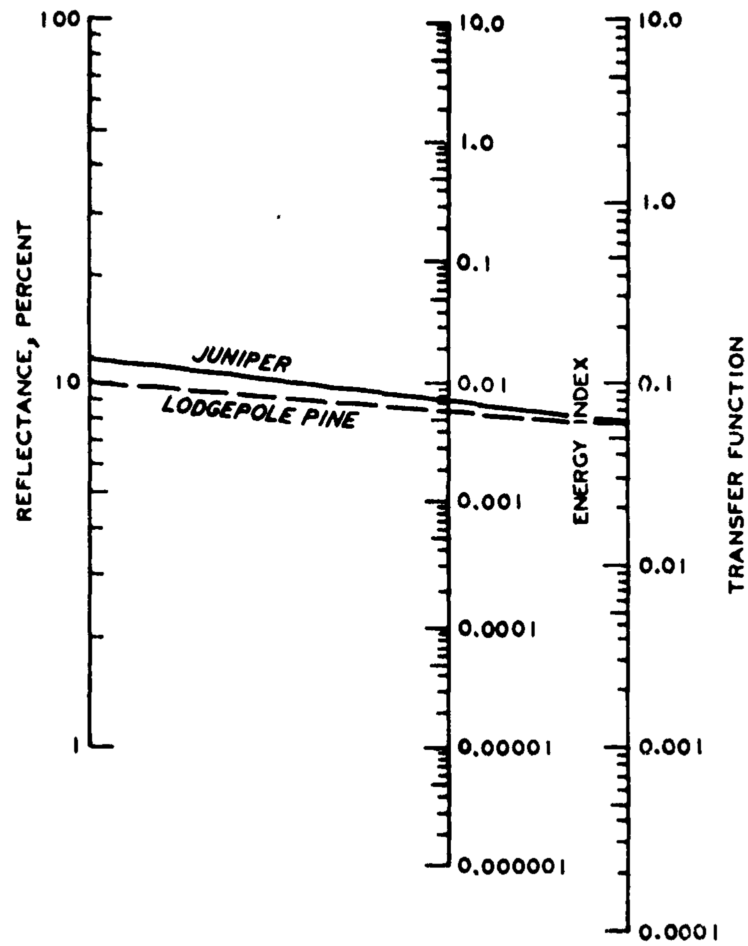

EXAMPLE OF COMPUTATION OF ENERGY INDEX VALUES FOR FEATURE AND BACKGROUND IN THE 0.58- TO 0.68-μM BAND

PLATE 10

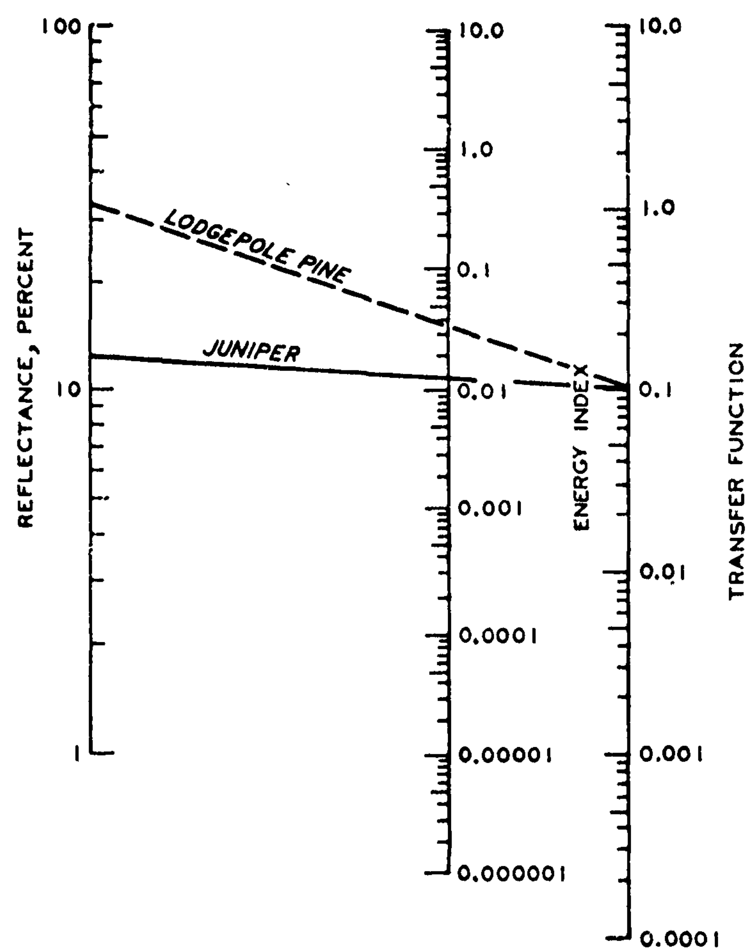

EXAMPLE OF COMPUTATION
OF ENERGY INDEX VALUES
FOR FEATURE AND BACKGROUND
IN THE 0.68- TO 0.80-μM BAND

PLATE 11

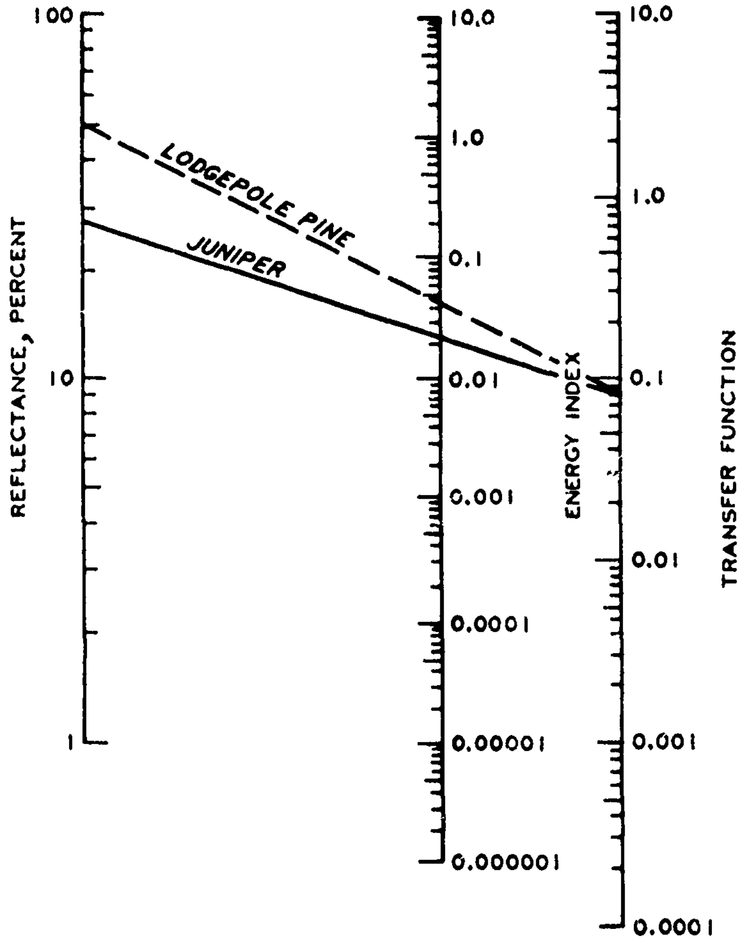

EXAMPLE OF COMPUTATION
OF ENERGY INDEX VALUES
FOR FEATURE AND BACKGROUND
IN THE 0.80- TO 0.93-μM BAND

PLATE 12

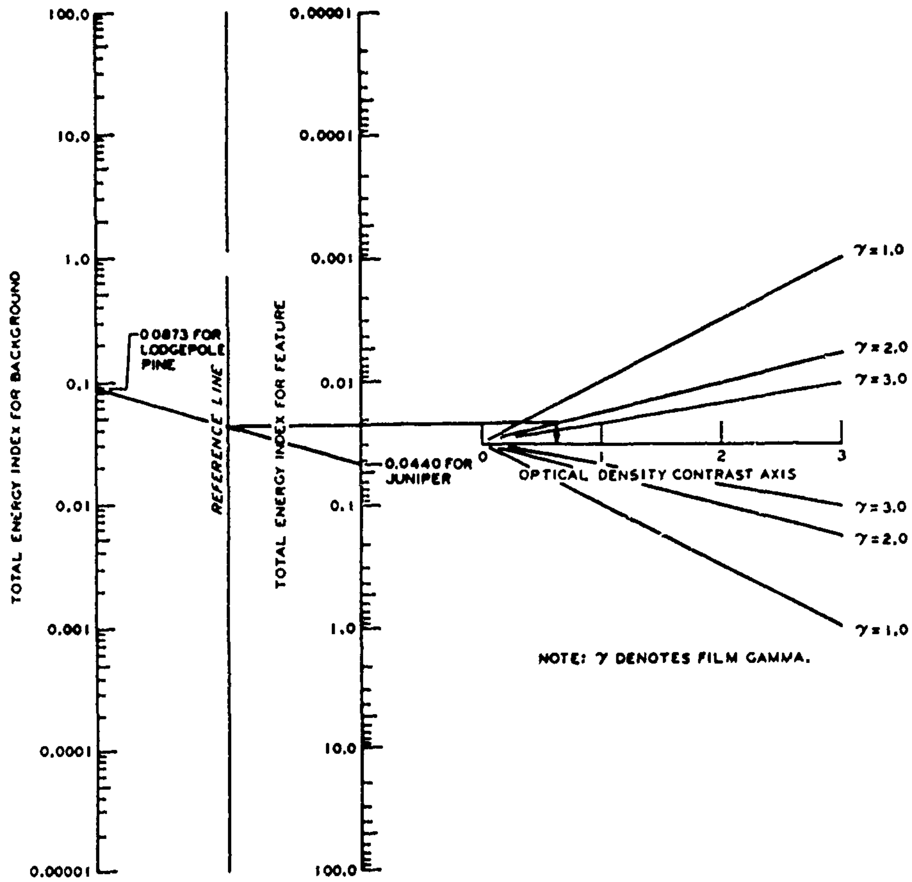

EXAMPLE OF COMPUTATION OF OPTICAL DENSITY CONTRAST USING POINT ON REFERENCE LINE AND APPROPRIATE γ CURVE

PLATE 13

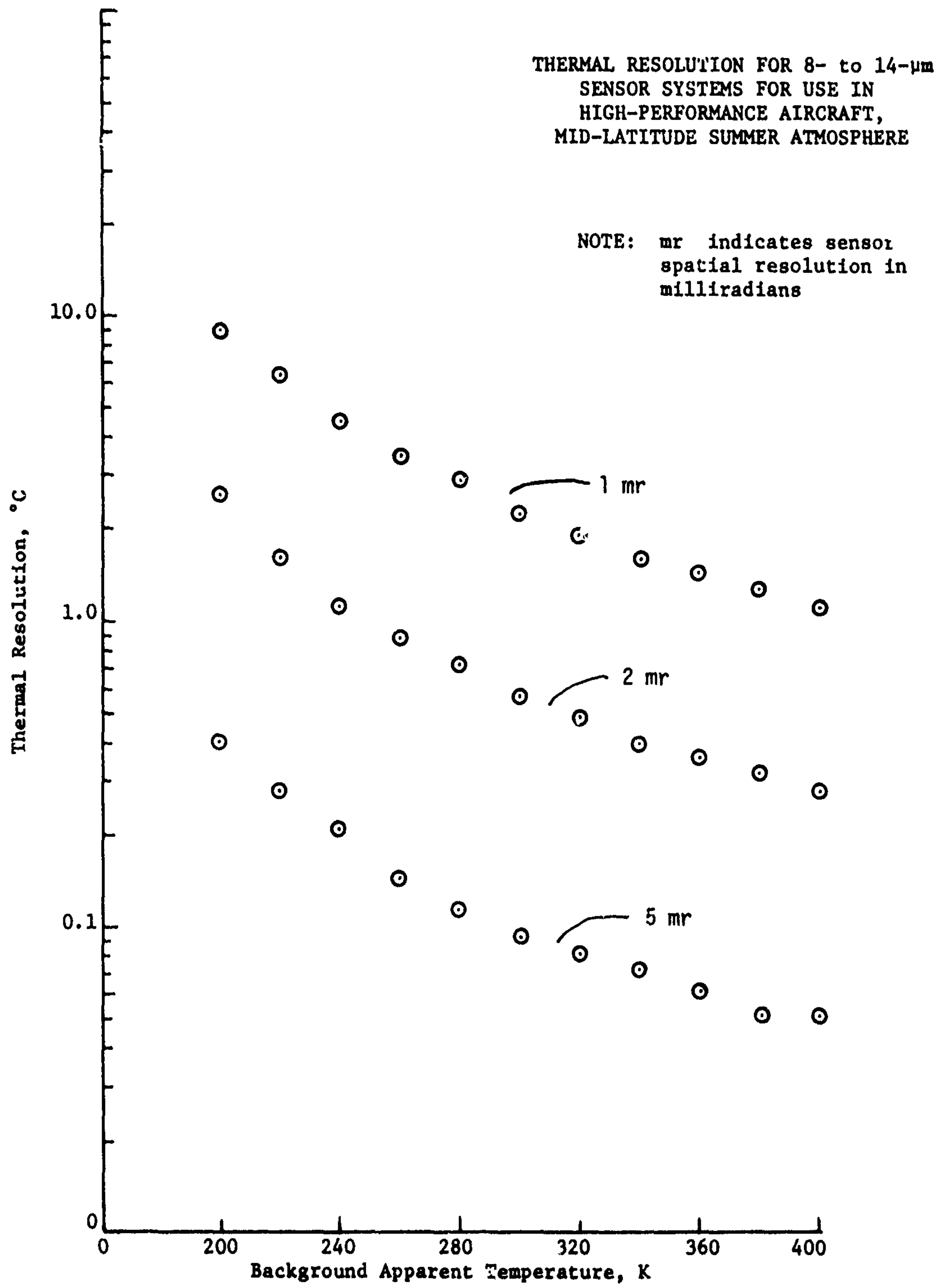
THERMAL RESOLUTION FOR 8- to 14-μm
SENSOR SYSTEMS FOR USE IN
HIGH-PERFORMANCE AIRCRAFT,
MID-LATITUDE SUMMER ATMOSPHERE
NOTE: mr indicates sensor
spatial resolution in
milliradians
10.0
1.0
0.1
0
Thermal Resolution, °C
1 mr
2 mr
5 mr
0
200
240
280
320
360
400
Background Apparent Temperature, K

PLATE 14

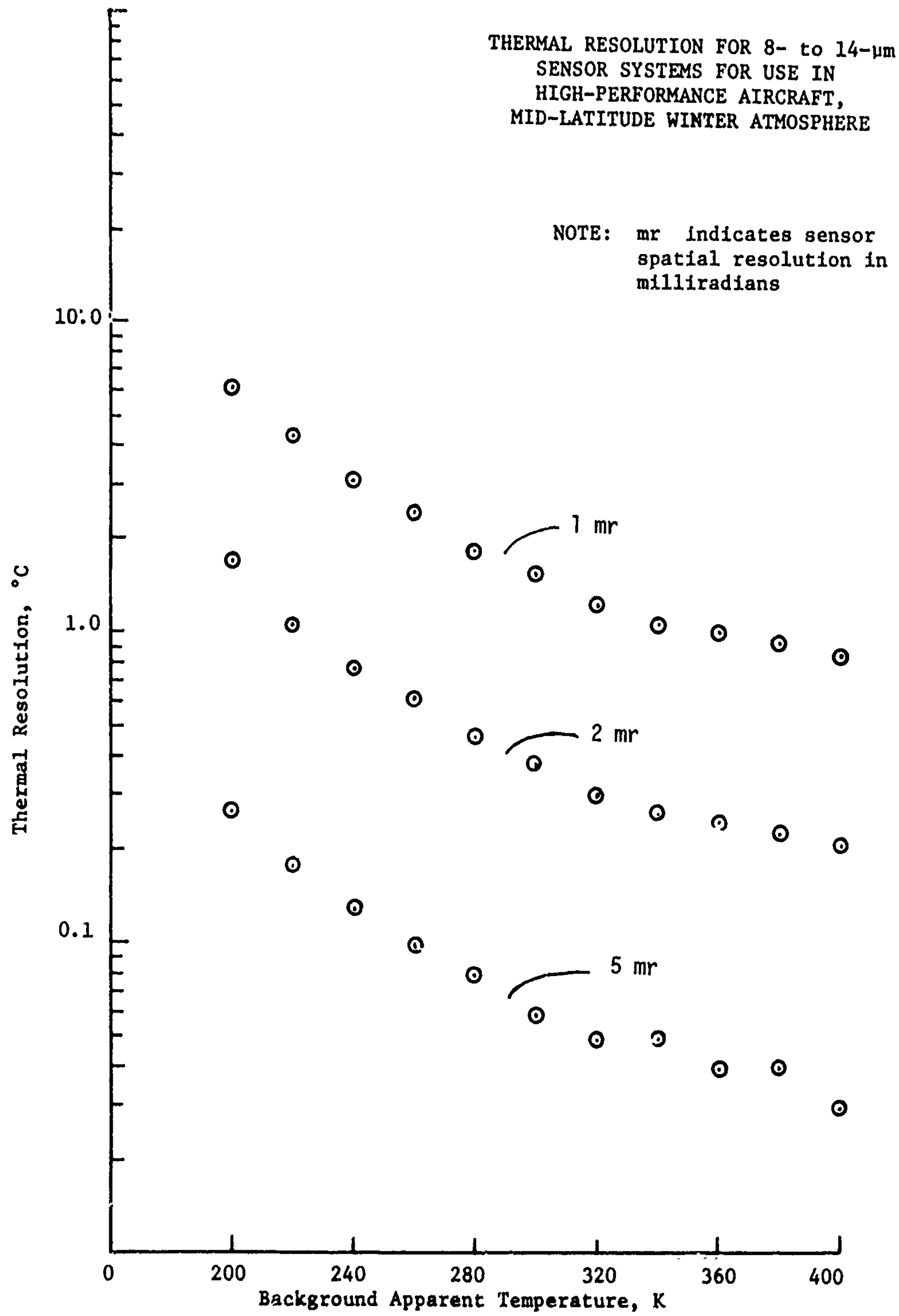
THERMAL RESOLUTION FOR 8- to 14-μm
SENSOR SYSTEMS FOR USE IN
HIGH-PERFORMANCE AIRCRAFT,
MID-LATITUDE WINTER ATMOSPHERE
NOTE: mr indicates sensor spatial resolution in milliradians
10.0
1.0
0.1
Thermal Resolution, °C
1 mr
2 mr
5 mr
0
200
240
280
320
360
400
Background Apparent Temperature, K

PLATE 15

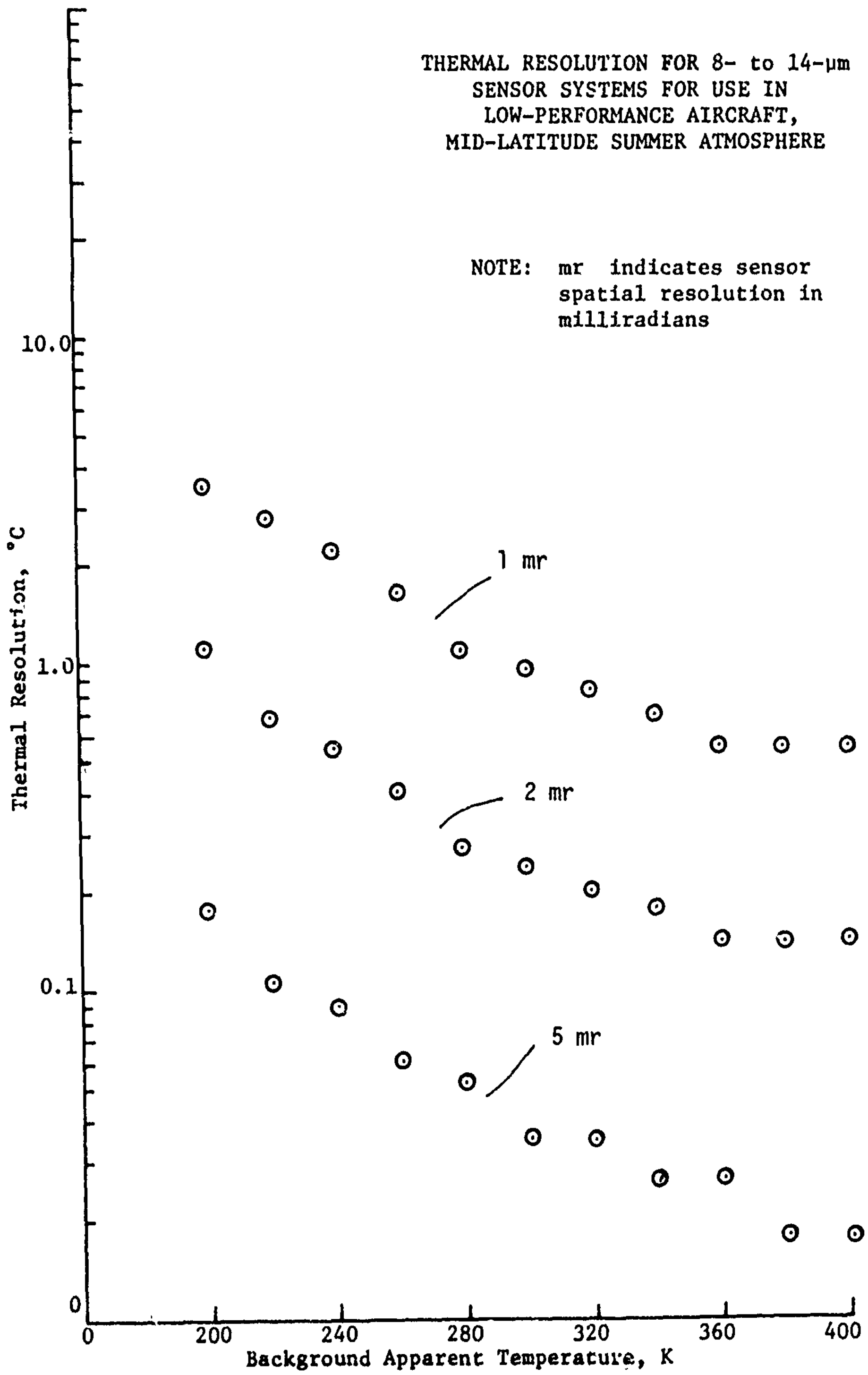
THERMAL RESOLUTION FOR 8- to 14-μm
SENSOR SYSTEMS FOR USE IN
LOW-PERFORMANCE AIRCRAFT,
MID-LATITUDE SUMMER ATMOSPHERE
NOTE: mr indicates sensor spatial resolution in milliradians
Thermal Resolution, °C
10.0
1.0
0.1
0
1 mr
2 mr
5 mr
0
200
240
280
320
360
400
Background Apparent Temperature, K

PLATE 16

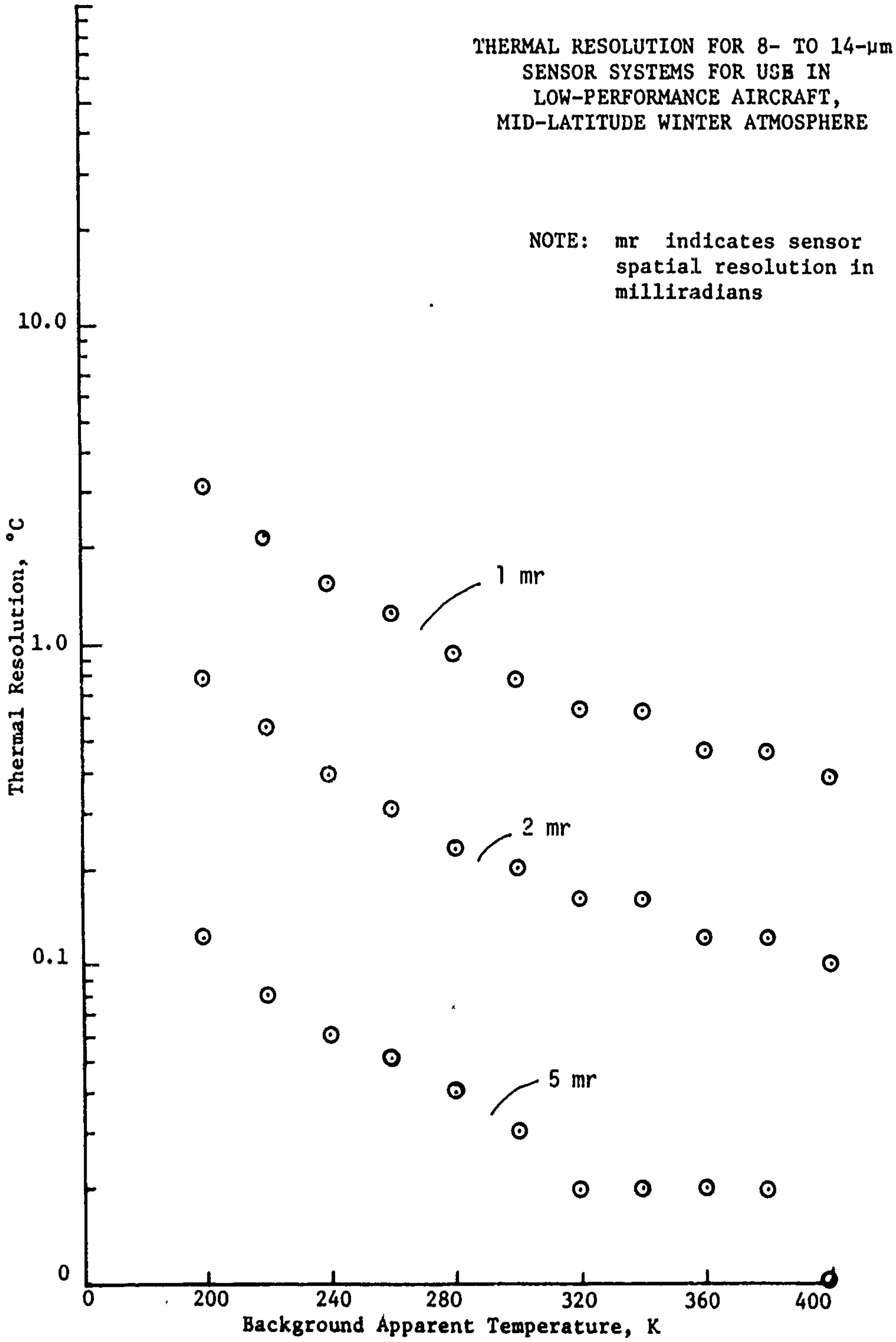
THERMAL RESOLUTION FOR 8- TO 14-μm
SENSOR SYSTEMS FOR USE IN
LOW-PERFORMANCE AIRCRAFT,
MID-LATITUDE WINTER ATMOSPHERE
NOTE: mr indicates sensor spatial resolution in milliradians
1 mr
2 mr
5 mr
Thermal Resolution, °C
10.0
1.0
0.1
0
0
200
240
280
320
360
400
Background Apparent Temperature, K

PLATE 17

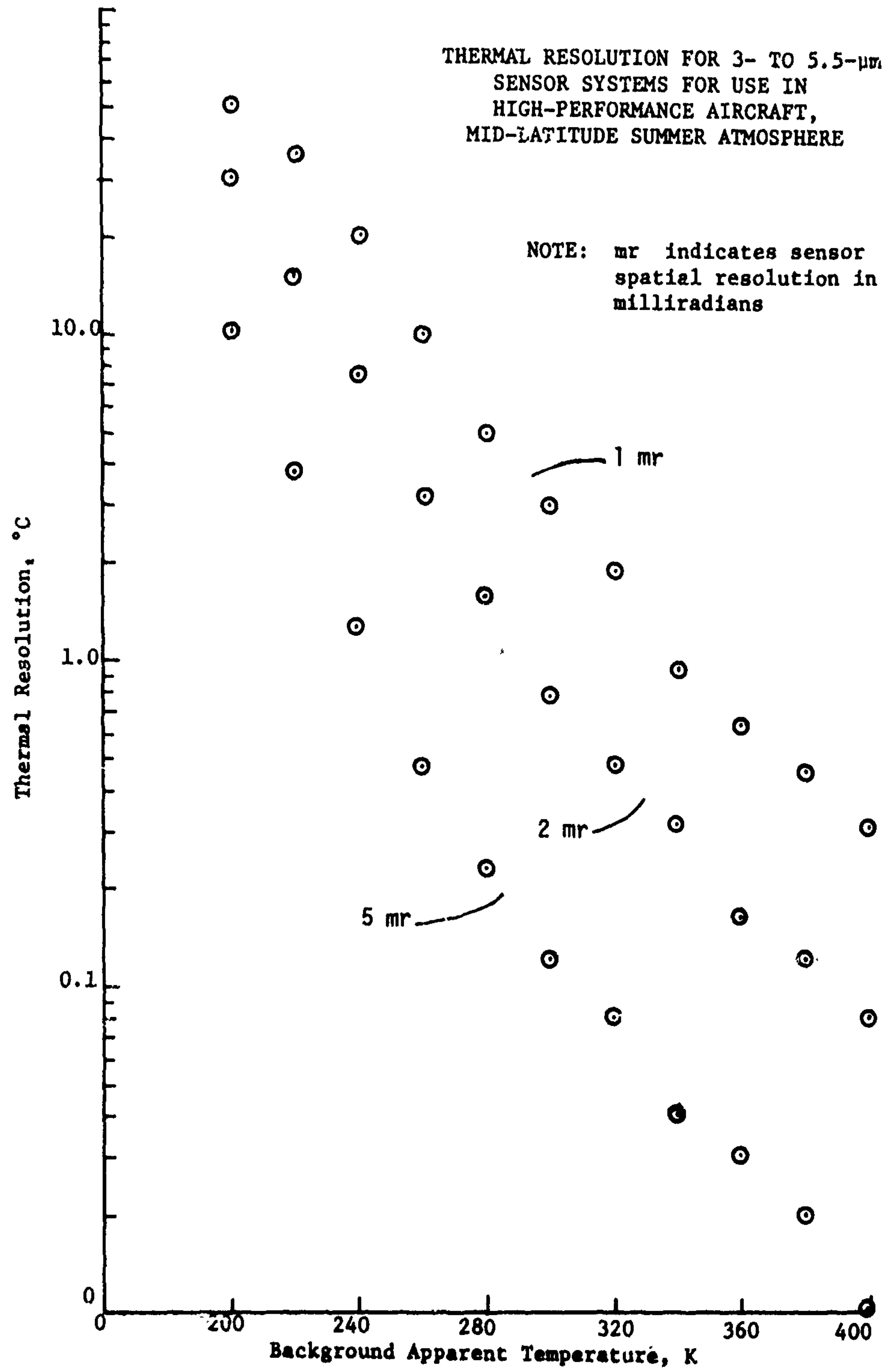
THERMAL RESOLUTION FOR 3- TO 5.5-μm SENSOR SYSTEMS FOR USE IN HIGH-PERFORMANCE AIRCRAFT, MID-LATITUDE SUMMER ATMOSPHERE
NOTE: mr indicates sensor spatial resolution in milliradians
1 mr
2 mr
5 mr
10.0
1.0
0.1
0
0
200
240
280
320
360
400
Thermal Resolution, °C
Background Apparent Temperature, K

PLATE 18

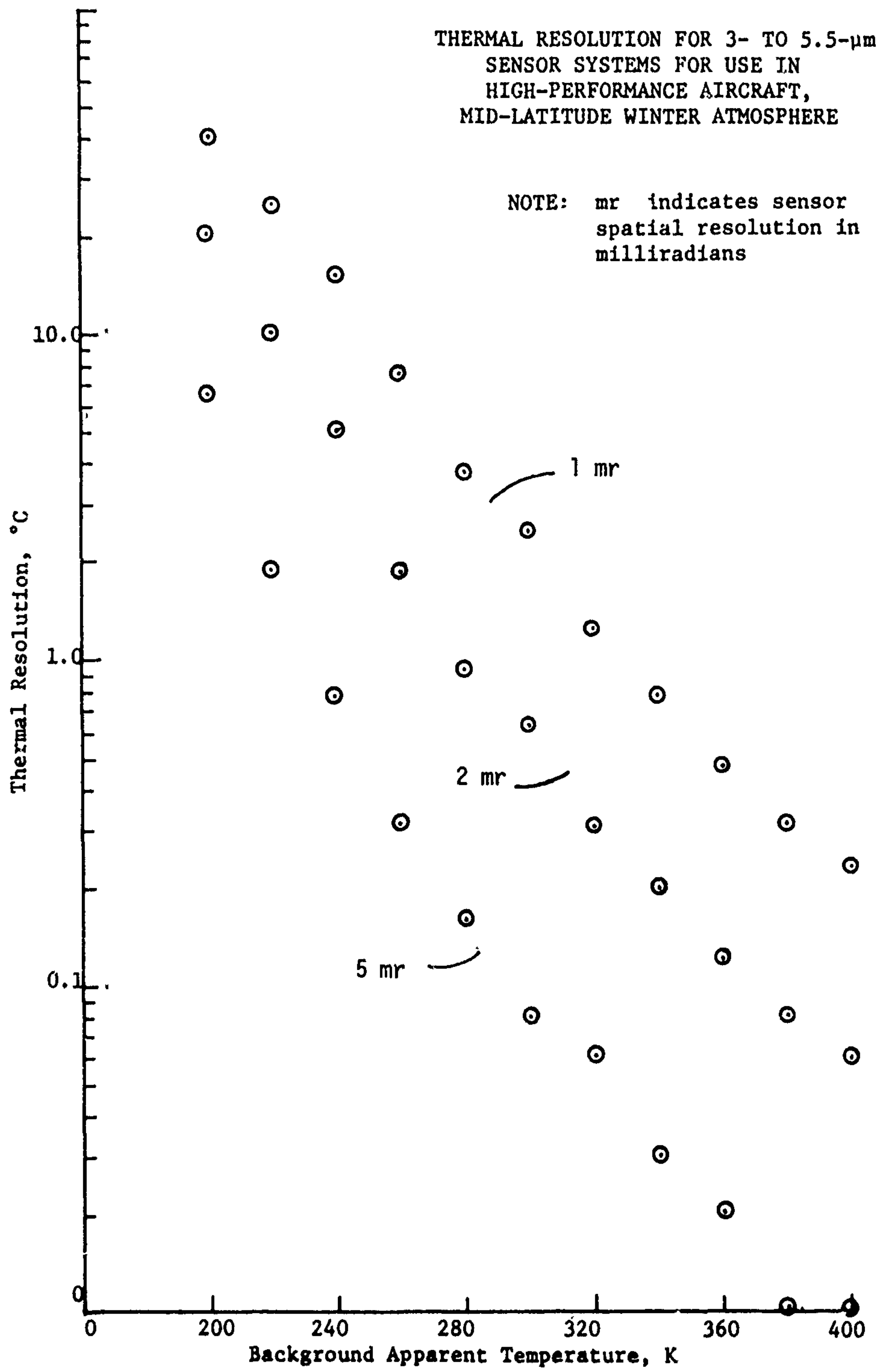
THERMAL RESOLUTION FOR 3- TO 5.5-μm
SENSOR SYSTEMS FOR USE IN
HIGH-PERFORMANCE AIRCRAFT,
MID-LATITUDE WINTER ATMOSPHERE
NOTE: mr indicates sensor spatial resolution in milliradians
1 mr
2 mr
5 mr
10.0
1.0
0.1
0
0
200
240
280
320
360
400
Thermal Resolution, °C
Background Apparent Temperature, K

PLATE 19

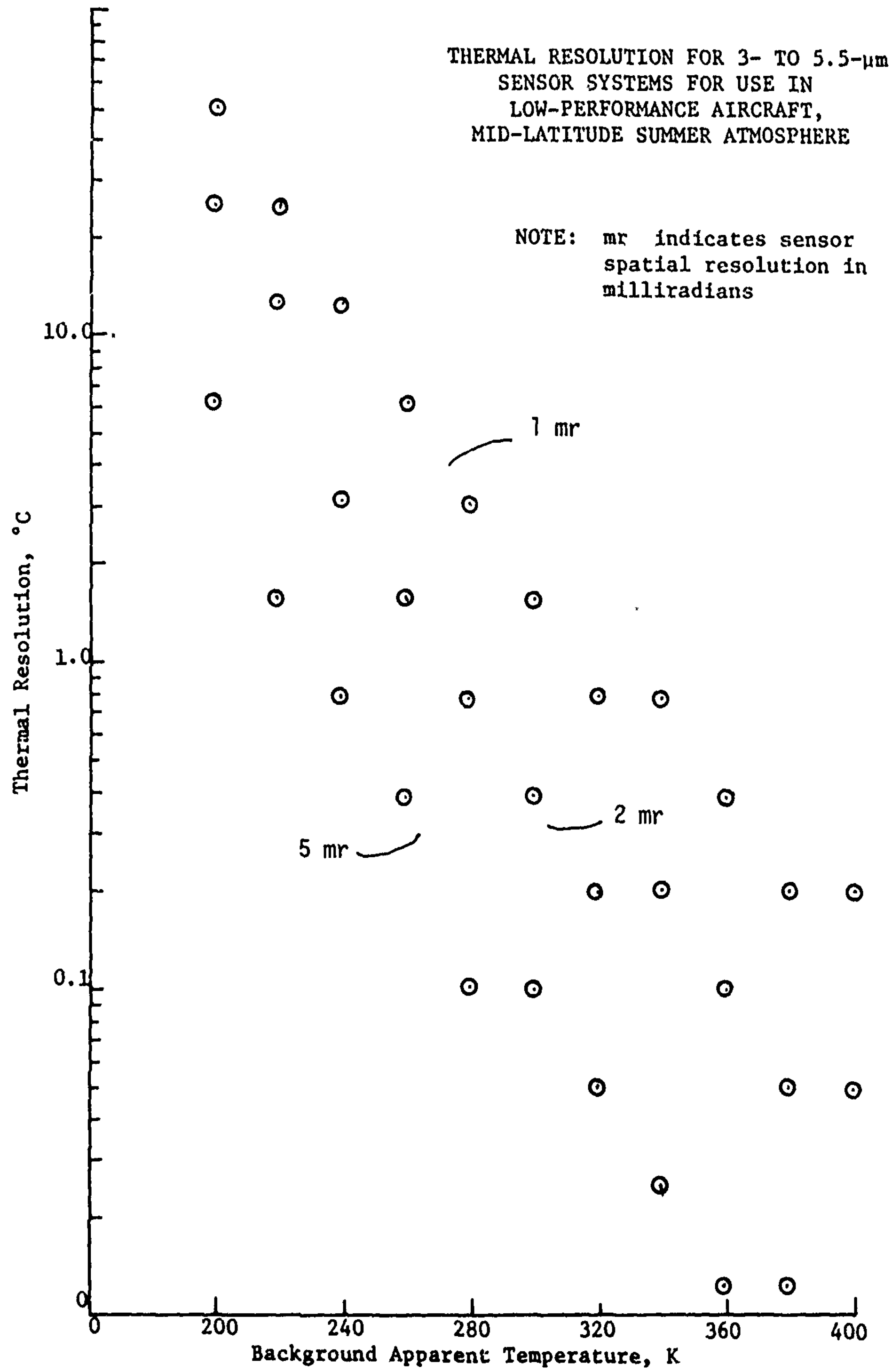

THERMAL RESOLUTION FOR 3- TO 5.5-μm SENSOR SYSTEMS FOR USE IN LOW-PERFORMANCE AIRCRAFT, MID-LATITUDE SUMMER ATMOSPHERE
NOTE: mr indicates sensor spatial resolution in milliradians
1 mr
2 mr
5 mr
10.0
1.0
0.1
0
Thermal Resolution, °C
0
200
240
280
320
360
400
Background Apparent Temperature, K

PLATE 20

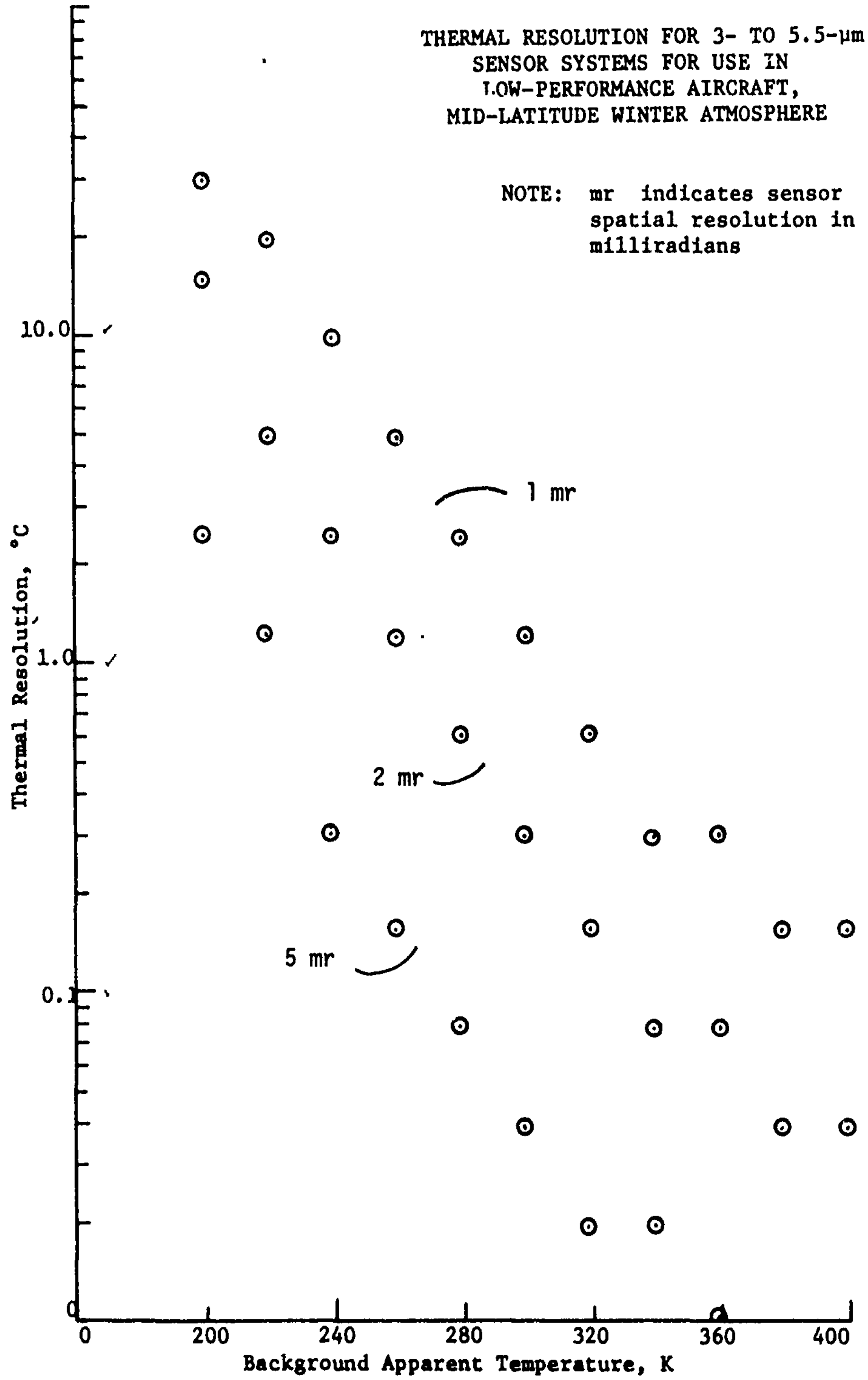
THERMAL RESOLUTION FOR 3- TO 5.5-µm
SENSOR SYSTEMS FOR USE IN
LOW-PERFORMANCE AIRCRAFT,
MID-LATITUDE WINTER ATMOSPHERE
NOTE: mr indicates sensor spatial resolution in milliradians
1 mr
2 mr
5 mr
10.0
1.0
0.1
0
Thermal Resolution, °C
0
200
240
280
320
360
400
Background Apparent Temperature, K

PLATE 21

APPENDIX A: BIBLIOGRAPHY

Aerojet Electrosystems Company, "Airborne Passive Microwave Measurements of NOAA Hydrology Sites," Report 1752FR-1, Jun 1973, U. S. Department of Commerce, National Oceanic and Atmospheric Administration, National Environmental Satellite Service, Hillcrest Heights, Md.

Badgley, P. C., "Planetary Exploration from Orbital Altitudes," Photogrammetric Engineering, Vol 32, No. 2, Mar 1966.

Bastuscheck, C. P., "Ground Temperature and Thermal Infrared," Photogrammetric Engineering, Vol 36, No. 10, 1970.

Bowersox, R. B., "Basic Properties of Radiation," Notes for Seminar Environmental Analyses by Remote Sensing, Colorado State University, Fort Collins, Colo., Jul 1968.

Buettner, K. J. K., "The Consequences of Terrestrial Surface Infrared Emissivity," Proceedings of the Third Symposium on Remote Sensing of the Environment, University of Michigan, Ann Arbor, Mich., Oct 1964.

Burgy, R. H., and Algazi, R. V., "An Assessment of Remote Sensing Applications in Hydrologic Engineering," Research Note No. 4, Sep 1974, U. S. Army Hydrologic Engineering Center, CE, Davis, Calif.

Cameron, H. L., "Radar as a Survey Instrument in Hydrology and Geology," Third Symposium on Remote Sensing of Environment, University of Michigan, Ann Arbor, Mich., 1964.

Cannon, P. J., "The Application of Radar and Infrared Imagery to Quantitative Geomorphic Investigations," Remote Sensing of Earth Resources, Vol II, University of Tennessee, Tullahoma, Tenn., Mar 1973.

Colwell, R. N., "A Summary of the Uses of Limitations of Multispectral Remote Sensing," Proceedings, First Annual International Remote Sensing Institute Symposium, Vol 2, Sacramento, Calif., 1969.

Condit, H. R., "The Spectral Reflectance of American Soils," Photogrammetric Engineering, Vol 36, No. 9, Sep 1970.

Dudley, S. Q., "Light in the Sea," Journal of the Optical Society of America, Vol 53, Feb 1963.

Egbert, D. D., "Spectral Reflectivity Data: A Practical Acquisition Procedure," CRES Technical Report 133-21, Nov 1970, University of Kansas, Lawrence, Kans.

Egbert, D. D., and Ulaby, F. T., "Effect of Angles on Reflectivity," Photogrammetric Engineering, Vol 38, No. 6, Jun 1972.

Eliason, J. R., and Foote, H. P., "Surface Water Movement Studies Utilizing a Tracer Dye Imaging System," Proceedings, Seventh Symposium on Remote Sensing of Environment, University of Michigan, Ann Arbor, Mich., 1971.

Herman, J. R., et al., "Radio Detection of Thunderstorm Activity with an Earth-Orbiting Satellite," Journal of Geophysical Research, Vol 80, No. 4, Feb 1975.

Hunter, G. T., and Bird, S. J. G., "Critical Terrain Analysis," Photogrammetric Engineering, Vol 36, No. 9, Sep 1970.

Ishaq, A. M., Application of Remote Sensing to the Location of Hydrologically Active (Source) Areas, Ph. D. Dissertation, The University of Wisconsin, Madison, Wis., 1974.

Jensen, N., Optical and Photographic Reconnaissance Systems, John Wiley and Sons, Inc., New York, 1968.

Joering, E. A., "Estimating Streamflow Characteristics Using Airphotos," Technical Note, U. S. Army Cold Regions Research and Engineering Laboratory, Hanover, N. H., 1969.

Krinov, E. L., "Spectral Reflectance Properties of Natural Formation," Technical Translation TT-439, 1953, National Research Council of Canada, Ottawa, Canada.

Krudristskii, D. M., et al., "Hydrographic Interpretation to Investigation of Aerial Photographs," Translation from the Russian by Shmutler and Stock, Israel Program for Scientific Translations, 1966.

Link, L. E., Jr., "Capability of Airborne Laser Profilometer to Measure Terrain Roughness," Proceedings, Sixth Symposium on Remote Sensing of Environment, Vol 1, October 1969.

Link, L. E., Jr., "Ground Truth Requirements for Remote Sensor Data Acquisition and Analysis," Miscellaneous Paper M-72-8, Nov 1972, U. S. Army Engineer Waterways Experiment Station, CE, Vicksburg, Miss.

Link, L. E., Jr., "Remote Sensing of Pollutant Discharges," Presented at the ASCE National Convention, Denver, Colo., Nov 1975.

Link, L. E., Jr., and Shindala, A., "Utilization of Remote Sensing in River Basin Studies," Proceedings, Eighth American Water Resources Conference, St. Louis, Mo., Oct 1972.

Lowe, D. S., "Line Scan Devices and Why Use Them," Proceedings of the Fifth Symposium on Remote Sensing of the Environment, University of Michigan, Ann Arbor, Mich., Apr 1966.

Manual of Color Aerial Photography, American Society of Photogrammetry, First Edition, 1968.

Manual of Photogrammetry, American Society of Photogrammetry, Vol 1, Third Edition, 1966.

Miers, B. T., and Oey, H. S., "An Evaluation of the Hydrometeorological Ground Truth Facility at White Sands Missile Range, New Mexico," Research and Development Technical Report ECOM-5557, Feb 1975, Atmospheric Sciences Laboratory, U. S. Army Electronics Command, White Sands Missile Range, N. Mex.

Myers, V. I., and Heilman, M. D., "Thermal Infrared for Soil Temperature Studies," Photogrammetric Engineering, Vol 35, No. 10, Oct 1969.

Oros, C. N., "River Current Data from Aerial Photography," Photogrammetric Engineering, Vol 18, No. 1, 1952.

Oswald, W. J., "Remote Sensing Data and Evaluation of Water Quality," Proceedings, First Annual International Remote Sensing Institute Symposium, Vol 2, Sacramento, Calif., 1969.

Parker, D. E., et al., "Flood Plain Delineation with Pan and Color," Photogrammetric Engineering, Vol 36, No. 10, 1970.

Parry, J. T., and Turner, H., "Infrared Photos for Drainage Analysis," Photogrammetric Engineering, Vol 37, No. 10, Oct 1971.

Reifsnyder, W. E., and Lull, H. W., "Radiant Energy in Relation to Forests," Technical Bulletin No. 1344, 1965, U. S. Department of Agriculture Forest Service, Washington, D. C.

Remote Sensing with Special Reference to Agriculture and Forestry, National Academy of Sciences, Washington, D. C., 1970.

Robinove, C. J., "Infrared Photography and Imagery in Water Research," Journal of the American Water Works Association, Vol 57, No. 7, 1965.

Sabins, F. F., Jr., "Flight Planning and Navigation for Thermal-IR Surveys," Photogrammetric Engineering, Vol 39, 1973.

Scherz, J., Aerial Photographic Techniques in Pollution Detection, Ph. D. Dissertation, University of Wisconsin, Madison, Wis., Jun 1967.

Schmugge, T. J., et al., "Hydrologic Applications of NUMBUS 5 ESMR Data," Goddard Space Flight Center Report X-910-74-51, Feb 1974, Green Belt, Md.

Schmugge, T. J., et al., "Remote Sensing of Soil Moisture with Microwave Radiometers," Journal of Geophysical Research, Vol 79, No. 2, 1974.

Schneider, W. J., "Color Photographs for Water Resources Studies," Photogrammetric Engineering, Vol 34, No. 3, March 1968.

Specht, M. R., Needler, D., and Fritz, N. L., "New Color Film for Water Penetration," Photogrammetric Engineering, Vol 39, No. 4, April 1973.

Sternberg, I., "Drainage Studies from Aerial Surveys," Photogrammetric Engineering, Vol 27, No. 4, 1961.

Stevens, A. R., et. al., "Alternatives for Land Use/Cover Mapping in the Tennessee River Watershed," Proceedings of the American Congress on Surveying and Mapping, 34th Annual Meeting, St. Louis, Mo., Mar 1974.

Stingelin, R. W., "Airborne Thermal Imaging," Report No. S-[illegible], Nov 1973, H. R. B. Singer, Inc., State College, Pa.

Strandberg, C. H., "An Aerial Water Quality Reconnaissance System," Photogrammetric Engineering, Vol 30, No. 1, Jan 1964.

Strandberg, C. H., "Color Aerial Photography for Water Supply and Pollution Control Reconnaissance," Proceedings, Third Annual Water Pollution, Sacramento, Calif., 1967.

Taylor, W. L., and Stingelin, R. W., "Infrared Imaging for Water Resources Studies," Journal of the Hydraulic Division, Proceedings of American Society of Civil Engineers, Vol 95, Jan 1969.

Texas Instruments, Inc., "Infrared System Design Considerations," Report SP14-GP68, May 1968, Dallas, Tex.

Wobber, F. J., "Orbital Photos Applied to the Environment," Photogrammetric Engineering, Vol 36, No. 8, Aug 1970.

APPENDIX B: DOCUMENTATION OF PHOTOGRAPHIC SYSTEMS SIMULATION MODEL COMPUTER PROGRAM

Program Identification

Program Title: Photographic Systems Simulation Model

Program Code Name: FTSKYL

Writers: L. E. Link and J. R. Stabler

Organization: U. S. Army Engineer Waterways Experiment Station, P. O. Box 631, Vicksburg, Mississippi 39180

Date: January 1976

Updates: 1

Version No.: 1

Source Language: FORTRAN IV, Honeywell G635

Availability: Source card deck and listing available on request from U. S. Army Engineer Waterways Experiment Station

Abstract: The Photographic Systems Simulation Model provides (1) a quantitative means of evaluating the applicability of photographic remote sensing systems for specific data acquisition jobs, (2) a means for selecting the best film-filter combination for a specific job, and (3) a guide for mission design to help ensure that the information desired can be obtained from the resulting photographs The model considers the major atmospheric, terrain, and sensor related parameters that influence image information content and most aerial photographic systems can be evaluated with the model.

Engineering Documentation

Narrative description

1. The Photographic Systems Simulation Model predicts the optical density contrast for specified features and backgrounds. The predictions are made as a function of sensor characteristics, altitude, and atmospheric conditions. The sensor conditions include lens focal length, lens F-stop setting, lens transmission film type, and filter type. The atmospheric conditions include solar zenith angle, a choice of two haze conditions (5- and 23-km visibility), and several atmosphere models (mid-latitude summer, mid-latitude winter, tropical, subarctic summer, and subarctic winter). Electromagnetic energy in the 0.4- to 1.0-μm wavelength region is considered, and any photographic system sensitive to visible or near-IR wavelengths can be analyzed with the model. The density contrast data can be used to evaluate the applicability of photographic remote sensing techniques to specific problems, selection of optimum photographic systems for a specific application, and guidance for image interpretation.

Method of solution

2. See text, Part II.

Program capabilities

3. The internal limitations and assumptions of the model are as follows:

   a. All files except atmospheric transmission must have the same starting position (1.0 μm wavelength) and end position (0.4 μm), and the data must be in the same increments.

b. Only wavelengths between 0.4 and 1.0 μm are considered.

c. Only photographic remote sensing systems can be evaluated.

d. The model assumes that all features are perfectly diffuse reflectors.

e. The increment (as a function of wavelength) between data points in any file must be greater than or equal to 50 cm^{-1} and be an even multiple of 50 cm^{-1}.

f. Predictions are made only for images obtained with the sensor directly above the features of interest.

Data inputs

4. The input data requirements for this model are as follows:

a. Sensor data

(1) Film number

(2) Filter number

(3) F-stop setting

(4) Starting wavelength-ending wavelength

b. Solar irradiance above the atmosphere

c. Spectral reflectance

(1) Feature

(2) Background

d. Transmission through the atmosphere (total atmosphere from energy source to ground)

e. Transmission through the atmosphere (from ground to sensor)

f. Skylight

g. Relative backscatter ratio

h. Filter transmission curve

i. Spectral sensitivity of film

j. Lens transmission

5. A list of input variables is shown in Table B1.

Program options

6. After one complete run, the program terminates automatically.

Printed output

7. An example of printed output is shown in Table B2.

Other outputs

8. Calcomp plots can be obtained by running a graphic program.

Flow chart

9. A condensed flow chart is shown in Figure B1.

System Documentation

Computer equipment

10. The model was developed at the U. S. Army Engineer Waterways Experiment Station using a Honeywell G635. The G635 is a dual processor system with a 192-K word (36 bit) memory. Memory cycle speed is 1.0 microsecond for fetching two words from memory. The system has a three-disc system; the dual channel DSU 180's with 168-million character capacity, the DSU 270's with 30-million character capacity, and the DSU 167's with 120-million character capacity. There are two magnetic tape subsystems with a total of three nine-track and six seven-track handlers, two printers (120 lpm), a cardpunch (100 cpm), card reader (900 cpm), and two G-DATANET-30 communications processors.

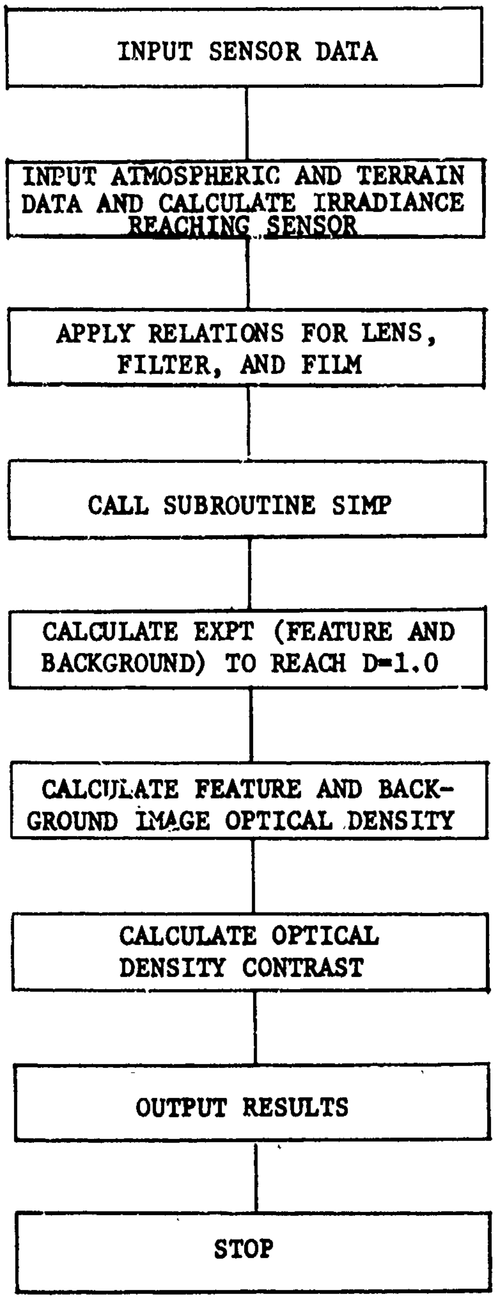

Figure B1. Condensed flow chart for remote sensing simulation model

Peripheral equipment

11. The following peripheral equipment is necessary to run this program: Honeywell G-DATANET-30 communication (16-K storage with 18-bit words) and a teletype communication terminal.

Source program

12. See availability.

Variables and subroutines

13. The variables in the simulation model and subroutine SIMP are listed in Table B3.

a. The function of the main program, subroutine, and system subprogram is as follows:

(1) Defines the dimension of the array of each variable.

(2) Identifies format for both input and output files.

(3) Reads input for all input files.

(4) Writes output for all output files.

(5) Activated subroutine at the proper time.

b. Subroutine SIMP calculates the area under functional curves using Simpson's rule.

c. Library programs used are:

(1) Cosine

(2) Common logarithm

Data structure

14. The formats of the input files are shown in Tables B4-B8. An example of each of the input files is shown in Tables B9-B13.

Storage requirements

15. The number of characters for the main program and subroutine is 15,360.

Maintenance and updates

16. The program was updated in January 1976.

Operating Instructions

Storage

17. The program is stored on a permanent disc file.

Operating messages

18. None.

Control cards

19. Control cards needed for this program are shown in Table B14.

Error recovery

20. Program must be restarted when error occurs.

Run time

21. Processor time for one complete run (i.e., one background-feature combination) with 12 film-filter combinations is about 0.0054 sec. The input-output time for this run was approximately 0.008 sec.

Table B1

List of Variables Input

Record No.	Variable	Format	Unit	Description
1-3	NAME	A68		Legend identification
4	NANGLE	Free field	deg	Zenith angle × 100
5	HEIGHT	Free field	km	Altitude
5	SCCF	Free field	-	Backscatter

Table B2

Example of Model Output

FILMN	FILTER	FEATURE EXPT FOR D=1.0 (SEC)	BACKGROUND EXPT FOR D=1.0 (SEC)	FEATURE DENSITY (DF)	BACKGROUND DENSITY (DB)	DF-DB
2402	12	0.002494	0.001151	1.000000	1.554152	0.554152
2403	12	0.000901	0.000375	1.000000	1.495396	0.495396
2402	47B	0.025486	0.015161	1.000000	1.372201	0.372201
2403	47B	0.010908	0.006589	1.000000	1.284555	0.284555
2402	58	0.012678	0.007130	1.000000	1.412479	0.412479
2403	58	0.006201	0.003484	1.000000	1.325541	0.325541
2402	25A	0.005029	0.001958	1.000000	1.675985	0.675985
2403	25A	0.001546	0.000542	1.000000	1.591475	0.591475
2402	3	0.001964	0.000915	1.000000	1.547256	0.547256
2403	3	0.000747	0.000318	1.000000	1.482382	0.482382
2448C	3	0.005550	0.002182	1.000000	1.810987	0.810987
2448Y	3	0.016650	0.007561	1.000000	1.685710	0.685710
2448M	3	0.004878	0.002803	1.000000	1.481103	0.481103
2443C	3	0.004505	0.003412	1.000000	1.181046	0.181046
2443Y	3	0.002366	0.001284	1.000000	1.398132	0.398132
2443M	3	0.003524	0.001349	1.000000	1.625664	0.625664
2443C	12	0.005106	0.004167	1.000000	1.132336	0.132336
2443Y	12	0.003775	0.002192	1.000000	1.354188	0.354188
2443M	12	0.003817	0.001446	1.000000	1.632168	0.632168
2424	12	0.000492	0.000441	1.000000	1.094734	0.094734
2424	25A	0.000508	0.000465	1.000000	1.076381	0.076381
2424	87C	0.002324	0.002517	1.069360	1.000000	0.069360
2424	89B	0.000574	0.000613	1.057942	1.000000	0.057942

LEGEND

FEATURE PONDEROSA PINE HEALTHY
BACKGROUND PONDEROSA PINE DISEASED
ATMOSPHERE MIDLATITUDE SUMMER HAZE-23 KM
ZENITH ANGLE 30 DEG.
DISTANCE TO SENSOR 1.50 KM

Table B3

Variable for Remote Sensing Simulation Model

Variable	Unit	Description
RAD		Conversion factor for changing degrees to radians
NCOUNT		Number of combinations
NOFILT		Filter number
NOSEN		Sensor number
FSTOP		F-stop settings
A1, ELL		Starting wavelength
A2, ELM		Ending wavelength
INAME		Storage for identification
NOPT, ICOUNT		Number of data points
N1, N3	cm^{-1}	Starting wave number
NDIFF, IDIFF	cm^{-1}	Wave number increments
SOLIR	$w/(cm^2 - \mu m)$	Storage for solar irradiance
POUTER, Y, NN, N		Storage for data values
REF		Storage for solar irradiance multiplied by spectral reflectance
NAME		Storage for legend identification
NANGLE, IANGLE	deg	Zenith angle × 100
GAMMA		Gamma values for films
F1	$w/(cm^2 - \mu m)$	Storage for filter curves
S1	$w/(cm^2 - \mu m)$	Storage for film sensitivity curves
CORX1		Conversion factor to correct data for zenith angle

(Continued)

Table B3 (Concluded)

Variable	Unit	Description
Model		Code: 1 - Tropical atmosphere model 2 - Mid-latitude summer 3 - Mid-latitude winter 4 - Subarctic summer 5 - Subarctic winter
IHAZE		Code: Haze condition 1 - 23 km 2 - 5 km
IH1	km	Minimum altitude × 10
IH2	km	Ground-to-sensor distance × 10
PREF	$w/(cm^2 - \mu m)$	Storage for irradiance reflected from feature or background
ATMREF	$w/(cm^2 - \mu m)$	Irradiance reaching sensor
IDENT		Filter identification number
T1		Film transmission for feature image
T2		Film transmission for background image
A3		Difference between feature image density and background image density
HIGH, DENMAX		Maximum diffuse density for films
TF	sec	Exposure time required to reach a density of 1.0 above fog for the feature
TB	sec	Exposure time required to reach a density of 1.0 above fog for the background
CLENS		Lens transmission
SKYL		Storage for skylight irradiance ratio
SCCF		Scattering coefficient

Table B4

Structure of Input File for Sensors

Record	Variable	Format	Description
1	NOSEN (JK)	Free field	Sensor number
	NOFILT (JK)	Free field	Filter number
	FSTOP (JK)	Free field	F-stop settings
	A1 (JK)	Free field	Starting wavelength
	A2 (JK)	Free field	Ending wavelength

Table B5

Structure of Input File for Spectral Sensitivity Curve

Record No.	Variable	Format	Description
1	FILMN	A6	Film identification number
2-4	INAME	A68	Identification
5	NOPT	I6	Number of data points
5	N1	I6	Starting wave number, cm^{-1}
5	NDIFF	I6	Wave number increment, cm^{-1}
6	S1	6E12.4	Data values

Table B6

Structure of Input File for Total and Ground-to-Sensor Atmospheres

Record No.	Variable	Format	Description
1	ICOUNT	I6	Number of data points
	N3	I6	Starting wave number, $cm^{-1} \times 10$
	NDIFF	I6	Wave number increment, $cm^{-1} \times 10$
	MODEL	I1	Code: 1 - Tropical atmosphere model 2 - Mid-latitude summer 3 - Mid-latitude winter 4 - Subarctic summer 5 - Subarctic winter
	IHAZE	I1	Code: 1 - 23-km (sea level) visual range 2 - 5-km (sea level) visual range
	IANGLE	I6	Zenith angle × 100, deg
	IH1	I6	Minimum altitude × 10, km
	IH2	I6	Ground-to-sensor distance × 10
2	NN, N	19I4	Data values for percent transmission $\times 10^4$

Table B7

Structure of Input File for Spectral Reflectance, Skylight Irradiance, and Solar Irradiance Above Atmosphere

Record No.	Variable	Format	Description
1-3	INAME	A68	Identification
4	NOPT	I6	Number of data points
	N1	I6	Starting wave number, cm^{-1}
	IDIFF	I6	Wave number increment, cm^{-1}
	POUTER, SOLIR, SKYL	6E12.4	Data values

Table B8

Structure of Input File for Filter Data

Record No.	Variable	Format	Description
1	IDENT	A3	Filter identification number
2-4	INAME	A68	Identification
5	ICOUNT	I6	Number of data points
	N1	I6	Starting wave number, cm^{-1}
	IDIFF	I6	Wave number increment, cm^{-1}
6	F1	6E12.4	Data values

Table B9

Example of Input File for Sensors

1,1,5.6,1.,.4

2,1,5.6,1.,.4

1,2,5.6,1.,.4

2,2,5.6,1.,.4

.

.

.

9,1,5.6,1.,.4

Table B10

Example of Input File for Film Spectral Sensitivity

```
10001 2424
10002KODAK INFRARED AEROGRAPHIC FILM
10003KODAK DATA FOR AERIAL PHOTOGRAPHY, PAGE 57
10004D=1.0 ABOVE GROSS FOG LEVEL
10005   301 10000     50
10006  0.          0.          0.          0.          0.          0.
10007  0.          0.          0.          0.          0.          0.
10008  0.          0.          0.          0.          0.          0.9135E 00
10009  0.2079E 01  0.3245E 01  0.4410E 01  0.5576E 01  0.6741E 01  0.7935E 01
10010  0.9136E 01  0.1006E 02  0.1028E 02  0.1050E 02  0.1071E 02  0.1093E 02
10011  0.1115E 02  0.1137E 02  0.1158E 02  0.1180E 02  0.1202E 02  0.1224E 02
10012  0.1234E 02  0.1240E 02  0.1247E 02  0.1253E 02  0.1259E 02  0.1265E 02
10013  0.1271E 02  0.1277E 02  0.1283E 02  0.1289E 02  0.1296E 02  0.1302E 02
10014  0.1308E 02  0.1314E 02  0.1320E 02  0.1308E 02  0.1296E 02  0.1284E 02
10015  0.1272E 02  0.1260E 02  0.1248E 02  0.1236E 02  0.1224E 02  0.1212E 02
10016  0.1200E 02  0.1188E 02  0.1176E 02  0.1164E 02  0.1152E 02  0.1140E 02
10017  0.1128E 02  0.1118E 02  0.1112E 02  0.1105E 02  0.1099E 02  0.1093E 02
10018  0.1086E 02  0.1080E 02  0.1074E 02  0.1068E 02  0.1061E 02  0.1055E 02
10019  0.1049E 02  0.1042E 02  0.1036E 02  0.1030E 02  0.1023E 02  0.1017E 02
10020  0.1011E 02  0.1004E 02  0.9962E 01  0.9830E 01  0.9698E 01  0.9566E 01
10021  0.9434E 01  0.9303E 01  0.9171E 01  0.9039E 01  0.8907E 01  0.8775E 01
10022  0.8643E 01  0.8511E 01  0.8379E 01  0.8247E 01  0.8115E 01  0.7983E 01
10023  0.7851E 01  0.7719E 01  0.7587E 01  0.7455E 01  0.7323E 01  0.7191E 01
10024  0.7082E 01  0.7024E 01  0.6965E 01  0.6907E 01  0.6848E 01  0.6790E 01
10025  0.6731E 01  0.6673E 01  0.6614E 01  0.6556E 01  0.6497E 01  0.6439E 01
10026  0.6380E 01  0.6322E 01  0.6263E 01  0.6204E 01  0.6146E 01  0.6087E 01
10027  0.6029E 01  0.5970E 01  0.5912E 01  0.5853E 01  0.5795E 01  0.5736E 01
10028  0.5678E 01  0.5619E 01  0.5532E 01  0.5429E 01  0.5327E 01  0.5225E 01
10029  0.5123E 01  0.5020E 01  0.4918E 01  0.4816E 01  0.4713E 01  0.4611E 01
10030  0.4509E 01  0.4406E 01  0.4304E 01  0.4202E 01  0.4100E 01  0.3997E 01
```

Table B11

Example of Input File for Atmospheric Transmission

```
  488  6500   50032     0     0    15     0
  016747133831488449015891583738087872984557707460634231158 174    0    0    0
 106    0    0    0 38410941949381535257847213747737151320    0   0697881118603
82658852883288418802875886247666643939083748212774643812388038382056363518O0
 184    3    0    0    0    0    0    0  23 495312860916308712773247804803881868246
8279814680188056813680787802740466307661462365126373384219 95 752 3221453  437
 232 74618212096619570067193746675157661776078347838783078327819758277737735
74107752773977057671732366215966439143916155310534072350189 2 816  411  458  835
 332 33118045338578861536313652770577338738673837197732873477335732373107298
72867274726272507209708368076508589054335554224741333501434264247001708670 74
70637051704070287017700569946983697169606949693769266915690468926881684868 03
66506378635564455853544748875144465951274622380650836450651963176356624165 57
61426138658266106599658865786567655765466536652565156504648664656428630861 79
62266311607961485984624863446359633463356309632062956295630062906280627062 60
61425333450543886210620061906180617061606126609860285953577558475711602856 00
59316053604360276011599759835974597259175966595659475937592859185909589958 90
58805871586158525843583358245814580557965786577757685758574957405730572157 12
57035693568456755666565756475638562956205611560255935584557555665557554855 39
55305521551255035494548554765467545954505441543254235414540553975388537953 70
53625353534453365327531853105301529252845275526652585249524152325223521552 06
51985189518151725163515551465138512951215113510450965087507950705062505350 45
50365028502050115003499449864978496949614953494449364928491949114903489448 86
48784869486148534845483648284820481248034795478747794771476247544746473847 30
47214713470546974689468146734664465646484640463246244616460846004591458345 75
45674559455145434535452745194511450344954487447944714463445544474439443144 23
44154407439943914383437543674359435143434335432843204312430442964288428042 72
42644256424942414233422542174209420141944186417841 70    0    0    0    0    0    0
```

Table B12

Example of Input File for Spectral Reflectance

0.6400E 00	0.6376E 00	0.6351E 00	0.6327E 00	0.6302E 00	0.6322E 00
0.6345E 00	0.6369E 00	0.6392E 00	0.6522E 00	0.6704E 00	0.6812E 00
0.6838E 00	0.6863E 00	0.6889E 00	0.6915E 00	0.6940E 00	0.6966E 00
0.6992E 00	0.7017E 00	0.7043E 00	0.7069E 00	0.7094E 00	0.7094E 00
0.7086E 00	0.7079E 00	0.7071E 00	0.7063E 00	0.7056E 00	0.7048E 00
0.7041E 00	0.7033E 00	0.7025E 00	0.7018E 00	0.7010E 00	0.7002E 00
0.7000E 00	0.7000E 00	0.7000E 00	0.7000E 00	0.7000E 00	0.7000E 00
0.7000E 00	0.7000E 00	0.7000E 00	0.7000E 00	0.7000E 00	0.7000E 00
0.7000E 00	0.7000E 00	0.7000E 00	0.6990E 00	0.6979E 00	0.6969E 00
0.6959E 00	0.6949E 00	0.6938E 00	0.6928E 00	0.6918E 00	0.6908E 00
0.6874E 00	0.6773E 00	0.6672E 00	0.6571E 00	0.6470E 00	0.6368E 00
0.6267E 00	0.6127E 00	0.5906E 00	0.5686E 00	0.5465E 00	0.5245E 00
0.5024E 00	0.4804E 00	0.4583E 00	0.4363E 00	0.4142E 00	0.3921E 00
0.3701E 00	0.3480E 00	0.3260E 00	0.3039E 00	0.2819E 00	0.2598E 00
0.2378E 00	0.2157E 00	0.1956E 00	0.1801E 00	0.1646E 00	0.1492E 00
0.1337E 00	0.1182E 00	0.1028E 00	0.8729E-01	0.7182E-01	0.7000E-01
0.7000E-01	0.7000E-01	0.7000E-01	0.7000E-01	0.7000E-01	0.7000E-01
0.7000E-01	0.7000E-01	0.7410E-01	0.7832E-01	0.8254E-01	0.8677E-01
0.9099E-01	0.9522E-01	0.9944E-01	0.1037E 00	0.1079E 00	0.1100E 00
0.1100E 00	0.1100E 00	0.1100E 00	0.1100E 00	0.1100E 00	0.1100E 00
0.1100E 00	0.1100E 00	0.1100E 00	0.1108E 00	0.1126E 00	0.1145E 00
0.1164E 00	0.1182E 00	0.1201E 00	0.1219E 00	0.1238E 00	0.1257E 00
0.1275E 00	0.1294E 00	0.1315E 00	0.1339E 00	0.1362E 00	0.1385E 00
0.1408E 00	0.1431E 00	0.1454E 00	0.1477E 00	0.1500E 00	0.1523E 00
0.1546E 00	0.1570E 00	0.1593E 00	0.1616E 00	0.1639E 00	0.1662E 00
0.1685E 00	0.1708E 00	0.1731E 00	0.1754E 00	0.1777E 00	0.1801E 00
0.1824E 00	0.1847E 00	0.1850E 00	0.1850E 00	0.1850E 00	0.1850E 00
0.1850E 00	0.1850E 00	0.1850E 00	0.1850E 00	0.1850E 00	0.1850E 00
0.1850E 00	0.1850E 00	0.1850E 00	0.1828E 00	0.1792E 00	0.1757E 00
0.1721E 00	0.1686E 00	0.1651E 00	0.1615E 00	0.1580E 00	0.1544E 00

Table B13

Example of Input File for Filter

0.9500E 00	0.9500E 00	0.9500E 00	0.9500E 00	0.9500E 00	0.9500E 00
0.9500E 00	0.9500E 00	0.9500E 00	0.9500E 00	0.9500E 00	0.9500E 00
0.9500E 00	0.9500E 00	0.9500E 00	0.9500E 00	0.9500E 00	0.9500E 00
0.9500E 00	0.9500E 00	0.9500E 00	0.9500E 00	0.9500E 00	0.9486E 00
0.9468E 00	0.9450E 00	0.9432E 00	0.9414E 00	0.9396E 00	0.9378E 00
0.9360E 00	0.9342E 00	0.9324E 00	0.9306E 00	0.9288E 00	0.9270E 00
0.9252E 00	0.9234E 00	0.9216E 00	0.9198E 00	0.9180E 00	0.9162E 00
0.9144E 00	0.9126E 00	0.9108E 00	0.9090E 00	0.9072E 00	0.9054E 00
0.9036E 00	0.9018E 00	0.9000E 00	0.8951E 00	0.8901E 00	0.8852E 00
0.8803E 00	0.8753E 00	0.8704E 00	0.8655E 00	0.8605E 00	0.8556E 00
0.8507E 00	0.8457E 00	0.8408E 00	0.8359E 00	0.8309E 00	0.8260E 00
0.8211E 00	0.8161E 00	0.8112E 00	0.8063E 00	0.8013E 00	0.7806E 00
0.7539E 00	0.7273E 00	0.7006E 00	0.6740E 00	0.6474E 00	0.6207E 00
0.5863E 00	0.5248E 00	0.4634E 00	0.4019E 00	0.3404E 00	0.2789E 00
0.2174E 00	0.1559E 00	0.1054E 00	0.8213E-01	0.5890E-01	0.3567E-01
0.1530E-01	0.1182E-01	0.8353E-02	0.4881E-02	0.1408E-02	0.
0.	0.	0.	0.	0.	0.
0.	0.	0.	0.	0.	0.
0.	0.	0.	0.	0.	0.
0.	0.	0.	0.	0.	0.
0.	0.	0.	0.	0.	0.
0.	0.	0.	0.	0.	0.
0.	0.	0.	0.	0.	0.
0.	0.	0.	0.	0.	0.
0.	0.	0.	0.	0.	0.
0.	0.	0.	0.	0.	0.
0.	0.	0.	0.	0.	0.
0.	0.	0.	0.	0.	0.
0.	0.	0.	0.	0.	0.
0.	0.	0.	0.	0.	0.

Table B14

List of Control Cards

Column No.		
1	8	16
$	IDENT	USER NO., IDENTIFICATION
$	OPTION	FORTRAN
$	FORTY	NFORM, NLNO
$	USE	.GTLIT
	Source Deck	
	.	
	.	
	.	
$	EXECUTE	
$	LIMITS	TIME, STORAGE
$	PRMFL	DEVICE NO.,R/W,L,USER NO./FILENAME
$	DATA	41

APPENDIX C: DOCUMENTATION OF SPECIFIC FORM OF THERMAL IR SYSTEMS SIMULATION MODEL COMPUTER PROGRAM

Program Identification

Program Title: Infrared Sensor Performance Prediction

Program Code Name: IRSPP6

Writers: L. E. Link and J. R. Stabler

Organization: U. S. Army Engineer Waterways Experiment Station,

P. O. Box 631, Vicksburg, Mississippi 39180

Date: February 1976

Updates: None

Version No.: 0

Source Language: FORTRAN IV, Honeywell G635

Availability: Source card deck and listing available on request from

U. S. Army Engineer Waterways Experiment Station

Abstract: The specific form of the Thermal IR Systems Simulation Model predicts the expected performance of specified thermal IR scanner systems for a specific feature-background combination. The model provides a quantitative means to evaluate individual sensor systems or types of sensor systems for specific data acquisition problems and to plan mission profiles to optimize imagery information content for specific data needs. Sensor systems operating in any portion of the 1.0- to 14.0-μm wavelength band can be evaluated and both reflected and radiated energy are considered in the model. The major atmospheric, terrain, and sensor parameters that influence imagery information

content are included in the model and the computational procedure used have been designed to require a minimum of inputs for execution ease.

Engineering Documentation

Narrative description

1. See text, Part III.

Method of solution

2. See text, Part III.

Program capabilities

3. The internal limitations and assumptions of the model are as follows:

   a. All files must have the same starting position (14.0 μm wavelength) and end position (1.0 μm) and the data must be in the same increments.

   b. Only wavelengths between 1.0 and 14.0 μm are considered.

   c. Only thermal infrared remote sensing systems can be evaluated.

   d. The increment (as a function of wavelength) between data points in any file must be greater than or equal to 50 cm^{-1} and be an even multiple of 50 cm^{-1}.

Data inputs

4. The input data requirements for this model are as follows:

   a. Sensor data

      (1) Electrical bandwidth (Hz)

      (2) Effective aperture area (sq cm)

      (3) Spatial resolution (mrad)

b. Detector data

(1) Relative response curve (v/w)

(2) Starting wavelength-ending wavelength (μm)

(3) Detector noise voltage index ($v\text{-}Hz^{-1/2}$)

(4) Peak response (v/w)

c. Terrain data

(1) Feature temperature, K and emissivity

(2) Background temperature, K and emissivity

(3) Feature area in m squared

(4) Feature reflectance curve (optional)

(5) Background reflectance curve (optional)*

5. A list of input variables is shown in Table C1.

Program options

6. After one complete run, the program is terminated. The user has the choice of either adding or not adding the reflected energy from the terrain. Enter 1 - without reflected energy or 2 - reflected energy for the variable NGO.

Printed output

7. An example of a printed output is shown in Table C2.

Flow chart

8. A condensed flow chart is shown in Figure C1.

System Documentation

Computer equipment

9. The model was developed at the U. S. Army Engineer Waterways

---

* Used only if daytime mission in 3- to 5.5-μm band is of concern.

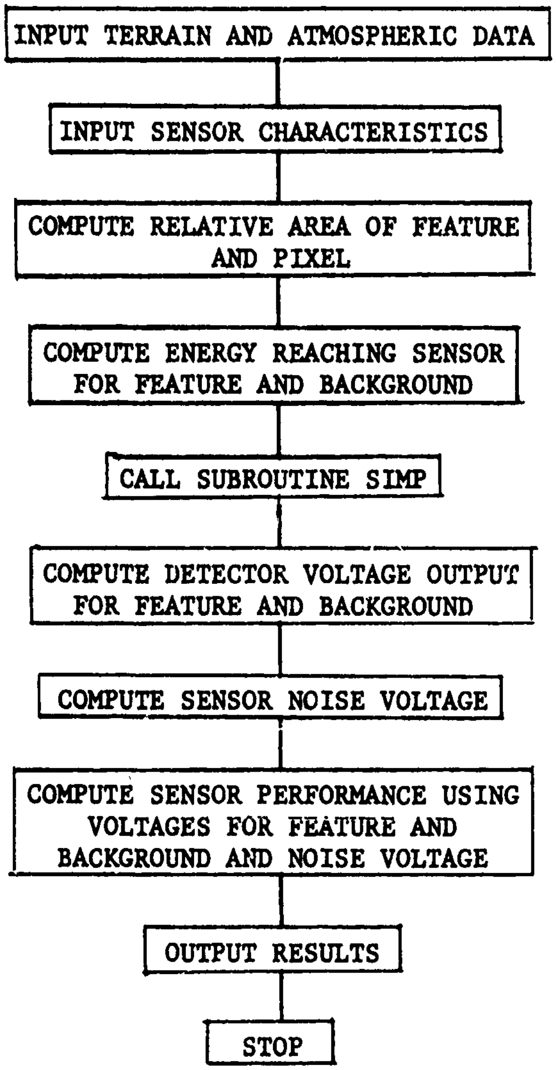

Figure C1. Condensed flow chart for specific form of Thermal IR Systems Simulation Model

Experiment Station using a Honeywell G635. The G635 is a dual processor system with a 192-K word (36 bit) memory. Memory cycle speed is 1.0 microsecond for fetching two words from memory. The system has three disc systems; the dual channel DSU 180's with 168-million character capacity, the DSU 270's with 30-million character capacity, and the DSU 167's with 120-million character capacity. There are two magnetic tape subsystems with a total of three nine-track and six seven-track handlers, two printers (1200 lpm), a card punch (100 cpm), card reader (900 cpm), and two G-DATANET-30 communications processors.

Peripheral equipment

10. The following peripheral equipment is necessary to run this program: Honeywell G-DATANET-30 communication (16-K storage with 18-bit words) and a teletype communication terminal.

Source program

11. See availability.

Variables and subroutines

12. The variables in the Thermal IR Systems Simulation Model, subroutine SIMP, and subroutine REFLEC are listed in Table C3.

a. The function of the main program, subroutines, and system subprogram are as follows:

(1) Defines the dimension of the array for each variable.

(2) Identifies format for both input and output files.

(3) Reads input for all input files.

(4) Writes output for all output files.

(5) Activates subroutines at the proper time.

b. Subroutine SIMP calculates the area under the functional curves using Simpson's rule.

c. Subroutine REFLEC calculates the amount of reflected energy contributed by the feature and background.

d. Library programs used are:

(1) Cosine

(2) Sine routine

Data structure

13. The formats of the input files are shown in Tables C4-C6. An example of each of the input files is shown in Tables C7-C11.

Storage requirements

14. The minimum amount of memory needed to load with all files open is 15 K.

Maintenance and updates

15. No updates of the program have been made.

Operating Instructions

Storage

16. The program and all files are stored on a permanent disc.

Operating messages

17. None.

Control cards

18. Control cards needed are shown in Table C12.

Error recovery

19. The program must be restarted when error occurs.

Run time

20. Processor time for one run is approximately 0.0022 sec. The input-output time is approximately 0.006 sec.

Table C1

List of Variable Input

Record No.	Variable	Format	Unit	Description
1	EMISS (1)	Free field		Feature emissivity
	EMISS (2)	Free field		Background emissivity
	TEMP (1)	Free field	K	Feature temperature
	TEMP (2)	Free field	K	Background temperature
2	RANGE	Free field	km	Altitude
3	AF	Free field	m^2	Feature area
	DELTAF	Free field	Hz	Electrical bandwidth
	AA	Free field	cm^2	Effective area aperture
	RAD1	Free field	mr	Number of milliradians
4	NODECT	Free field		Number of detectors to be considered
5	JNAME	A40		Latitude-season identification
6	ID1	Free field	[illegible]	Haze condition
7	A2	Free field	µm	Ending wavelength
	A3	Free field	µm	Starting wavelength
	DNVI	Free field	$v\ Hz^{-1/2}$	Detector noise voltage index
	RPEAK	Free field	v/w	Peak response
8	NGO	Free field		Code: 1 - No reflected energy 2 - Reflected energy
9	NANGLE	Free field	degree	Zenith angle × 100

Table C2

Example of Model Output of IR Sensor Performance Prediction

Temperature K	Feature Emissivity	Voltage v	Temperature K	Background Emissivity	Voltage v	Noise Voltage, v	Voltage Ratio
300.0	0.90	0.00270	303.0	0.85	0.00267	0.00001677	1.70036

LEGEND

Sensor Characteristic

Detector Type: HGCDTE
Detector Noise Voltage Index (volt/sqrt (Hertz)): 0.1000E 07
Electrical Bandwidth (Hertz): 0.1250E 07
Spatial Resolution (milliradians): 2.5
Wavelength Band (micrometers): 14.0
Effective Aperture Area (cm^2): 40.0
Peak Response (volt/watt): 0.2000E 04

Atmosphere Condition

Latitude-Season: Mid-latitude Summer
Haze (km): 23
Altitude (km): 1.5

If voltage ratio >1.0, detection is possible.

Table C3

Variables for Thermal IR System Performance Prediction

Variable	Unit	Description
AA	cm^2	Effective aperture area
NODECT		Number of detectors
INAME, KNAME, JNAME		Storage for identification
POUTER	v/w	Storage for relative response curve
A2	μm	Ending wavelength
A3	μm	Starting wavelength
DNVI	$v\text{-}Hz^{-1/2}$	Detector noise voltage index
DELTAF	Hz	Electrical bandpass of sensor
IH1	km	Minimum altitude × 10
IH2, RANGE	km	Ground-to-sensor distance × 10
ICOUNT, NOPT		Number of data points
N3, N1	cm^{-1}	Starting wave number
NDIFF	cm^{-1}	Wave number increment
MODEL		Code: 1 - Tropical atmosphere 2 - Mid-latitude summer 3 - Mid-latitude winter 4 - Subarctic summer 5 - Subarctic winter
IHAZE		Code: Haze condition 1 - 23 km 2 - 5 km
EMISS		Storage of emissivity
VND	volts	Detector voltage noise

(Continued)

(Sheet 1 of 3)

Table C3 (Continued)

Variable	Unit	Description
WRE		Storage of emissivity multiplied by ground-to-sensor atmosphere data
RADI	mr	Number of milliradians
AG		Geometric correction factor
APG	m^2	Ground pixel area
AF	m^2	Feature area
PARFAR		Ratio between feature area and ground pixel area
PARBAR		Difference between 1 and parfar
W2	$w/(cm^2-\mu m)$	Storage of energy reaching sensor
WW	v/μm	Storage of energy reaching sensor multiplied by detector response curve, aperture area, and geometric correction factor
REA	volts	Storage for area under curve for feature and background
VFB	volts	Voltage resulting from simultaneous sensoring of feature and background
RDIFF	volts	The voltage difference between two adjacent pixels
VDIFF		Ratio between voltage difference between two adjacent pixels and detection voltage noise
TEMP	K	Temperatures for feature and background
ID1	km	Haze condition
RPEAK	v/w	Peak detector response
M1		Storage for atmosphere data (ground to sensor)

(Continued)

(Sheet 2 of 3)

Table C3 (Concluded)

Variable	Unit	Description
REF	w/(cm^2-μm)	Storage for irradiance reflected from feature or background
N	w/(cm^2-μm)	Storage for total atmosphere
SOLIR	w/(cm^2-μm)	Storage for solar irradiance
ANGLE2	degree	Zenith angle/100
SPEC	w/(cm^2-μm)	Storage for spectral reflectance
CORX1		Conversion factor to correct data for zenith angle
RAD		Conversion factor for changing degrees to radians

(Sheet 3 of 3)

Table C4

Structure of Input File for Total and Ground-to-Sensor Atmospheres

Record No.	Variable	Format	Description
1	ICOUNT	I6	Number of data points
	N3	I6	Starting wave number, $cm^{-1} \times 10$
	NDIFF	I6	Wave number increment, $cm^{-1} \times 10$
	MODEL	I1	Code: 1 - Tropical atmosphere model 2 - Mid-latitude summer 3 - Mid-latitude winter 4 - Subarctic summer 5 - Subarctic winter
	IHAZE	I1	Code: 1 - 23-km (sea level) visual range 2 - 5-km (sea level) visual range
	IANGLE	I6	Zenith angle $\times$ 100, deg
	IH1	I6	Minimum altitude $\times$ 10, km
	IH2	I6	Ground-to-sensor distance $\times$ 10
2	NN, N	19I4	Data values for percent transmission $\times 10^4$

Table C5

Structure of Input File for Spectral Reflectance and Solar Irradiance Above Atmosphere

Record No.	Variable	Format	Description
1-3	INAME	A68	Identification
4	NOPT	I6	Number of data points
	N1	I6	Starting wave number, cm^{-1}
	IDIFF	I6	Wave number increment, cm^{-1}
	POUTER, SOLIR, SKYI.	6E12.4	Data values

Table C6

Structure of Input File for Relative Response Curve

Record No.	Variable	Format	Description
1	INAME	A12	Detector identification
2-3	KNAME	A68	Identification
4	NOPT	I6	Number of data points
	N1	I6	Starting wave number. $cm^{-1} \times 10$
	NDIFF	I6	Wave number increment, $cm^{-1} \times 10$
5	POUTER	6E12.4	Data values

Table C7

Example of Variable Input

```
1.,1.,300.,303.

1.5

100.,1.E6,40.,2.5

1.

Mid-latitude Summer

23.

14.,8.,1.E-8,1000.

2.

3000.
```

Table C8

Example of Solar Irradiance File

```
SOLAR IRRADIANCE ABOVE ATMOSPHERE

DECEMBER 6, 1973     1245 HOURS
  301 10000     50
```

0.080000	0.080900	0.081800	0.082700	0.083600	0.084500
0.085400	0.086300	0.087200	0.088100	0.089000	0.089900
0.090800	0.091700	0.092600	0.093500	0.094400	0.095300
0.096200	0.097100	0.098000	0.098900	0.099800	0.100700
0.101600	0.102500	0.103400	0.104300	0.105200	0.106100
0.107000	0.107900	0.108800	0.109700	0.110600	0.111500
0.112400	0.113300	0.114200	0.115100	0.116000	0.116900
0.117800	0.118700	0.119600	0.120500	0.121400	0.122300
0.123200	0.124100	0.125000	0.125840	0.126680	0.127520
0.128360	0.129200	0.130040	0.130880	0.131720	0.132560
0.133400	0.134240	0.135080	0.135920	0.136760	0.137600
0.138440	0.139280	0.140120	0.140960	0.141800	0.142640
0.143480	0.144320	0.145160	0.146000	0.146840	0.147680
0.148520	0.149360	0.150200	0.151040	0.151880	0.152720
0.153560	0.154400	0.155240	0.156080	0.156920	0.157760
0.158600	0.159440	0.160280	0.161120	0.161960	0.162800
0.163640	0.164480	0.165320	0.166160	0.167000	0.167840
0.168680	0.169520	0.170360	0.171200	0.172040	0.172880
0.173720	0.174560	0.175400	0.176240	0.177080	0.177920
0.178760	0.179600	0.180440	0.181280	0.182120	0.182960
0.183800	0.184640	0.185480	0.186320	0.187160	0.188000
0.188840	0.189680	0.190520	0.191360	0.192200	0.193040
0.193880	0.194720	0.195238	0.195595	0.195952	0.196309
0.196666	0.197023	0.197380	0.197737	0.198094	0.198451
0.198808	0.199165	0.199522	0.199879	0.200236	0.200593
0.200950	0.201307	0.201664	0.202021	0.202378	0.202735
0.203092	0.203449	0.203806	0.204163	0.204520	0.204877
0.205234	0.205591	0.205948	0.206305	0.206662	0.207019
0.207376	0.207733	0.208090	0.208447	0.208804	0.209161
0.209518	0.209875	0.210232	0.210589	0.210946	0.211303

Table C9

Example of Input File for Detector Relative Response Curve

```
INSB
RELATIVE RESPONSE CURVE
MARCH 10,1976   1015 HOURS
   187    700    50
  0.            0.            0.            0.            0.            0.
  0.            0.            0.            0.            0.            0.
  0.            0.            0.            0.            0.            0.
  0.            0.            0.8040E-01    0.1860E 00    0.2916E 00    0.4297E 00
  0.5865E 00    0.7433E 00    0.9000E 00    0.9288E 00    0.9575E 00    0.9863E 00
  0.1000E 01    0.1000E 01    0.1000E 01    0.1000E 01    0.9840E 00    0.9670E 00
  0.9500E 00    0.9430E 00    0.9360E 00    0.9290E 00    0.9220E 00    0.9150E 00
  0.9080E 00    0.9010E 00    0.8910E 00    0.8805E 00    0.8700E 00    0.8595E 00
  0.8490E 00    0.8385E 00    0.8280E 00    0.8175E 00    0.8070E 00    0.7975E 00
  0.7900E 00    0.7825E 00    0.7750E 00    0.7675E 00    0.7600E 00    0.7525E 00
  0.7450E 00    0.7375E 00    0.7300E 00    0.7225E 00    0.7150E 00    0.7075E 00
  0.7000E 00    0.6950E 00    0.6900E 00    0.6850E 00    0.6800E 00    0.6750E 00
  0.6700E 00    0.6650E 00    0.6600E 00    0.6550E 00    0.6500E 00    0.6450E 00
  0.6400E 00    0.6350E 00    0.6300E 00    0.6250E 00    0.6200E 00    0.6150E 00
  0.6100E 00    0.6050E 00    0.6000E 00    0.5961E 00    0.5922E 00    0.5883E 00
  0.5844E 00    0.5805E 00    0.5766E 00    0.5727E 00    0.5688E 00    0.5649E 00
  0.5610E 00    0.5571E 00    0.5532E 00    0.5493E 00    0.5454E 00    0.5415E 00
  0.5376E 00    0.5337E 00    0.5298E 00    0.5259E 00    0.5220E 00    0.5181E 00
  0.5142E 00    0.5103E 00    0.5064E 00    0.5025E 00    0.4986E 00    0.4947E 00
  0.4908E 00    0.4869E 00    0.4830E 00    0.4791E 00    0.4752E 00    0.4713E 00
  0.4688E 00    0.4670E 00    0.4652E 00    0.4634E 00    0.4616E 00    0.4598E 00
  0.4580E 00    0.4562E 00    0.4544E 00    0.4526E 00    0.4508E 00    0.4490E 00
  0.4472E 00    0.4454E 00    0.4436E 00    0.4418E 00    0.4400E 00    0.4382E 00
  0.4364E 00    0.4346E 00    0.4328E 00    0.4310E 00    0.4292E 00    0.4274E 00
  0.4256E 00    0.4238E 00    0.4220E 00    0.4202E 00    0.4184E 00    0.4166E 00
  0.4148E 00    0.4130E 00    0.4112E 00    0.4094E 00    0.4076E 00    0.405[illegible] 00
  0.4040E 00    0.4022E 00    0.4004E 00    0.3986E 00    0.3968E 00    0.3950E 00
  0.3932E 00    0.3914E 00    0.3896E 00    0.3878E 00    0.3860E 00    0.3842E 00
  0.3824E 00    0.3806E 00    0.3788E 00    0.3770E 00    0.3752E 00    0.3734E 00
  0.3716E 00    0.3698E 00    0.3680E 00    0.3662E 00    0.3644E 00    0.3626E 00
```

Table C10

Example of Input File for Atmospheric Transmission

```
   488  6500   50032      0      0     15      0
   0167471338314884490158915637380878729845577074606342311158 174    0    0    0
 106    0    0    0 38410941949382153525784721374773715132 0    0    0697881118603
8265885288328841880287588624766664393908374821277464381238803838205636351800
 184    3    0    0    0    0    0    0   23 495531286091630871277324780480388186 8246
82798146801880568136807878027404663076614623651263733842 1995  752  3221453  437
 232  746182120966195700671937466751576617760783478387830783278197582777 37735
741077527739770576717323662159664391439161553105340723501892  816  411  458  835
 332  331180453385788615363136527705773387386738371977328734773357323731 07298
7286727472627250720970836807650858905433555422474133350143426424700170867074
7063705170407028701770056994698369716960694969376926691569046892688168486803
6650637863556445585354474887514446595127462238065063645065196317635662416557
6142613865826610659965886578656765576546653665256515650464866465642863086179
6226631160796148598462486344635963346335630963206295629563006290628062706260
6142533345054388621062006190618061706160612660986028595357755847571160285600
5931605360436027601159975983597459725917596659565947593759285918590958995890
5880587158615852584358335824581458055796578657775768575857495740573057215712
5703569356845675566656575647563856295620561156025593555845575556655575548553 9
5530552155125503549454855476546754595450544154325423541454055397538853795370
5362535353445336532753185310530152925284527552665258524952415232522352155206
5198518951815172516351555146513851295121511135104509650875079507050625053504 5
5036502850205011500349944986497849694961495349444936492849194911490348944886
4878486948614853484548364828482048124803479547874779477147624754474647384730
4721471347054697468946814673466446564648464046324624461646084600459145834575
4567455945514543453545274519451145034495448744794471446344554447443944314423
4415440743994391438343754367435943514343433543284320431243044296428842804272
42644256424942414233422542174209420141944186417841 70    0    0    0    0    0    0
```

Table C11

Example of Spectral Reflectance File

PONDEROSA PINE NEEDLES, DISEASED

OCTOBER 28,1975 1440 HOURS

188 650 50

0.1000E-01	0.1000E-01	0.1325E-01	0.1567E-01	0.1675E-01	0.1783E-01
0.1892E-01	0.2000E-01	0.2000E-01	0.2000E-01	0.1860E-01	0.1680E-01
0.1500E-01	0.1780E-01	0.2060E-01	0.2340E-01	0.2988E-01	0.4125E-01
0.4409E-01	0.2500E-01	0.2500E-01	0.2500E-01	0.1788E-01	0.2141E-01
0.4384E-01	0.6627E-01	0.8429E-01	0.8000E-01	0.8263E-01	0.8525E-01
0.8787E-01	0.9050E-01	0.9312E-01	0.9575E-01	0.9837E-01	0.9280E-01
0.7390E-01	0.5500E-01	0.5010E-01	0.4520E-01	0.4030E-01	0.3540E-01
0.3050E-01	0.2560E-01	0.2070E-01	0.1957E-01	0.1906E-01	0.1856E-01
0.1805E-01	0.1754E-01	0.1704E-01	0.1653E-01	0.1603E-01	0.1552E-01
0.1502E-01	0.1451E-01	0.1401E-01	0.1350E-01	0.1299E-01	0.1249E-01
0.1198E-01	0.1148E-01	0.1097E-01	0.1047E-01	0.1375E-01	0.6250E-01
0.1112E 00	0.1600E 00	0.1587E 00	0.1573E 00	0.1560E 00	0.1547E 00
0.1533E 00	0.1520E 00	0.1507E 00	0.1493E 00	0.1480E 00	0.1467E 00
0.1453E 00	0.1440E 00	0.1427E 00	0.1413E 00	0.1400E 00	0.1387E 00
0.1373E 00	0.1360E 00	0.1347E 00	0.1333E 00	0.1320E 00	0.1307E 00
0.1293E 00	0.1280E 00	0.1267E 00	0.1253E 00	0.1240E 00	0.1227E 00
0.1213E 00	0.1200E 00	0.1187E 00	0.1173E 00	0.1160E 00	0.1147E 00
0.1133E 00	0.1120E 00	0.1107E 00	0.1093E 00	0.1080E 00	0.1067E 00
0.1053E 00	0.1040E 00	0.1027E 00	0.1013E 00	0.1000E 00	0.9867E-01
0.9733E-01	0.9600E-01	0.9467E-01	0.9333E-01	0.9200E-01	0.9067E-01
0.8933E-01	0.8800E-01	0.8667E-01	0.8533E-01	0.8400E-01	0.8267E-01
0.8133E-01	0.8000E-01	0.7867E-01	0.7733E-01	0.7600E-01	0.7467E-01
0.7333E-01	0.7200E-01	0.7067E-01	0.6933E-01	0.6800E-01	0.6667E-01
0.6533E-01	0.6400E-01	0.6267E-01	0.6133E-01	0.6000E-01	0.5867E-01
0.5733E-01	0.5600E-01	0.5467E-01	0.5333E-01	0.5200E-01	0.5067E-01
0.4933E-01	0.4800E-01	0.4667E-01	0.4533E-01	0.4400E-01	0.4267E-01
0.4133E-01	0.4000E-01	0.3867E-01	0.3733E-01	0.3600E-01	0.3467E-01
0.3333E-01	0.3200E-01	0.3067E-01	0.2933E-01	0.2800E-01	0.2667E-01
0.2533E-01	0.2400E-01	0.2267E-01	0.2133E-01	0.2000E-01	0.1867E-01
0.1733E-01	0.1600E-01	0.1467E-01	0.1333E-01	0.1200E-01	0.1067E-01

Table C12

List of Control Cards

Column No.		
1	8	16
$	IDENT	USER NO., IDENTIFICATION
$	OPTION	FORTRAN
$	FORTY	NFORM, NLNO
$	USE	.GTLIT
	Source Deck	
	.	
	.	
	.	
$	EXECUTE	
$	LIMITS	TIME, STORAGE
$	PRMFL	DEVICE NO.,R/W,L,USER NO./FILENAME
$	DATA	41

APPENDIX D: DOCUMENTATION OF GENERAL FORM OF THERMAL IR SYSTEMS SIMULATION MODEL COMPUTER PROGRAM

Program Identification

Program Title: Minimum Detectable Temperature Difference

Program Code Name: MDTD01

Writers: L. E. Link and J. R. Stabler

Organization: U. S. Engineer Waterways Experiment Station,
P. O. Box 631, Vicksburg, Mississippi 39180

Date: February 1976

Updates: None

Version No.: 0

Source Language: FORTRAN IV, Honeywell G635

Availability: Source card deck and listing available on request from
U. S. Engineer Waterways Experiment Station

Abstract: The general form of the Thermal IR Systems Simulation Model predicts the thermal resolution (minimum detectable apparent temperature difference) as a function of background (average terrain) apparent temperature for individual sensor systems or types of sensor systems. The thermal resolution data (in tabular or graphical form) are directly applicable for evaluating the capabilities of sensor systems for specific jobs or for planning missions to optimize imagery information content. The major variables that influence imagery information content are included and the model has been designed to minimize the required inputs for ease of execution.

Engineering Documentation

Narrative description

1. See text, Part III.

Method of solution

2. See text, Part III.

Program capabilities

3. The internal limitations and assumptions of the model are as follows:

   a. All files must have the same starting position (14.0-μm wavelength) and end position (1.0 μm) and the data must be in the same increments.

   b. Only wavelengths between 1.0 and 14.0 μm are considered.

   c. Only thermal infrared remote sensing systems can be evaluated.

   d. The increment (as a function of wavelength) between data points in any file must be greater than or equal to 50 cm^{-1} and be an even multiple of 50 cm^{-1}.

Data inputs

4. The input data requirements for this model are as follows:

   a. Sensor data

      (1) Electrical bandwidth (Hz)

      (2) Effective aperture area (sq cm)

      (3) Spatial resolution (mrad)

   b. Detector data

      (1) Relative response curve

      (2) Starting wavelength-ending wavelength (μm)

(3) Detector noise voltage index ($v\text{-}Hz^{-1/2}$)

(4) Peak response (v/w)

c. Terrain data

(1) Starting temperature, K

(2) Ending temperature, K

(3) Temperature interval, K

(4) Initial temperature change, K

d. Transmission through atmosphere (ground to sensor)

5. A list of input variables is shown in Table D1.

Program options

6. After one complete run, the program is terminated.

Printed output

7. An example of a printed output is shown in Table D2.

Other output

8. An example of a graphical output is shown in Figure D1.

Flowchart

9. A condensed flowchart is shown in Figure D2.

System Documentation

Computer equipment

10. The model was developed at the U. S. Engineer Waterways Experiment Station using a Honeywell G635. The G635 is a dual processor system with a 192-K word (36 bit) memory. Memory cycle speed is 1.0 microsecond for fetching two words from memory. The system has three disc systems; the dual channel DSU 180's with 168-million character capacity, the DSU 270's with 30-million character capacity, and the DSU 167's with 120-million character capacity. There are two

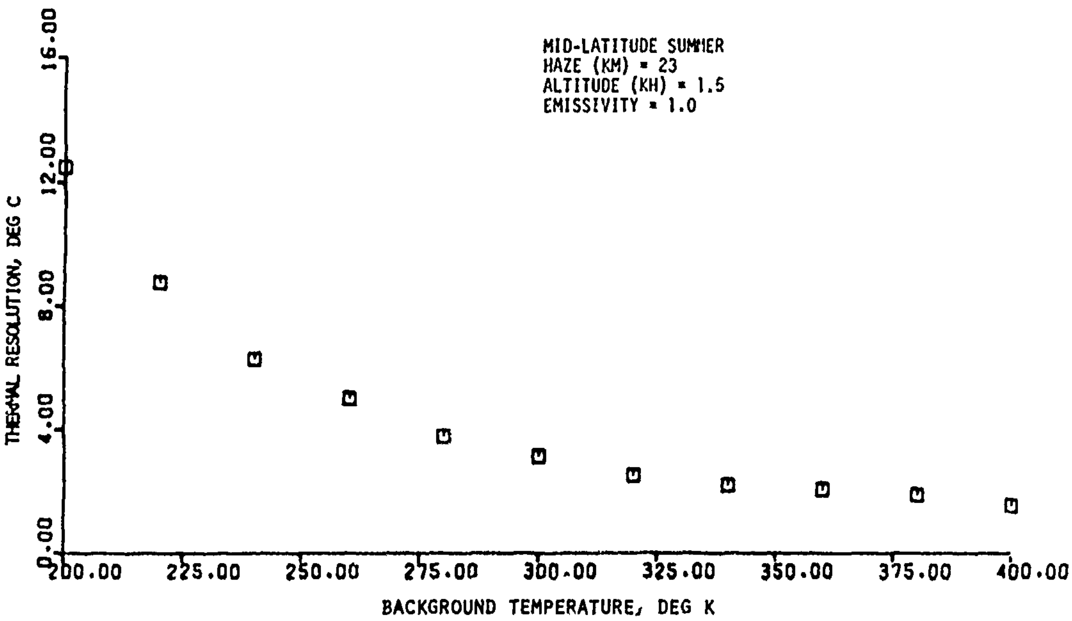

LEGEND
DETECTOR - HGCDTE
DETECTOR NOISE VOLTAGE INDEX (volt/sqrt (Hz)) = 0.00000001
ELECTRICAL BANDWIDTH (Hz) = 1000000.
SPATIAL RESOLUTION (milliradians) = 2.6
WAVELENGTH BAND (micrometer) = 14.0-8.0
EFFECTIVE APERATURE AREA (cm^2) = 40.0
PEAK RESPONSE (volt/watt) = 200.0

Figure D1. Example of graphical form of model output

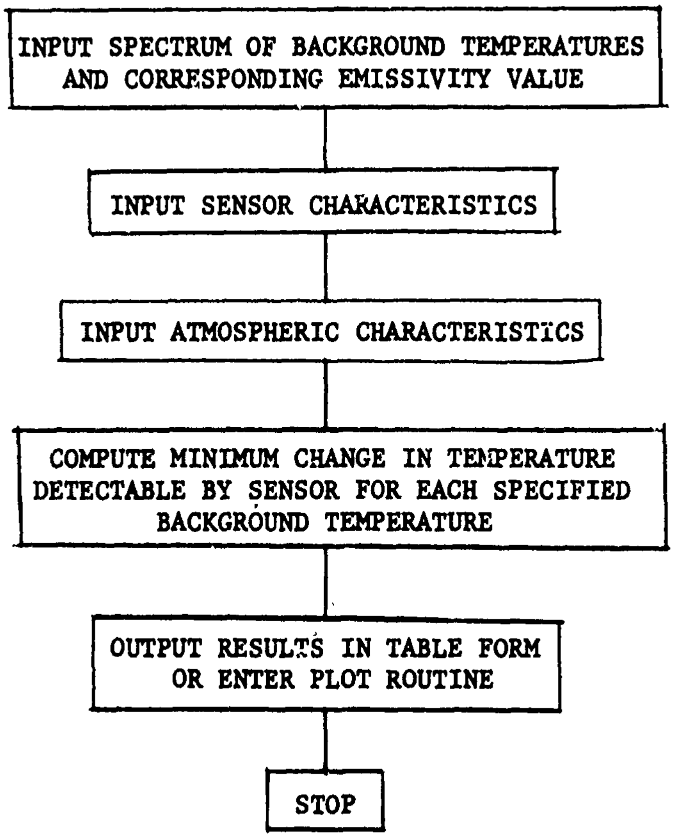

Figure D2. Condensed flowchart for specific form of Thermal IR Systems Simulation Model

magnetic tape subsystems with a total of three nine-track and six seven-track handlers, two printers (120 lpm), a card punch (100 cpm), card reader (900 cpm), and two G-DATANET-30 communications processors.

Peripheral equipment

11. The following peripheral equipment is necessary to run this program: Honeywell G-DATANET-30 communication (16-K storage with 18-bit words) and a teletype communication terminal.

Source program

12. See availability.

Variables and subroutines

13. The variables in the minimum detectable temperature difference model, subroutine SIMP, and subroutine TPLOT are listed in Table D3.

a. The functions of the main program, subroutines, and system subroutine are as follows:

(1) Define the dimension of the array for each variable.

(2) Identify format for both input and output files.

(3) Read input for all input files.

(4) Write output for all output files.

(5) Activate subroutines at the proper time.

b. Subroutine SIMP calculates the area under the functional curves using Simpson's rule.

c. Subroutine TPLOT produces output plots for thermal resolution (minimum detectable temperature difference, ^{o}C) versus background temperature (K).

d. Library programs used are:

(1) Cosine

(2) Sine routine

Date structure

14. The formats of the input files are shown in Tables D4 and D5. An example of each of the input files is shown in Tables D6 to D8.

Storage requirements

15. The minimum amount of memory needed to load with all files open is 17 K.

Maintenance and updates

16. No updates of the program have been made.

Operating Instructions

Storage

17. The program and all files are stored on a permanent disc.

Operating messages

18. None.

Control cards

19. Control cards needed are shown in Table D9.

Error recovery

20. The program must be restarted when error occurs.

Run time

21. Processor time for one complete run is about 0.0038 sec. The input-output for this run was approximately 0.003 sec.

Table D1

List of Variables Input

Record	Variable	Format	Unit	Description
1	NTEMPS	Free field	K	Starting temperature
	NTEMPE	Free field	K	Ending temperature
	NTEMPI	Free field	K	Initial temperature interval
	DELTAT	Free field	K	Initial temperature change
2	RANGE	Free field	km	Altitude
3	JNAME	Free field	A40	Latitude-season identification
4	ID1	Free field	km	Haze condition
5	DELTAF	Free field	Hz	Electrical bandwidth
	AA	Free field	cm^2	Effective area aperture
	RADI	Free field	mrad	Number of milliradians
	EMISS	Free field		Emissivity
6	A2	Free field	μm	Ending wavelength
	A3	Free field	μm	Starting wavelength
	DNVI	Free field	$v\text{-}Hz^{-1/2}$	Detector noise voltage index
	RPEAK	Free field	v/w	Peak detector response
7	XSTART	Free field		Starting X-axis value (output plot)
	YSTART	Free field		Starting Y-axis value (output plot)
	XINCRE	Free field		X-axis increment
	YINCRE	Free field		Y-axis increment
	XSCALE	Free field		X-axis scale factor
	YSCALE	Free field		Y-axis scale factor
	XSIZE	Free field	inch	Length of X-axis
	YSIZE	Free field	inch	Length of Y-axis

Table D2

Example of Graphical Output of Model

Prediction of Minimum Detectable Temperature Difference		
Temperature K	Emissivity	Minimum Detectable Temperature Difference °C
200.0	1.0	2.50
220.0	1.0	1.56
240.0	1.0	1.09
260.0	1.0	0.86
280.0	1.0	0.70
300.0	1.0	0.55
320.0	1.0	0.47
340.0	1.0	0.39
360.0	1.0	0.35
380.0	1.0	0.31
400.0	1.0	0.27

LEGEND

Sensor Characteristics
Detector Type: HGCDTE
Detector Noise Voltage Index (volt/sqrt (Hertz)): 0.1000E 07
Electrical Bandwidth (Hertz): 0.1250E 07
Spatial Resolution (milliradians): 2.0
Wavelength Band (micrometers): 14.0-8.0
Effective Aperture Area (cm^2): 40.0
Peak Response (volt/watt): 2000.0

Atmosphere Condition
Latitude-Season: Mid-latitude Summer
Haze (km): 23
Altitude (km): 1.5

Table D3

Variable for Minimum Detectable Temperature Difference Model

Variable	Unit	Description
NTEMPS	K	Starting temperature
NTEMPE	K	Ending temperature
NTEMPI	K	Temperature interval
DELTAT	K	Initial temperature change
RANGE	km	Altitude
ICOUNT, NOPT		Number of points
N3, N1	cm^{-1}	Starting wave number
NDIFF	cm^{-1}	Wave number increments
MODEL		Code: 1 - Tropical atmosphere model 2 - Mid-latitude summer 3 - Mid-latitude winter 4 - Subarctic summer 5 - Subarctic winter
IHAZE		Code: Haze condition 1 - 23 km 2 - 5 km
IANGLE	degree	Zenith angle × 100
IH1	km	Minimum altitude × 100
IH2	km	Ground to sensor altitude × 10
M1, POUTER	$w/(cm^2\text{-}\mu m)$	Storage for data values
JNAME		Legend identification
ID1	km	Haze condition
DELTAF	Hz	Electrical bandwidth
AA	m^2	Feature area

(Continued)

Table D3 (Concluded)

Variable	Unit	Description
RAD1	mr	Number of milliradians
EMISS		Emissivity
A2	μm	Starting wavelength
A3	μm	Ending wavelength
DNVI	$v\text{-}Hz^{-1/2}$	Detector noise voltage index
VND	volt	Voltage noise
REA		Storage for area under curve for feature and background
RDIFF	volt	Difference for feature area and background area
TDIFF	^{o}C	Storage for minimum detectable temperature difference
Y(I)	μm	Storage for wavelength
XSIZE	inch	Length of X-axis
YSIZE	inch	Length of Y-axis
XSTART		Starting value of X-axis
YSTART		Starting value of Y-axis
XINCRE		X-axis increments between tic marks
YINCRE		Y-axis increments between tic marl
XSCALE		X-axis scale factor
YSCALE		Y-axis scale factor

Table D4

Structure of Input File for Ground-to-Sensor Atmospheres

Record No.	Variable	Format	Description
1	ICOUNT	I6	Number of data points
	N3	I6	Starting wave number, $cm^{-1} \times 10$
	NDIFF	I6	Wave number increment, $cm^{-1} \times 10$
	MODEL	I1	Code: 1 - Tropical atmosphere 2 - Mid-latitude summer 3 - Mid-latitude winter 4 - Subarctic summer 5 - Subarctic winter
	IHAZE	I1	Code: 1 - 23 km (sea level) visual range 2 - 5 km (sea level) visual range
	IANGLE	I6	Zenith angle × 100, deg
	IH1	I6	Minimum altitude × 10, km
	IH2	I6	Ground-to-sensor distance × 10
2	M1	19I4	Data values for percent transmission $\times 10^4$

Table D5

Structure of Input File for Relative Response Curve

Record No.	Variable	Format	Description
1	INAME	A12	Detector identification
2-3	KNAME	A68	Identification
4	NOPT	I6	Number of data points
	N1	I6	Starting wave number, $cm^{-1} \times 10$
	NDIFF	I6	Wave number increment, $cm^{-1} \times 10$
5	POUTER	6E12.4	Data values

Table D6

Example of Variable Inputs

200, 400., 20., 10.
1.5
Mid-latitude summer
23
1.E6, 40., 2.5, 1.0
14., 8., 1.E-8, 2000.
200., 0., 25., 5., .04, .2, 8., 5.

Table D7

Example of Input File for Atmospheric Transmission

```
  488  6507   50032      0      0     15      0
  01674713383148844901589158373808787298455770746063423115 8 174    0    0    0
 106    0    0    0 38410941949382153525784721374773715132 0    0   0697881118603
8765885288328841880287588624766664393908374821277464381238803838205636351800
 184    3    0    0    0    0    0    0   23 495312860916308712773247804803881868246
8279814680188056813680787802740466307661462365126373384219 95  752  3221453  437
 232  746182120966195700671937466751576617760783478387830783278197582777 37735
7410775277397705767173236621596643914391615531053407235018 92  816  411  458  835
 332  3311804533857886153631365277057733873867383719773287347733573237 3107298
7286727472627250720970836807650858905433555422474133350143426424700170867074
7063705170407028701770056994698369716960694969376926691569046892688168486803
6650637863556445585354474887514446595127462238065083645065196317635662416557
6142613865826610659965886578656765576546653665256515650464866465642863086179
6226631160796148598462486344635963346335630963206295629563006290628062706260
6142533345054388621062006190618061706160612660986028595357755847571160285600
5931605360436027601159975983597459725917596659565947593759285918590958995890
5880587158615852584358335824581458055796578657775768575857495740573057215712
5703569356845675566656575647563856295620561156025593558455755566555755485539
5530552155125503549454855476546754595450544154325423541454055397538853795370
5362535353445336532753185310530152925284527552665258524952415232522352155206
5198518951815172516351555146513851295121511351045096508750795070506250535045
5036502850205011500349944986497849694961495349444936492849194911490348944886
4878486948614853484548364828482048124803479547874779477147624754474647384730
4721471347054697468946814673466446564648464046324624461646084600459145834575
4567455945514543453545274519451145034495448744794471446344554447443944314423
4415440743994391438343754367435943514343433543284320431243044296428842804272
4264425642494241423342254217420942014194418641784170    0    0    0    0    0    0
```

263

Table D8

Example of Detector Relative Response File

```
INSP
RELATIVE RESPONSE CURVE
MARCH 10,1976    1015 HOURS
  187    700    50
 0.          0.          0.          0.          0.          0.
 0.          0.          0.          0.          0.          0.
 0.          0.          0.          0.          0.          0.
 0.          0.          0.8040E-01  0.1860E 00  0.2916E 00  0.4297E 00
 0.5865E 00  0.7433E 00  0.9000E 00  0.9288E 00  0.9575E 00  0.9863E 00
 0.1000E 01  0.1000E 01  0.1000E 01  0.1000E 01  0.9840E 00  0.9670E 00
 0.9500E 00  0.9430E 00  0.9360E 00  0.9290E 00  0.9220E 00  0.9150E 00
 0.9040E 00  0.9010E 00  0.8910E 00  0.8805E 00  0.8700E 00  0.8595E 00
 [illegible]90E 00  0.8385E 00  0.8280E 00  0.8175E 00  0.8070E 00  0.7975E 00
 0.7900E 00  0.7825E 00  0.7750E 00  0.7675E 00  0.7600E 00  0.7525E 00
 0.7450E 00  0.7375E 00  0.7300E 00  0.7225E 00  0.7150E 00  0.7075E 00
 0.7000E 00  0.6950E 00  0.6900E 00  0.6850E 00  0.6800E 00  0.6750E 00
 0.6700E 00  0.6650E 00  0.6600E 00  0.6550E 00  0.6500E 00  0.6450E 00
 0.6400E 00  0.6350E 00  0.6300E 00  0.6250E 00  0.6200E 00  0.6150E 00
 0.6100E 00  0.6050E 00  0.6000E 00  0.5961E 00  0.5922E 00  0.5883E 00
 0.5844E 00  0.5805E 00  0.5766E 00  0.5727E 00  0.5688E 00  0.5649E 00
 0.5610E 00  0.5571E 00  0.5532E 00  0.5493E 00  0.5454E 00  0.5415E 00
 0.5376E 00  0.5337E 00  0.5298E 00  0.5259E 00  0.5220E 00  0.5181E 00
 0.5142E 00  0.5103E 00  0.5064E 00  0.5025E 00  0.4986E 00  0.4947E 00
 0.4908E 00  0.4869E 00  0.4830E 00  0.4791E 00  0.4752E 00  0.4713E 00
 0.4688E 00  0.4670E 00  0.4652E 00  0.4634E 00  0.4616E 00  0.4598E 00
 0.4580E 00  0.4562E 00  0.4544E 00  0.4526E 00  0.4508E 00  0.4490E 00
 0.4472E 00  0.4454E 00  0.4436E 00  0.4418E 00  0.4400E 00  0.4382E 00
 0.4364E 00  0.4346E 00  0.4328E 00  0.4310E 00  0.4292E 00  0.4274E 00
 0.4256E 00  0.4238E 00  0.4220E 00  0.4202E 00  0.4184E 00  0.4166E 00
 0.4148E 00  0.4130E 00  0.4112E 00  0.4094E 00  0.4076E 00  0.4058E 00
 0.4040E 00  0.4022E 00  0.4004E 00  0.3986E 00  0.3968E 00  0.3950E 00
 0.3932E 00  0.3914E 00  0.3896E 00  0.3878E 00  0.3860E 00  0.3842E 00
 0.3824E 00  0.3806E 00  0.3788E 00  0.3770E 00  0.3752E 00  0.3734E 00
 0.3716E 00  0.3698E 00  0.3680E 00  0.3662E 00  0.3644E 00  0.3626E 00
```

Table D9

List of Control Cards

Column No.		
1	8	16
$	IDENT	USER NO., IDENTIFICATION
$	OPTION	FORTRAN
$	FORTY	NFORM, NLNO
$	USE	.GTLIT
	Source Deck	
	.	
	.	
	.	
$	EXECUTE	
$	LIMITS	TIME, STORAGE
$	PRMFL	DEVICE NO.,R/W,L,USER NO./FILENAME
$	DATA	41

APPENDIX E: RELATION OF ABSOLUTE AND APPARENT TEMPERATURE

1. The relation between absolute and apparent temperature can be formulated from Planck's Law and the definition of apparent temperature. For the purposes of this study, apparent temperature, T_{app}, is defined as the temperature of a blackbody (a material with $\varepsilon = 1.0$) that radiates (within the wavelength band of interest) the same amount of EM energy as a material wit . ' ı absolute temperature, T, and an emissivity, ε, less than 1.0.

2. From Planck's Law the EM energy radiated as a function of wavelength from a blackbody is as follows:

$$W_{\lambda bb} = \frac{C_1}{\lambda^5}\left[e^{(C_2/\lambda T)} - 1\right]^{-1}$$

where

$C_1 = 3.74 \times 10^4$, W μm^4 cm^{-2}

$C_2 = 14,388$, μm K

λ = wavelength, μm

e = base to natural logarithm

T = absolute temperature, K

Similarly, the energy radiated by a nonperfect radiator (a gray body; a material having an ε less than 1.0) is as follows:

$$W_{\lambda} = \frac{\varepsilon_{\lambda} C_1}{\lambda^5}\left[e^{(C_2/\lambda T)} - 1\right]^{-1} \qquad \text{(E1)}$$

where

ε_{λ} = emissivity at wavelength λ.

Since the apparent temperature of the material whose radiation properties are described by Equation E1 is the temperature of a blackbody radiating the same amount of energy, the following relation can be formulated within a wavelength band of interest:

$$W_\lambda = \frac{\varepsilon_\lambda C_1}{\lambda^5}\left[e^{(C_2/\lambda T)} - 1\right]^{-1} = W_{\lambda bb} = \frac{C_1}{\lambda^5}\left[e^{(C_2/\lambda T_{app})} - 1\right]^{-1} \qquad \text{(E2)}$$

Solving this relation for ε_λ results in the following:

$$\varepsilon_\lambda = \frac{\left[e^{(C_2/\lambda T)} - 1\right]}{\left[e^{(C_2/\lambda T_{app})} - 1\right]}$$

Ignoring the -1 in the brackets (the effects of this step is addressed in paragraph 5) and taking the logarithm of both sides of the equation results in the following:

$$\ln \varepsilon_\lambda = \frac{C_2}{\lambda T} - \frac{C_2}{\lambda T_{app}}$$

which reduces to

$$\ln \varepsilon = \frac{C_2}{\lambda}\left(\frac{1}{T} - \frac{1}{T_{app}}\right)$$

Assuming ε is a constant for a given wavelength band (a fairly valid assumption for the 3- to 5.5-µm or 8- to 14-µm wavelength bands) λ_1 to λ_2 and integrating

$$\ln \varepsilon \int_{\lambda_1}^{\lambda_2} d\lambda = C_2\left(\frac{1}{T} - \frac{1}{T_{app}}\right) \int_{\lambda_1}^{\lambda_2} \frac{d\lambda}{\lambda}$$

resulting in

$$\Delta\lambda \ln \varepsilon = C_2 \left(\frac{1}{T} - \frac{1}{T_{app}}\right) \ln \left(\frac{\lambda_2}{\lambda_1}\right)$$

where $\Delta\lambda = \lambda_2 - \lambda_1$ and

$$\frac{\Delta\lambda \ln \varepsilon}{C_2 \ln (\lambda_2/\lambda_1)} = \frac{1}{T} - \frac{1}{T_{app}}$$

Rearranging this equation results in a final expression for apparent temperature:

$$T_{app} = \frac{1}{\frac{1}{T} - \frac{\Delta\lambda \ln \varepsilon}{C_2 \ln (\lambda_2/\lambda_1)}} \qquad \text{(E3)}$$

Examination of the above equation reveals that the apparent temperature of a material is a function of the wavelength band of interest as well as emissivity and absolute temperature. A graphical presentation of this equation is given in Figures E1 and E2.

3. The graphs shown in Figures E1 and E2 reveal two important items. First, by comparing the graphs in the two figures it is obvious that the relation between absolute and apparent temperature is significantly different for the two wavelength bands. For example, the

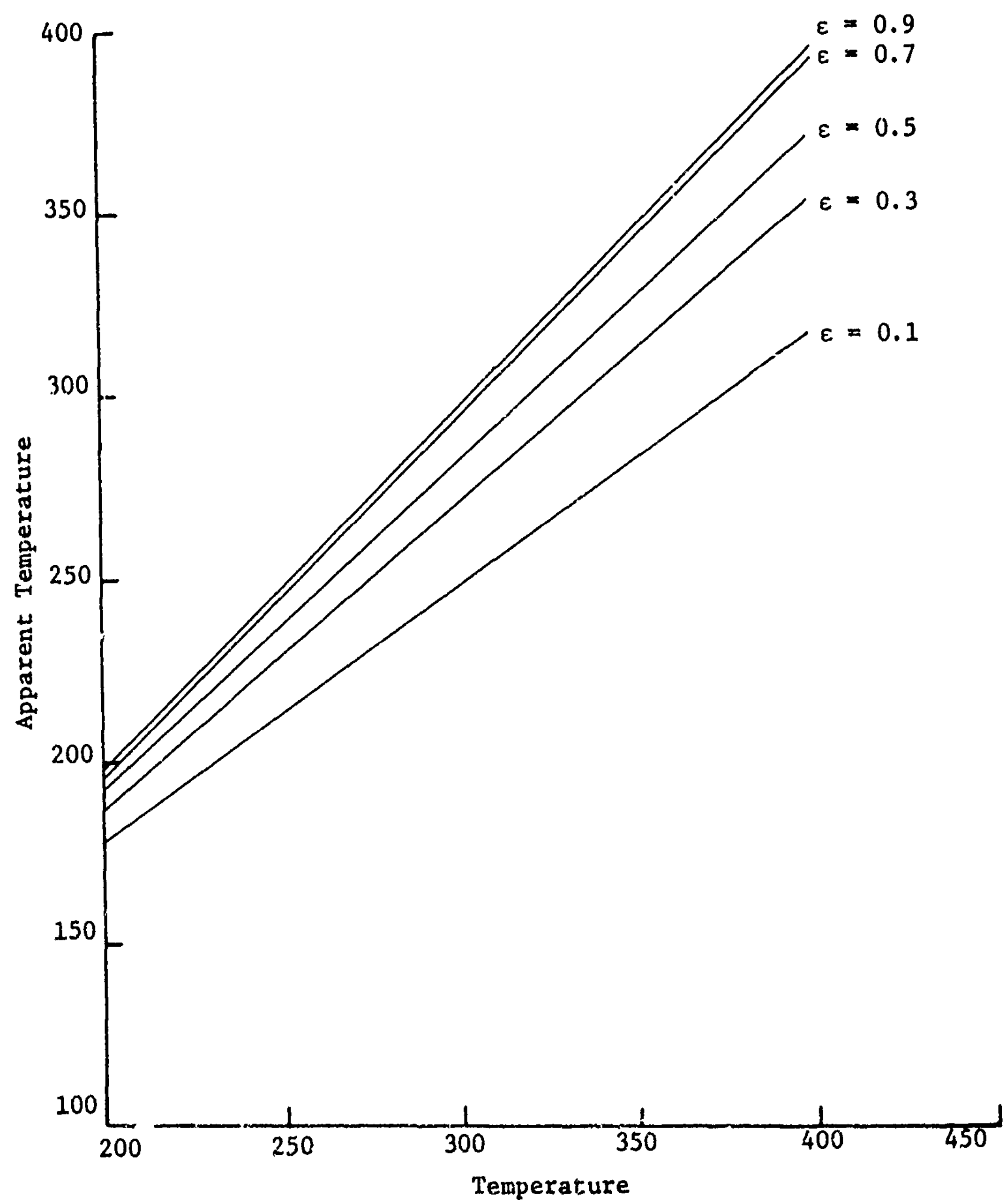

Figure E1. Apparent temperature versus actual temperature and emissivity for the 3.0- to 5.5-μm wavelength band

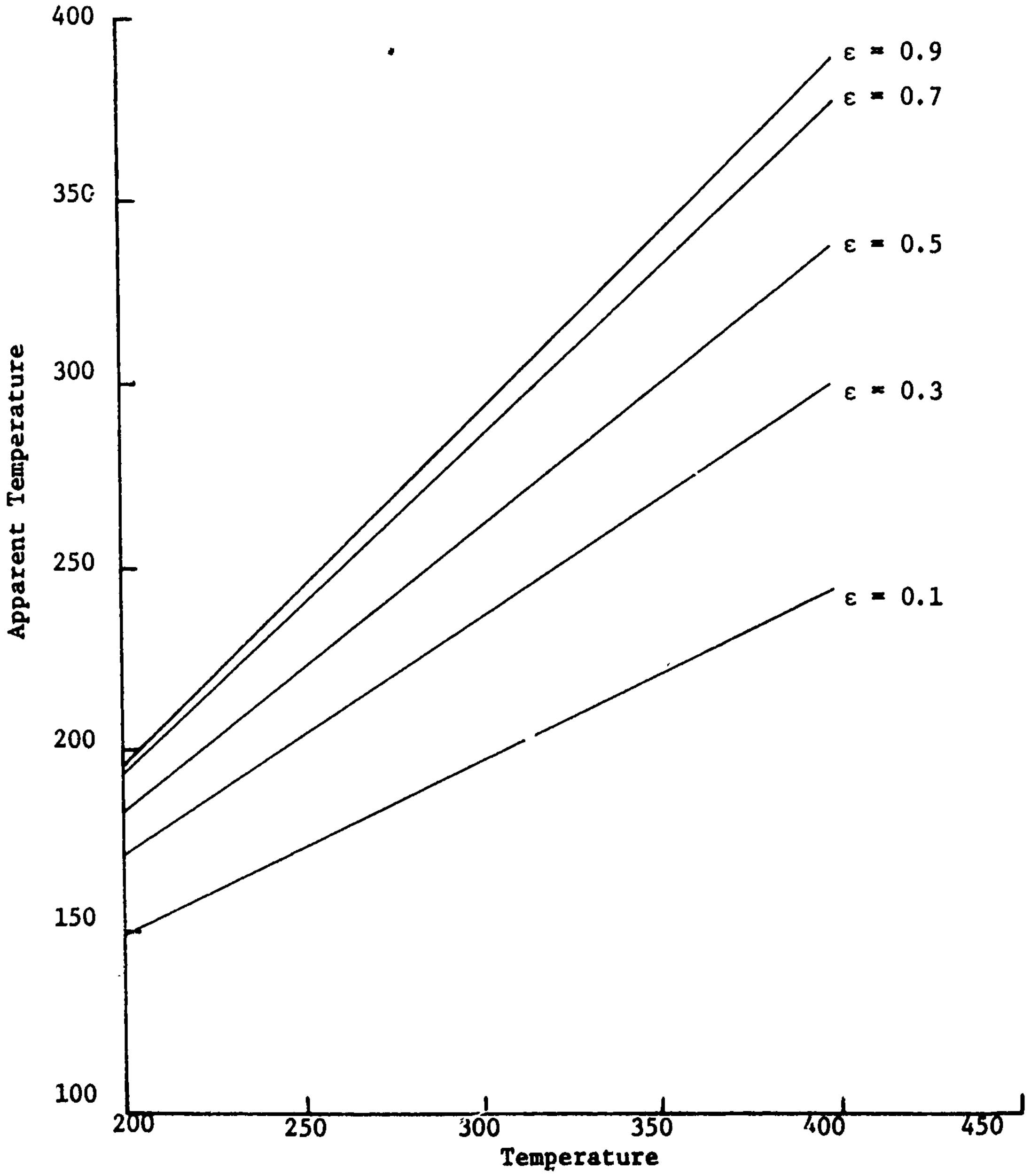

Figure E2. Apparent temperature versus actual temperature and emissivity for the 8- to 14-μm wavelength band

apparent temperature of a material having an absolute temperature of 300 K (roughly ambient for terrain materials) and emissivity of 0.7 is 295 K and 280 K for the 3.0- to 5.5- and 8- to 14-μm wavelength bands, respectively. A portion of the apparent temperature difference between the wavelength bands is due to the larger bandwidth for the 8- to 14-μm band.

4. The second item concerns the functional relationship between absolute and apparent temperature. Examination of the graphs in Figures E1 and E2 shows that the relationship described by Equation E3 is almost linear within the wavelength bands for which calculations were made (i.e. 3- to 5.5- and 8- to 14-μm). Within the normal ambient temperatures observed for terrain materials (i.e. between 250 and 350 K) the assumption of linearity within a single wavelength band is probably adequate for the purposes of this study.

5. The effect of eliminating the "-1" from the expression

$$\left[e^{(C_2/\lambda T)} - 1\right]$$

(as described in paragraph 2) was evaluated by calculating the value of the expression with and without the "-1" for a wavelength of 10 μm and a spectrum of temperatures. The results were as follows:

T, K	$e^{(C_2/\lambda T)}$	$\left[e^{(c_2/\lambda T)} - 1\right]$	Percent Difference
250			
300	120.7	119.7	0.8
350	60.9	59.9	1.6
400	36.4	35.4	2.8
450	24.4	23.4	4.0

Examination of these data show that the percent difference of the values for the two forms of the expression is essentially negligible for ambient terrain temperatures (i.e. approximately 300 K) and increases slightly with an increase in temperature.

In accordance with ER 70-2-3, paragraph 6c(1)(b), dated 15 February 1973, a facsimile catalog card in Library of Congress format is reproduced below.

Link, Lewis E

Procedures for the systematic evaluation of remote sensor performance and quantitative mission planning, by Lewis E. Link, Jr. Vicksburg, U. S. Army Engineer Waterways Experiment Station, 1976.

xix, 272 p. illus. 27 cm. (U. S. Waterways Experiment Station. Technical report M-76-8)

Prepared for Office, Chief of Engineers, U. S. Army, Washington, D. C., under Project 4A162121A896, Task 01.

Literature cited: p. 142-144.

1. Infrared scanners. 2. Mathematical models. 3. Remote sensing. 4. Sensors. I. U. S. Army. Corps of Engineers. (Series: U. S. Waterways Experiment Station, Vicksburg, Miss. Technical report M-76-8)

TA7.W34 no.M-76-8